Master of Science Thesis

# Finite Element Analysis of Inflatable Structures Using Uniform Pressure

## Inflatable beam validation and leading edge inflatable tube kite structural modeling in Madymo

J.F.J.E.M. Schwoll

July 2012

Delft University of Technology

Challenge the future

Faculty of Aerospace Engineering

# Finite Element Analysis of Inflatable Structures Using Uniform Pressure

*Inflatable beam validation and Leading Edge Inflatable tube kite structural modeling in Madymo*

J.F.J.E.M Schwoll

June 25, 2012

# Finite Element Analysis of Inflatable Structures Using Uniform Pressure

## Inflatable beam validation and Leading Edge Inflatable tube kite structural modeling in Madymo

Master of Science Thesis

For obtaining the degree of Master of Science in Aerospace Engineering
at Delft University of Technology

J.F.J.E.M Schwoll

June 25, 2012

Faculty of Aerospace Engineering · Delft University of Technology

Delft University of Technology

Delft University Of Technology
Institute
Applied Sustainable Science Engineering and Technology

The undersigned hereby certify that they have read and recommend to the Faculty of Aerospace Engineering for acceptance a thesis entitled **"Finite Element Analysis of Inflatable Structures Using Uniform Pressure"** by **J.F.J.E.M Schwoll** in partial fulfillment of the requirements for the degree of **Master of Science**.

Dated: June 25, 2012

Readers:

Prof.dr. W.J. Ockels

Dr.-ing. R. Schmehl

Dr.ir. O.K. Bergsma

Dr.ir. J. Breukels

Dr.ir. M.G.A. Tijssens

# Preface

This Master thesis will end a fantastic time studying Aerospace Engineering. Sustainability is a very interesting and challenging topic, however being part of such an onnovative concept inspired me for the rest of my life.

I would like to thank Prof. Dr. Wubbo J. Ockels for starting the kite powered energy concept with a innovative and original idea, and giving me the opportunity to do this research. Special thanks to my supervisor Dr.-Ing. Roland Schmehl for his patience and who guided me through my research, which was not easy. I am grateful for the great feedback and insight that Dr. Ir. Martin G. A. Tijssens provided on my work and for being part of my graduation committee. I would like to share my gratitude for the help, inspiration and being part of my graduation committee to Dr. Ir. Jeroen Breukels. Last but not least, for taking part in my graduation committee, my appreciation goes out to Dr. Ir. Otto K. Bergsma.

I would like to thank the people from TASS, especially Ir. Peter Ritmeijer, MSc. Cindy Charlot and Dr. Ir. Willy Koppens, who provided me the opportunity to work with Madymo. For giving me advice and assistance on a challenging topic.

Thanks to everyone in the Kite Power group with whom I worked with the past, nearly, two years. The knowledge about kites, the system and the enthusiasm of everyone involved made this research an interesting, exiting and informative time. Special thanks to Nana Saaneh, who helped me with settling down and arranging my forms and paper work.

For helping me with my Thesis structure and grammar, which was a difficult task for me, I would like to thank my friends Ir. Mareijn Willems, Ir. Edwin Terink and Jasper Vijverberg for their support.

Most importantly, I would like to thank my parents and my girlfriend who supported and believed in me.

Delft, University of Technology J.F.J.E.M. Schwoll
Juli 2012

# Summary

Kite wings might be the future in sustainable electricity generation. Delft University of Technology developed a concept with a flexible Leading Edge Inflatable (LEI) kite to generate the energy, which can maneuver at higher altitudes where the power density is much higher and the wind velocity is much more consistent compared to operating altitudes of conventional wind turbines. Using a realistic kite computer simulation the design of the kites can be improved, by better understanding the structural behavior of the kites. The existing kite models are able to reproduce the general behavior of the kite. However, the local effects, such as the actual shape of the structure, wrinkling, stresses and collapse are difficult topics that cannot be examined in the existing models. The models are also not able to use physical inputs and predict the behavior. In this thesis the method that is set to investigate the local effects as well as general structural behavior of the kite is the Finite Element Method (FEM). This is a predictive method, which means that the actual material properties, geometrical and external loads are used as inputs of the model. The FEM solver that is used for this research is called Madymo. This is a general purpose FEM, CFD and multi body solver and used in the automotive industry for crash investigation. The internal pressure of the LEI kite is assumed to be equally distributed inside the struts and the leading edge. In Madymo, the method that is used for this purpose is called the Uniform Pressure (UP) method. A cantilever inflatable cylindrical beam applied with a tip load is the first case study that is discussed. For validation, linear theory and an experiment are compared to a reference case of the FEM model. Also a parameter sensitivity study is performed. The second case study consists of modeling the V2 LEI Mutiny kite, including the bridle system, in FEM. The kite was qualitatively compared to a test with three load cases: gravity, load in the center of the leading edge and a falling mass. The results of the inflatable beam were very promising in the linear and first non linear states, compared to the theory. The model and theory showed a deviant behavior from the experiment, and for collapse, further study is needed. The model of the kite proved to be much stiffer compared to the real kite; however, as a first study it showed to be very promising to model the kite with FEM. Further study is needed for optimizing the model of the bridle system and to model the local effects of the kite, such as the connections between the leading edge and the struts.

# Acronyms

| | |
|---|---|
| **2D** | Two Dimensional |
| **3D** | Three Dimensional |
| **ASSET** | Applied Sustainable Science Engineering and Technology |
| **AWE** | Airborne Wind Energy |
| **BP** | Bridle Point |
| **CAD** | Computer-Aided Design |
| **CFD** | Computational Fluid Dynamics |
| **CST** | Constant strain triangle |
| **DOF** | Degrees of freedom |
| **DUT** | Delft University of Technology |
| **FBD** | Free Body Diagram |
| **FEM** | Finite Element Method |
| **GUI** | Graphical User Interface |
| **KCU** | Kite Control Unit |
| **LE** | Leading Edge |
| **LEI** | Leading Edge Inflatable |
| **Madymo** | MAthematical DYnamic MOdel |
| **MB** | Multi Body |
| **NURBS** | Non-Uniform Rational B-Splines |
| **o/i** | Output/Input |
| **Rhino** | Cad program Rhinoceros |
| **TE** | Trailing Edge |
| **UP** | Uniform Pressure |
| **WIP** | Work In Progress |
| **WPD** | Wind Power Density |
| **XML** | Extensible Markup Language |

# List of Symbols

## Greek Symbols

| | |
|---|---|
| $\alpha$ | Rayleigh Damping Coefficient |
| $\alpha$ | Angle of attack |
| $\pi$ | Ratio of the circumference of a circle to the diameter |
| $\rho$ | Air density |
| $\epsilon$ | Strain |
| $\gamma$ | Shear Strain |
| $\lambda$ | Artificial poisson ratio |
| $\nu$ | Poisson's ratio |
| $\psi$ | Shear Stress |
| $\sigma$ | Stress |
| $\tau$ | Shear Stress |
| $\theta$ | Circumferential angle |

## Roman Symbols

| | |
|---|---|
| $D$ | Drag Force |
| $L$ | Lift Force |
| $I$ | mass moment of inertia |
| $p$ | Internal pressure |
| $r$ | Radius |
| $S$ | $2^{nd}$ Piola Kirchhoff stress tensor |
| $C$ | Compliant Matrix |

| | |
|---|---|
| $D$ | Damping Matrix |
| $G$ | shear modulus |
| $K$ | Stiffness Matrix |
| $M$ | Mass Matrix |
| $M$ | Moment |
| $Y$ | Mass mixture |
| $a$ | Acceleration vector |
| $u$ | Mass-specific internal energy |
| $u$ | displacement in x direction |
| $v$ | Velocity vector |
| $v$ | displacement in y direction |
| $E$ | E modulus |
| $t$ | Time |
| $V_W$ | Wind velocity |

# Contents

# Chapter 1

# Introduction

Inflatable structures applications can be found in a wide variety of industries. Entertainment, sports, nautical, civil, space and aerospace are just a number of industries where inflatable structures are used. In space engineering especially there is an interest in using inflatable structures, mainly because of the light weight and stiffness after inflation in space. In space engineering the inflatable structure research is a part of a wider study, which is called thin film (or Gossamer) structures (Veldman, 2005).

This thesis is performed at the Delft University of Technology (DUT) kite power group, where kites are used to convert wind energy to electrical energy. This form of energy production is called Airborne Wind Energy (AWE) and could possibly be competitive with conventional wind turbines in future. AWE has the potential to be competitive because of the flexible operating altitude and location. Also the devices are constructed using lighter material compared to conventional wind turbines. The DUT kite power group uses a Leading Edge Inflatable (LEI) kite to convert the kinetic energy of the wind into mechanical energy. This LEI kite consists of an inflatable tubular structure that provides stiffness to the structure of the kite.

One of the major shortcomings of the current state the LEI research is the lack of a reliable and realistic computer model of the structure of the kite. There are two main motivations to perform a thorough scientific study into modeling kites. The first motivation is that the kite is a highly flexible structure compared to aircraft. The structural dynamics of the LEI kite is strongly coupled with the fluid dynamics of the wind. The inflatable structure influences the aerodynamic flow and the aerodynamic flow is influenced by the flexible structure. This interaction is called fluid structure interaction (FSI), which is complex. Conventional aircraft are also complex systems, however conventional aircraft are considered to be less flexible compared to kites (Breukels, 2011). The second motivation for modeling LEI kites is that it is difficult to validate a kite wing model in airflow. The kite used in the DUT kite group is 25 $m^2$ so it is difficult to test a kite in a wind tunnel. Scaling down a kite might also be difficult because of the fabrics that are used in the kites. This is different with conventional aircraft. If the kite is scaled down, the fabric might be scaled down accordingly, together with seams and the bridle. The scaling of the kite could possibly influence the aerodynamics differently compared to a full size kite. Kite testing and measuring of realistic flight conditions, poses a problem that the wind field is not uniform and cannot be controlled. At this moment, this is the only choice that is done for validation.

## 1-1 Problem statement

The existing kite models describe the kite either as a point mass, rigid body, multi-plate model or a multi-body model. The multi plate and the multi body model incorporate flexibility. However, this flexibility is modeled as fitted parameters that mimic the flexibility of inflatable structures. These models describe the general behavior of the kite, but cannot display local effects, such as wrinkling or stresses in the material. These models contain no physical properties that describe the behavior of inflatable structures. With the existing models it is not possible to "predict" the behavior of the beam by the input of the physical properties of the inflatable structure.

## 1-2 Research questions

In order to investigate the inflatable structures locally, a higher level of complexity compared to multi body dynamics is required. Finite Element Method (FEM) provides this higher level of complexity and is a predictive method. The material inputs are physical properties such as the E modulus and density and in this way the FEM method predicts the behavior of the structure. Different materials, external forces and geometries can be implemented as inputs. The FEM method however is computationally more expensive compared to multi body model. Also material research is needed to acquire the material input with woven fabrics this is complex due to interaction of the threads in the fabric. The following research questions will be answered in this thesis are:

- Is it possible to describe a FEM model of an inflatable structure with UP (uniform pressure) method with a triangular membrane mesh? The UP method equally distributes the internal pressure on the surface inside an enclosed inflatable structure.
- How accurate will a cylindrical beam model be able to predict the behavior in comparison with experiments and theory using a model that has a reasonable computation time?
- What is the influence of changes in the model parameters to the inflatable beam model performance?
- Is it possible to model the structural dynamics of a LEI kite model including the bridle system with FEM method using the Uniform Pressure (UP) assumption applied to the inflatable tubular structure?

## 1-3 Scope of the thesis

The method to examine and analyze the inflatable structure is the FEM. The discretization that is used is a triangulated membrane mesh. The pressure inside the inflatable structure is a uniform pressure. The main focus within this thesis is the analysis of inflatable structures in taut, or linear behavior. The inflatable structures are loaded with static loads and the analysis will not include dynamic analysis. There is no aerodynamic load applied to the inflatable structure and The FEM tool used is Madymo (Mathematical Dynamic Model) and is a general purpose FEM, CFD and multi body solver.

## 1-4 Thesis structure

This thesis is built up in two parts. The first part consists of the background of the research. In Chapter 2 the DUT kite project is explained. This will give the motivation to perform research to access the Airborne Wind Energy (AWE) using a pumping kite concept. In Chapter 3 a theoretical background of inflatable structures is discussed. First the existing kite models are discussed, however, literature of structural research on LEI kites is rare. One of the main components of a LEI kite is the inflatable tubular structure. The inflatable cylindrical beam is examined thoroughly, thus covering inflatable beam structure theory. Since MAthematical DYnamic MOdel (Madymo) is used as a FEM tool with the uniform pressure assumption, Chapter 4 describes the theoretical background of the uniform pressure method. In this Chapter, the finite element method and the multi-body model are also explained.

The second part consists of the main part of this thesis. In Chapter 6 the modeling inputs for the FEM model with uniform pressure method are described. In this Chapter, the inputs are discussed that are needed for the FEM model in Madymo. The Chapter is concluded with an approach for two case studies, the first is a cylindrical inflatable beam and second is the V2 LEI Mutiny kite. In Chapter 7 a case study is performed on a cantilever cylindrical inflatable beam FEM model. Results are given and the FEM model is compared and validated with the experiment and linear beam theory. Next a parameter sensitivity study is performed that describes the influences of the different parameters of the model. In the results of this parameter sensitivity study, the variation of the parameters are compared to the reference case and the experiment(s). In Chapter 8 The V2 LEI Mutiny kite is modeled including the bridle. The results are qualitatively compared to an experiment which is described. This chapter will be concluded with a discussion of the model and the comparison between the model and the experiment. Finally conclusions and recommendations will be given in Chapter 9.

# Part I

# Literature Study

Chapter 2

# Kite technology for energy generation

This chapter discusses the new field of research to access the wind energy with respect to the conventional wind turbines: kite power. Section 2-1 describes the wind energy that is not generated using conventional wind turbines, which is called Airborne Wind Energy (AWE). The DUT has a kite research group that investigates the accessibility of this AWE using a pumping kite concept. This is explained in Section 2-2. In Section 2-3 the kite is analyzed, which is one of the components of the DUT kite research group. Section 2-4 describes the specific kite that has been used for this thesis: the leading edge inflatable (LEI) V2 Mutiny kite.

## 2-1 Airborne Wind Energy (AWE)

In this section AWE is explained. The motivation for developing AWE is to provide a competitive alternative to conventional wind turbines. In order to be competitive, the aim of AWE is to generate energy at lower costs, access the wind energy with more flexibility and have a lower environmental impact compared to conventional wind turbines.

One example of accessing the wind energy more flexible is the ability of AWE to access the wind energy at higher altitudes. Wind at higher altitude is stronger and more consistent compared to wind accessible by conventional wind turbines. Tethered airfoils could be a way to access this energy at these higher altitudes.

AWE started as wind energy production at altitudes above the altitudes of conventional wind turbines (rotor tip height of 200m). Fig. 2-1a shows the average wind velocities at different altitudes measured at the meteorological station of de Bilt in the Netherlands between 1960 and 1980. The Kite power research group of DUT, which is part of Applied Sustainable Science Engineering and Technology (ASSET) institute, has been investigating the possibilities of AWE by means of a pumping kite system. The first incentive for using tethered airfoils to generate energy was described by Ockels (2001).

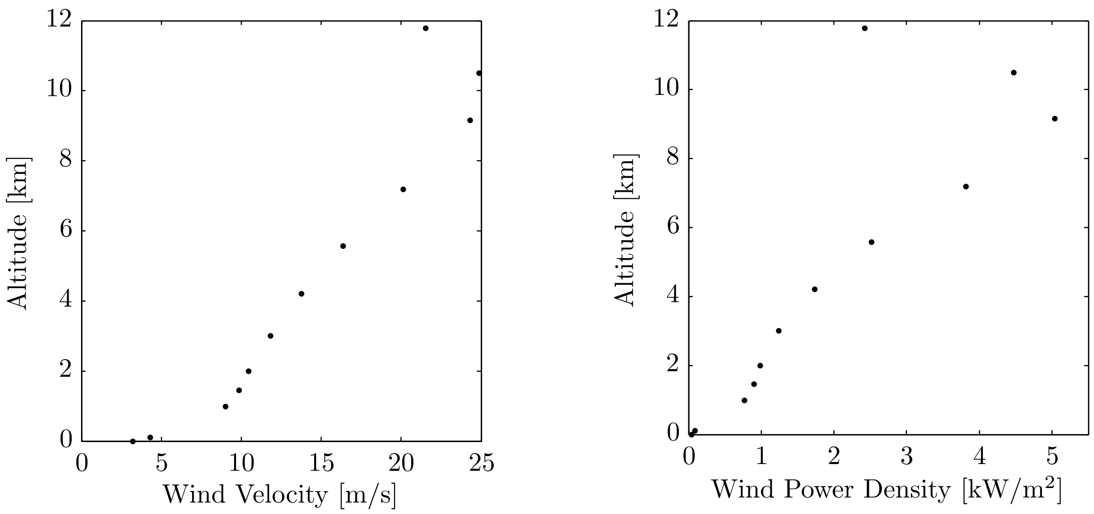


**(a)** Average Wind velocity

**(b)** Average Wind Power

**Figure 2-1:** Wind data from KNMI averaged from 1960 - 1980 (Ockels et al., 2004)

The Wind Power Density (WPD) is given by Equation 2-1, where $WPD$ is given in $kW/m^2$. Here $\rho$ is the density and $V_W$ is the wind velocity.

$$WPD = \frac{1}{2}\rho V_W^3 \tag{2-1}$$

The power per square meter stored in the wind is shown in Fig. 2-1b and the average wind measurements shown in Fig. 2-1a. In Fig. 2-1b, an increase in wind power density is shown with a maximum at approximately 9 km altitude. The increase in wind power density is strong between 0.1 km and 1 km, so small increase in altitude shows a large increase in wind power density. This increase in wind power density as a function of altitude is interesting to investigate the possibilities for AWE.

A down side of accessing the wind energy at high altitudes are the air traffic regulations; however with AWE it might be possible to access the wind energy.

## 2-2 DUT Kite power project

In the previous section, it has become clear that the wind energy at higher altitudes is a very interesting source of energy. At the DUT a research group explores the possibilities of accessing AWE. In this section the kite power system of the DUT is explained. The pumping concept of the kite power project of the DUT is first explained including five power cycles are discussed. As last, the components of the kite project are introduced.

The kite power project of DUT consists of a system where wind energy is converted into mechanical energy by means of a pumping cycle. A pumping cycle consists of a reel-out phase and a reel-in phase. In Fig. 2-2a the two phases are shown. In the reel-out phases of the periodic cycles, the kite flies Figures-of-eight perpendicular to the wind velocity to achieve high traction force. From (Loyd, 1980), high traction force is proportional to high mechanical power. The traction force pulls the tether from a drum (onto which the tether is rolled) that drives an electrical generator that converts this mechanical energy into electrical energy. This is shown at the top of Fig. 2-2a. In Fig. 2-2b, the Figure-of-eight flight pattern during the reel-out phase is shown at during an actual test. When the tether is rolled out to the maximum length, the orientation of the wing is changed by active control, such that the aerodynamic forces on the kite are as low as possible. This is done by pitch rotation of the wing. At this time, the tether is reeled in back on the drum, which is defined as the reel-in phase of the pumping cycle. This is shown at the bottom of Fig. 2-2a. The reel-in phase of the pumping cycles consumes energy, however the energy generated during the reel-out phase is larger than the energy consumed during the reel-in phase, resulting in a net output over the complete cycle. Sufficient storage capacity is used to equalize energy over the cycle (Wachter, 2010).

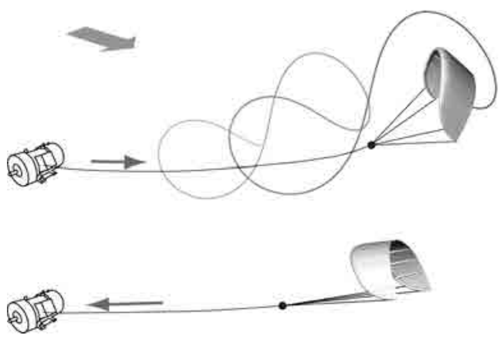

**(a)** Pumping kite power system cycle (Schmehl & Fechner, 2012)

**(b)** Figure-of-eight during test demonstration (Wachter, 2010)

**Figure 2-2:** Concept of the pumping kite power system of DUT

In Fig. 2-3 the instant mechanical output as a function of time is shown of five pumping cycles during an actual test operation of the kite power system. The positive mechanical power output is generated during the reel-out phase of the cycle. The mechanical output increases during each of the reel-out phases. This could be caused due to the higher wind velocity at higher altitudes and smoother and bigger Figure-of-eight patterns that are flown at increasing tether length. The reel-in phase is shown in Fig. 2-3 by the negative mechanical power output during the cycle and it represents the energy consumed during the reel-in phase. The reel-out phases take more time compared to the reel-in phases and the mechanical energy output is larger during the reel-out phases. So there is a positive mechanical energy output by the kite power system.

The former airfield at Valkenburg is used as a test location of the kite power system of DUT (Schmehl, 2011b). The maximum operating altitude of the current system during testing is approximately 500 m. Testing at higher altitudes is not possible at Valkenburg. This is due to regulations and since Valkenburg airfield is located near Schiphol. As a comparison the largest wind turbine has a tip height of 198 m, a rotor diameter of 126 m, and with 7 MW is

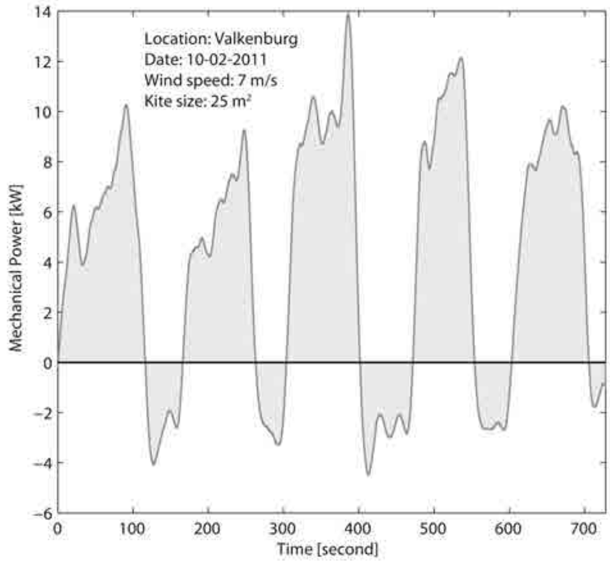


**Figure 2-3:** Instant mechanical power output during five pumping cycles during actual test operation of the kite power system (Schmehl, 2011a)

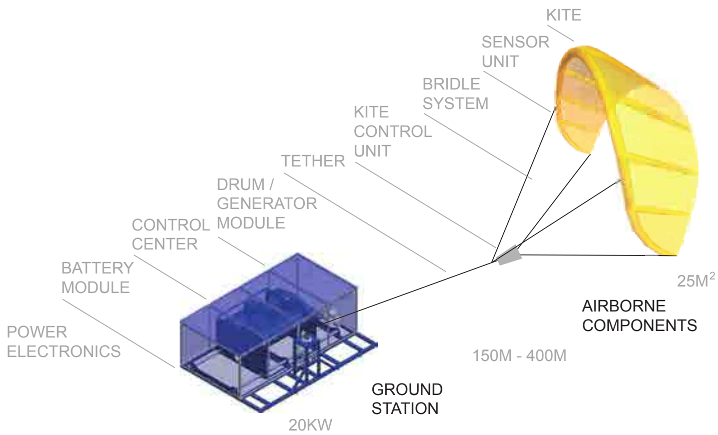


**Figure 2-4:** Kite power system components (Schmehl & Fechner, 2012)

the world's largest-capacity wind turbine since its introduction in 2007 (Thomas, 2008). The nominal average cycle power of the kite power system is 6.5 kW (Schmehl, 2012). In order to be competitive with conventional wind turbines and a lot of research has to be performed.

The components for the kite power system demonstrator of the DUT kite power group are shown in Fig. 2-4. With this system, the mechanical energy is generated of Fig. 2-3. Here the complexity of the system is shown.

In Fig. 2-5a a complete cycle without crosswind is shown to present the principle of the pumping power cycle. These are given in steady state flight where all the forces are acting on one point. The forces are in equilibrium so no accelerations or moments are introduced. Fig. 2-5b represents the orientation of the kite profile during reel-out here the velocity and force equilibrium is shown without cross-wind. The increase in angle of attack ensures the increase lift and thus traction force, this results ina high mechanical energy output. In Fig. 2-5c, the velocity and force balance is shown for the reel-in flight phase. Here the aerodynamic force is smaller compared to the reel-out phase, this is due to the lower angle of attack. The lower the aerodynamic force is, the lower the energy needed for reel-in of the kite. The $F_{aero}$ = $-F_{tether}$ holds only with the assumption that the kite is massless.

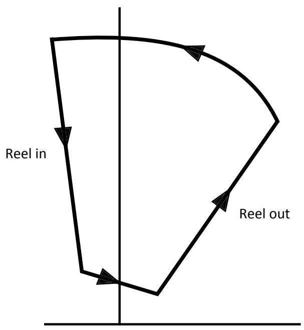


**(a)** Velocity profile of reel-in, reel-out and transition phases

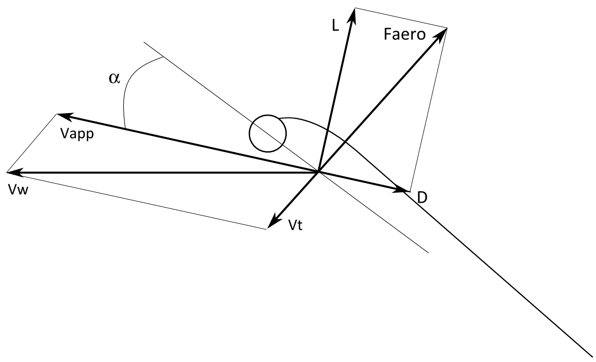


**(b)** Velocity and force diagram during reel-out phase diagram

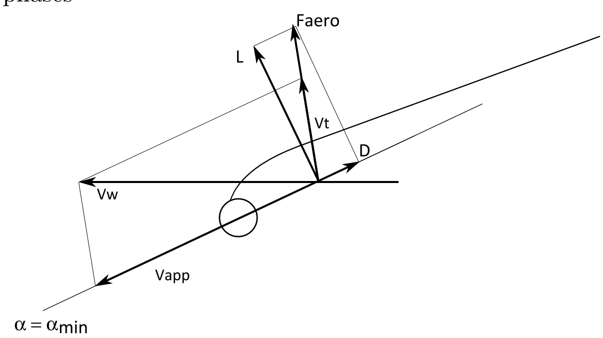


**(c)** Velocity and force diagram during reel-in phase diagram

**Figure 2-5:** Concept of the pumping kite power system of DUT

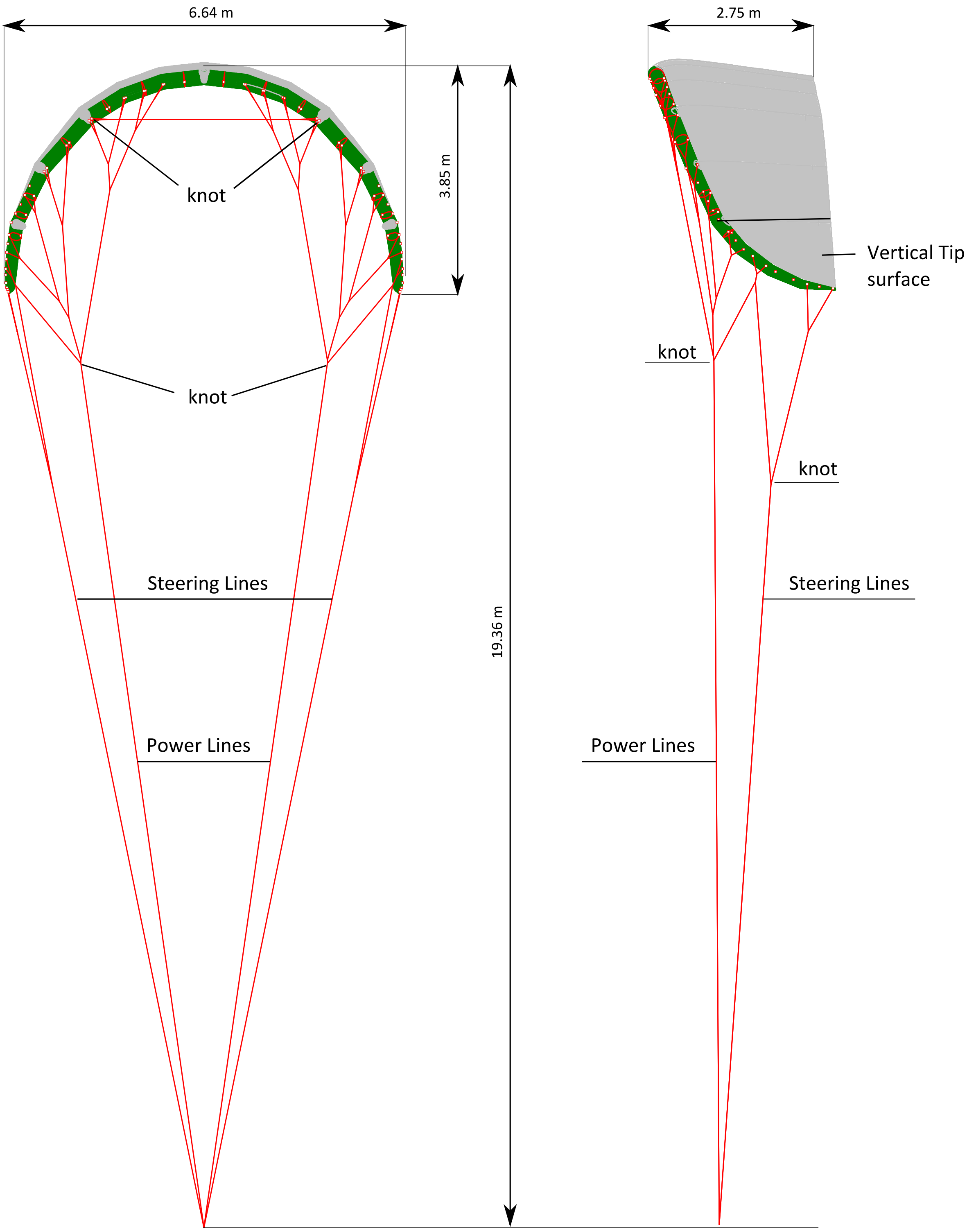


**Figure 2-6:** CAD representation V2 Mutiny kite in CAD software Rhino

The actual kite controls the pitch by elongating (for reel-in phase) and shortening (for reel-out phase) the steering lines such that the force on the steering lines is low for the reel-in phase and high for the reel-out phase. In Fig. 2-6, a CAD representation of the V2 Mutiny kite is shown including the bridle.

The forces in the V2 Mutiny kite are given in Fig. 2-5b for reel-out phase and Fig. 2-5c for the reel-in phase. Because the force and velocity of the kite during reel-out phase are higher compared to the reel-in phase, the mechanical energy is also higher.

In Fig. 2-7a and Fig. 2-7b a side view of the Mutiny kite is given. In Fig. 2-6, front and side views are displayed. In Fig. 2-7b a Free Body Diagram (FBD) of a kite is shown in the reel-out phase of the pumping cycle also with the actual Computer-Aided Design (CAD) representation of the V2 Mutiny kite. The resultant force (tether force) acting on the kite are the aerodynamic loads lift force, drag force and an aerodynamic moment and the loads acting on the steering- and power lines. In the reel-in phase, the forces in the steering lines are approximately zero. The angle of attack ($\alpha$) changes and the tether force reduces. In Figure 2-7a the FBD of the kite in reel-in phase is shown. To enable the reel-in phase of the pumping cycle, the steering force should be as small as possible. This is done in the real kite by elongating the steering lines. By this elongation, the angle of attack is decreased and reduced to approximately zero and is called "flagging". This way the forces acting on the kite are small to enable the kite to be reeled in with a small force.

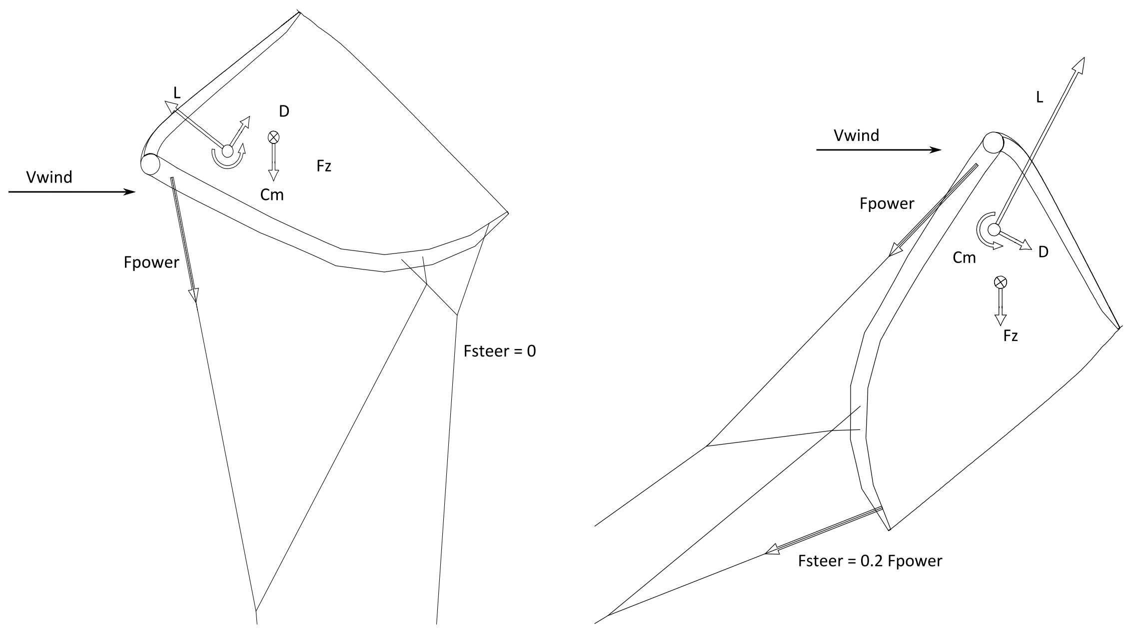


**(a)** Reel-in phase **(b)** Reel-out phase

**Figure 2-7:** FBD (free body diagram) of the kite in both phases of a pumping cycle

## 2-3 Kite analysis for energy generation

In Section 2-2 the project of the DUT is explained. In this project of the DUT the kite is an important component of the complete project. The structural dynamics of the leading edge inflatable kite is the topic of this thesis. First, an overview is given of the energy conversion from the kinematic energy of the flow to the mechanical energy of the kite on the tether. Next functional requirements of the LEI kite are graphically displayed.

There has been a lot of interest in the past for inflatable structures especially in the space research. But also in other fields, the inflated structure is applied. In civil engineering there are tents that are a distinct form of inflatable structure (Veldman, 2005).

Curtain airbags exist for a long time in the automotive industry. An example of a curtain airbag is shown in figure 2-8a. This structure is similar to the inflatable structure of a LEI kite and a possibility for research.

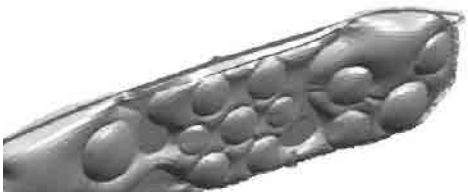

**(a)** Example of a curtain airbag (TRW, 2003)

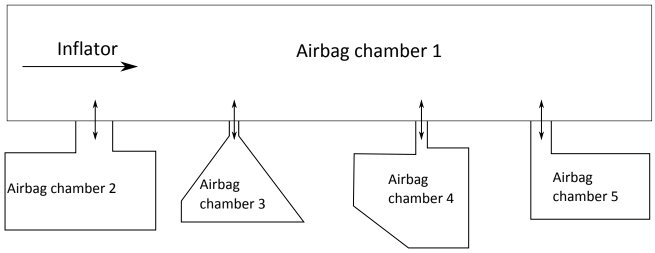


**(b)** Schematic representation (TASS, 2010d)

**Figure 2-8:** Example and schematic representation of a curtain airbag

The kite group of the DUT uses LEI kites to convert the kinetic energy of the air flow into mechanical energy. In Figure 2-9 the energy conversion process is displayed. In this figure, the steps are shown from the kinematic energy in the flow until the electrical energy through rotating motion of the drum where the tether is rolled on.

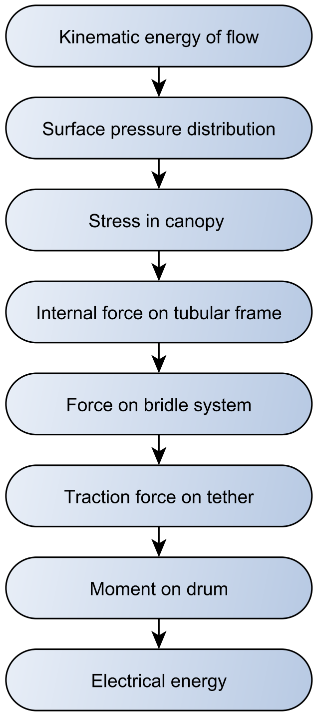


**Figure 2-9:** Energy conversion process

The objective for the pumping kite power system to generate maximum energy output. The kite is the object that converts the kinetic energy of the flow into the traction force in the tether. There are other requirements that are important for the kite power system. In Fig. 2-10, a mind map is displayed of the energy generation with pumping kite cycles. This chart is defined only by the kite, bridle and kite control unit for maneuvering. The functional requirements are concluded in the "branches" of the chart. One branche is taken and shown as an example. For a high traction force the functional requirements are:

- High $C_L$ at design $\alpha$.
- Large projected area
- High L/D

The chart in Figure 2-10 will be used to discuss some of the design choices that are made for the existing V2 Mutiny kite that is used in the kite power project of the DUT. This will be explained in the next section.

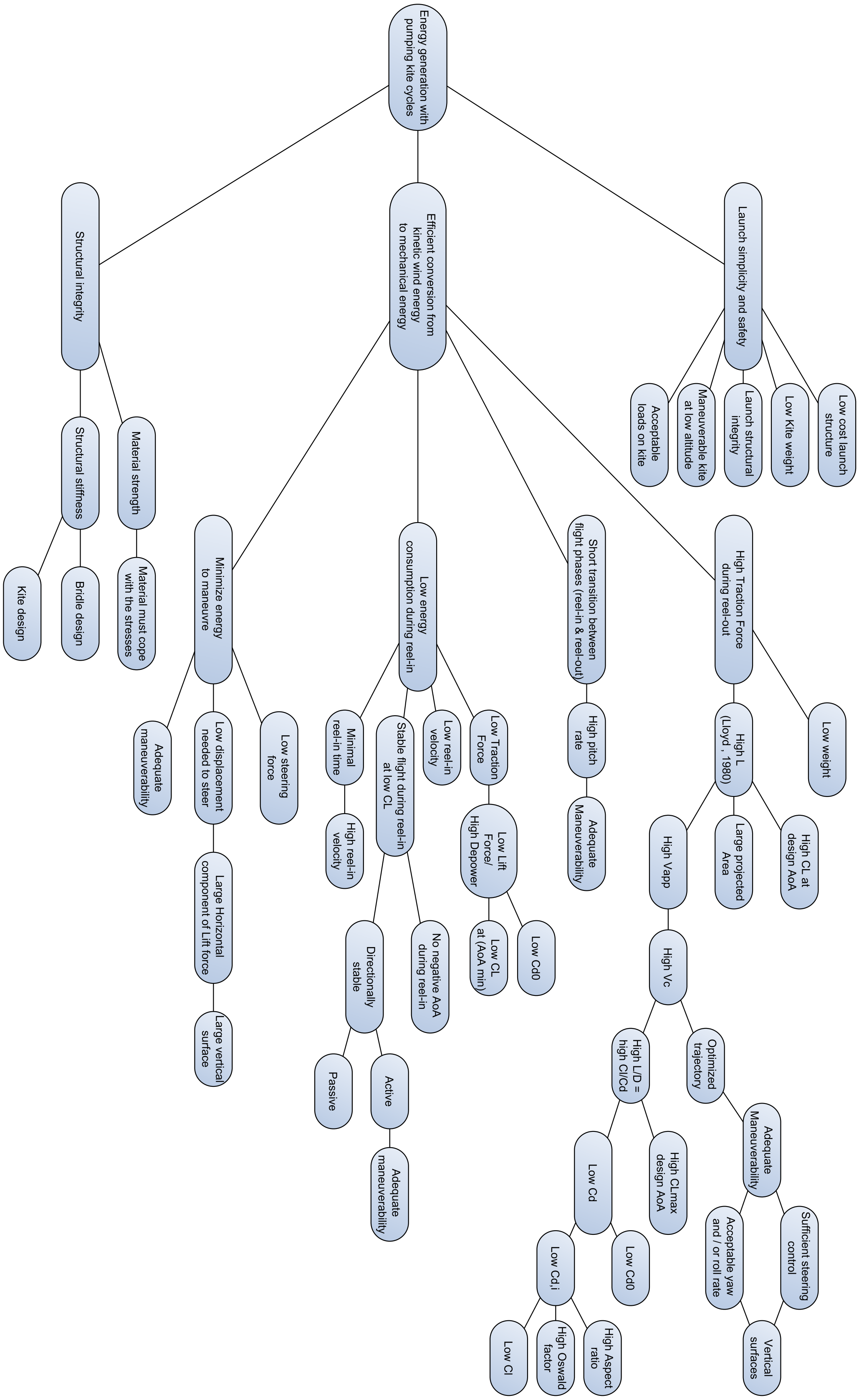


**Figure 2-10:** Kite Diagram

## 2-4 Kite in DUT kite power project: V2 Mutiny Kite

In this section the design of the V2 Mutiny kite will be explained. First a graphical CAD representation will be given. The functional requirements from the previous section are used for the analysis of the LEI V2 Mutiny kite. This is done from the design to the functional requirements. At the end of this section, a weight breakdown of the kite including the bridle is given.

The 25 $m^2$ V2 Mutiny Kite is an inflatable tube kite and is in fact a large version of a C-shaped LEI surf kite. The complete kite includes the canopy, the tubular inflatable structure (Leading Edge (LE) connected with seven struts) and a bridle system, see Fig. 2-11. The designer of the V2 Mutiny kite is Henry Rebbeck (Wachter, 2010) and the V2 is the second kite after an iteration of the V1 Mutiny kite. In Figure 2-6 the front and the side views of the CAD representation of the LEI V2 Mutiny kite including dimensions are displayed.


**Figure 2-11:** V2 Mutiny kite

With the design of the kite and the mind map in Fig. 2-10 the design choices of the V2 Mutiny kite will be explained.

The inflatable tubular structure is chosen for its structural stiffness. The stiffness of the kite is increased by adding a large and complex bridle system. The bridle system is added to support the inflatable leading edge of the kite. The shape of the kite is a C-shape kite with large vertical tip surfaces. These large vertical surfaces, see Fig. 2-6, have a number of positive and negative consequences these are:

- Difficult to change the $\alpha$ of the kite. This leads to difficult to De-power the kite during the reel-in phase.

- Limited projected surface. The surface of the kite is 25 $m^2$, while the projected surface is 17 $m^2$.
- Large drag due to the vertical surfaces that do not contribute to the traction force.
- Stable kite, because the horizontal lift force on the vertical surfaces of the kite helps to remain the shape of the kite.
- Highly manoeuvrable. The kite reacts very fast to steering inputs given.

In order to De-Power this C-shaped kite, pulleys were added to the bridle system. This was necessary because of the force equilibrium in the bridle (Heuvel, 2011).

In Fig. 2-12 and Fig. 2-13, the difference between the change in $\alpha$ of a flat plate and a C-shaped kite is denoted. Here the a and b are lengths of the line from the leading edge to the knot during the reel-out phase. The $\alpha$ of flat plate and the C-shaped kite are changed to the $\alpha$ during reel-in phase. The line lengths are changed from a and b to a' to b'. For the flat plate, a and b are equal to a' and b'. This is not the case for the C-shaped kite.

In order to change the $\alpha$ of the C-shaped kite, the line lengths a and b must be changed into a' and b'. This is done in the design of the V2 Mutiny kite with pulley addition in the bridle. The addition of pulleys in the bridle adds more complexity to the bridle design.

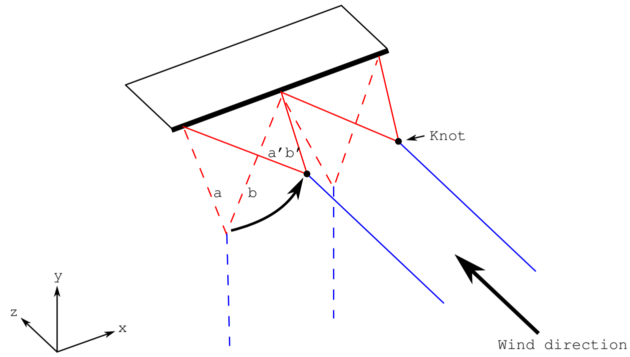


**Figure 2-12:** Rotation of the bridle of a flat plate (Heuvel, 2011)

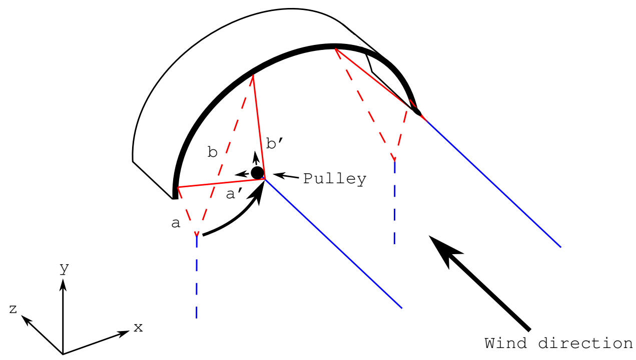


**Figure 2-13:** Rotation of the bridle of a C-shaped kite with pulleys (Heuvel, 2011)

The inflatable structure with the leading edge and the struts are made of an internal bladder to make the structure air tight to ensure the internal pressure inside of the structure see Fig. 2-14. The material of the bladder is TPU (thermoplastic polyurethane) and the material of the outer layer is Dacron. The Dacron layer is the layer that must carry and redirect the loads from the aerodynamics forces to the bridle system.

The function of the canopy is to redirect the aerodynamic forces to the inflatable structure. The material that is used for the canopy is Ripstop nylon. This is a customary material used

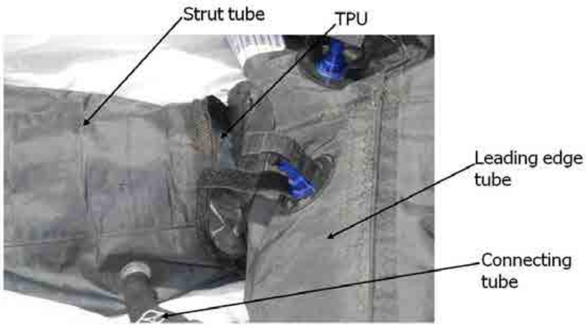


**Figure 2-14:** Internal bladder and Dacron section

in kites that are used for kite surfing.
The bridle system consists of bridle lines, knots and pulleys. The main function of the lines is to convert the forces from the LE to the main cable. Knots are two lines bound together. There are six knots in the complete bridle system, three each side. The function of each knot is different, the knot at the bottom is to connect the power lines to the steering lines. The function of this knot is to lower the steering force. The knot at the top connects two Bridle Points (BPs) to a horizontal line. The function of this line is to increase the load. The function of the pulleys in the bridle is to change the angle of attack ($\alpha$) of the kite from reel-out setting to reel-in phase. The bridle is attached only to the LE and for the complete bridle system where knots, BPs (bridle points) and pulleys are highlighted, see Figure 2-15.

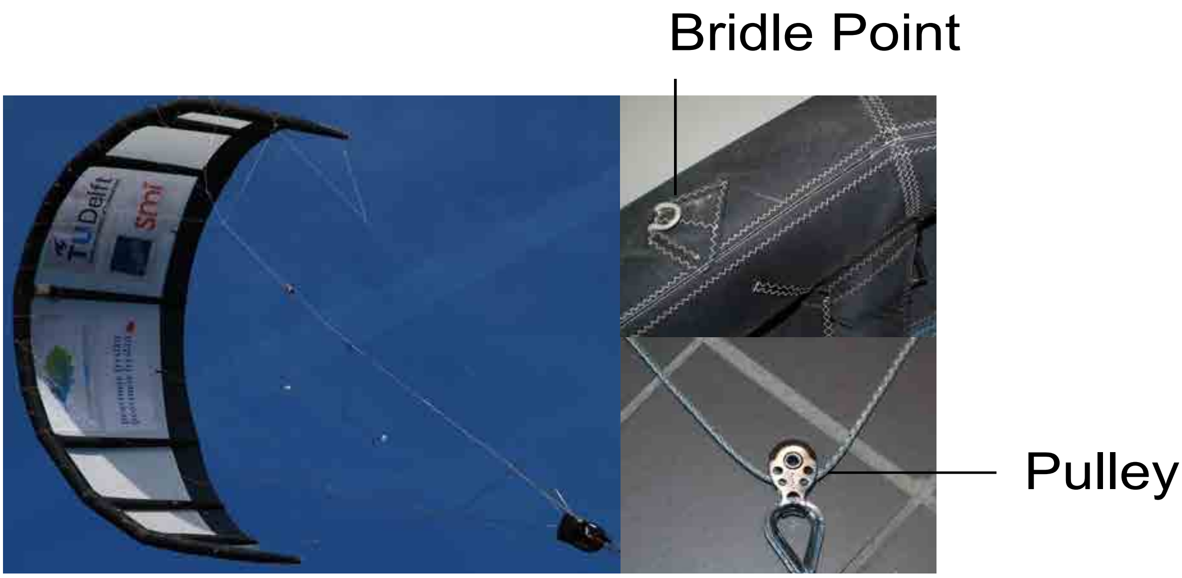


**Figure 2-15:** Bridle system, pulleys knots and bridle point

All over the kite, there are extra reinforcements that are needed to cope with stress concentrations in all flight phases. The mass of the kite is 11.49 kg including the bridle system and excluding the kite control unit (KCU), see table 2-1.

In the column "Mass Estimate", the mass of each component of the kite is calculated by multiplying the area of each component times the specific material weight in $kg/m^2$. The areas are taken from the CAD model made in Cad program Rhinoceros (Rhino) The specific material weight for Dacron is 0.13 kg/m$^2$, for TPU (thermoplastic polyurethanes) is 0.17 kg/m$^2$, for spinnaker the specific weight is 0.05 kg/m$^2$ and for the sponsor logos, the specific weight is 0.08 kg/m$^2$ (Verheul, 2010). These values in the column "Mass Estimate" are not measured, but calculated with the specific material weights multiplied by the different areas. The complete kite including bridle is the only measured data.

However, many small reinforcements have been placed on the kite, and this is included in the column: "$TotalMass$". The contributions of the small reinforcements are estimated, based on the quantity of the reinforcements (Verheul, 2010).

**Table 2-1:** Mass breakdown of the kite, including the bridle excluding the KCU (kite control unit) (Verheul, 2010)

| Component | Area | Mass Estimate | Mass<br>Total Mass | % Mass | Measured |
|---|---|---|---|---|---|
| unit | m$^2$ | kg | kg | - | kg |
| Canopy weight (rip-stop) | 25.00 | 1.25 | 1.38 | 11.97 | |
| Sponsor Logos | 5.30 | 0.42 | 0.42 | 3.69 | |
| LE Dacron | 8.70 | 1.48 | 2.07 | 18.03 | |
| Struts Dacron | 6.10 | 1.04 | 1.45 | 12.64 | |
| LE bladder | 8.70 | 1.13 | 1.47 | 12.80 | |
| Struts bladder | 6.10 | 0.79 | 1.03 | 8.97 | |
| Dacron reinforcements | 4.20 | 0.71 | 0.71 | 6.22 | |
| Bridle | NA | 2.00 | 2.00 | 17.41 | |
| Other | NA | 0.95 | 0.95 | 8.27 | |
| Total Mass | NA | 9.78 | 11.49 | 100 | 11.49 |

# Chapter 3

# Inflatable tubular structures

In Chapter 2, kite power has been elaborated. The kite that is going to be discussed in this thesis consists of a inflatable tubular structure. In Section 3-1, the different kite models of the DUT are discussed. Inflatable beams are an important part of the inflatable tubular structure of the kite, so in section 3-2 the basics of inflatable beams are explained. In Section 3-3, a multi-body approach by (Breukels, 2011) to model inflatable beam is described. Lastly some of the FEM inflatable beam applications are discussed.

## 3-1 Kite models

In this section the kite models are explained. There are a lot of different models present that model the behavior of the kite. In this Section an overview is given with the existing models and the models that are needed for analyzing, modeling and validation of the models.

The scientific research of structural deformations on inflatable structures is a challenging and an engineering opportunity. The research and kite design nowadays is based mostly on experience and trial and error. Since the LEI tube kites are used to generate power and increase in size, there is a need for a scientific approach to investigate the kite power system. There are multiple models for modeling the behavior of kites. These models show different levels of complexity starting from point mass to fluid structure interaction (FSI) using FEM and Computational Fluid Dynamics (CFD). See Fig. 3-1 where the complexity is plotted against the calculation time. With increasing complexity of the model the more computation time is required.

The point mass model Fig. 3-1 is the most simple kite model. The forces and apparent velocity component act in one point. The kite is controlled by artificially changing the direction of the lift and drag forces. This model is suitable for preliminary flight analysis of the kite and rough trajectory determination.

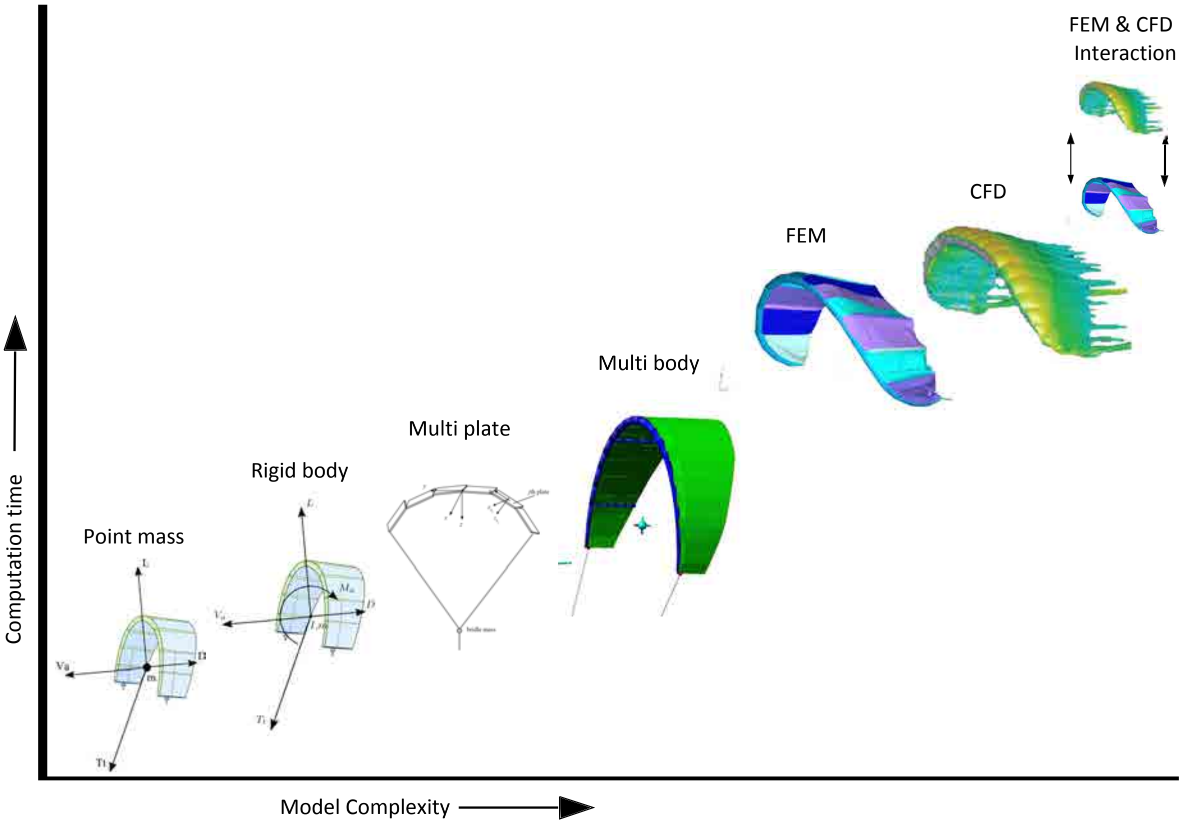


**Figure 3-1:** System level representing the complexity of different kite models

The rigid body model of the kite is described by 6 degrees of freedom. These are three translational and three rotational degrees of freedom and inertia is included. The flight dynamics of this model treats the kite as an aircraft.

There is no flexibility embedded in both the point mass model and the rigid body model. However the actual kite models deforms due to aerodynamic- or control forces. To get a realistic behavior of the kite, flexibility should be incorporated in the models.

The multi-plate model includes flexibility by hinging plates at the leading edge. In the plate models the natural control of kite can be implemented directly. The flexibility is not incorporated in the plates, but in the hinge between the plates. This model rough

In the multi-body model by (Breukels, 2011), the kite is discretized in approximately 400 parts. The inflatable structure of the kite is modeled by discretizing the beams into smaller rigid elements. In between spherical joints are modeled on which three dimensional torque vectors act. These torque vectors act as springs and give the beam the bending stiffness. Linear springs are used to model the canopy and tether. An aerodynamic model is created that distribute the aerodynamic forces on the canopy.

The multi-body model is created to give the general shape of the kite in a flight condition. The disadvantage of this model is that the model is based on artificial and no physical inputs.

In this thesis not only the general behavior, but also local behavior, such as wrinkling and stresses of inflatable structures are investigated. A different approach is required with a higher level of complexity.

## 3-2 Inflatable beam theory

In the previous section, multiple inflatable structures are given as an example. Scientifically, the structures were not scientifically analyzed. This Section will discuss the structural dynamics of the cylindrical inflatable beam. The cylindrical inflatable beam has been analyzed analytically, with multi-body dynamics and with FEM. The basic principles of the inflatable beam will be explained, based on membrane analogy based on (Stein & Hedgepeth, 1961), (Wielgosz & Thomas, 2002), (Thomas & Wielgosz, 2004), (Le & Wielgosz, 2005), (Veldman, 2006).

The focus in this section will be on modeling an inflatable clamped cantilever beam in bending load condition. The external loads on the beam are considered a tip force and an internal pressure. These external forces must be equal to the internal material stresses see Eq. 3-2 and Eq. 3-3.

The inflatable beam has three different conditions for the beam at different tip forces (Veldman, 2005):

1. Taut
2. Slack/collapse
3. Wrinkled

Different theories define the three conditions of the inflatable beam. These theories are based on a stress criterion, a strain criterion or combined (Veldman, 2005). In this Section, the stress criterion from (Stein & Hedgepeth, 1961) and (Comer & Levi, 1963) is used. The conditions are explained by (Veldman, 2005) as:

$$\begin{aligned} Taut \rightarrow \ & \sigma_2 \ > \ 0 \\ Slack/Collapse \rightarrow \ & \sigma_1 \ \leq \ 0 \\ Wrinkled \rightarrow \ & \sigma_1 \ > \ 0 \ \& \ \sigma_2 \leq 0 \end{aligned} \tag{3-1}$$

Where $\sigma_1$ is the maximum stress condition in principle direction. $\sigma_2$ is the minimum stress condition in principle direction (Veldman, 2005). The principal stress directions is a condition where the only stresses acting in a plane are normal stresses and no shear stresses (Hibbeler, 1997).

### 3-2-1 Inflatable beam theory: taut condition

This Sub-section provides expressions of equilibrium of forces and moments in the taut region and in the wrinkled region. The theory presented here is described by (Comer & Levi, 1963) and (Veldman, 2005). The latter based the theory by (Stein & Hedgepeth, 1961).

A thin walled cylindrical inflatable beam with a tip force and an internal pressure is analysed. The beam is shown in Fig. 3-2. The beam is considered thin walled if $r > 5t$ holds.

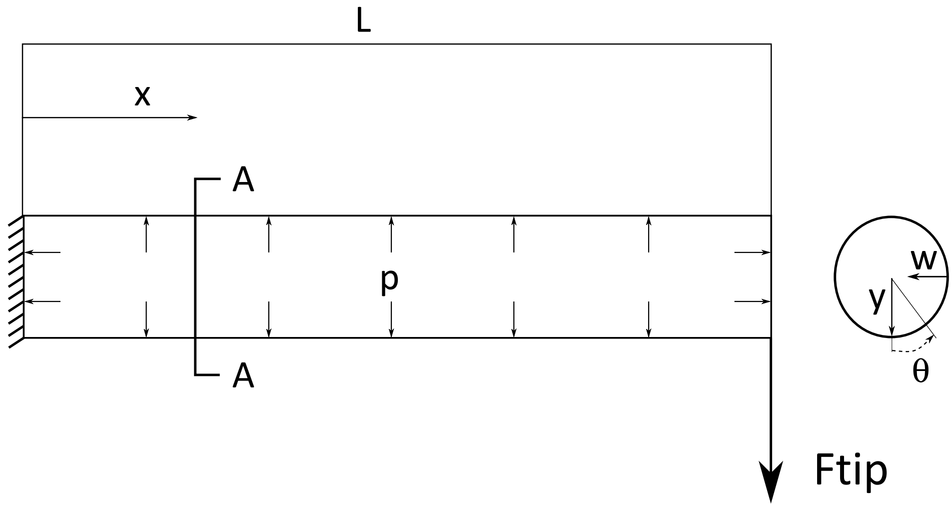


**Figure 3-2:** Clamped end cylindrical inflatable beam including sign conventions

The internal pressure and the tip force introduce internal stresses in the material. In Fig. 3-3 these stresses are shown in cross section A-A. The stresses are displayed qualitatively. The tip force creates a shear force, that results in a shear stress ($\tau$). Next to the shear stress, the tip force creates a moment. This moment creates a normal stress ($\sigma_{xForce}$).

The pressure introduce only normal stresses.

$$p\pi r^2 = t\int_0^{2\pi} \sigma_x r d\theta \tag{3-2}$$

$$M = -r^2 t\int_0^{2\pi} \sigma_x \cos\theta d\theta \tag{3-3}$$

In the taut condition, the stress distribution due to pressurization and a transverse tip load Ftip will be described by:

$$\sigma_x = \frac{pr}{2t} - \frac{F_{tip}\,(L-x)}{\pi r^2 t}\cos\theta \tag{3-4}$$

$$\sigma_\theta = \frac{pr}{t} \tag{3-5}$$

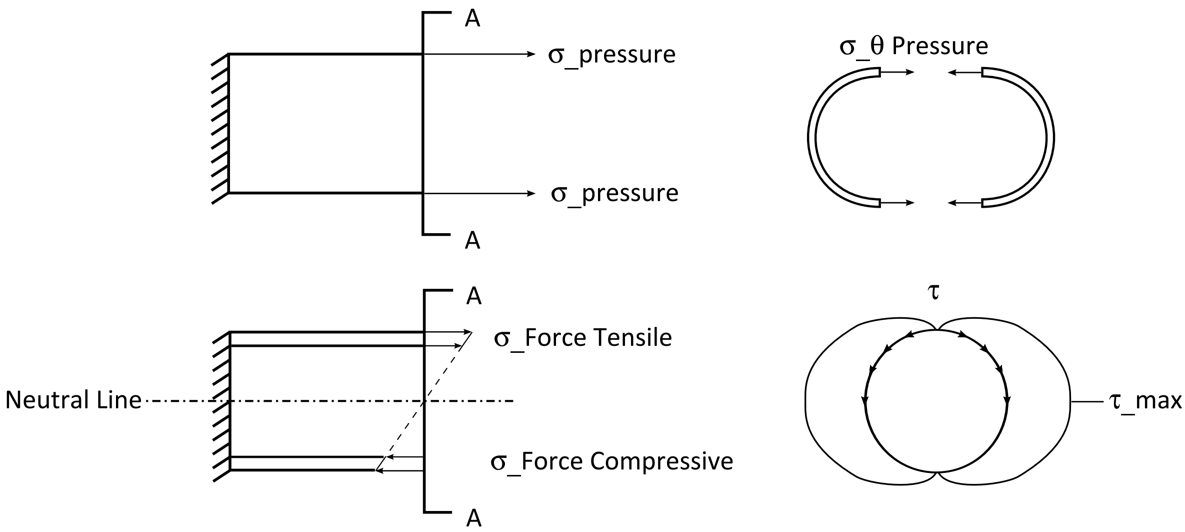


**Figure 3-3:** Stresses in the beam due to a tip force and an internal pressure

$$\tau_{x\theta} = \frac{F_{tip} \sin\theta}{\pi r t} \tag{3-6}$$

The stress strain relations are:

$$\epsilon_x = \frac{\sigma_x}{E_x} - \frac{\nu_{x\theta}\ \sigma_\theta}{E_x} \tag{3-7}$$

$$\epsilon_\theta = \frac{\sigma_\theta}{E_\theta} - \frac{\nu_{\theta x}\sigma_x}{E_\theta} \tag{3-8}$$

$$\gamma_{x\theta} = \frac{\tau_{x\theta}}{G_{x\theta}} \tag{3-9}$$

In this case the Poissons ratios are defined according to Maxwells law.

### 3-2-2 Inflatable beam theory: wrinkled condition

In this section, the wrinkled condition of the beam loaded by tip force is discussed. The stress criterion by (Stein & Hedgepeth, 1961), (Comer & Levi, 1963) and (Veldman, 2005) is considered.

The stress criterion describes that when the resultant minimal stress $\sigma_2 = 0$ at $\theta = 0$, wrinkles occur. This means that when the $\sigma_x$ due to the moment is equal to the $\sigma_x$ due to the pressure at $\theta = 0$. The wrinkling angle is shown in the beam see Fig. 3-4. Both (Comer & Levi, 1963) as well as (Veldman, 2005) wrinkling angle as: $\theta_0$ respectively $\theta_w$. When the force and thus the moment is increased, the wrinkling angle increases. Figure 3-4 shows the slack region, which is fully wrinkled. The stress $(\sigma_x) = 0$.

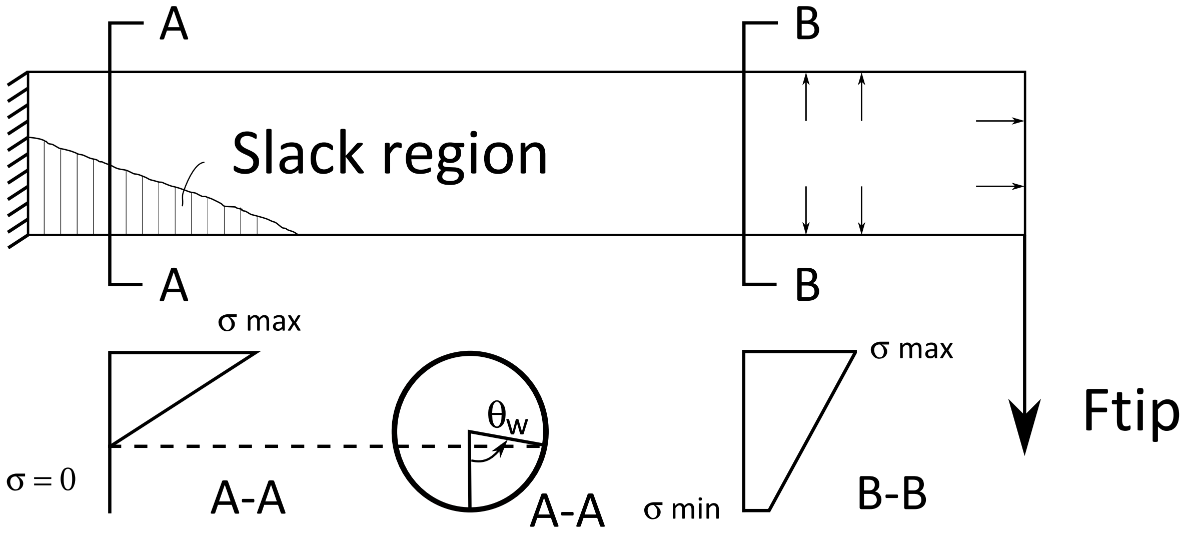


**Figure 3-4:** Clamped end cylindrical inflatable beam

In (Stein & Hedgepeth, 1961) the Poisson ratio is replaced by a parameter $\lambda_{x\theta}$ in the wrinkled case so that the stress $\sigma_x$ would remain zero. This is for the case that the material is assumed to be a true membrane. The true membrane can only resist in plane loading and no bending. This theory is elaborated and adjusted by (Veldman, 2005).

In this wrinkled region the behavior of the deflection of the beam behaves non linear (Stein & Hedgepeth, 1961), (Comer & Levi, 1963) and (Veldman, 2005).

### 3-2-3 Inflatable beam theory: collapse condition

The objective of this section is to give an overview of the different collapse moments. In Table 3-1 an overview is given from (Veldman, 2005) showing the different theories and collapse moments.

*"The bending moment at which collapse takes place is regarded as the moment at which an increase in deflection does not result in an increase in moment"* (Veldman, 2005). All three regions taut, wrinkled and collapse are graphically shown in Fig. reffig:TautwrinkleCollapse. Here the taut (unwrinkled) region is assumed to be linear. The wrinkled region is non linear and finally the collapse is shown.

Basically there are three different basic theory schemes investigating collapse of pressurized beams or structures. The first theory is to consider the beam as a shell structure ((Brazier, 1927), (Flugge, 1932), (Axelrad & Emmerling, 1987), (Seide et al., 1965), (Baruch & Zhang, 1992), (Jamal, 1998), (Veldman, 2005). The second theory is to consider the beam as a membrane structure: ((Stein & Hedgepeth, 1961), (Pappa et al., 2001), (Tsunoda & Senbokuya, 2002), (Wielgosz & Thomas, 2002), (Kroeplin & Wagner, 2004), (Le & Wielgosz, 2005), (Thomas & Wielgosz, 2004), (Wielgosz et al., 2008), (Jetteur & Bruyneel, 2008), (Lampani & Gaudenzi, 2010) etc.). A third option that is investigated is a combination of a shell and membrane structure: ((Veldman, 2005), (Veldman et al., 2005)).

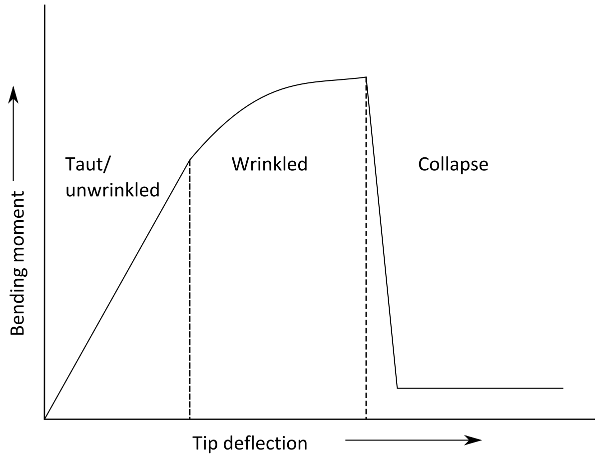


**Figure 3-5:** Taut, wrinkled and collapse regions of an inflatable beam (Breukels, 2011)

For the shell theories, two types of collapses have been identified. The first theory is the theory of (Brazier, 1927) in which it is stated that the collapse of an infinite long beam is due to the ovalisation of the beam subjected to a bending load. On the other hand there is (Flugge, 1932) who states that the collapse of short beams is due to axial wrinkling on the compression side of the inflatable beam also known as shortwave buckling or bifurcation instability.

In figure 3-6, an overview is given of collapse moments for shell theories. In this figure, four different beams are defined: a very short cylinder is with $0 \leq L/R \leq 1$ a short beam: $1 \leq L/R \leq 5$, a moderate long beam is given by $5 \leq L/R \leq 20$ and finally, a long beam is assumed $L/R > 20$ (infinite long beam). The beams of the kite, leading edge and struts fall in the category moderate long beam.

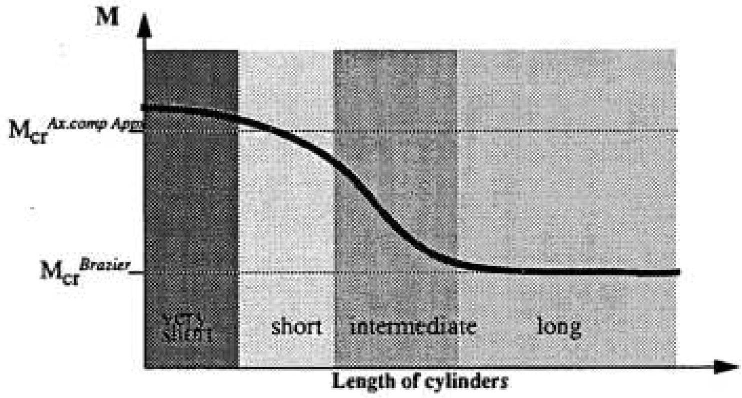


**Figure 3-6:** Different collapse load theories as a function of beam length (Jamal 1998)

## 3-3 Multi body modeling of an inflatable beam

For the behavior of the inflatable tubes of the kite, (Breukels, 2011) performed experiments regarding bending and torsion of inflatable beams. (Breukels, 2011) model of an inflatable beam is modeled in multi-body (Multi Body (MB)) environment MSC Adams. This multi-body model divided the inflatable beam into several rigid sections. Between these rigid sections spherical joints have been placed, these joints allow rotations around all three axes. To model the stiffness of the inflatable beam, there are 3D torque vectors (2 bending- and 1 torsion vector) acting on the joints that represent the stiffness of the inflatable beam. These stiffness vectors are functions that need to be derived for the inflatable beams. In the taut region, the deflection is assumed linear (linear spring stiffness), in the wrinkled region, the spring stiffness decreases with increasing force and at collapse the spring stiffness is assumed zero. The analogy is according to membrane theory proposed by (Stein & Hedgepeth, 1961).
Breukels performed experiments with different inflatable beams (see Chapter 7) for the stiffness- coefficients, functions and collapse. To find these functions, the experiment data ($F_{tip}$ versus deflection) was fitted to create a function that represented the spring stiffness (Breukels, 2011). The function of the spring stiffness was used as the input for the inflatable beams and could be used for different pressures, beam radii and tip deflections. For the collapse region, a different function was found. This was done by replacing the deflection by the collapse deflection ($v_{collapse}$) as a function of $r$ and $p$. These algorithms have been implemented in MSC ADAMS and verified with glass fiber braided inflatable beam and a polyester fiber cloth beam.

This approach is limited for the use of the beam length and material. If a new material or beam length is used, the behavior of the inflatable beam could be different. To deduce the functions for the spring stiffness of the beam, new experiments should be performed. To introduce another approach to investigate the behavior of inflatable beams, the FEM is chosen.

## 3-4 Finite Element analysis of an inflatable beam

In this section, FEM analysis have been performed in order to study the behavior of inflatable beams. The FEM is a method where the material properties, geometrical properties and external loads are implemented in a FEM solver and the behavior of the beam is investigated. This method should predict the behavior of an inflatable beam using different materials, different geometries and different external loads. The analysis should be used not be limited by the taut region, but should also be valid to predict the wrinkling and collapse behavior of the inflatable beam.

- (Veldman, 2005) performed an FEM static analysis of cylindrical beams in FEM Abaqus. Here a new theory was proposed to model the behavior of an inflatable beam, this theory was validated with both experiments and FEM models.

- (Lampani & Gaudenzi, 2010) compared the FEM explicit (central difference time integration) versus implicit time integration scheme for different cases. The conclusions of (Lampani & Gaudenzi, 2010) are that for different problems, specific elements and specific time integration schemes should be used. The quantitative results of the numerical simulation showed a serious deviation from the physical solution. However some qualitative aspects could be used for preliminary design (Lampani & Gaudenzi, 2010). These qualitative results are for example based on the prediction of wrinkling patterns in a membrane.

- (Davids & Zhang, 2008) investigated a quadratic Timoshenko beam element nonlinear analysis of pressurized fabric beamcolumns. The study showed the importance of modeling fabric wrinkling of inflatable beams at different pressures and showed promising results for more complex inflatable structures.

- (Le & Wielgosz, 2005) proposed a theory for inplane bending and stretching of an inflatable beam loaded with a tip force. The solution of the theory was compared to FEM of both deflection of the beam as well as the wrinkling load. This was performed at different pressures and different beam diameters. The analytical solution holds only if the pressure is greater than the wrinkling pressure.

In the theory it was shown inflatable beams can be described with FEM.

## 3-5 Concluding remarks

In this chapter, first the existing kite models have been evaluated. The model with the highest complexity was the multi body model, which incorporates the flexibility of the kite and inflatable beam by fitted parameters of experimental data. The FEM is proposed as a different approach for modeling LEI inflatable kites.

**Table 3-1:** Overview cylindrical beam bending load theories (Veldman2005)

| | Element | | Pressure included | | Material properties | | | Beam Length | Collapse Moment |
|---|---|---|---|---|---|---|---|---|---|
| | Shell | Mem | No | Yes | Iso | Aniso | Not | | |
| Brazier(1927) | ■ | | ■ | | ■ | | | Long | $M_{Brazier} = \frac{2\sqrt{2}}{9}\frac{\pi E r t^2}{\sqrt{1-\nu^2}}$ |
| Wood(1958) | ■ | | | ■ | ■ | | | Long | $M_{Wood} = \frac{2\sqrt{2}}{9}\pi E r t^2 \sqrt{\frac{1}{1-\nu^2} + 4\frac{\rho}{E}\left(\frac{r}{t}\right)^3}$ |
| Baruch(1992) | ■ | | ■ | | | ■ | | Long | $M_{Baruch} = \frac{2\sqrt{2}}{9}\pi r t^2 \sqrt{\frac{E_x E_\theta}{1-\nu_{x\theta}\nu_{\theta x}}}$ |
| Veldman(2005a) | ■ | | | ■ | | ■ | | Long | $M_{cr} = \frac{2}{9}\sqrt{2}\pi E_x r t^2 \sqrt{\frac{E_\theta}{E_x}}\sqrt{\frac{1}{1-\nu_{x\theta}\nu_{\theta x}} + 4\frac{pr^3}{E_\theta t}}$ |
| Stein(1961) | | ■ | | ■ | | | ■ | | $M_{Stein} = \pi p r^3$ |
| Zender(1962) | ■ | ■ | | ■ | ■ | | | | $M_{Zender} = \pi p r^3 + \frac{\pi E r t^2}{2\sqrt{3\left(1-\nu^2\right)}}$ |
| Seide(1965) | ■ | | | ■ | | ■ | | | $M_{Seide} = 0.8\pi p r^3 + \pi E_x r t^2 \left(\frac{1-0.731\left(1-e^{-\phi}\right)}{\sqrt{3(1-\nu_{x\theta}\nu_{\theta x})}} + \Delta\gamma\right)$ |
| Wielgosz(2002) | | ■ | | ■ | | | ■ | | $M_{Wielgosz} = \frac{\pi}{4}\pi p r^3$ |
| Veldman(2005) | ■ | ■ | | ■ | | ■ | | L/D > 10 | $M_{cr} = \left(\frac{\pi}{2}\right)^2 p r^3 + \frac{1}{2\sqrt{3}}\pi E_x r t^2 \sqrt{\frac{E_\theta}{E_x}}\sqrt{\frac{1}{1-\nu_{x\theta}\nu_{\theta x}} + 4\frac{p}{E_{theta}}\left(\frac{r}{t}\right)^2}$ |

# Chapter 4

# Uniform Pressure method in Finite Element application with Madymo

As discussed in the previous chapter, the LEI leading edge inflatable kite will be modeled with finite element method (FEM). The FEM program that will be used is Madymo. The uniform pressure (UP) method will be used to model the internal pressure on the inflatable tubular structure. In this chapter the background of Madymo will be explained, because it is a relatively unknown FEM program and used primarily in the automotive industry. First a short introduction will be given of Madymo. In Section 4-1, the FEM application in Madymo will be elaborated. In the Section4-2, the uniform pressure theory will be explained. For the bridle system, belts (that are used to model seat belts) will be used in Madymo. Belts are modeled with multi-body (MB) theory. The belts are briefly addressed in Section 4-3.

> "*Madymo is a computer program that simulates the dynamic behavior of physical systems emphasizing the analysis of vehicle collisions and assessing injuries sustained by passengers.*" (TASS, 2010d)

The inflated multi-chamber airbag (for example curtain airbag) that can be modeled with Madymo and resembles a LEI kite without a tether. In Chapter 3 an example of a curtain airbag is shown. Here the multiple chambers can be seen. The curtain airbag is very similar to the LEI tubular structure of the kite.

Madymo is chosen to model the kite for four reasons:

1. The inflation process can be modeled with an inflator that actually inflates the kite with air. This resembles the physical inflation process used in real time. The method that is used in this thesis behind the modeling with an inflator is called the UP method. This assumes a uniform pressure distribution at the interior of the inflatable structure. Inside the inflatable tubular structure of the kite, it is assumed that there is little flow of air during normal flight. The pressure is assumed to act uniformly inside the struts and the leading edge.

2. Using an airbag chamber has the advantage of having a lot of sensors already built in.
3. Non linear modeling possible for solving the equations of motion, geometry and material.
4. Multibody parts (for example belt systems) and FEM parts can be linked to each other. This gives an opportunity to attach the belt segments as a bridle system to the inflatable LE at the BPs.

The theory that will be treated in this chapter is based on three items: uniform pressure method, finite element application within Madymo and belts. The theory as used in Madymo is explained and is used as background knowledge. The theory behind Madymo that is described here comes from the Madymo manual and from Filippa (2000b) for the corotational description. Unfortunately not all techniques and algorithms used by the program are publicly available.

## 4-1 Finite Element Method (FEM) in Madymo

The leading edge inflatable (LEI) kite will be modeled in Madymo with the FEM. In this section, the finite element method (FEM) is explained. In FEM, a geometry is discretized into elements. The elements are interconnected by the nodes. The FEM module of Madymo can solve problems fully non linear. In Madymo an explicit time is used to solve the equations of motion at each time step using information of the previous time step. In Fig. 4-1 the FEM concept is shown for a single time step.

In this section, the theory is limited to the use of triangular Constant strain triangle (CST) membrane elements (MEM3 elements in Madymo).

- The material Dacron that is used in the kite is assumed to behave as a membrane.
- The elements could be distorted during loading of the inflatable structure. CST membrane elements are can be distorted significantly (TASS, 2010d).
- The elements should be able to be refined for complex structures, triangulated mesh is better in refinement compared to quadrilateral elements.

The forces at the nodes are known, through the equations of motion. This way the accelerations can be calculated. The velocities and the displacements at the nodes are calculated with a explicit time integration scheme. The time integration scheme that is used is called the central difference method. This will be explained in detail in Section 4-1-1. A next step is to go from the nodal displacements to the element displacements. This done using the shape functions of the element. The element considered is the MEM3 element in Madymo. To calculate the strains and the stresses in the "MEM3.element" for a non linear problem, Madymo uses a corotational kinematic strain/displacement formulation. In this corotational formulation, rigid body modes and deformations are decoupled. The corotational formulation in combination with the Green-Lagrange strain measure, the strains are calculated. In

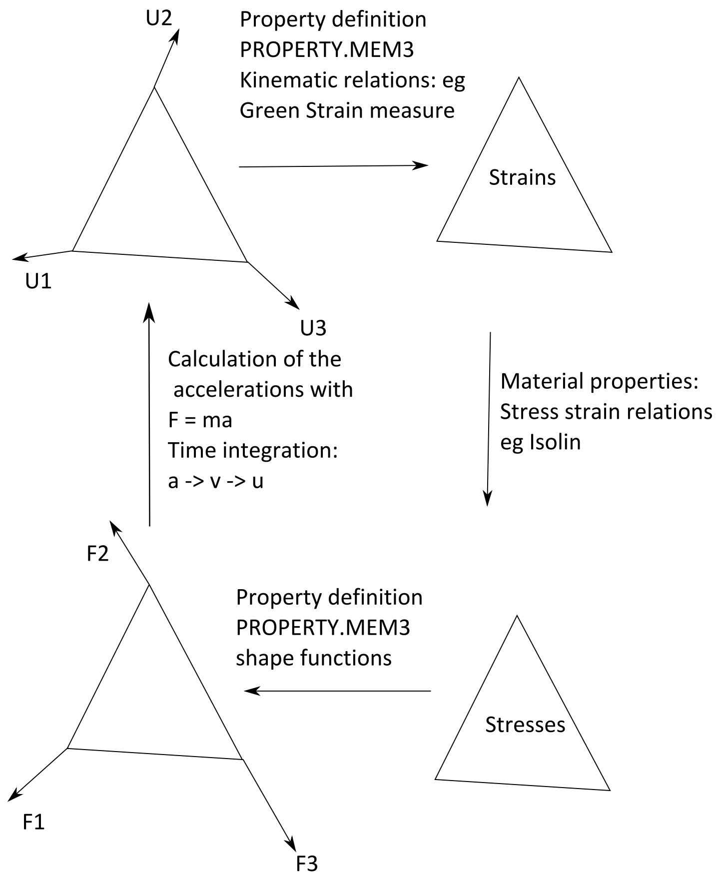


**Figure 4-1:** Finite Element concept in Madymo (TASS, 2010b)

Section 4-1-2 the element type and the kinematic formulation are described. With the material, or constitutive relations, the stresses are calculated from the strains. With the shape functions and the geometry of the element, the internal forces can be calculated again at a new time increment. The equations of motion are solved again with the new external- and internal forces in the new timestep to get the new nodal accelerations.

## 4-1-1 Equations of motion

In this section, the equations of motion are explained that describe the calculations from the forces to the nodal displacements, velocities and accelerations.

The finite element method is used to reduce a continuous structure to a discrete numerical model. The equations of motion of a finite element model can be written as Eq.( 4-1). The equations of motion are solved with the known nodal forces and the mass to get the nodal displacements.

$$\underline{\underline{M}}\ \underline{a} + \underline{\underline{D}}\ \underline{v} = \underline{F}_{ext} - \underline{F}_{int}(u, v) \tag{4-1}$$

Where $\underline{\underline{M}}$ and $\underline{\underline{D}}$ are the mass and damping matrices; $\underline{F}_{ext}$ is the vector of externally applied loads; $\underline{F}_{int}$ is the vector of internal nodal forces and a, v and u are the nodal acceleration, velocity and displacement vectors, respectively. The matrix $\underline{\underline{D}}$ is generally not assembled out of element damping matrices. The damping matrix is constructed from the mass and stiffness matrix of the complete element assemblage. In numerical calculation, an artificial damping is used (TASS, 2010d). This artificial damping is called Rayleigh damping and is assumed by Eq.( 4-2) (TASS, 2010d).

$$\underline{\underline{D}} = \alpha \underline{\underline{M}} + \beta \underline{\underline{K}} \tag{4-2}$$

Where $\alpha$ and $\beta$ are damping coefficients. This Rayleigh damping coefficient is an artificial representation of the actual damping in the entire system. The coefficient $\alpha$ may be a function of time. The stiffness matrix is not assembled and calculated in Madymo. The stiffness is represented by the tangential component of the force - displacement relation. For a non linear system, this tangential stiffness is not represented by a constant (for example infinitely small displacements with a linear material behavior) but it changes in time as can be seen in Fig. 4-2. The stiffness matrix is not constructed, hence $\beta$ is set to zero.

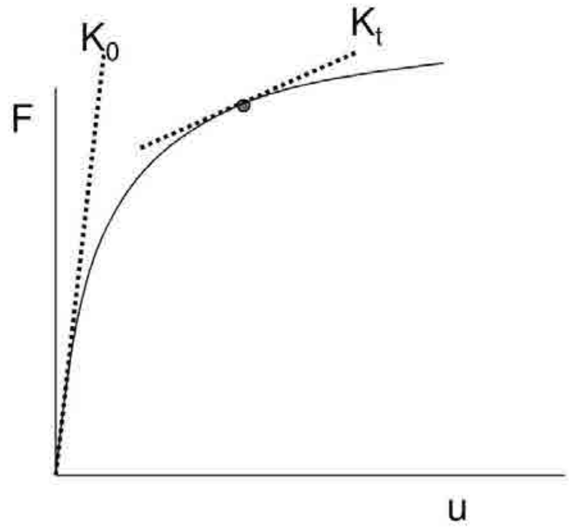


**Figure 4-2:** Non linear tangential stiffness (TASS, 2010b)

Madymo is a fully non linear solver and the stiffness contribution is incorporated in the internal forces. The final equation of motion is given in equation 4-3.

$$\underline{\underline{M}}\,(\underline{a} + \alpha\ \underline{v}) = \underline{F}_{ext} - \underline{F}_{int}(u, v) \tag{4-3}$$

Equation 4-3 the only matrix that must be assembled is the mass matrix. A diagonal mass matrix is very desirable, since the mass matrix is inverted. In Madymo this is done by mass lumping (TASS, 2010d). Lumping is a method to translate the surface entity of the element to the nodes. Lumping is used for element mass or surface pressure. There are two possibilities for Lumping for the CST within Madymo:

1. Each node has 1/3 of the element surface mass or pressure, this is called "WORK_EQUIVALENCE" lumping method (TASS, 2010c).
2. The pressure force or mass on the element is distributed over the nodes depending on the enclosed angle between the adjacent sides. So for a triangular element with enclosed angles 30, 60, and 90 degrees, the nodal forces equal 1/6, 1/3 and 1/2 of the element force, respectively. In Madymo this lumping method is called "GEOMETRICAL" (TASS, 2010c).

The default lumping method is chosen, both methods have been tested and this resulted in little differences between the two methods.

The nodal accelerations follow directly from the solving the equations of motion at time t. With an explicit integration scheme, the nodal velocities and displacements can be determined at time step t + Δt/2. This explicit time integration scheme is called the central difference method.

$$\begin{aligned} \underline{v}_{n+\frac{1}{2}} &= \underline{v}_{n-\frac{1}{2}} + \Delta t \underline{a}_n \\ \underline{u}_{n+1} &= \underline{u}_n + \Delta t \underline{v}_{n+\frac{1}{2}} \end{aligned} \tag{4-4}$$

Substituting equation 4-4 into equation 4-3, results in equation 4-5.

$$\underline{v}_{n+\frac{1}{2}} = A_1 \underline{v}_{n-\frac{1}{2}} + A_2 \underline{\underline{M}}^{-1} \left( \underline{F}_{ext} - \underline{F}_{int} \right) \tag{4-5}$$

where

$$\begin{aligned} A_1 &= (1 - \alpha \Delta t) \, / \, (1 + \alpha \Delta t) \\ A_2 &= (\Delta t) \, / \, (1 + \alpha \Delta t) \end{aligned} \tag{4-6}$$

In the central difference method, the displacements and velocities are calculated from quantities at previous points in time only. This method is called an explicit time integration method and is conditionally stable, which implies that the timestep must be smaller then the Courant time step (TASS, 2010d).

$$\Delta t = L/c \tag{4-7}$$

The speed of sound for linear elastic material is given by c and L is the characteristic length of the element. This condition requires that the time step is small enough to ensure that sound wave may not cross the smallest element during one time step. The speed of sound for linear elastic material is a function of the elasticity and density of the material (TASS, 2010d), see Eq. 4-8.

$$c = \sqrt{E/\rho} \tag{4-8}$$

The stability of the system depends on the size of the smallest element (TASS, 2010d). A safety margin of 10 % reduction on the Courant condition is sufficient for practical non linear problems (TASS, 2010d).

For the CST element, the Courant stability criterion is defined as the minimum element length see Eq. 4-9.

$$L_{min} = \frac{2A}{max\,(l_i)} \tag{4-9}$$

### 4-1-2 Element type and kinematic relation

In the previous section the equations of motion were elaborated. The nodal displacements, velocities and accelerations are calculated from the nodal forces. Also the stability condition is explained. In this Section, the approach and methods are explained in order to calculate the element displacements from the nodal displacements. The element displacements are necessary to calculate the strains in the elements.

There are three important relations and/or formulations that need to be clear:

1. Element type that is used is the CST (or the linear membrane) element.
2. Kinematic formulation that can cope with geometrical nonlinearities, large rotations large displacement and preferably large strain. In Madymo a corotational formulation is used.
3. Within this kinematic formulation, a strain/displacement relation that relates the element displacements to the strains. In Madymo, the Green-Lagrange relation is recommended.

Before the CST element is explained, the context of the corotational formulation is clarified. In Madymo the corotational formulation is one of the three possible geometrical non linear kinematic Lagrangian descriptions used in present day engineering. It is the newest formulation and has a limitation and the reason why "*CR has not penetrated the major general-purpose FEM codes that cater to nonlinear analysis*" (Filippa, 2000b), (Filippa, 2000a). The reason is that displacements and rotations may be arbitrarily large, but deformations must be small (strains < 5 %) (Filippa, 2000a). The principle of the corotational formulation is to decouple the rigid body motions and the deformations of each element. This is done by decomposition of the reference composition into two configurations:

1. Base $C^0$, this is the initial or base configuration.
2. Corotational configuration $C^R$. This the configuration that varies from element to element and represents the rigid body motion. From this configuration the deformations ,or in other words the strains in all elements, are determined.

In Fig. 4-3 a visual representation of the corotational kinematic description is shown. Note that the deformed (current) state at time t is exaggerated.

Each membrane element has a separate element coordinate system, see Fig. 4-4. This element is called the CST element because the interpolation functions are linear. The strains

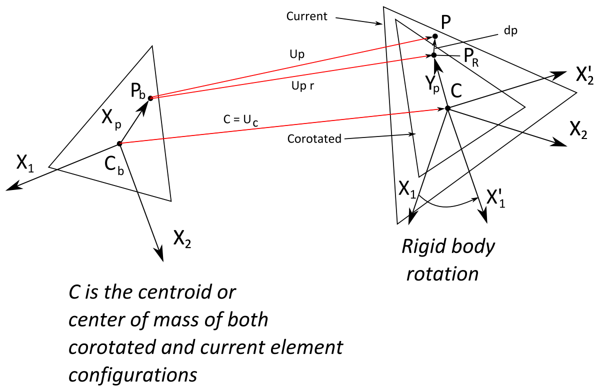


**Figure 4-3:** Corotational kinematic description from base configuration to deform (Filippa, 2000b)

determined either with the linear strain measure or the Green-Lagrange strain measure are constant (Bathe, 1982). As a consequence, the element displacements are continuous across the element boundaries but the strains (and the stresses) are not continuous across the element boundaries. The element that used is called the Belytschko Tsay element. The definition of the element coordinate system is given in (TASS, 2010d): "*Each membrane element has its own right-handed, orthogonal, local element coordinate system. The element plane is defined as the plane through the three nodes of the element. The $\xi$ and $\eta$ axis lie in the element plane. The $\zeta$ axis is perpendicular to the element plane. The direction of the $\xi$ axis is from the first to the second node specified in the Elements Table. The $\eta$ axis is perpendicular to the $\xi$ axis pointing into the direction of the third node. The $\zeta$ axis follows from the outer product of vectors along the positive $\xi$ and $\eta$ axis (see Fig. 4-4). The order in which the node numbers are given therefore defines the direction of the $\zeta$ axis. The positive direction of the $\zeta$ axis can be easily determined as it corresponds with the direction of a right-handed screw if rotating from node 1 past node 2 towards node 3.*"

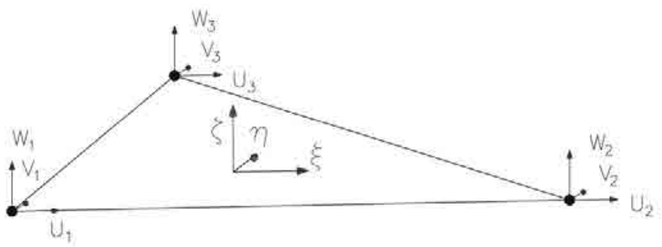


**Figure 4-4:** Three noded membrane element (TASS, 2010d)

The rigid mode displacements of the nodes and the deformation displacement of each element at each time-step is known. In order to calculate the strains the element displacement are important. To determine the strains in the element, two strain measures are used. The first is the linear or engineering strain measure, see equation 4-10 (Bathe, 1982), (TASS, 2010d). Here $\underline{\underline{F}}$ is the deformation gradient. The deformation gradient is the derivative of the element location with respect to a reference (for example the corotational) element configuration, see figure 4-3.

$$\underline{\underline{E}}_{lin} = \underline{\underline{\epsilon}}_{lin} = \underline{\underline{F}} - \underline{\underline{I}} \tag{4-10}$$

$$\underline{\underline{F}} = \frac{\partial(x,y,z)}{\partial(X,Y,Z)} = \begin{pmatrix} \frac{\partial x}{\partial X} & \frac{\partial x}{\partial Y} & \frac{\partial x}{\partial Z} \\ \frac{\partial y}{\partial X} & \frac{\partial y}{\partial Y} & \frac{\partial y}{\partial Z} \\ \frac{\partial z}{\partial X} & \frac{\partial z}{\partial Y} & \frac{\partial z}{\partial Z} \end{pmatrix} = \nabla \underline{x} \tag{4-11}$$

This equations right hand side is written in Jacobian format (Filippa, 2000b). In Eq. 4-12, the linear strain measure with respect to the displacements is given in Eq. 4-12.

$$\underline{\underline{E}}_{lin} = \underline{\underline{\epsilon}}_{lin} \quad = \quad = \frac{1}{2}\left(\nabla \underline{u}^T + \nabla \underline{u}\right) \tag{4-12}$$

where $\nabla$ is the nabla operator. This formulation is in general not objective and the results obtained can depend on the element nodal topology. Objectivity means that the orientation of the element has no influence on the strain calculation.

Equation 4-10 can now be written as a function of displacements. The element considered is a CST element, which only caries plane strains and stresses in (x,X,y,Y) plane.

The LEI kite deforms significantly during flight. Due to this flexibility, the kite is assumed to steer. This flexibility leads to geometrical non linearities. The Green Lagrange strain formulation can cope with these geometrical non linearities and therefore this strain measure is used.

This incorporates geometrical non linearities (TASS, 2010d), (Filippa, 2000b). Together with the corotational formulation, the Green-Lagrange strain measure is objective, because the rigid body motion does not have influence on the Green-Lagrange strains, this is derived in (Filippa, 2000b) and (Bathe, 1982).

The Green-Lagrange strain measure is noted in (TASS, 2010d) as given in Eq. 4-13. The virtual work equivalent to the Green-Lagrange strain measure is the $2^{nd}$ Piola Kirchoff stress tensor (Bathe, 1982).

$$\underline{\underline{E}}_{GL} = \frac{1}{2}\left(\underline{\underline{F}}^T \underline{\underline{F}} - \underline{\underline{I}}\right) \tag{4-13}$$

With a relation between the element coordinate and the element displacement:

$$\underline{x} = \underline{X} + \underline{u} \tag{4-14}$$

The deformation matrix can also be expressed as a function of the element displacements. This is derived in the following equation, using Eq. 4-11 and substituting equation 4-14.

$$\underline{\underline{F}} = \frac{\partial(x,y,z)}{\partial(X,Y,Z)} = \begin{pmatrix} \frac{\partial X+u_x}{\partial X} & \frac{\partial X+u_x}{\partial Y} & \frac{\partial X+u_x}{\partial Z} \\ \frac{\partial Y+u_y}{\partial X} & \frac{\partial Y+u_y}{\partial Y} & \frac{\partial Y+u_y}{\partial Z} \\ \frac{\partial Z+u_z}{\partial X} & \frac{\partial Z+u_z}{\partial Y} & \frac{\partial Z+u_z}{\partial Z} \end{pmatrix} = \nabla(\underline{X} + \underline{u}) \tag{4-15}$$

It is also possible to derive the Green-Lagrange strain measure as a function of the displacement. Substitution of Eq. 4-15 leads to

$$\begin{aligned} \underline{\underline{E}}_{GL} = \underline{\underline{\epsilon}}_{GL} &= \frac{1}{2}\left([\nabla(\underline{X}+\underline{u})^T][\nabla(\underline{X}+\underline{u})^T]^T - \underline{\underline{I}}\right) \\ &= \frac{1}{2}\left([\underline{\underline{I}} + \nabla\underline{u}^T][\underline{\underline{I}} + \nabla\underline{u}^T]^T - \underline{\underline{I}}\right) \\ &= \frac{1}{2}\left(\nabla\underline{u}^T + (\nabla\underline{u}^T)^T + (\nabla\underline{u}^T)(\nabla\underline{u}^T)^T\right) \end{aligned} \tag{4-16}$$

If the equation is written in matrix form, the equation 4-16 can be written as

$$\underline{\underline{E}}_{GL} = \underline{\underline{\epsilon}}_{GL} = \begin{pmatrix} \epsilon_{xx} & \psi_{yx} & \psi_{zx} \\ \psi_{xy} & \epsilon_{yy} & \psi_{zy} \\ \psi_{xz} & \psi_{yz} & \epsilon_{zz} \end{pmatrix} \tag{4-17}$$

The Green-Lagrange strain matrix for a CST element is displayed as:

$$\begin{aligned} \epsilon_{xx} &= \frac{\partial u_x}{\partial X} + \frac{1}{2}\left[\left(\frac{\partial u_x}{\partial X}\right)^2 + \left(\frac{\partial u_y}{\partial X}\right)^2\right] \\ \epsilon_{yy} &= \frac{\partial u_y}{\partial Y} + \frac{1}{2}\left[\left(\frac{\partial u_x}{\partial Y}\right)^2 + \left(\frac{\partial u_y}{\partial Y}\right)^2\right] \\ \psi_{yx} = \psi_{xy} &= \frac{1}{2}\left(\frac{\partial u_y}{\partial X} + \frac{\partial u_x}{\partial Y}\right) + \frac{1}{2}\left[\frac{\partial u_x}{\partial X}\frac{\partial u_x}{\partial Y} + \frac{\partial u_y}{\partial X}\frac{\partial u_y}{\partial Y}\right] \\ \epsilon_{zz} &= \psi_{xz} = \psi_{zx} = \psi_{yz} = \psi_{zy} \qquad = 0 \end{aligned} \tag{4-18}$$

The Green-Lagrange strains disappear in the rigid motion (Bathe, 1982), (TASS, 2010d) and (Filippa, 2000b). The linear strain measure is found as the first term of the right hand side in equation 4-18. The Green-Lagrange strain measure has a non linear contribution with respect to the linear strains.

The elements can be distorted significantly during the analysis. The performance is best when they are close to an equilateral triangle (TASS, 2010d).

There are limitations in the use of the CST element. the most important restriction is known as locking (Chatzikonstantinou, 1999). The CST element can only resist in plane deformation. However, if the elements are subjected to in plane bending, the elements cannot deform and the stiffness of such elements is much higher compared to the actual situation (MacNeal, 1994). This can be solved by:

1. Using different elements for example quadrilateral elements, that have linear strain displacement relation (in contrast to constant strain in CST elements).
2. Using small CST elements.
3. Using triangular membrane elements with non-linear shape functions (for example by adding nodes on the middle of each element boundary).
4. Using shell elements that can incorporate bending.

For this thesis only the CST elements are considered, so it is important to know these limitations.

### 4-1-3 Constitutive stress strain relation and material models in Madymo

In Fig. 4-1 we have just computed the element strains with the kinematic relations described in section 4-1-2. The element stresses are computed using the constitutive relations in this Section. This is the relation between the strains and stresses in the element. This constitutive relation is given by the material properties.

A lot of material models are available in Madymo. Two material models will be explained. The first one is the isotropic linear (ISOLIN is Madymo) material. The second model is used for woven material. This model can represent linear as well as non-linear material behavior. These two material model will be used for both Dacron and Ripstop of the kite. The Uni- and Bi axial stress tests for these two material types are described in Chapter 6-2.

Isolinear material model was chosen, because of the data available. The only data available was the E modulus in one direction. The linear material model is the most simple one. With the biaxial stress test data, the woven material model was used in Madymo.

#### ISOLIN material model

The ISOLIN material model stands for Isotropic homogeneous linear material model. This means:

- homogeneous = the smallest part cut from the body possesses the same specific mechanical properties as the body.
- isotropic = the properties are the same in all directions.

The mechanical behavior of materials is specified as the relationship between the stresses and strains, constitutive equations.

$$\underline{\sigma} = \underline{\underline{K}}\ \underline{\epsilon} \tag{4-19}$$

where $K$ is the stiffness matrix with elasticity coefficients and where $\sigma$ and $\epsilon$ are column vectors with the following stress and strain components:

$$\begin{aligned} \underline{\sigma}^T &= (\sigma_{xx}, \sigma_{yy}, \sigma_{zz}, \tau_{xy}, \tau_{yz}, \tau_{zx}) \\ \underline{\epsilon}^T &= (\epsilon_{xx}, \epsilon_{yy}, \epsilon_{zz}, \psi_{xy}, \psi_{yz}, \psi_{zx}) \end{aligned} \tag{4-20}$$

The stiffness matrix can be inverted in order to obtain the strains in terms of the stresses, $\underline{\underline{C}}$ is called the compliance matrix.

$$\underline{\epsilon} = \underline{\underline{C}}\;\underline{\sigma} \tag{4-21}$$

$$\underline{\underline{C}} = \begin{pmatrix} 1/E & -\nu/E & -\nu/E & 0 & 0 & 0 \\ -\nu/E & 1/E & -\nu/E & 0 & 0 & 0 \\ -\nu/E & -\nu/E & 1/G & 0 & 0 & 0 \\ 0 & 0 & 0 & 1/G & 0 & 0 \\ 0 & 0 & 0 & 0 & 1/G & 0 \\ 0 & 0 & 0 & 0 & 0 & 1/G \end{pmatrix} \tag{4-22}$$

In Eq. 4-22 $E$ is Youngs modulus, $\nu$ is the Poissons ratio and $G$ the shear modulus. The relationship between these constants is:

$$G = \frac{1}{2}\frac{E}{1+\nu} \tag{4-23}$$

This means that only two constants, $E$ and $\nu$, have to be specified for linear isotropic material behavior. In membranes, a plane stress state is often assumed. In the CST element (membranes) the z-direction is perpendicular to the surface, this leads to Eq. 4-24.

$$\sigma_{zz} \;=\; \tau_{yz} \;=\; \tau_{zx} \;=\; 0 \tag{4-24}$$

The stiffness matrix $K$ for isotropic materials reduces to Eq. 4-25.

$$\underline{\underline{K}} = \frac{E}{1-\nu^2}\begin{pmatrix} 1 & \nu & 0 \\ \nu & 1 & 0 \\ 0 & 0 & \frac{1-\nu}{2} \end{pmatrix} \tag{4-25}$$

With this relation, the Cauchy stresses in the elements can be calculated. However, in section 4-1-2, the stress measure used is called the $2^{nd}$ Piola Kirchoff stress measure ($\underline{\underline{S}}$). This is the work equivalent to the Green-Lagrange strain measure.

$$\underline{\underline{S}} = \frac{\rho}{\rho_{ref}}\underline{\underline{F}}^{-1}\underline{\underline{\sigma}}\;\underline{\underline{F}}^{-T} \tag{4-26}$$

#### Material fabric shear: woven material model

This material model is used for non-linear material airbag modeling. The material that is used for the LE inflatable kite is a plain-woven material. This is a material model that actually models the fabric.

The initial warp and fill directions of the yarns can be chosen arbitrarily. Relative rotations are allowed between the yarns, because the orientation of the threads is updated each time-step. The stiffness of the fabric can introduced into the warp and fill direction. The first part is the Young's modulus in the warp and weft thread direction. The input can be a constant E modulus or a user-defined function, which represents the material stress-strain relation (TASS, 2010c). The second part is the shear modulus that is determined in the 45 degree (bias) direction. The user defined function could be deduced from different stress tests:

- Single yarn uni-axial test
- Whole fabric uni-axial test (necessary in three direction)
- Whole fabric bi-axial (main directions (warp, weft (or fill) and the bias direction.

In Madymo two different types of woven fabric material can be modeled, loose and tightly woven fabric. The difference between the two is that the tightly woven fabric can incorporate in-plane shear stiffness as discussed above (TASS, 2010d). This is also the material model that is most applicable for Dacron and Ripstop materials.

There is a huge disadvantage for using the woven fabric model. That is that the material directions have to be incorporated into the directions of the elements (TASS, 2010a). This means that the inflatable structure must be unfolded.

## 4-2 Uniform Pressure (UP) method in Madymo

This section describes the theory of uniform pressure used in Madymo. In the FEM method, described in the previous section, the uniform pressure method is used to model the internal pressure of the inflatable structure. The structure will be regarded as an airbag chamber (FEM in Madymo is focused on airbag analysis).

The uniform pressure method is based on the assumptions of uniform pressure and a uniform temperature distribution of a gas in an airbag chamber. The gas that is used is air and the assumption is that the composition of air is not changed. Air is assumed and treated as an ideal gas, with the ideal gas law the temperatures and the pressures are calculated. In case of the LE inflatable kite, after inflation the pressure and temperature are equal for every chamber, since all chambers (LE and the struts) are connected to each other. Transport of air from one chamber to another is possible.

Figure 4-5 represents a schematic view of the leading edge and the strut that are connected. The pressure is uniformly distributed on the nodes. The LE and strut have each internal conditions such as temperature and pressure. For the LE T1,p1 and for the strut T2,p2

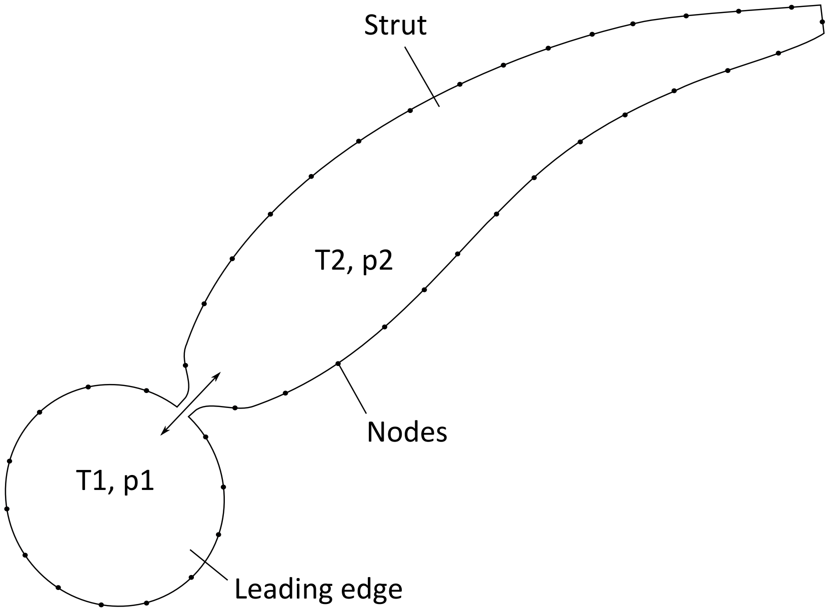


**Figure 4-5:** Schematic representation of the leading edge and strut

indicating that mass flow can be interchanged between chambers untill a new equilibrium is found.

In the Appendix A, the theory behind the uniform pressure is presented.

## 4-3 Multibody (MB) belts in Madymo

The kite will be modeled with the FEM with a uniform pressure distribution, which is discussed in the previous section. The bridle system of the kite will be modeled with "belts" in Madymo. Belts are used to model seat belts in Madymo.

A nice feature of Madymo is that the multi-body model and the structural FEM model can be simulated in one program. As shown in the Chapter 2-4, the bridle system consists of bridle lines, knots and pulleys. The bridle lines can be modeled as belt segments. The pulley will be modeled as tyings. These tyings behave in a similar way compared to pulleys. In these pulleys, coulomb friction coefficients can be applied to model the friction of a pulley (TASS, 2010d). The end of a belt segment can be connected to a FEM node.

# Chapter 5

# Preliminary conclusions

From the literature study, the potential of the AWE by using kites is explained. At higher altitudes, the wind is stronger and more consistent compared to the conventional wind turbine altitudes. The kite power research group at the DUT uses a pumping cycle that generates 20 kW nominal mechanical power. The kite that is used in order to generate power is the 25 $m^2$ V2 Mutiny kite. This is a very complex structure that including a lot of pulleys in the bridle system to enable the change in $\alpha$ that is needed for reel-out and reel-in phase of the kite. The cylindrical inflatable beam is investigated quite extensively. The analysis of an inflatable beam can be divided in three states: taut, wrinkled and collapse. In the taut region the beam is supposed to behave linear, however in the wrinkled and near collapse the behavior was shown to be highly non-linear. Few attempts have been made to model kites (let alone LEI kites) with the FEM. FEM is chosen for modeling the V2 LEI Mutiny kite. The program in which it is going to be modeled is Madymo.

In order to model LEI kite with FEM there are two motivations:

1. FEM is a predictive and physical way to model structures. Such a model could eventually be used as a validation tool.
2. FEM can be modeled in detail and could be used as a design tool. The structural behavior of the kite depends mostly on local effects and to show these local effects, FEM might be a adequate tool.

To model inflatable with FEM structures was proven to be quite a challenge because of the complex behavior of the inflatable beam. An extensive background is given where the principles behind Madymo are given.

This leads to the main research questions provided in Chapter 1. The following sub questions are formulated, how these main questions are to be answered in this Thesis.

1. Is it possible to create the geometry of an inflatable beam model and the LEI kite that can be imported in Madymo?
2. What material properties are important for the material models?
3. Is it possible to create and analyze a straight inflatable beam model, which can be loaded with a tip force and a desired internal pressure?
4. If this is possible, then how accurate does this model describe the load versus deflection curve compared the experiment performed by (Breukels, 2011) and theory?
5. Is it possible to analyze the beam in the linear state. For example to check strains and stresses in the beam?
6. What parameters influence the model?
7. Is it possible to create a structural model of the LE inflatable kite with the LE and the struts inflated to a desired internal pressure?
8. Is it possible to model the LEI kite including the bridle and does the bridle interact with the kite at different loads?
9. Does the response qualitatively match the actual kite?

# Part II

# Case studies

# Chapter 6

# Model input requirements for Madymo

In this chapter the input requirements for Madymo are given and an approach will be given on how the research questions are going to be answered in this thesis.

The behavior of inflatable structures should be modeled with three inputs: geometry, external loads (including internal pressure and supports/constraints) and material properties see Fig. 6-1.

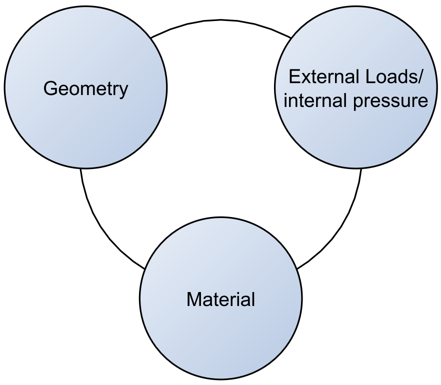


**Figure 6-1:** Trinity between geometry, external loads and material based on (Veldman, 2005)

The three required inputs shown in Fig. 6-1 must be discussed first before an inflatable beam can be created in Madymo.

The discretized geometry cannot be created in Madymo. A mesh program is needed in order to create a discretized geometry that can be used as an input for Madymo. One objective is to create a CAD geometry of a leading edge inflatable kite. There is no process that creates the geometrical input that is necessary for Madymo. So in Section 6-1 a process will be described in order to create a discretized geometry from CAD to a mesh program that can eventually be used as an geometry input for Madymo. This process is created in such a way that different geometries can be discretized as a triangulated mesh. In this section, the geometries from the cylindrical beam till the final kite will be created from the requirements.

In Section 4 material requirements are given. Two material models are used and described for the FEM model. The first model is called isotropic linear (ISOLIN) material model and the second material model is called material fabric shear. The latter material model is able to model woven fabrics that is able to incorporated non-linear material characteristics.

The internal pressure within the inflatable beam using UP method is used in this thesis by two methods. The first method is called the LOAD.PRES method. This model creates a equal pressure on the beam elements that describes a pressure function over time. The second method is the UP inflation or airbag method. In this method, the internal pressure is applied by an inflator. This inflator uses mass flow of air to inflate the structure. The pressure is uniformly distributed over all the elements in an enclosed chamber. The external loads applied to the inflatable structure are discussed in Section 6-3.

In (Breukels, 2011) an experiment of an inflatable beam made of Dacron with an internal bladder is performed. This beam experiment results in a force versus deflection curve. Different beam diameters, loads and internal pressures are measured. The accuracy of the model will be discussed by first creating a reference model that has a diameter of 0.13 m, a length of 1 m, an internal pressure of 0.3 bar overpressure. Next, the load versus deflection curve will be compared to the measurements of (Breukels, 2011).

The stresses and the strains in the beam could be important for detailed analysis. The stresses and strains could be displayed by contour plots.

## 6-1 Geometry input

In this section, the geometry input will be discussed. A process will be described for any geometry as a triangular mesh input for Madymo. The beam, kite and the kite including the bridle will be discussed in three process steps: CAD, triangulated mesh and import into Madymo. This is done by first setting the requirements for each step in the design process and next find suitable solutions for the challenges and design difficulties.

The research sub-question that is answered in this Section is:

**Is it possible to create the geometry of an inflatable beam model and the LEI that can be imported in Madymo?**

There is no (standard) procedure for generating a geometry for Madymo. For the mesh a CST membrane element is chosen. The requirements for the input for a triangulated mesh in Madymo consist out:

1. nodes with a node id, a x-, y-, and z coordinate see table 6-1 and Figure 6-2a for an example.

2. elements (connectivity between the nodes) with an element id, part id, node id $i$, node id $j$ and node id $k$ see table 6-1 Fig. 6-2b for an example.

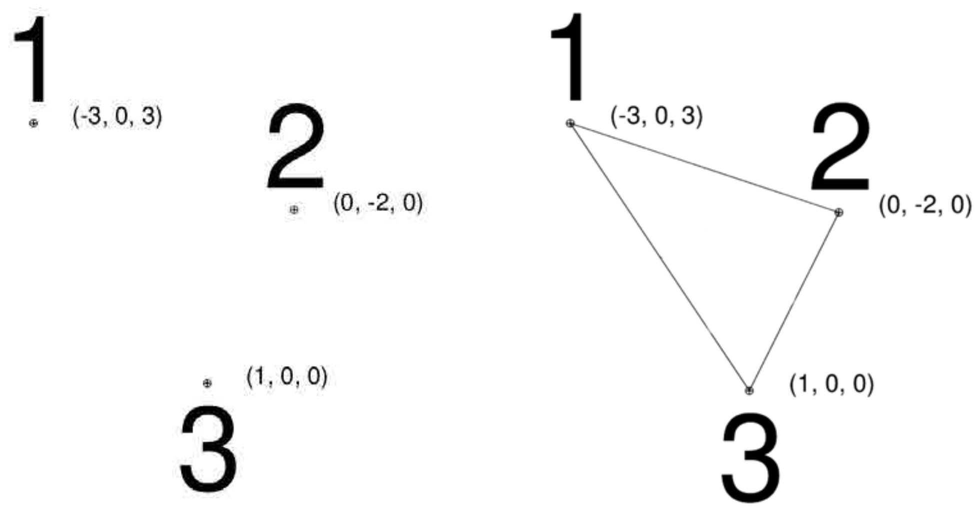


**(a)** Three nodes **(b)** Element

**Figure 6-2:** Examples that represent three nodes and one element for the connectivity between the nodes

**Table 6-1:** Node table input for Madymo

| Node ID # | x- coordinate | y-coordinate | z-coordinate |
|---|---|---|---|
| 1 | -3 | 0 | 3 |
| 2 | 0 | -2 | 0 |
| 3 | 1 | 0 | 0 |

**Table 6-2:** Element table input for Madymo showing the connectivity between the nodes

| Element ID # | Part ID # | node $i$ | node $j$ | node $k$ |
|---|---|---|---|---|
| 1 | 1 | 1 | 2 | 3 |

A mesh in Madymo consist of a number of nodes that are connected through elements. These elements and nodes are built up in different parts that form a discretized representation of a geometry. However with a complex geometry, there are many parts, nodes and elements. To discretize the geometry into a complete mesh, there are mesh programs that can create a mesh from a complex CAD geometry. So in Table 6-3 and Table 6-4 a general representation is shown for number of nodes from $n_1$ to $n_v$ with coordinates $x_1$ to $x_v$, $y_1$ to $y_v$ and $z_1$ to $z_v$. And for the elements from for example the element numbers from 1 to $f$,the part numbers from 1 to $g$ and the three node numbers $n_i$, $n_j$ and $n_k$

**Table 6-3:** Node table input for Madymo

| Node ID # | x- coordinate | y-coordinate | z-coordinate |
|---|---|---|---|
| 1 | -3 | 0 | 3 |
| 2 | 0 | -2 | 0 |
| 3 | 1 | 0 | 0 |
| ⋮ | ⋮ | ⋮ | ⋮ |
| v | $x_v$ | $y_v$ | $z_v$ |

**Table 6-4:** Element table input for Madymo showing the connectivity between the nodes

| Element ID # | Part ID # | node 1 | node 2 | node 3 |
|---|---|---|---|---|
| 1 | 1 | 1 | 2 | 3 |
| 2 | 1 | 5 | 2 | 7 |
| ⋮ | ⋮ | ⋮ | ⋮ | ⋮ |
| f | g | $n_i$ | $n_j$ | $n_k$ |

### 6-1-1 Geometry Process Overview

In this section, two different processes in order to create the geometry of an inflatable beam and a LEI kite are discussed. The first process represents the complexity of the geometry. The second process describes the three different stages from CAD, mesh and geometry import in Madymo.

Figure 6-3 shows the chart of the process development representing the complexity of the entire process, developing a kite in the three process steps (CAD, mesh and FEM). In Fig. 6-3a a chart is given and in Fig. 6-3b the steps out of the chart are given by images out of Rhino.

The process from CAD, mesh to the FEM solver is shown in Fig. 6-4 and is called the horizontal process. There are a number of requirements in each horizontal process step, which will be discussed in this chapter. These are the requirements that must be met in

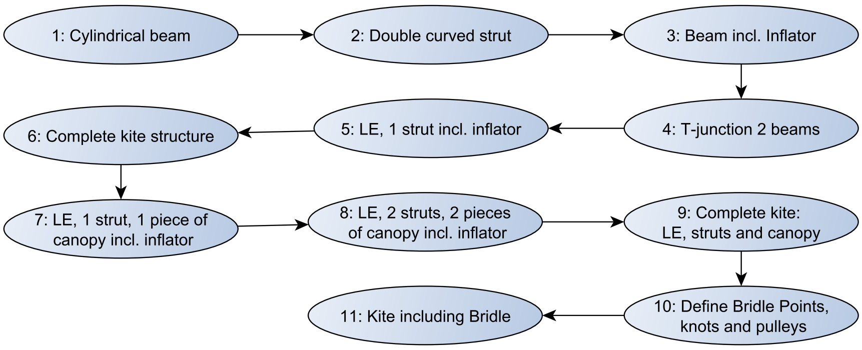


**(a)** Vertical flow chart

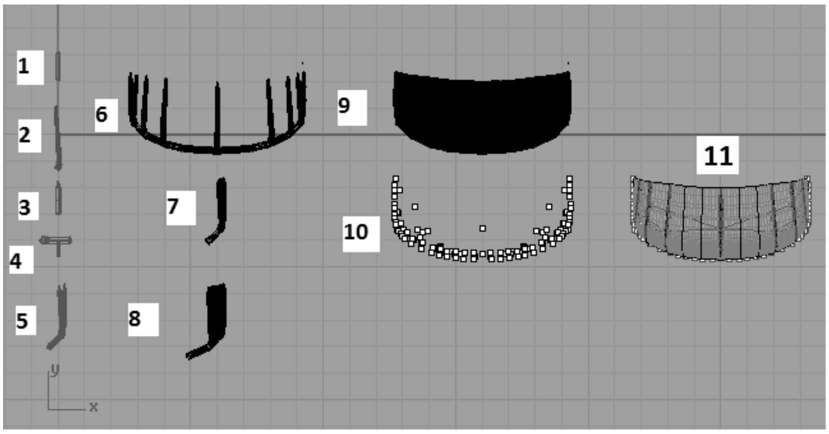


**(b)** CAD chart in CAD program Rhino

**Figure 6-3:** Process development representing the complexity of the entire process

every process step. There are two types of requirements:

1. Process requirements. The process requirements are driven not only in the process itself, but also by the other two processes (mesh and FEM solver).
2. Output/Input (o/i) requirements. These are requirement that are only applicable to the process steps which are consecutive. So the input requirements of the process $i+1$ drives the output requirements of process $i$ see Fig.6-4.

The final objective of developing a process is, at the end of the process, provide the base of the Madymo model that can be analyzed. In every step of the process shown in Fig. 6-3, different challenges must be solved.

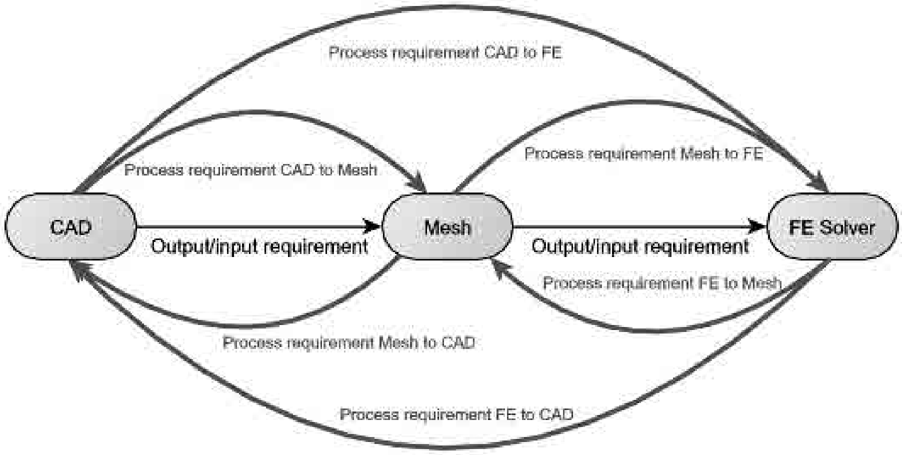


**Figure 6-4:** Horizontal chart including iterative coupling of both types of requirements: (Process requirements and output/input requirements)

### 6-1-2 Reshaping CAD geometry for meshing

In this section, the requirements for the CAD process is explained. The kite was already represented in Rhino. This visual representation was the design of the kite during flight, however it was not suitable for a mesh because the surface consisted of a large number of seams and small surfaces not suitable for meshing.

The kite had to be created from scratch with the original drawing as a benchmark.

First the requirements of each step with respect to the CAD are given. Only the cross sections of this CAD representation were maintained.

**Requirements CAD for CAD**

- The kite must be able to be drawn in a CAD environment such that it represents the actual shape (within limits) of the kite.
- This must be a surface representation of the kite, since internal pressure has to provide stiffness for the inflatable structure.
- Non manifold surfaces are three (or more) surfaces that share a single seam/edge. Examples of the kite are: the connection with the struts and the leading edge and connection of the canopy, strut and leading edge.

### Requirements mesh for CAD

- Surface mesh, so all the meshed parts should be surfaces.
- At the manifold surfaces: an example of a non manifold mesh with three surfaces that join one edge see Fig. 6-5. On the edge, nodes are placed that share elements on all three surfaces.

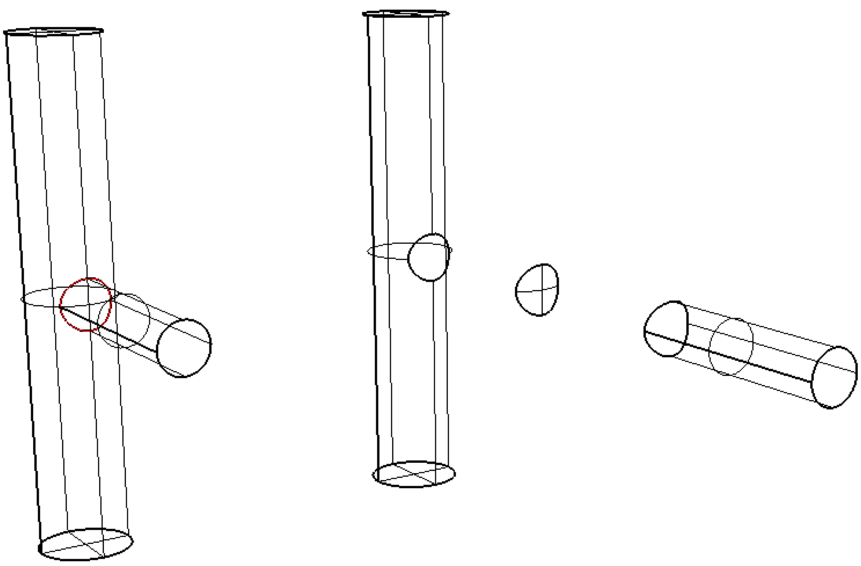

**Figure 6-5:** Non manifold surfaces

### o/i requirements mesh for CAD

- The output of the CAD should be exported, such that the mesh program can import the CAD output.

### Requirements FEM for CAD

- Within Madymo it is required to have an inflator as a mesh part, in CAD this should be taken into account. Both chambers (inflator and the beam) should be sharing a surface.

The 25 $m^2$ V2 Mutiny kite was already drawn in Rhino 4. This was used as a start, number 1, for the beam see Fig. 6-3. The four most important requirements for this challenge were:

1. Create a surface for a surface mesh, without surfaces that restricts the mesh into sharp angles.

2. In the CAD application, make sure that there are not too much "lines" that could restrict the triangulation in the mesh.
3. Solve non manifold surface issue.
4. Make sure that the output of Rhino is compatible with the input of the mesh program.

Preferably the non manifold surface would be taken care of in a CAD environment.

There are 5 CAD packages used for developing a process from CAD, mesh towards FEM. These are: Rhino 3,4 and 5 Work In Progress (WIP), CATIA V5R19, ProEwildfire2.0, SolidWorks2010(x64) edition. Rhino 5 beta is specialized with surfaces. The curves and surfaces are translated into Non-Uniform Rational B-Splines (NURBS). This is a mathematical representation of a geometry, Two Dimensional (2D) or Three Dimensional (3D). However non of the packages could deal with the non manifolding surfaces.

From the chart in Fig. 6-3, the first step is to create a beam including an inflator satisfying the requirements mentioned above.

With this information, the CAD of the beam including an inflator and the non-manifold surface that connects the beam and the inflator can be created. In Rhino it is very easy to create surfaces. Every line, arc, circle, square etc. can be extruded to a surface. In this case, it is very straight-forward in Rhino, because what must be created are in fact two cylinders with a non-manifold surface in between. Rhino 5.0 beta was used, because of the user friendly Graphical User Interface (GUI), compared to Rhino 4.

The CAD package will be Rhino 5 beta package, and an additional requirement for the mesh program: CAD applications in the mesh program to deal with the non-manifold surface.

The output of the Rhino drawing depends on the mesh program used. Different mesh programs require different inputs.

### 6-1-3 Meshing kite components

In the previous section, the CAD process was discussed. In this section the mesh has to be created. First the process- and the output/input requirements are determined. Next three mesh programs are discussed and the best suited mesh program is chosen. As a result, the results of the meshed geometries are shown and finally the process to flatten a mesh which is required for the woven material model is discussed and shown.

From the horizontal flowchart see Fig. 6-4 again the requirements for the mesh in the process are set.

**Requirements CAD for mesh**

- Create non manifold surfaces e.g. for connection between the LE and the struts, connection for the inflator and the beam/kite, connection between the struts and the canopy and the connection between the LE and the canopy).
- The mesh should follow within limits follow the shape of the CAD input.

**Requirements mesh for mesh**

- Triangulated mesh.
- Surface mesh.
- closed mesh without gaps.
- At the manifold mesh surfaces: the nodes at the edge of the three adjacent surfaces should be connected to the elements in all three adjacent surfaces.
- The mesh should give a mesh that is an accurate representation of the CAD drawing within certain predefined limits, important question is this: what is good enough?

**Requirements FEM for mesh**

- The mesh should be airtight, this means no gaps or holes between the elements.
- The mesh has to be just rough enough that the least computational time is needed to reach a certain accuracy with respect to theory or experiments.
- Non manifold surfaces must be specified for as long as multiple airbag chambers are defined e.g. beam connection with inflator, LE connection with struts and inflator).
- The FEM experts from TASS recommend strongly a 3 node membrane element. This element can deal with distortions the best in Madymo.
- The BPs should be connected to the BPs. The BPs are points of the bridle, which are connected to the kite. In the case of the 25 $m^2$ V2 Mutiny kite, the BPs are connected to the LE.
- The mesh should be able to be flattened for the thread direction in Madymo. This is the only way that woven material model could be defined.

Next to the requirements for the mesh, the input/output requirements must be set.

**o/i requirements FEM for mesh**
The input requirements of Madymo are defined in two tables:

1. Node table: In this table the nodes are defined by a Node ID, x-coordinate, y-coordinate and a z-coordinate of each node.
2. Element table: In this table the connectivity of the nodes are defined. This is represented in the element table by: by a Element ID, a part number, Node 1, node 2 and node 3 which define the element. This set-up only holds for a triangulated mesh.

The output of the mesh program should be such, that the input requirements are met of Madymo. In the introduction of this chapter the input requirement for Madymo regarding the mesh was already explained.

Three mesh programs are taken into account: mesh within Rhino, GMSH and Ansys Icem.

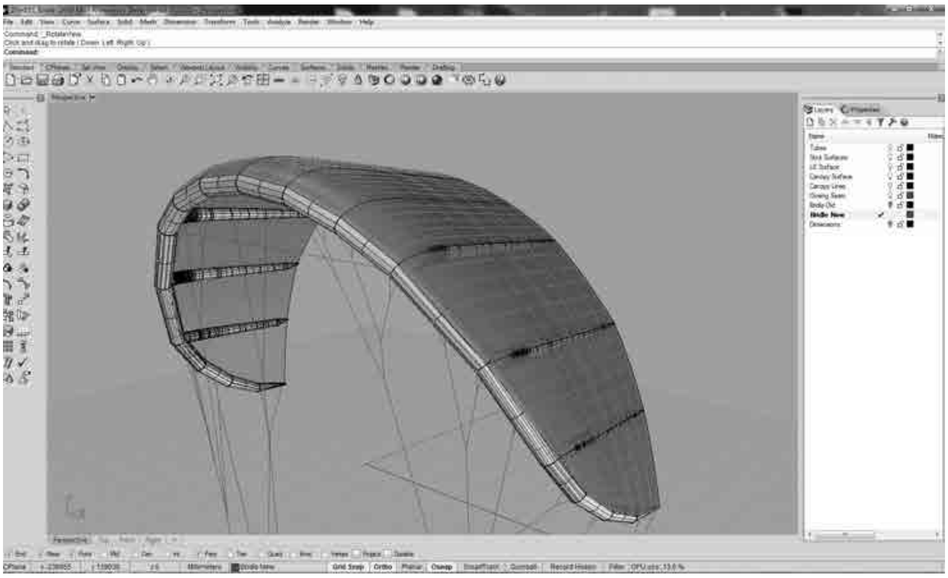

**Figure 6-6:** Bridle Points that connected to the Leading Edge of the 25 $m^2$ V2 Mutiny kite

### Mesh in Rhino 5 beta

The most obvious choice is using the mesh capabilities of Rhino 5 WIP. In Rhino the mesh is built up from polygon surfaces. The mesh capabilities has improved a lot compared to previous versions of Rhino.In Rhino 5 beta some basics could be used for meshing However, the quality of the triangles in circumferential surfaces (e.g. cylindrical beams, LE or struts) is very poor. This result can be seen in Fig. 6-7. The triangles are not evenly distributed about length of the beam, in contrary to the circumferential mesh distribution. This clearly does not hold for the polygon mesh of Rhino 5 beta.

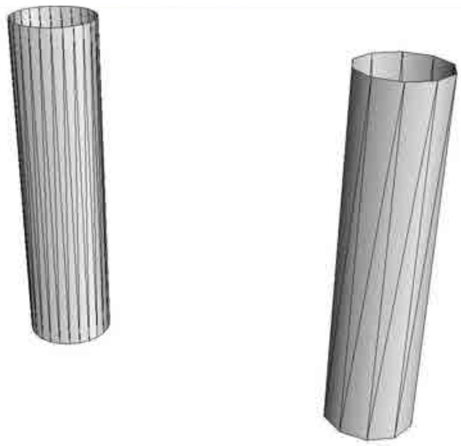

**Figure 6-7:** Mesh quality of a beam with r = 0.25 m in Rhino

Rhino gives no control over the mesh algorithm, which should be used (e.g. adaptive, Delaunay). The mesh attribute of Rhino 5 WIP is not suited as a mesh tool for the beam or kite.

## GMSH

GMSH is an open source mesh program, which is used in diverse FEM applications (Geuzaine & Remacle, 2010). An open source code is advantageous, because the source code could be adapted to increase the possibilities in using the mesh.

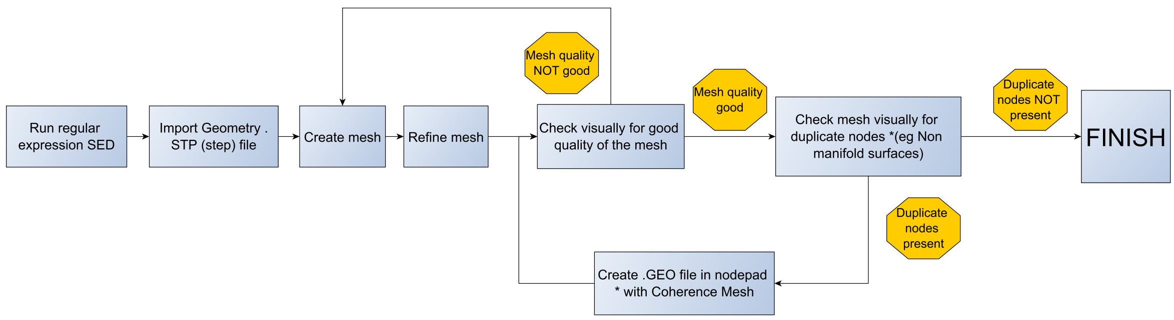


**Figure 6-8:** Flow chart of the mesh process in GMSH

The structure build-up for the process development (see Fig. 6-3) shows that the CAD and the mesh process goes from a cylindrical beam towards a complete kite including a complete bridle system. If the requirements are taken into the consideration, which are discussed above, 2 requirements are important:

1. The mesh should be without gaps or holes.
2. Manifold surface should be meshed with all three surfaces connected.

As a next step, from the FEM requirement in Madymo for the mesh, the inflator is necessary, thus resulting in a beam including an inflator (see Fig. 6-3 sub Figure beam including inflator).

This implies that a non manifold surface must be used between the inflator and the beam, to ensure two requirements: Multiple airbag chambers must be defined, so the mesh must be "airtight" (no gaps) between the chambers and non manifold surfaces must be defined. Mesh check for quality and two complications:

1. Duplicate nodes at approximately the same location.
2. Non closed mesh.

The beam in various shapes is explored, to get familiar with setting up the process. Because the LE and the struts are more or less beams, this cylindrical beam is the natural first. However one requirement (Manifold surfaces) is not in the picture. For the beam and strut without non-manifold surfaces, GMSH had some good results, see Figure 6-9.

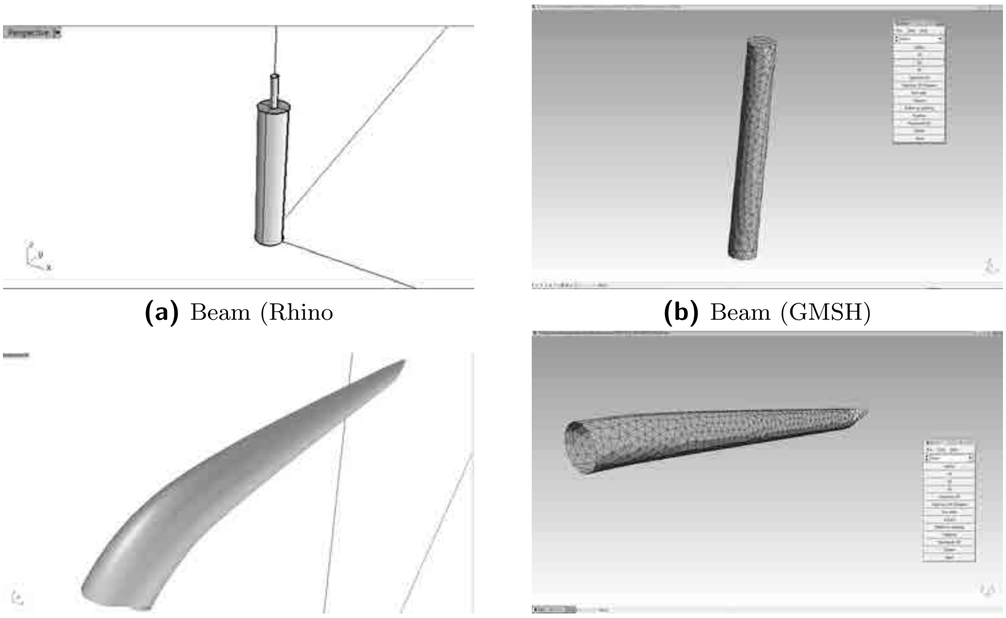

**(a)** Beam (Rhino

**(b)** Beam (GMSH)

**(c)** Strut (Rhino)

**(d)** Strut (GMSH)

**Figure 6-9:** Cylindrical beam with r =0.25 m and a strut represented in Rhino and GMSH

The next step is the the beam including the inflator, see step 3 in Fig. 6-3. It is discussed that the Non-manifold surface application only works with Rhino 5 WIP. It is also been shown that the Non-manifold surface application cannot be exported from Rhino 5 WIP. When this beam including the inflator is meshed, only two surfaces can be connected to each other. In the mesh for non-manifold surfaces, it is important that the nodes on the edge of the non-manifold surface in fact share the three adjacent surfaces, see Fig. 6-10. However, within GMSH, there is no CAD function, which connects, glues or sews all three surfaces. A maximum of two surfaces can be connected to each other. This results in two connected surfaces and the third surface is disconnected with regard to the connected surfaces, see Figure 6-10. So in Figure 6-10 wrong mesh from GMSH is shown. The nodes of the different parts should be aligned on the edge that shares three or more surfaces. In Figure 6-10 the misalignment of the nodes is shown and the surfaces are not connected. The misaligned nodes are seen on the edge of the edge and in the red circle.

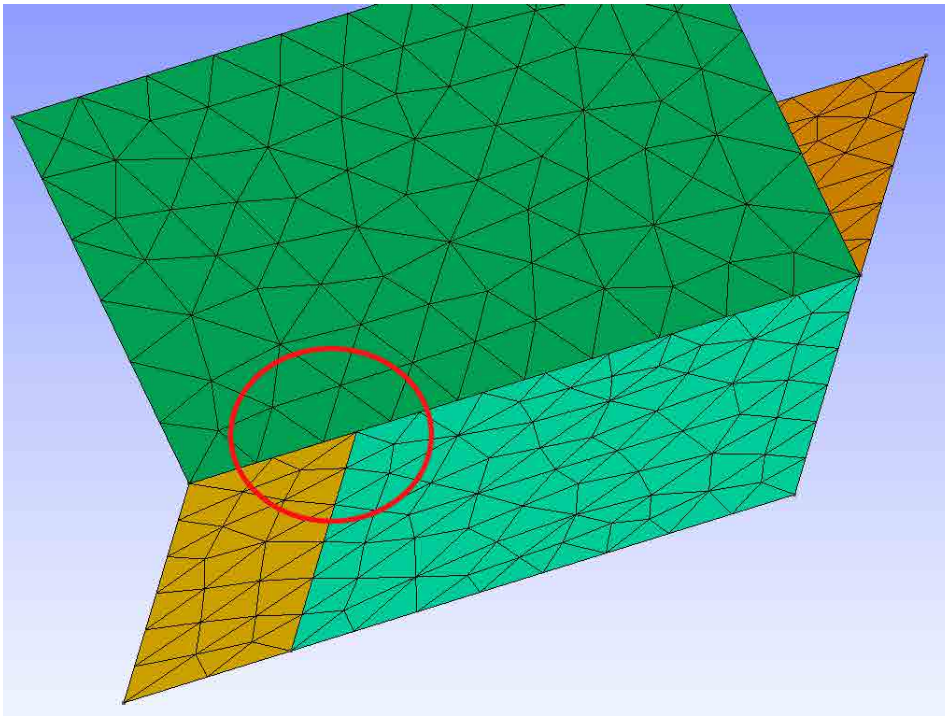

**Figure 6-10:** Hanging nodes of the mesh simple non manifold surfaces

So the quality regarding the mesh shape is good. The non-manifold surface mesh cannot be implemented in GMSH. GMSH is not suited as a mesh program for complex surface structures.

### Ansys ICEM

In Fig. 6-11 the flow chart of the mesh process in Ansys Icem is shown. Some steps in the vertical process need some extra work, for example attaching the canopy to the struts and the LE.

The main challenge of a new mesh tool is: create a mesh, which has the same (or better) mesh quality compared to the GMSH mesh for the beam and a mesh that can deal with non-manifold surfaces. There was experience within the ASSET kite group with Ansys ICEM, which should be able to cope with non-manifold surfaces because of different CAD functionalities that are included in Ansys ICEM. Within the DUT, this package is used in different faculties, hence this was a logical next step in the process. This was important because Rhino 5 WIP could deal with non-manifold surfaces, however, the CAD drawing with non-manifold surfaces could not be exported as such. Non-manifold surfaces were a vital issue in modeling every step from the beam including the inflator to the kite in the mesh and FEM. The CAD requirement for these non-manifold surfaces is redirected to the mesh

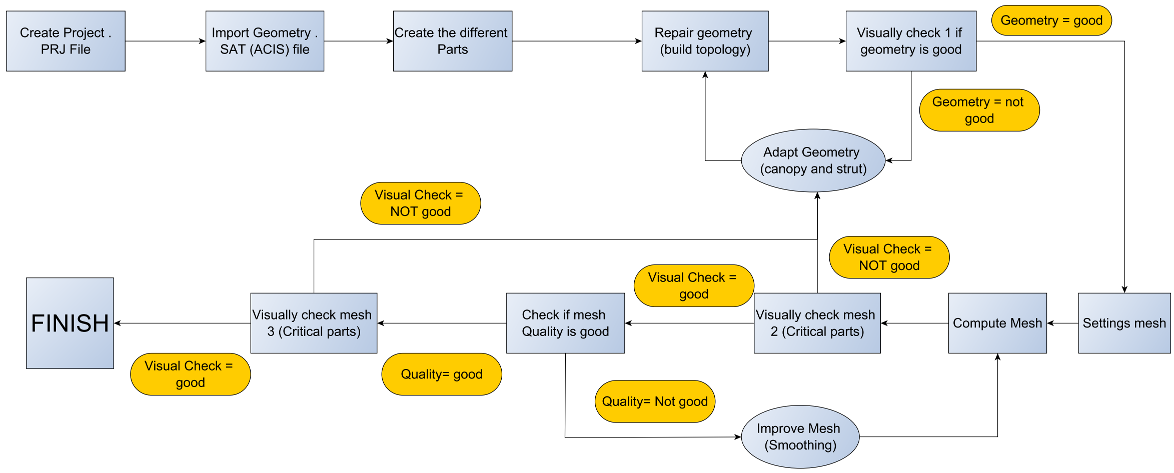


**Figure 6-11:** Flow chart of the mesh process in Icem

process step. This is not preferable, because the clearest and most structured overall process is reached when all the process steps itself are well defined and completed. In this case, that is impossible, so the mesh process step must solve a CAD process step requirement. This means evidently that the CAD- and the mesh process steps overlap each other.

### Mesh process with Ansys ICEM

The mesh process is given below.

- Export only the surfaces of the Rhino drawing as a .sat (ACIS) file.
- Importing of the Rhino drawing.
- Visual check of the drawing.
- Create different parts, for example for the different mesh densities.
- Build topology, non-manifold check. This is done by checking connectivity between the parts (see (Ansys, 2007)
- Meshing.

- Mesh check visual, for deformed mesh, difference between the imported CAD drawing. And check for two complications:
  1. Errors: Duplicate elements, Uncovered faces, Missing internal faces.
  2. Possible problems: multiple edges, Single edges, Overlapping elements, unconnected vertices.
- Mesh quality check, for the quality of the mesh.
- Improve quality if necessary (smooth Mesh Globally). The mesh quality should be as high as possible (better mesh means a better result) without reducing the the difference between the mesh and the actual CAD drawing.
- Output of Ansys ICEM as a RADIOSS file or as LS DYNA output in case of mesh flattening. in case of LS DYNA, the file must not be exported, but ”save as” must be used. If the mesh has been exported in the usual way (see C) there is no connectivity between the nodes.
- Make the output of Ansys ICEM compatible as an Input of Madymo by scripts in python.

### 6-1-4 Mesh flattening for woven material model

In Madymo various material models can be described. For the material fabric shear model, the stiffness and material properties can be assigned to the two thread directions in the woven fabric. Next to the stiffness there is the shear stiffness, which can be assigned in the model. In order to be able to assign the thread directions in the woven fabric material model, the mesh of the object (in this case the cylindrical part of the beam) can be flattened. See as an example Fig. 6-12. In this figure, an example of a passenger airbag is shown in the reference (blown up) state and the flattened state.

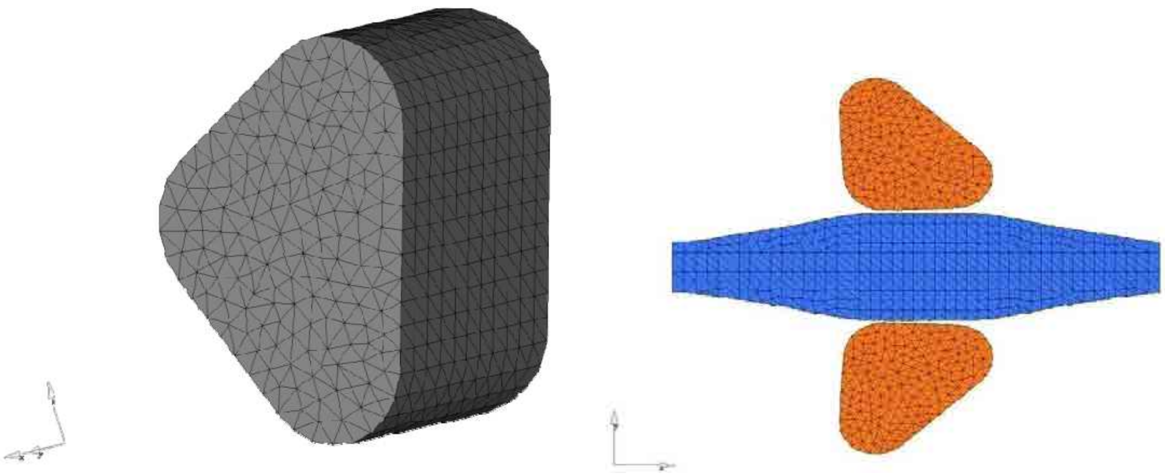

**(a)** Initial mesh **(b)** Flattened mesh

**Figure 6-12:** Example of a initial- and flattened mesh of a passenger airbag in Madymo

### Preprocessing for flattening: in ICEM

In Madymo, there are two methods to assign a woven material model to the geometry. By mapping the material directions to the curved geometry and to flatten the geometry and assign the material directions there. The possibilities for flattening are to be explored and show that this is possible, for possible future application. Within ICEM, there is no function or functionality, that can cope with mesh flattening or mesh unfolding. The flattening must be done in a different way. For this purpose, an existing matlab script is used. This matlab script has multiple ways that can flatten a mesh. The beam is used to test the flattening, to see if this is suitable for the application of beam and kite. The cylindrical reference mesh of the beam was used to test the flattening matlab script. All the seams of the cylindrical mesh needed to be identified. For this beam, this is a straightforward procedure, since in ICEM, the seams are really visible see Fig. 6-13. The nodes at the seam are split into two nodes. So two different nodes have the same coordinates.

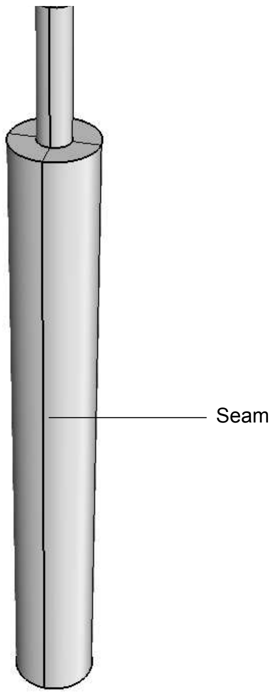


**Figure 6-13:** Seams of the beam

This is done along the seam of the cylindrical part of the beam, where the nodes with the same coordinates are connected with different elements. In Fig. 6-14, the connectivity is shown between the nodes and elements on the seams in the original (reference) and the split mesh.

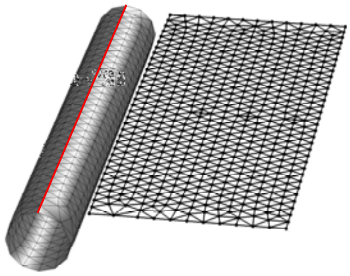

**Figure 6-14:** Split procedure of the nodes

#### Preprocessing for flattening: in matlab

So it is clear that the connectivity between the elements remains the same apart from the nodes and elements adjacent to the seams. The input for the matlab file:

Mesh flattening procedure in matlab. In this method, the mesh is flattened along the seam in the x- and y- direction comparable to the x- and y- direction of the beam in Madymo. The first trial, in order to check the mesh flattening was a square open beam with 8 elements and 8 nodes.

So for the first trial only the cylindrical part of the diamond shaped beam is considered. In Fig. 6-14, the two phases of the flattening are shown. First the nodes have to be split and assigned to the right elements. The next step is to flatten the mesh in such a way that the material direction can be assigned. In order to flatten or unfold the beam, the nodes at the edges have to be duplicated. In this way, the beam is not a closed entity, but an open beam that must be flattened into a flat square unfolded beam.

### 6-1-5 Mesh results for inflatable structures

In the previous Section, the mesh is created for the geometries that are required. The output/input requirements are set in order to import the mesh into Madymo. In this Section the result of the imported mesh is discussed. Three different discretized geometries are imported into Madymo. These different geometries are: inflatable beam including an inflator, a triangulated mesh of the V2 LEI Mutiny kite and as last a triangulated mesh of the V2 LEI Mutiny kite including the existing bridle system.

For the Madymo simulations, three different geometries are important for this research to answer the research questions.

1. Cylindrical beam including inflator.

2. Kite including inflator, LE, struts and canopy.

3. Kite including inflator, LE, struts and canopy and bridle system.

**Requirements CAD for FEM**

- Non manifold surfaces (e.g. for connection between the LE and the struts, connection for the inflator and the beam/kite, connection between the struts and the canopy and the connection between the LE and the canopy).
- The mesh should, within limits, follow the shape of the CAD input.

**Requirements mesh for FEM**

- Surface mesh
- Triangulated mesh
- At the manifold mesh surfaces: the nodes at the edge of the three adjacent surfaces should be connected to the elements in all three adjacent surfaces see Fig. 6-5
- The mesh should provide a response that is accurate within certain predefined limits, for example theory or convergence study.
- There should be nodes at the locations of the BPs on the LE

**Requirements FEM for FEM**

- The mesh has to be watertight.
- The mesh has to be just rough enough that the least computational time is needed to reach a certain accuracy.
- The BPs should be connected to the locations at the kite. The BPs are points of the bridle, which are connected to the kite. In the case of the 25 $m^2$ V2 Mutiny kite, the BPs are connected to the LE, see Figure 6-16.

From the requirements, the FEM process can be started. The basic set-up for Madymo consist of an Extensible Markup Language (XML) file. The steps to create a geometry of an inflatable model in Madymo (see (TASS, 2010d)) are:

- Importing node- and element tables from the output of the RADIOSS or (in case of mesh flattening) LS DYNA python scripts
- Include and check if parts correspond to the parts in Ansys ICEM
- Introduce holes as parts and in element table
- If woven material is used set the initial and flattened reference mesh

- Create element properties for three- node membrane elements (CST)
- Create FE groups for airbag chambers
- Creating airbag chambers, outward pointing normals with AUTO VOLUME ON
- Creating the bridle system by creating bodies at the nodes at the locations of the BPs.
- Check if the nodes of the kite are connected to the bodies of the BPs.
- Creating the belts (by connecting the correct BPs) as bridle lines and connect the correct bridle lines with tyings (as pulleys) or with knots.

As a result the geometry of the inflatable beam and the 25 $m^2$ V2 Mutiny kite as shown in Madymo can be seen in figures 6-15 and 6-16. These geometries are modeled in Madymo and used for the simulations and analysis. An important step has been made. The geometry of an entire kite including inflatable struts and a LE, canopy, inflator and the complete bridle system.

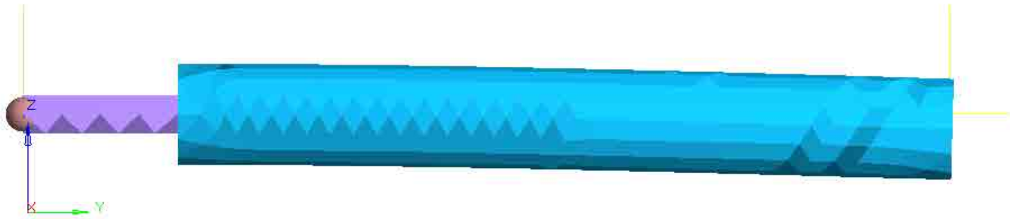


**Figure 6-15:** Madymo representation of an inflatable beam including inflator

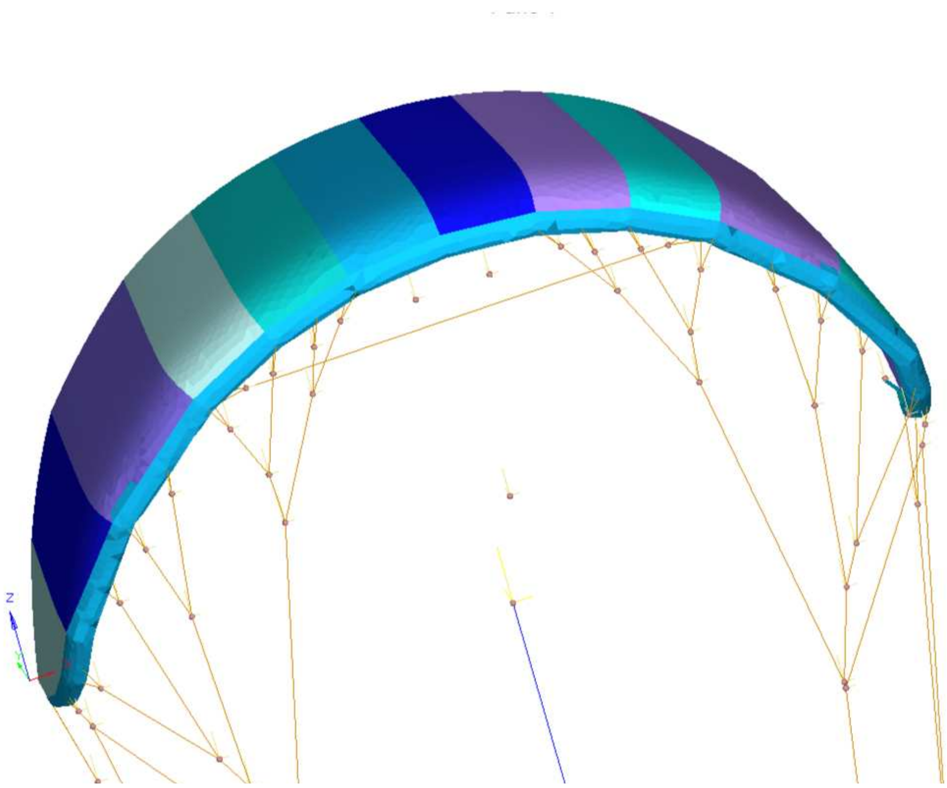

**Figure 6-16:** Madymo representation of a leading edge inflatable kite including inflator and bridle

## 6-2 Material input

This Section will explain the material inputs that are necessary in Madymo for three different material models. Material input is very important for an FEM analysis the material information determines for a great deal the behavior of a structure (Veldman, 2005).

The research sub question that is going to be answered in this Section is:

**What material properties are important for the material models?**

As explained in the introduction of this chapter, FEM should be predictive which means that with certain input variables the behavior of the inflatable structures is comparable to an actual experiment. This also accounts for the material input. The inflatable tubular structure consists of a Dacron outer layer and TPU bladder. The function of the bladder is to keep the pressure inside of the beam. The function of the Dacron outer layer is to withstand the loads transfered onto the structure. As last, the canopy consists out of Ripstop nylon. Some uni-axial tests of Dacron and Ripstop nylon have been performed by (Verheul et al., 2009) in order to discuss the requirements for fabrics that could be used for Airborne Wind Energy AWE. However, these material properties were presented very limited. The data in (Verheul et al., 2009) was limited to the stresses at four different strains. This is not sufficient for the finite element method. The raw test data was available, however there was no test description present, only the E modulus is used.

In Madymo there is an opportunity to incorporate the material properties of different material models. To model the behavior of the cylindrical inflatable beam, two models are chosen to model the fabric: isotropic linear material (ISOLIN) and a woven fabric material model (MATERIAL_FABRIC.SHEAR). In order to model the thread directions of the fabric, the mesh is chosen to be flattened according to Section 6-1-4.

In the Chapter 4-1-2, the theoretical background of the three material models are explained. Woven fabric is very difficult to model. This is due to the fact that the woven material consist out of threads. Each thread has material characteristics and the threads are woven into each other. This interaction between the threads in the different direction is called crimp (TASS, 2010d). This leads to a complex structure, of which, little data is available.

For the woven material model, more information was required and a bi-axial stress test was been performed additionally. This bi-axial stress test was performed for two reasons:

1. Acquire information that is required for the material data in Madymo for the woven material models.
2. Get more knowledge of the materials that have been used.

In order to know what information is required as material input for Madymo, the requirements of Madymo are given.

In the following sections the material requirements for the models in Madymo are explained. After the requirements of Madymo the material test results are presented. First the Isolin material model will be explained followed by the results of the uni-axial stress test. Next the requirements for the woven material models in Madymo are presented followed by the results of the bi axial stress test.

### 6-2-1 Requirements on material model ISOLIN

The first material model that is explained is the Isolin material model. Two different modules within Madymo that describe the material behavior. The first module is the material model itself. The requirements for the Isolin material model using the UP method are:

- $\rho$: Mass density of the material in kg/m$^3$.
- $E$ Modulus: Modulus of elasticity (Young) in N/m$^2$
- $\nu$: Poissons ratio in -
- TENSION_ONLY: Represents material behavior that incorporates reduced compressive stiffness
- DAMP_COEF: Material damping coefficient
- REDUCTION_FACTOR Stress reduction factor.

Next to the material model, it is important to indicate in what way the material behaves. In Madymo the material can behave as solid-, shell- or membrane elements. For fabrics, the membrane element is recommended by Madymo experts (TASS, 2010b).

- $t$: Material thickness in $m$.
- Strain_Form: The strain- and stress measures that are used.

The material density, E modulus, material thickness and strain form are obligatory inputs in order to make the model work. These are the minimal requirements to run a simulation. However, tension only is set to ON to mimic the non compressive behavior of the fabric. Material damping is derived based on experts at TASS (TASS, 2010b). When TENSION_ONLY is set to ON, the negative principal stresses are scaled down by REDUCTION_FACTOR. This reduces the ability to withstand compressive loads in the material. The reduction factor RF ($0 < RF < 1$) is a constant with which the E modulus is multiplied.

An important note must be made according to the thickness input. The E-modulus and material density of fabrics usually not given in $N/mm^2$ and $kg/m^3$. These properties are given in $N/m$ and $kg/m^2$. With the thickness of the material, the input for Madymo can be calculated.

**Density** The TPU bladder inside of the inflatable beams of the leading edge and the struts of the kite see Section 2-4 is assumed not to contribute the the strength. However it contributes considerably to the mass of the inflatable beam. The mass per unit area of Dacron is 0.170 kg/m$^2$ and the mass per unit area of TPU is 0.130 kg/m$^2$, (Verheul, 2010). Because the Dacron layer must provide all of the strength, this is modeled as one layer. To include the mass of the TPU bladder, the layer of Dacron gets a mass per unit area of 0.300 (0.130+0.170) kg/m$^2$. This, however is not the complete density breakdown. In the LE and the struts, there are seams that increase the weight of the structure and Dacron reinforcements are added distributed more or less evenly over the complete inflatable surface. The weight of the seams and reinforcements are considerable. If the weights of the seams and the reinforcements are included, the total density is approximately 2046 kg/m$^3$, this is an increase of 10 % to the specific mass. For Ripstop, the mass of the logos and the mass of the canopy itself is taken into account. The thickness of Ripstop is measured in the same way as the Dacron thickness. The thickness of 10 layers of Ripstop were measured and resulted in a thickness of 0.08 mm per layer. The sponsor logos are assumed not to contribute to the strength of the canopy, however the contribution to the density is considerable. The mass per unit area of Ripstop is 0.05 kg/m$^2$ and the mass per unit area of a sponsor logo is 0.08 kg/m$^2$ (Verheul, 2010). This leads to a density of approximately 750 $kg/m^3$.

**E modulus** Two important material inputs are required: $E$ (Young's modulus) and $\nu$ (Poisson's ratio). In order to get information about Dacron and Ripstop, uni- and bi-axial stress tests have been performed. These will be explained later in this Chapter.

**Strain Form** With respect to the strain form, the Green strain measure is recommended because the Green strain rate is objective and the time integration is objective for finite time increments (TASS, 2010d). This is confirmed by theory (Bathe, 1982) and Section 4-1-2. The stress measure that is used is the 2$^{nd}$ Piola Kirchhoff stress measure.

**Material damping** The material damping coefficient $\mu$ is assumed to be 0.1.

## 6-2-2 Results uni axial test

The uni-axial stress test was performed by (Verheul et al., 2009). The focus for the FEM application will be on two materials: Dacron and Ripstop. The uni-axial stress test for fabrics was performed according to the standard stress test for fabrics, see (ASTM, 2003). In this uni-axial stress test, the fabric is made out of strips of 50 mm wide and the length depended on the type machine used. Some results can be found in (Verheul et al., 2009). From the test only the E modulus was available. This was used in the model.

The stress/strain curves were taken from directly from the raw data from the test bench machine at the DUT. For each material (or test case) 5 strips were made and measured in the thread direction. The thickness is given as 0.17 mm for Dacron and 0.08 mm for Ripstop and the width of the test strips were 50 mm. From this test it could not be concluded whether the E modulus of Dacron and Ripstop were equal in both thread directions.

The average E modulus of Dacron is approximately 1360 $N/mm^2$ and the result of the measurement of Ripstop is approximately 600 $N/mm^2$ resulted from the analysis of the test bench software, this corresponds also to the material output in (Verheul et al., 2009).

For the Isolin material model only one E modulus is required, the preliminary assumption is made that the E modulus of both thread directions is similar.

$w^\circ$

## 6-2-3 Requirements on woven material model MATERIAL_FABRIC_SHEAR

Material fabric shear is a material model that needs a little more information compared to the isolinear material model. However the basic information is the same compared to the isolin material model. The major difference is that the Young's modulus in both thread directions (warp and weft/fill) needs to be inserted. The uni-axial stress test only gives information in one direction, therefore a bi-axial stress test is performed.

### 6-2-4 Results bi-axial test

The bi-axial test was performed at Empa. A method was developed for measuring stress/strain relation for woven materials. In this method, different load cases are evaluated. These load cases are described as ratio's between the load in warp- and weft (fill) direction. In total, 5 load ratio's were evaluated: 1:1; 1:2; 2:1; 1:5; 5:1; 1:0 and 0:1. To use these in a comparable situation for the warp and weft direction, the load ratios are normalized in warp and weft/fill direction (Galliot & Luchsinger, 2009). In appendix D, all the results of the bi-axial stress- and shear test can be found.

Each load case of the bi-axial stress test was repeated 5 times in order to remove the residual strains (Galliot & Luchsinger, 2009). The input results that are important for material models in Madymo are given in Table 6-5 in Section 6-2-5 for both Dacron and Ripstop. The $E_w$ is the Young's modulus in warp direction, the $E_f$ is the Young's modulus in fill/weft direction. The Poisson's ratios are also given in Section 6-2-5.

The shear modulus was also measured in a different bi-axial stress test. The results are shown in Appendix D

For Dacron, it can be concluded that in the thread directions the behavior behaves isolinear, because the E moduli in both directions are similar. For Ripstop, there is a difference in E modulus in both thread directions.

The bi axial stress tests are shown in Appendix D-1. The assumption that Dacron is equally strong in both thread directions is justified. The E modulus in the fill (weft) direction, denoted as $E_f$, is 0.91*E modulus in the warp direction denoted as $E_f$. The average E-modulus is assumed to be: (358,9 + 326)/(2*0.00017) = 2014*$10^3$ kN/m$^2$. The results of the shear modulus are given in Appendix D-3 shear modulus, denoted by $G_{wf}$, is between 28 and 50 kN/m. This results in a range between 165*$10^3$ kN/m$^2$ and 294*$10^3$ kN/m$^2$.

For Ripstop, the assumption that the E modulus in both thread directions is equal does not hold. This is due to an increase in thread densities in one direction. The threads in warp direction are 10 % more dense than in fill direction the source of this conclusion was given by C. Galliot through correspondance. Here the E-modulus in fill (weft) direction is 0.68*E-modulus in warp direction direction. The E-modulus of Ripstop in the warp direction is 104.4/0.00008 = 1305*$10^3$ kN/m$^2$. In fill (weft) direction this is 71.2/0.00008 = 890*$10^3$ kN/m$^2$. The results of the shear modulus, denoted by $G_{wf}$, are given in Appendix D-4 shear modulus is between 28 and 50 kN/m. This results in a range between 22.5*$10^3$ kN/m$^2$ and 27.5*$10^3$ kN/m$^2$ for the shear modulus.

An important note should be made at the tests, and that is that usually thicker fabrics are tested on this machine. It has the ability to exert a force of 10 kN on each side while, from the Uni axial tests, the breaking force of Dacron was approximately 1700 N. This is 17 % of the capability of the machine. For the shear test of Ripstop, the machine was operating in the lowest regions of the bi axial machine see comments from C. Galliot in Appendix D. The big question that remains is how accurate are the material tests?

## 6-2-5 Material input summary for inflatable structures

In this section it is shown what the input requirements are needed in Madymo. In order to respond to these requirements, uni- and bi axial stress tests have been performed. However, it is shown in the previous Section 6-1-4 that in order to include the different E moduli in both thread directions, the mesh needs to be flattened, which proved to be a difficult procedure.

In Table 6-5, the material inputs are summarized for Dacron and Ripstop from the several tests that have been performed.

**Table 6-5:** Summary material inputs for Dacron and Ripstop

| Material | | Uni-axial test | | Bi-axial test | | | |
|---|---|---|---|---|---|---|---|
| | $\rho$ (kg/m$^3$) | t (mm) | E (kN/m$^2$) | $E_w$ (kN/m$^2$) | $E_f$ (kN/m$^2$) | $\nu$ (-) | $G_{wf}$ (kN/m$^2$) |
| Dacron | 2046 | 0.17 | 1360*10$^3$ | 2011*10$^3$ | 1920*10$^3$ | 0.33 | (165-294)*10$^3$ |
| Ripstop | 750 | 0.08 | 600*10$^3$ | 1305*10$^3$ | 850*10$^3$ | 0.37 | (22.5-27.5)*10$^3$ |

There are two important conclusions from the biaxial stress tests performed at EMPA. The first conclusion is that the E modulus of Dacron is approximately equal in both thread directions, while the E modulus of Ripstop shows a difference between both thread directions. The second conclusion after discussion with C. Galliot is that the behavior of both Dacron and Ripstop could be considered linear orthotropic see comments of C. Galliot in Appendix D.

## 6-3 External load input

In this Section, the external loads are described as an input for Madymo. The three different loads that are discussed are: gravity load, Internal pressure and as last the tip force.

### 6-3-1 Gravity load for inflatable structures

In Madymo, the gravity load can be introduced on the beam as a gravity field. This gravity field can act on different SYSTEM.MODEL in Madymo and in this case only the SYSTEM.MODEL in which the beam is described. The acceleration field is denoted by LOAD.SYSTEM_ACC in Madymo. Within this acceleration field, a acceleration function must be assigned. In this case, the function is a constant line at -9.81 which corresponds to a gravitational acceleration of 9.81 $m/s^2$ in a negative direction.

### 6-3-2 Creating a constant internal pressure

There are two different methods to introduce internal pressure on the inflatable structure. The first method that will be discussed is the airbag inflation method. The second method is an artificial pressure and is called load.pres in Madymo.

#### Airbag inflation

The inflation process needs to be defined in order to put internal pressure on the beam. This process is built to maintain the volume in the beam (similar to the experiment by (Breukels, 2011)).

**Inflator**
The first item that is needed to make the inflation possible is the inflator. With the UP method in FEM, there is no jet needed for inflating the beam. An inflator in Madymo consist of a FEM part that is made from the same triangular elements (MEM3) as used for the beam. The inflator is noted as a airbag chamber, so every information, which is needed, could be made visible. In order to assign the inflator as such in Madymo, a body (BODY.RIGID including a joint) has to be assigned to the inflator. Next to this geometrical shape, a function is needed that prescribes the mass flow of air in $kg/s$. When different shapes, volumes, a lot of airbag chambers are necessary, it might be not convenient to recalculate the mass flow function for every model. So a mass flow is chosen that ensures the pressure of different beams and/or pressures.

The inflation process is modeled in a similar way compared to the experiment. The internal pressure inside the beam is induced by an inflator. The inflator introduces a mass flow of air with a prescribed mass flow function. Between the inflator and the beam, there is a hole in the connecting surface between the beam and the inflator. See Figure 6-17, for the set-up. The internal pressure is measured inside the beam. This pressure is linked to a switch and when the pressure hits the target pressure (in the reference case this is an overpressure of 0.3 bar), the hole connecting the inflator and the beam, and the mass flow to the beam is stopped. Now there is a fixed volume of air inside the beam, representing the case described in the experiment. Now including a load at the tip, this should eventually lead to a decrease in volume. This deformation, where the volume changes due to the force should lead to an increase in pressure,however since uniform pressure is assumed, the pressure is everywhere equal.

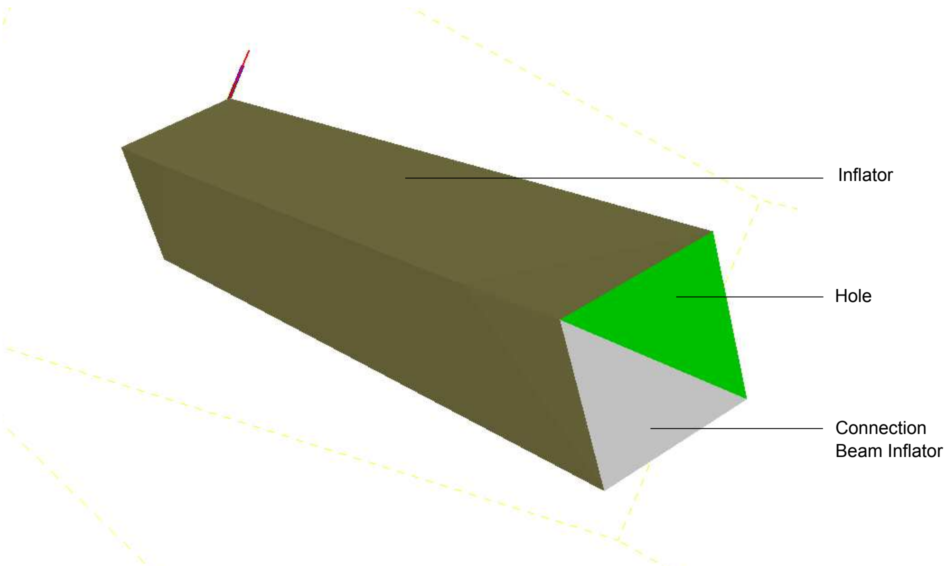


**Figure 6-17:** Inflator and connection between the Inflator and the beam including the hole

Both the inflatable beam and the inflator are considered as airbag chambers. In these airbag chambers, there are multiple sensors that can measure different variables (pressure, temperature, volume etc). These airbag chambers consist of the FEM groups of the different parts that create one airbag chamber. For example, the inflator consist of the FEM parts: inflator, connection_inflator_beam and hole. The beam consist of the FEM parts: BEAM, CONNECTION_BEAM_INFLATOR, HOLE, CONNECTION_BEAM_REF and the ENDCAP.

To model the inflation process in Madymo the sensors of the airbag chamber in Madymo are used. A lot of information is pre-set as an output entity of the airbag chamber such as temperature, pressure, mass flow rate, volume etc. see (TASS, 2010c).

Next a hole is needed to let the mass flow of air flow, from the inflator to the airbag chamber. A hole in Madymo is a material property that could be assigned to every element(s). In this particular case, the airbag chamber is the inflatable beam part. The hole has to be located in the connection surface between the beam and the inflator. The size of the hole can be scaled so that a larger or smaller mass flow flows through the hole. The hole could be connected to a SWITCH, to close the hole. HOLE_MODEL.1 should be used (TASS, 2010c). The switch is connected to a sensor, so when the pressure inside the airbag reaches the target pressure, switch is activated and the mass flow is stopped to the beam.

#### Instant static loading

This is a more artificial method compared to the airbag inflation method in order to apply internal pressure on the inflatable structure. The pressure with load.pres is created with a function that describes the pressure on the elements of the structure.

The function is in this case a constant, thus a straight line with a desired prescribed over-pressure.

### 6-3-3 Tip force

The tip force on the beam can be applied on the inflatable structure on three different ways:

1. Assign a constant acceleration field that is applied on varying masses.
2. Assign a variable acceleration field that is applied on a constant mass.
3. Assign a force function that acts on node(s).

## 6-4 Modeling approach

In the previous sections the three inputs (geometry, material and external loads) to create a FEM model using UP method in Madymo of a kite and a beam is explained.

In this section, the modeling approach is discussed.

Based on the approach, there are three steps that are performed: first a reference case FEM model will created of a cantilever beam, clamped at one end and loaded with a tip force. The next step is to see what inputs have influences on the behavior of the deflection of the inflatable beam applied with a tip force. Lastly, an experiment has to be prepared and a complete model of the kite is made, a and a similar model must be created in order to compare the experiment and the model. This because of three reasons:

1. In (Breukels, 2011) the deflection of multiple cantilever beams, made of Dacron and TPU bladder, clamped at one end, were measured in an experiment.
2. Gain confidence in using FEM in Madymo for the kite.

The reference case will be compared to an experiment and linear inflatable beam theory. The linear state of the beam will be the main focus. The input influences on the inflatable beam will be studied with a parameter sensitivity study. The important parameters will be changed one by one to indicate, whether the parameter has an influence onthe behavior on the beam. The main focus of the parameter study is the linear, or taut state of the inflatable beam. The kite will be modeled and compared to an experiment in the linear state.

The hypotheses that starts with this research is:
*If the beam is modeled accurately according to the tests and experiments in the linear state, then more complex structures, which consist of inflatable beams can be modeled also in the same method and approach.*

# Chapter 7

# Case study I: validation of a tip loaded inflated cantilever beam

In this chapter, the inflatable beam is analyzed. An experiment with an inflatable cylindrical beam is performed by (Breukels, 2011), this experiment is described in Section E and in (Breukels, 2011). The overview of the experiment is displayed in Fig. 7-1and a reference beam is modeled in FEM in Section 7-1 with inputs obtained from the previous chapter. The results of the FEM model, beam theory from (Le & Wielgosz, 2005) and the experiment are compared and discussed in Section 7-3. In Section 7-4 the results are discussed based with regard to the linear beam theory (Le & Wielgosz, 2005), experiment, input and model. To investigate the influence of the important parameters of the FEM model, a parameter sensitivity study is performed in Section 7-5. Some of the parameters have also been measured in the experiment so the parameter study is concluded with a comparison between the experiment and the models. Lastly a conclusion is given.

The experiment overview is given and shown in Fig. 7-1.

## 7-1 FE Madymo model set-up

The research subquestions that will be answered in this section is:

- **Is it possible to create and analyze a straight inflatable beam model, which can be loaded with a tip force and a desired internal pressure?**
- **How accurate does this model describe the load versus deflection curve compared the experiment performed by (Breukels, 2011) and theory?**
- **Is it possible to analyze the beam in the linear state. For example to check strains and stresses in the beam?**

**Figure 7-1:** Overview of the experiment (Breukels, 2011)

In order to validate the FEM model, a beam has been created comparable to the experiment, described in Breukels (2011) and Section E. A few comments must be made. The seams of the beam, which are present in the actual inflatable beam are not included in the model. Also the way the forces are introduced to the beam is different. In the actual model, the force is introduced by a small strap. In the model, the force is introduced via the whole surface of the endcap. Another difference is the measurement of the deflection. In the actual beam, the deflection is measured in $z$ direction at the bottom of the plate on which the masses are introduced. In the model a node at the endcap is taken to measure the displacement in $z$ direction. The strap might introduce stress concentrations near the contact surface of the strap, however, this was not recorded during the experiment. The clamping of the beam is also not equal. In the model, the Degrees of freedoms (DOFs) of the nodes in the endcap attached to the wall are all fixed. It is not possible to "freeze" all DOFs, but this is done as best as possible by fixing the end at a wooden frame, which is fixed to the big frame. In this section the model set-up in Madymo will be discussed. The FEM beam model is expected to behave similar to the experiment in the linear region if the input of material, geometry and external forces are correctly implemented. The mass of the beam in the experiment, behind the strap where the force is connected is neglected in the FEM model. This beam part has a length of 0.2 m, a diameter of 0.13 m and a specific mass of Dacron and TPU is 0.3 kg/m$^2$. This leads to a mass of 0.028 kg.

### 7-1-1 Beam geometry

In the model there are several parts generated from the mesh program ICEM. This is split-up in order to get a distinction between the parts. These are the parts for the complete inflatable beam:

1. Inflator
2. Connection_beam_inflator

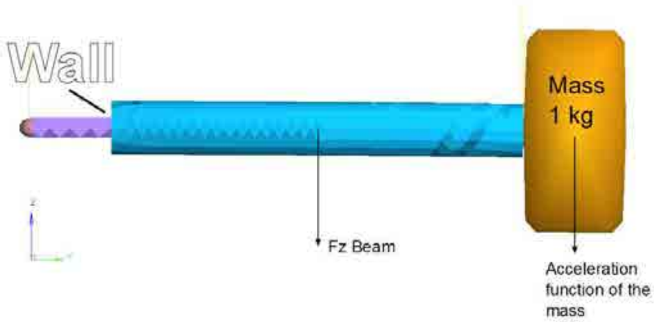


**(a)** Mass model

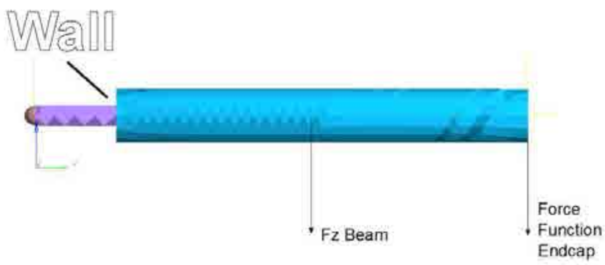


**(b)** Element Mass model

**Figure 7-2:** The two different models of the inflatable beam for the reference case

3. Hole
4. Beam
5. Connection_beam_ref
6. Endcap

See Fig. 7-3 for the model and the location of the parts. The inflator is a cylinder that has a hole at one end that ensures the inflation of the beam. This part is connected to the reference space (attached to the earth). The connection_beam_inflator part is the part that connects the beam and the inflator and is the non manifold surface. The beam part has a cylindrical (depending on the number of elements) shape. The last part is the endcap where the forces will be applied at.

The distinction between the parts is important because of several reasons:

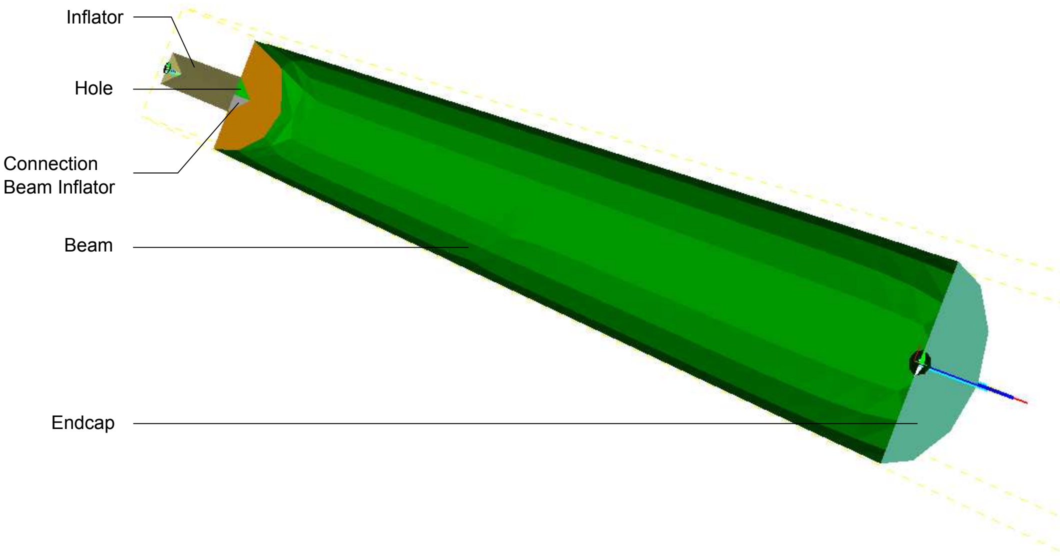


**Figure 7-3:** Intersection of the beam including the parts of the FE model in Madymo

1. The DOFs of the nodes in the parts inflator and the Connection_beam_ref are fixed. This means that the nodes remain in the same location. The stresses and the strains will increase however this will not influence the parts that are of interest for the deflection of the beam.
2. The cylindrical part (beam) might be flattened in a later stage.
3. The hole to ensure for the mass flow of air from inflator and the beam. When the desired predescribed pressure is reached, the hole is closed. This is done by multiplying the massflow by zero.
4. At all the nodes of the endcap, the force (forces, or mass attachment) is applied.

The number of elements is important for accuracy and computation time (Bathe, 1982). This will be described later in Section 7-3-1 as a convergence study.

## 7-1-2 Beam material in Madymo

A model set-up in Madymo for bending will be given in this section. However the fundamentals of the Madymo model should be explained. The material inputs for two Madymo material models can be found in Chapter 6-2-5. The model set-up will be given based on a reference case. This reference case is a beam with length of 1 m, diameter of 0.13 m, E-modulus of 1360 N/mm$^2$ material thickness of 0.17 mm, density of 2046 kg/m$^3$, isolin material model.

The material model used in Madymo for the reference case is isolin. This a linear material model, which means that there is a linear function between the strain and the stress of the material used. This means a constant E-modulus for the complete of the material range. The linear relation between strain and stress was concluded from the bi-axial material test performed by EMPA is Switzerland. There after performing the biaxial test, a linear relation was found that fitted quite good with respect to the material tests (correspondence EMPA). In chapter D the bi-axial test results can be seen as well as the uni-axial stress test results.

At the actual beam, there are material imperfection and the beam is sewn together manually leaving folded closing seams closing up the beam. Furthermore, only the Dacron material layer is modeled, because the $TPU$ bladder does not add to the stiffness of the beam. The material stiffness originates fully from the Dacron material layer. However, the mass of the $TPU$ bladder is taken into account into the density of the material.

**Element type**
A triangulated mesh including CST membrane element is used. For the kite it might be necessary to refine the elements, this can be done with triangulated CST membrane elements. This membrane element cannot withstand out of plane bending moments (TASS, 2010d). Dacron and Ripstop are assumed to behave like a membrane and that the materials cannot compress.

## 7-1-3 External loads

Three external loads are explained in this Section. The first load is the internal pressure on the beam, the second load is the tip force and the third load is the gravity.

#### Internal pressure

The internal pressure is also an external load. It is applied externally on the elements. For the UP method, two different methods are used. These are load.pres and airbag inflation, both processes are described in Section 6-3-2. This is described for a general case, now the internal pressures of the beam will be discussed.

**Airbag inflation**

A recap of the airbag inflation process is given first. The input of the airbag inflation is a mass flow of air that is coupled to the inflator. The air flows through a hole, which is in "open" state into a closed volume that is denoted as an airbag chamber. In this airbag chamber, a sensor is connected to a switch. If the pressure inside the beam reaches a predescribed reference pressure, the switch is activated and the hole is "closed". The volume inside the airbag chamber and thus the beam will remain equal, however the pressure can increase during the bending of the beam. This is due to the change in shape and thus volume when the tip force is applied. The pressure inside the inflator does not have influence on the behavior of the clamped cantilever beam, because the (DOFs) of all the nodes of the inflator are fixed.

#### Tip force

The tip force on the beam are modeled in two methods:

1. Attaching a Mass of 1 kg to the endcap and apply a linear rampfunction of the gravity field from from 0 to 98.1 m/s$^2$ from t = 0 to t = 18 seconds. The complete simulation takes 20 seconds, however the first 2 seconds are used for inflation of the beam and settling of the beam. In this time, no force is applied to the beam. The mass of 1 kg combined with a acceleration field results in a linear function of the tip force from 0 to 98.1 N in 18 seconds. The center of gravity is located at the center of the endcap and all the nodes are connected to the mass. This is called the Mass model, see Fig. 7-2a. The center of gravity is attached to a node in the middle of the endcap. The shape is merely for visual representation.
2. Using Element.Mass (EM) in Madymo and apply forces on the nodes of the endcap from 0 to 98.1 N in 18 seconds see Fig. 7-2b.

### 7-1-4 Beam Support and constraints

For the clamping of the beam, all the DOFs of both the nodes of the inflator and the endcap connected to the inflator are fixed. This is shown in Fig. 7-4, where the dots represent the nodes of the inflator and the connection between the reference space and the beam. The restraints are shown by triangles.

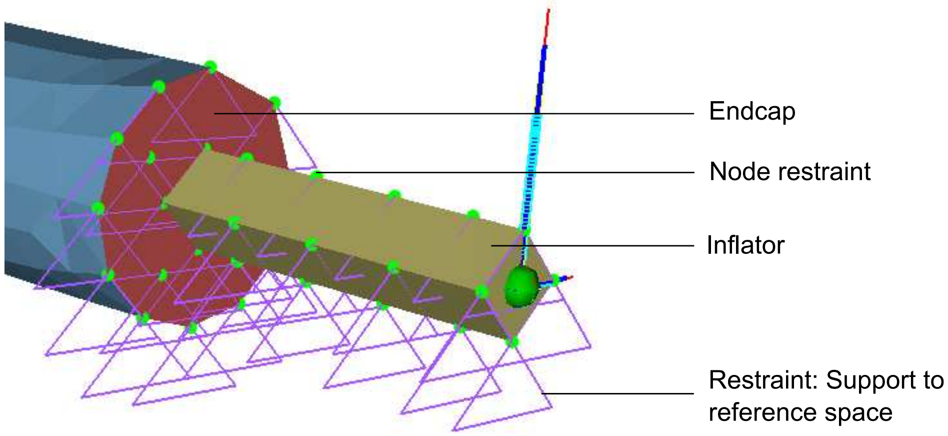


**Figure 7-4:** Clamped end of the model

## 7-2 Reference case input summary

In this section a summary is given of the parameters that are used for the reference model. A reference case has been created to compare the results of the inflatable beam. The parameters of the reference case for the beam are split in four groups: geometrical-, external load-, material-, "general" Madymo parameters.

The details are given in Table 7-1

The constant Rayleigh damping ($\alpha = 1000$) is used for the tip force method 1, the varying Rayleigh damping is a step function from that steps from $10e^4$ to 10 at t=0.1 is used for tip force method 2. The Rayleigh damping of 10 corresponds to a realistic value and is advised to be used by (TASS, 2010b).

**Table 7-1:** Input parameters of the reference case for the inflatable beam

| Group | Parameter (Unit) | Value |
|---|---|---|
| Geometry | Diameter (m) | 0.13 |
| | Length (m) | 1 |
| | Element - | CST |
| | Number of elements for the cylindrical beam | 1000 |
| External loads | Internal (over)pressure (bar) | 0.3 |
| | Tip force method 1* (N) | Varying |
| | Tip force method 2** (N) | Varying |
| | Gravity: constant acceleration field ($m/s^2$) | 9.81 |
| Material | Material Damping $\nu$ (-) | 0.1 |
| | Material thickness (mm) | 0.17 |
| | E-modulus $N/mm^2$ | 1360 |
| | Density $\rho$ ($kg/m^3$) | 2046 |
| | Poisson's ratio $\mu$ (-) | 0 |
| Madymo setting | Rayleigh damping $\alpha$ (-) | 1000 |
| | Rayleigh damping $\alpha$ (-) | Varying |

* Tip force method 1: constant mass and rampfunction gravitational field.
** Tip force method 2: element.mass and rampfunction force field on endcap.

## 7-3 Results of the reference case

In this section, the results are shown of the reference case. First the preparation of the model is described. This preparation describes methods to apply the force to the tip of the beam and the slope of the force function is discussed. Next a hypotheses is given to indicate the expectations based on literature, theory and the experiments. The results are given as animated frame shots of the general behavior of the inflatable beam. As a third result, deflection curve as a function of tip force. Lastly the stresses are shown of the elements at a cross section of the beam.

### 7-3-1 Preparation of the reference case

For this reference case, the results of the simulation can be shown and compared to the measurement data from the experiment. Especially as the load is applied on the beam, there are some variations. In Fig. 7-5 and Fig. 7-6 the response is shown to three different force ramps for EM tip force and the Mass model is plotted in the figures:

1. The first force ramp is from 0 to 98.1 N in 18 seconds
2. The second force ramp is from 0 to 98.1 N in 48 seconds
3. The third force ramp is from 0 to 98.1 N in 98 seconds

The objective of this comparison is to determine if the 18 second ramp is not too steep. The main focus is at the taut region and is the linear part of Fig. 7-6.

There are several interesting results be seen in Fig.7-6. In this figure, the force ramp of 18 seconds is almost equal in the EM models with other two force ramps. Secondly, the Mass model behaves a little more stiff compared to the EM models. It is expected that this is the reason for the Rayleigh Damping of 1000.

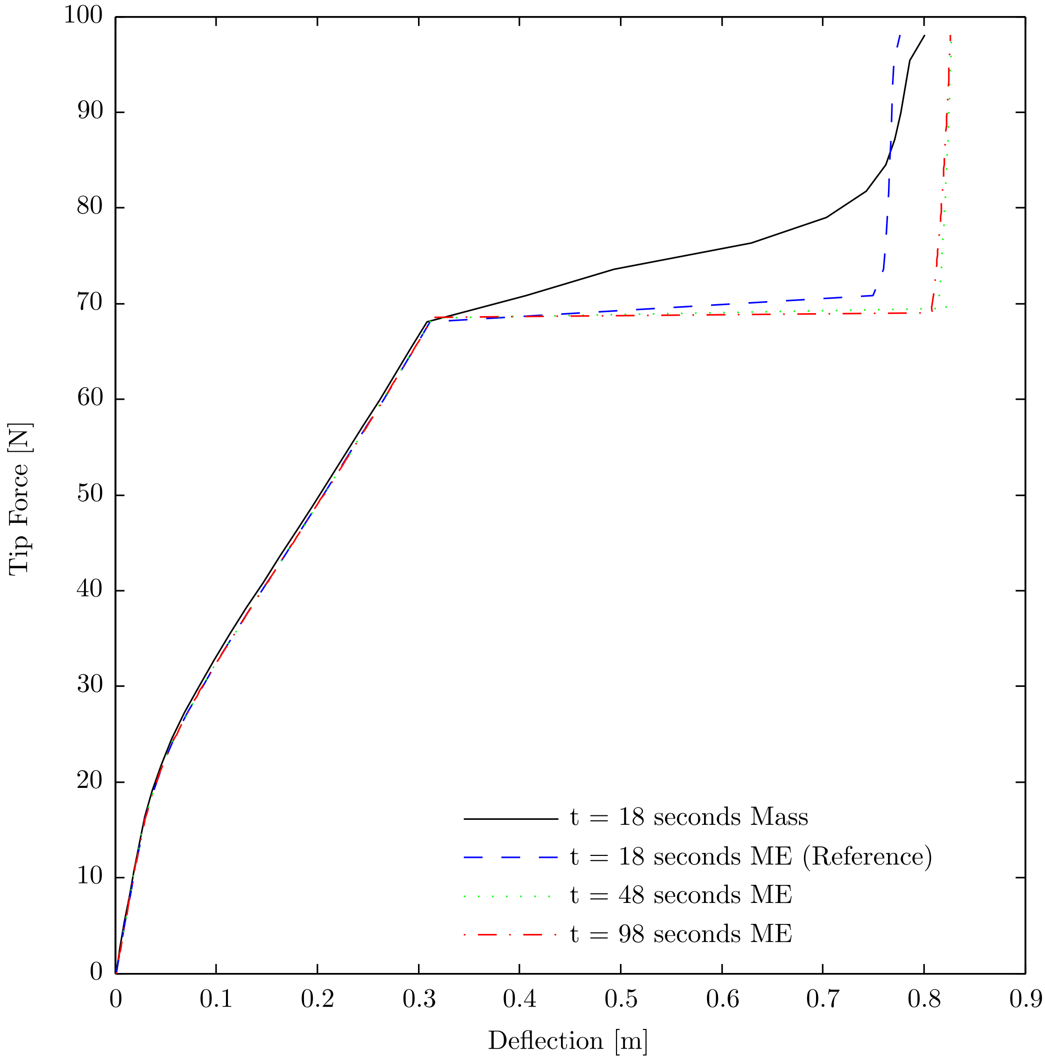


**Figure 7-5:** Influence force rampfunction at different ramp slopes

## Mesh convergence

To determine the number of elements, a convergence study is made, see Fig. 7-7 for the result. The tip force function applied to the beam described in the previous section. In Fig. 7-7 deflection of the beam as a function of the number of elements, see Fig. 7-7. On the horizontal axis, the deflection is shown and on the vertical axis, tip force is displayed. In Fig. 7-8 a detail is shown from Fig. 7-7.

Fig. 7-8 the linear, or taut, part of the curves that ranges from 0 to approximately 14 N the behavior seems very similar. In the non linear, or wrinkled part, ranges from 14 till 23 N, the difference is larger between the curves in number of elements.

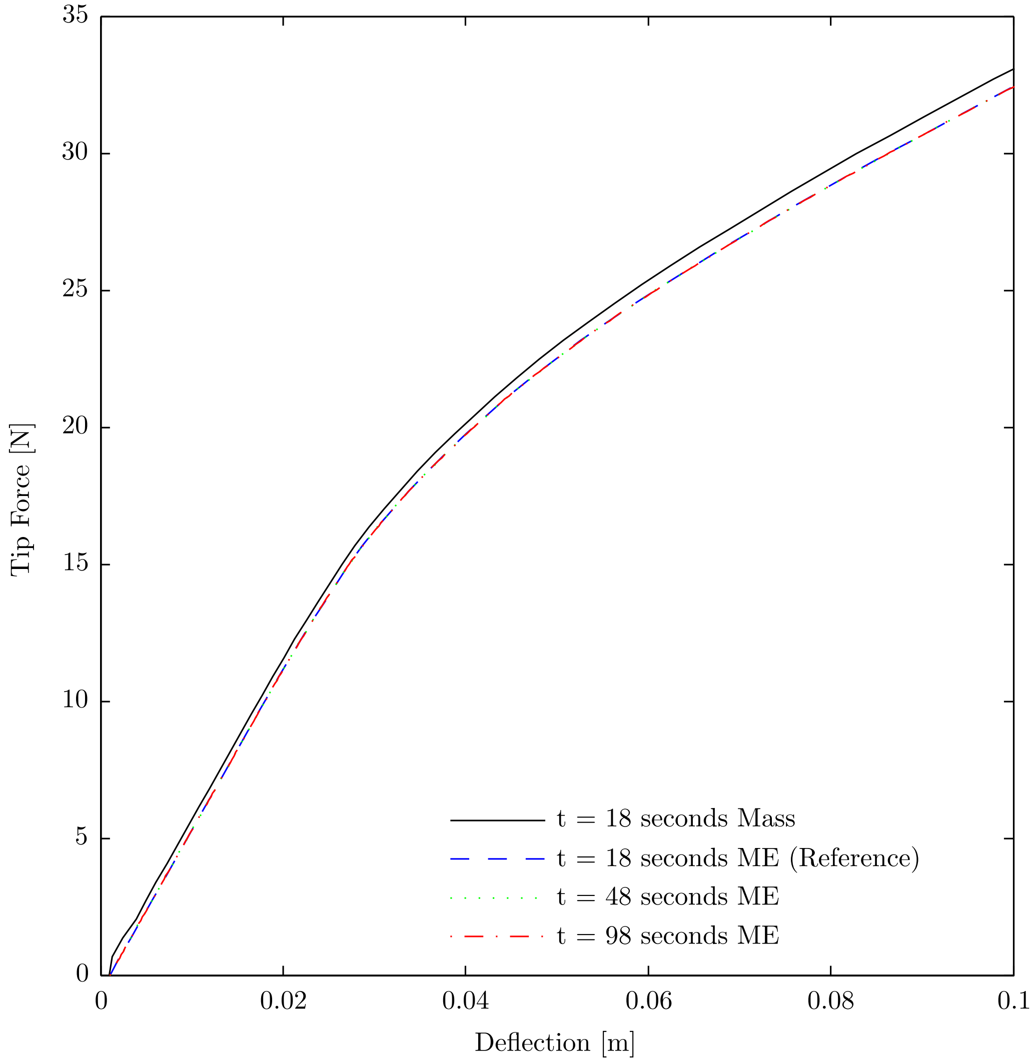


**Figure 7-6:** Detail of Fig. 7-5

The behavior of the beam behaves like expected from theory see Fig 3-5 in Section 3-2-3. the three states of inflatable beam behavior, taut, wrinkle and collapse, can be seen in the Fig. 7-7.

The curves in Fig. 7-8 are very close to each other, so in order to get a clear view of the convergence, the deflection of the beams with different number of elements are plotted at different tip forces. This is shown in Fig. 7-9, where the general behavior seem converge with increasing numbers of elements.

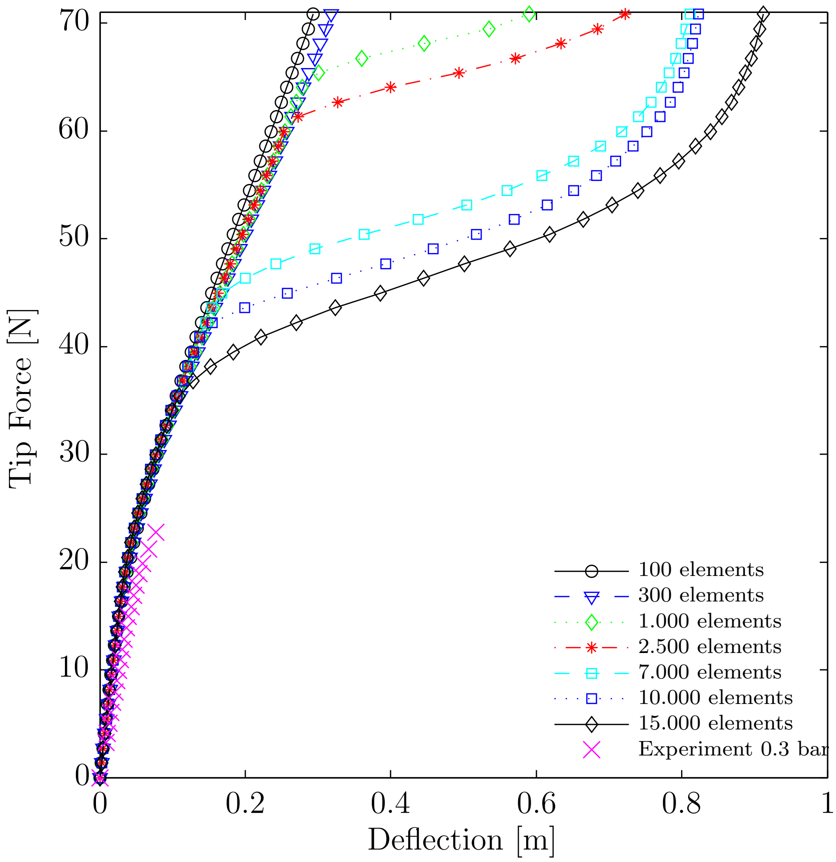


**Figure 7-7:** Convergence study of inflatable beam at different forces

For the analysis of the linear or taut region, the beam of 1000 elements is going to be used. In the convergence Fig. 7-9, 1000 elements is considered converged to a solution only the linear part, this to reduce computation time for the simulations. The collapse cannot be taken into account the results might be unreliable because for collapse, the solution is not converged.

## 7-3-2 Hypotheses

In this section a hypotheses is given for the results of the reference case. In this hypotheses the prognoses are set for the three regions of inflatable cylindrical beams: taut, wrinkled and collapse region of the beam.

The tip deflection of the model is given with respect to the experiment by (Breukels, 2011) and described in E-3-2 both for the taut and the wrinkled region. In the taut region, the tip deflection is compared to theory described in (Le & Wielgosz, 2005), because the theory is valid with the assumption of small displacements.

Equation 7-1 describes the theory of the displacement v(x) at tip load $F_{tip}$.

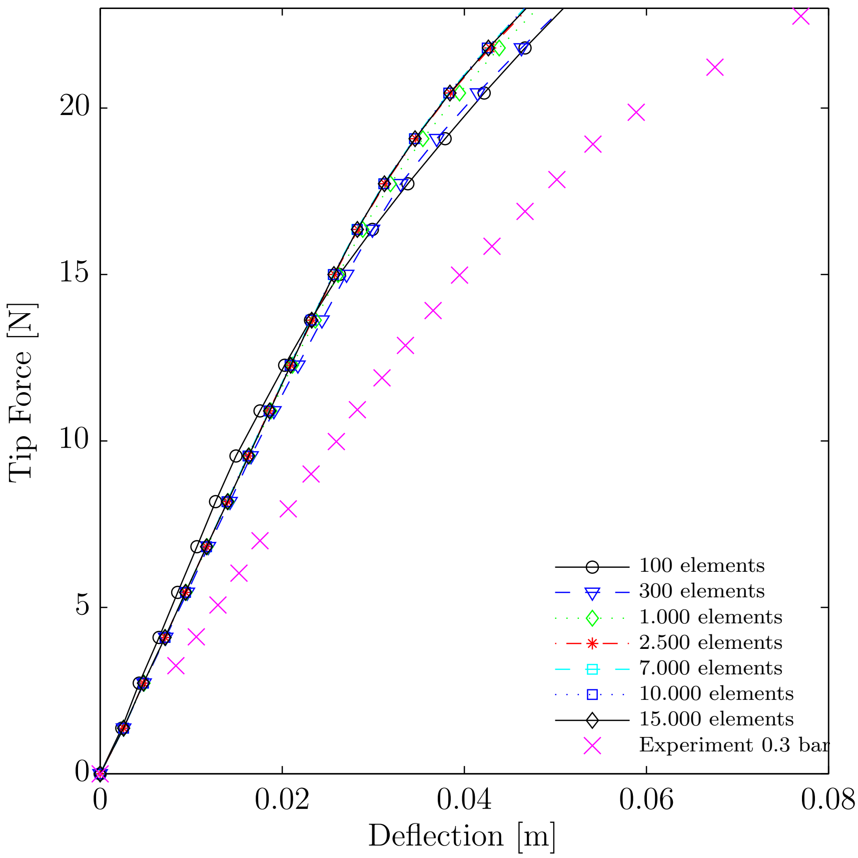


**Figure 7-8:** Convergence study of inflatable beam at different forces detail of Fig. 7-8

$$v(x) = \frac{F_{tip}}{(E + pA/S)\, I} \left( \frac{Lx^2}{2} - \frac{x^3}{6} \right) + \left( \frac{F_{tip}x}{pA + kGS} \right) \tag{7-1}$$

Here E is the E modulus of Dacron, S is the area of the cross section at t = 0 seconds, A is the surface of the endcap of the beam, p is the internal pressure, I is the $2^{nd}$ moment of inertia, k is the correction shear coefficient and is 0.5 for circular thin walled tubes (Le & Wielgosz, 2005), G is the shear modulus. The hypotheses is that in the taut region with a tip force of 6 N and 9 N is accurate within 5 % of the average between the theory of (Le & Wielgosz, 2005) and the experiment. In the wrinkled region with a tip force of 20 N, the error is estimated to be 10 %. The values of thickness, radius and length of the beam (and thus I, A, S and L) all depend on the pressure. These values are calculated using formulations for small strain analytical solutions (Le & Wielgosz, 2005).

Collapse is not considered to be a focus in this thesis. The collapse values shown especially in the graph with 1000 elements should be evaluated with care, because in the collapse region for 1000 elements, the mesh is not converged yet. It is even a question if the beam is converged at collapse with 15000 elements. However, taken the simulation time in consideration and

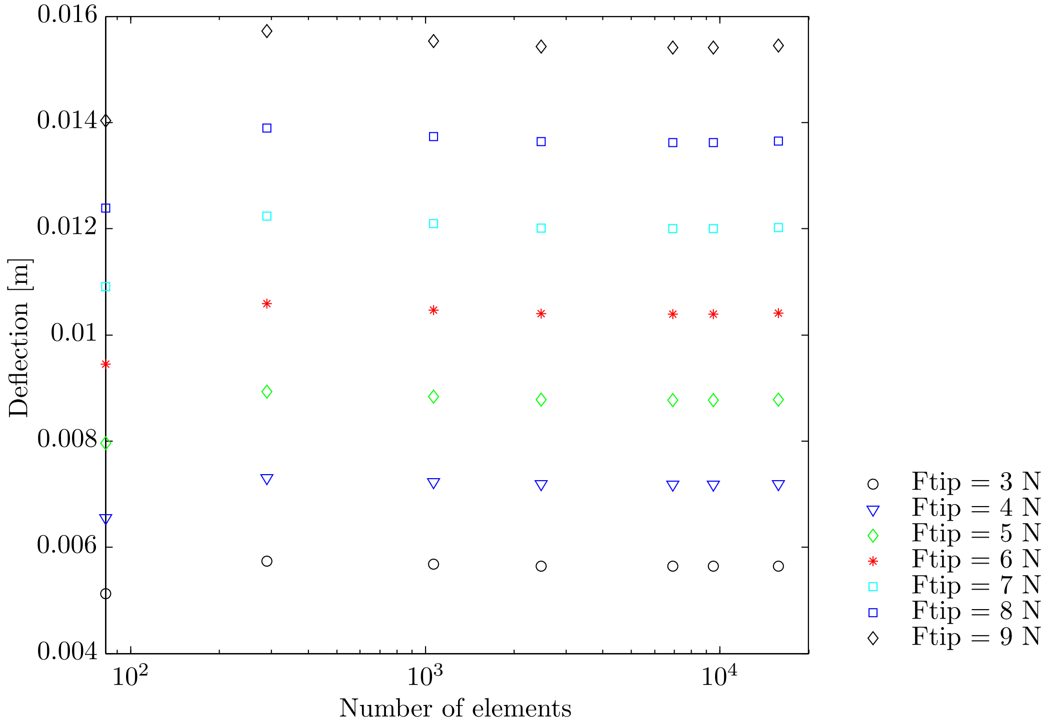


**Figure 7-9:** Deflection of the beam at different tip forces

the main focus in this thesis is the linear and first wrinkle states, further refinement was not included. The collapse proved to be more difficult to validate with FEM compared to the taut region as shown in (Veldman, 2005). The collapse theory that is taken from (Stein & Hedgepeth, 1961). The collapse research proved to be not suited as a goal in this thesis. In Table 7-2, the overview is shown with the collapse at 15.00 elements.

**Table 7-2:** Results inflatable beam collapse force

| Region | Collapse force (N) | | |
|---|---|---|---|
| | Experiment | Theory Stein(1961) | FEM model 15.000 elements |
| Collapse | 22.8 | 25.9 | 38 |

### 7-3-3 Internal pressure of an inflatable beam with a tip force

In Fig. 7-10 the pressure sensor of the airbag is shown as a function of time and the switch activation as a function of time is given. Here the pressure 0.3 bar overpressure is displayed. In Fig. 7-11 the pressure of the inflator is displayed. The pressure increases in the inflator to a pressure of $3.2 * 10^6$ N/m$^2$. This is high, however, because the degrees of freedom of the inflator and the endcap connected to the inflator are locked the pressure is assumed not to have an influence of the bending behavior of the inflatable beam.

Outward pointing normals for the airbag chamber pointing outward of the airbag. This can be set with AutoVolume = ON. This is assumed to be necessary because in between the beam and the inflator, there the non manifold surface see Section 6-1-2. This surface shares two volumes, the volume of the inflator and the volume of the beam. The volume calculation in Madymo defines the volume inside a chamber if all element normals point out of the enclosed volume and secondly, the mesh must be closed.

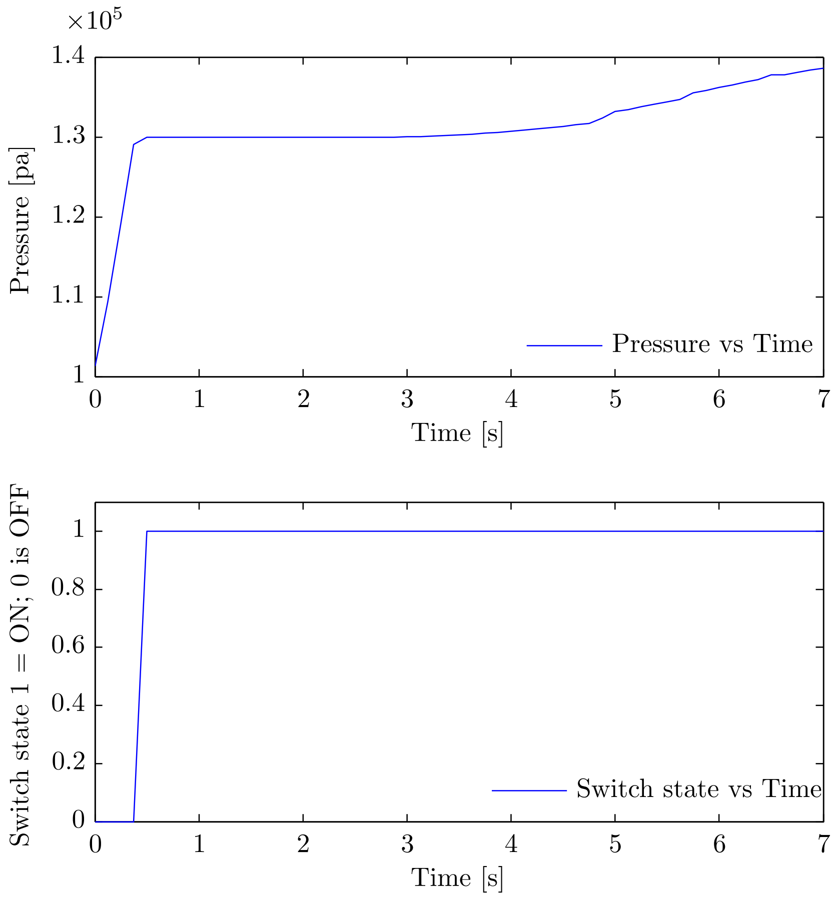


**Figure 7-10:** Pressure sensor of the airbag and the switch activation

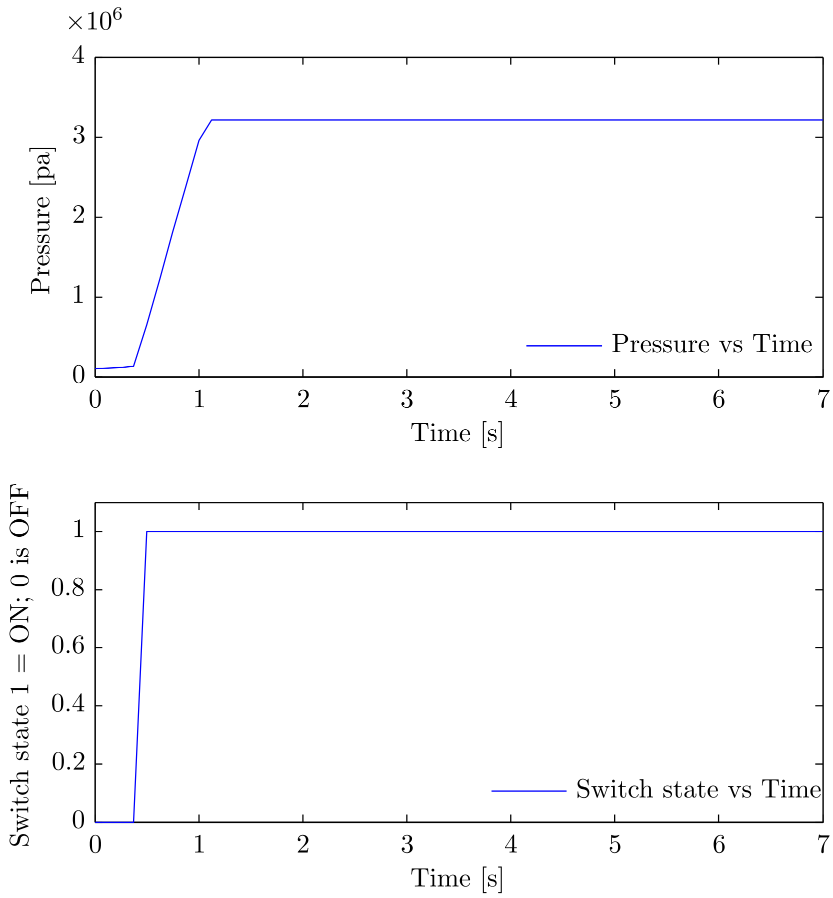


**Figure 7-11:** Pressure sensor of the inflator after the hole is closed

## 7-3-4 Deflection versus tip force curve

In the Fig. 7-12 and Fig. 7-13 the results of the deflection as a function of the tip force are shown.

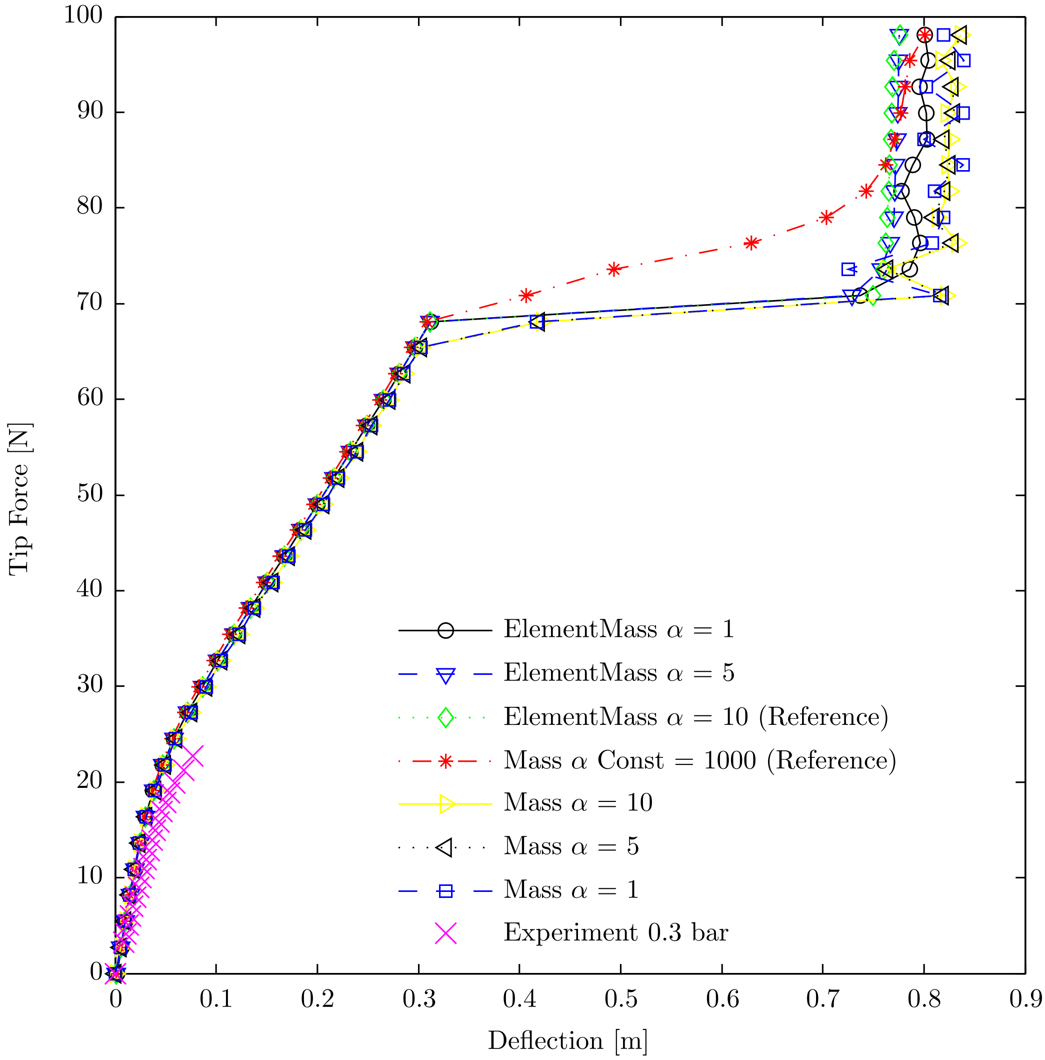


**Figure 7-12:** Reference case study

The plots of the experiment show deflection versus tip force. The Madymo output are time history plots, the input of the tip force acting on the beam is also a function of the time. In Matlab, these two plots are converted into one plot that shows the deflection as a function of the tip force.

In Fig. 7-12, Fig. 7-13 and Fig. 7-14 the results are shown of different Rayleigh Damping coefficients of EM and Mass models together with the experiment and theory described in Eq. 7-1.

For the Element Mass models, the Rayleigh Damping coefficient show little differences between the different curves of EM with Rayleigh Damping coefficient of 1, 5 or 10. The curve of

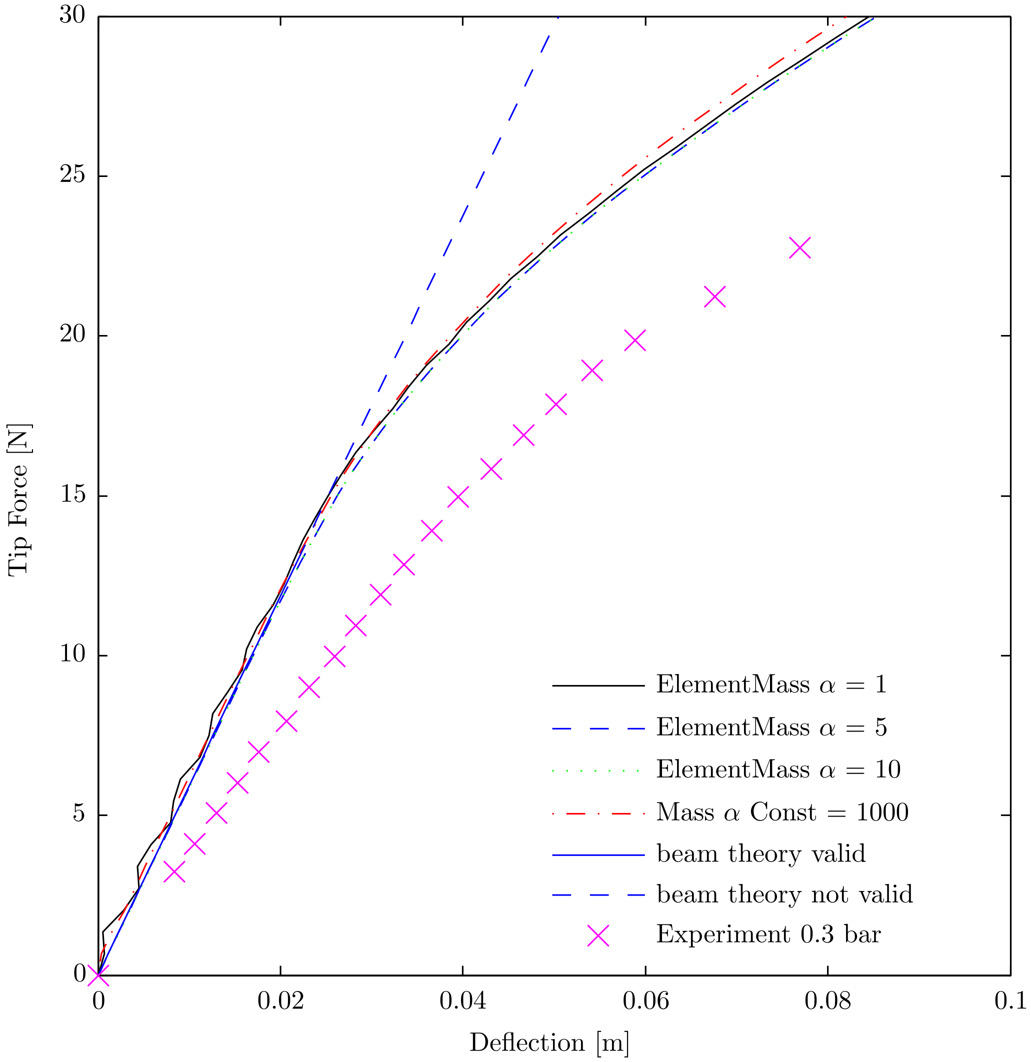


**Figure 7-13:** Reference case study detail of Figure 7-12

Rayleigh Damping of 1, shows a vibrating motion from F = 0 to F ≈ 12 N. From the Mass model, the curves of a Rayleigh Damping coefficients of 1, 5 and 10 also coincide. However with the Mass model, the curves show a vibration in the range from a force of 0 N to force of 30 N. The curve shows this vibrating motion probably due to the introduced moment of inertia of the mass. The Mass model with Rayleigh Damping coefficient of 1000 show steady behavior. The curves with a vibrating motion cannot be used for the analysis, so for the EM model a Rayleigh Damping coefficient of 10 is chosen and for the Mass model a Rayleigh Damping coefficient of 1000 is chosen. This value is high, however the force motion is slow, so this has little effect on the behavior of the beam. For the EM model, a Rayleigh Damping

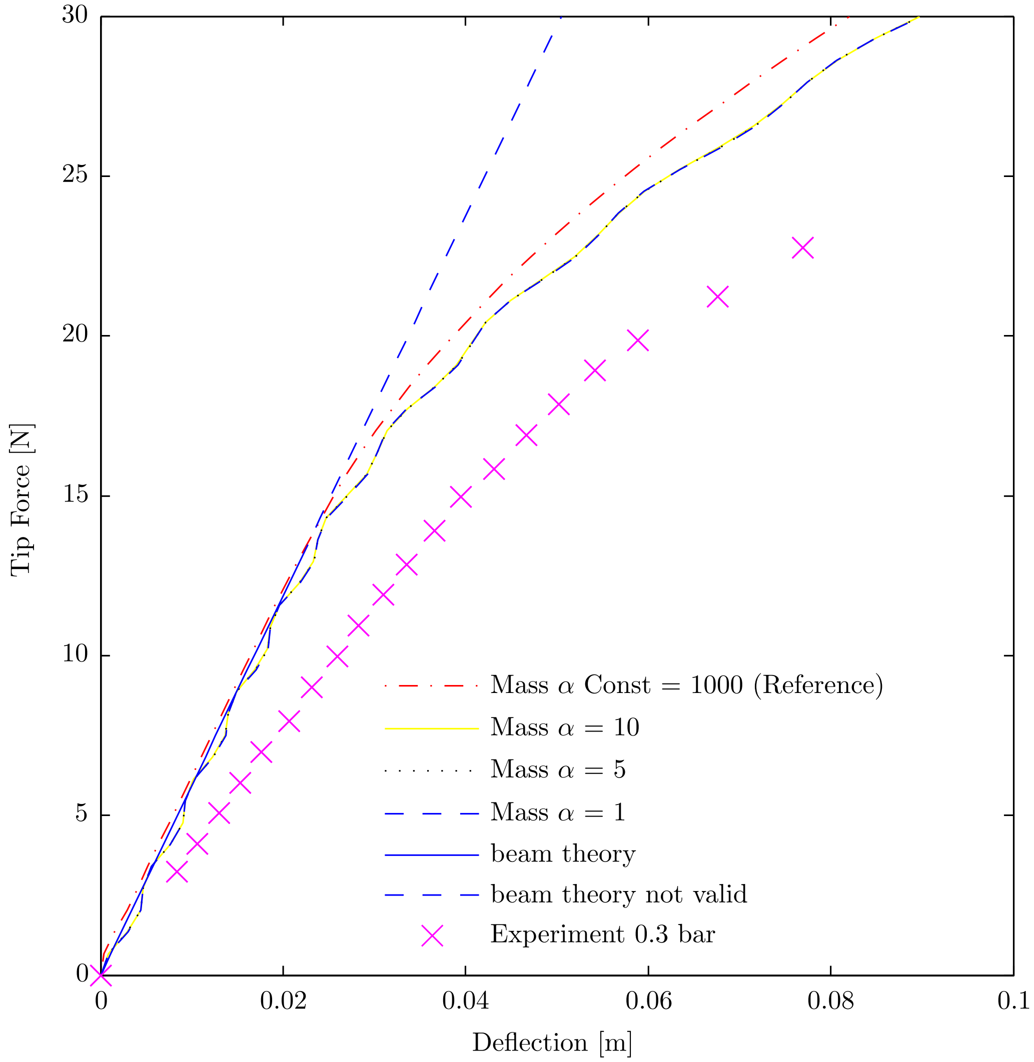


**Figure 7-14:** Reference case study Mass and gravity field

of 10 is chosen to exclude vibration to distort the measurements.

In Fig. 7-15, there are four different frame shots from the inflatable beam of the Mass model with $\alpha = 1000$.

In Fig. 7-16a, Fig. 7-16b and Fig. 7-16c stresses in the material are shown in the taut region. In the wrinkled region, the stresses are shown in Figure 7-17a and in Figure 7-17b, the stresses are shown during collapse. In Figure 7-17c another method to visualize the stresses is shown. Here the stresses are shown by vectors and colors. As expected is the stress near the clamped part the largest and near the collapse moment (approximately t = 12.72 s). The actual value of the principle stresses cannot be observed in these plots, another visualization is necessary

**(a)** t = 0.0, Ftip = 0 N s

**(b)** t = 2.0, Ftip = 10.9 N s

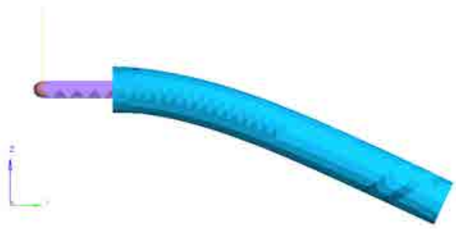

**(c)** t = 12.6, Ftip = 68.7 N s

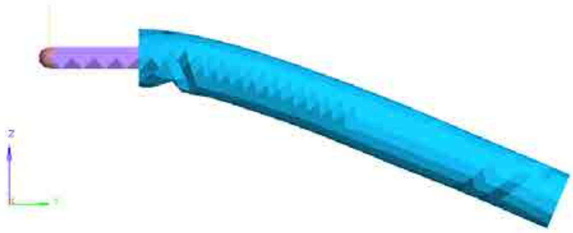

**(d)** t = 12.64 Ftip = 68.9 N s

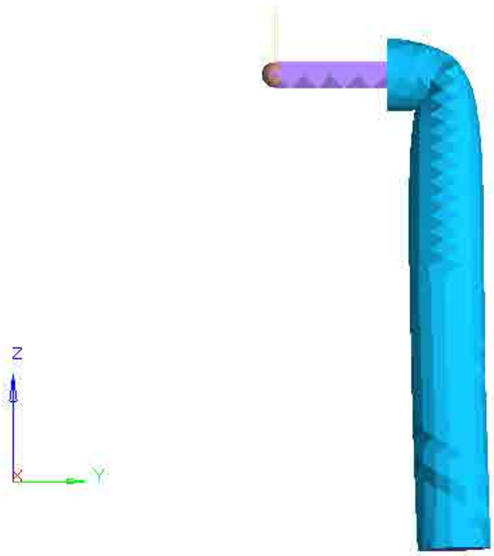


**(e)** t = 12.72 Ftip = 69.3 N s

**Figure 7-15:** Frameshots of the dynamic model

to investigate the loacation of wrinkling ($\sigma_2 \leq 0$)In contrast to membrane theory ((Stein & Hedgepeth, 1961), (Wielgosz & Thomas, 2002)), here the stresses are assumed zero when wrinkles begin to occur.

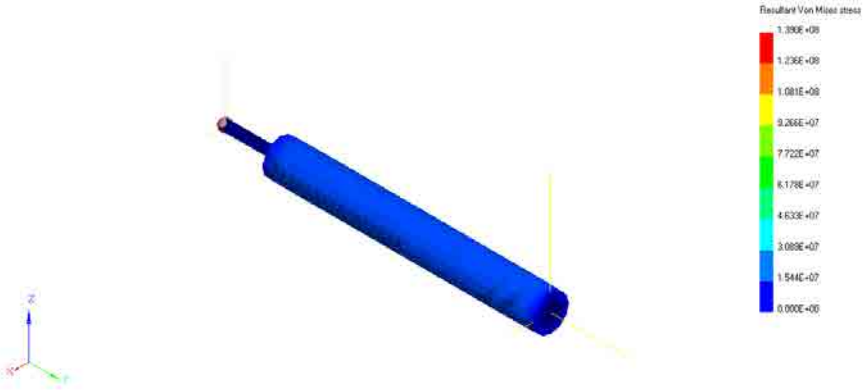


**(a)** t = 0.0, Ftip = 0 N s

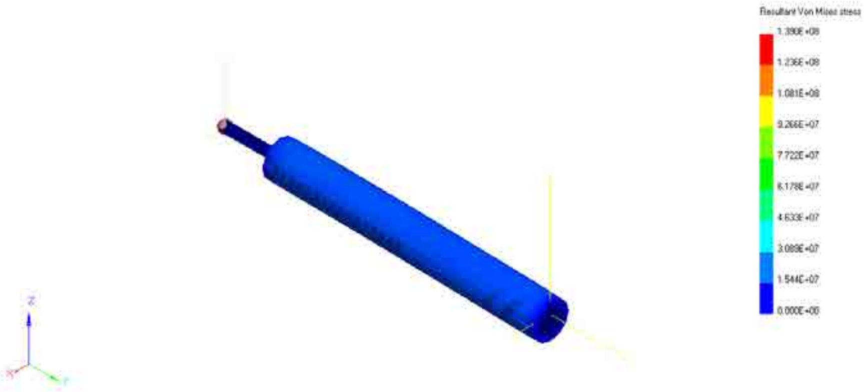


**(b)** t = 2.0, Ftip = 10.9 N s

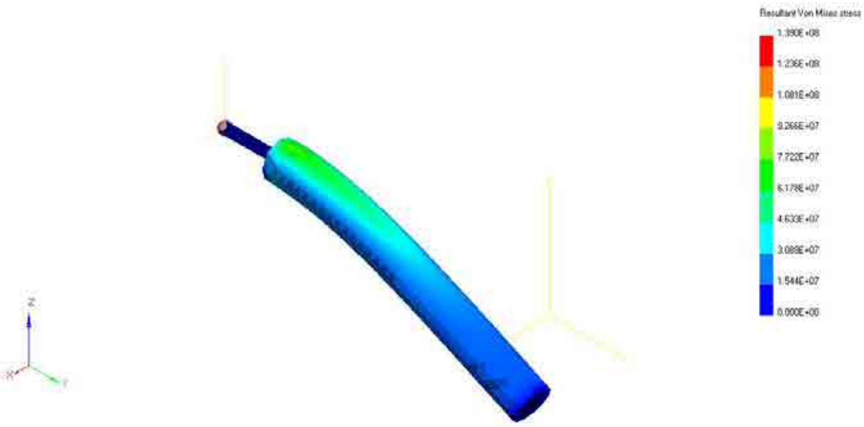


**(c)** t = 12.6, Ftip = 10.9 N s

**Figure 7-16:** Von mises stresses in the beam at different points in time in taut region

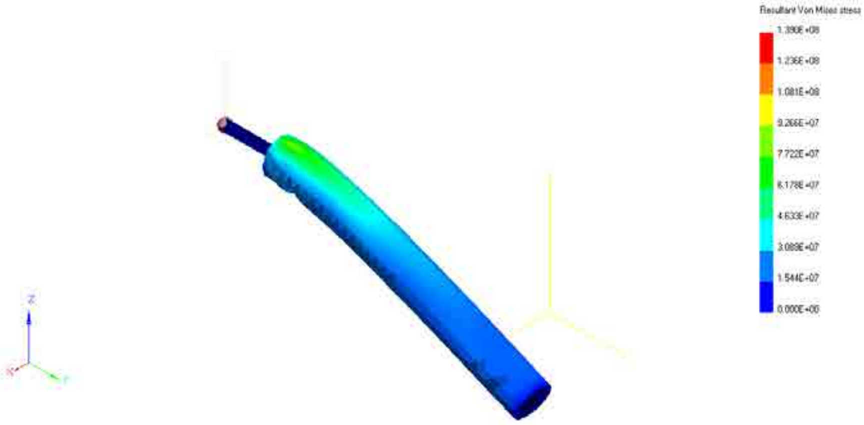


**(a)** t = 12.64, Ftip = 68.7 N s

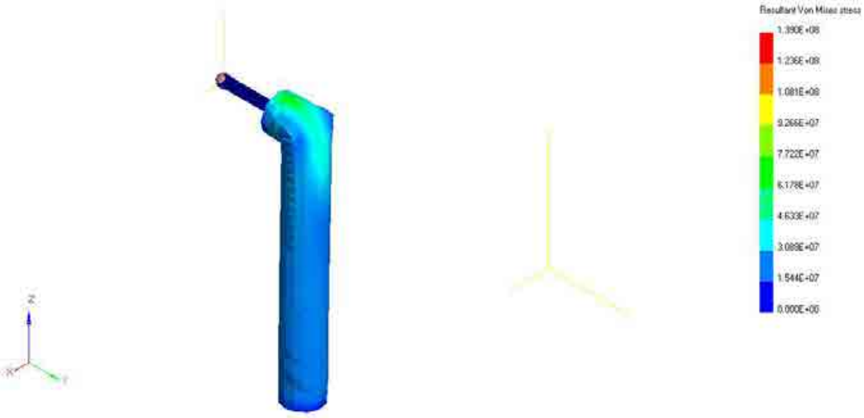


**(b)** t = 12.72, Ftip = 69.3 N s

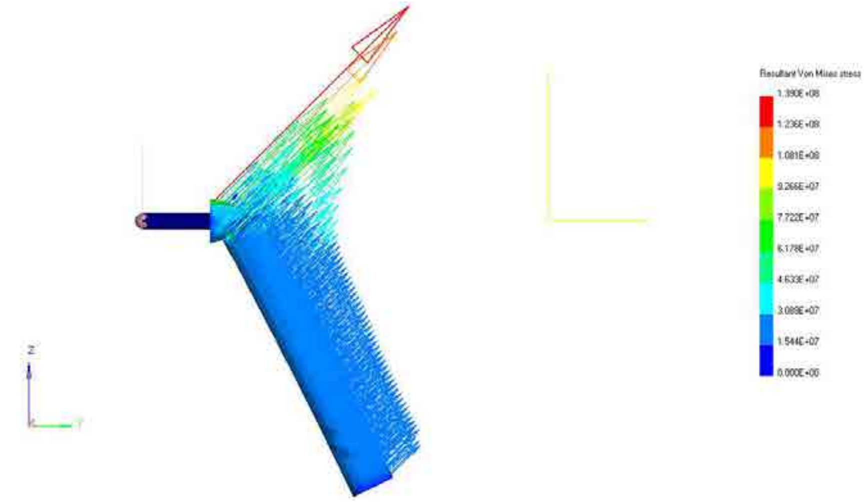


**(c)** t = 12.72, Ftip = 69.3 N s

**Figure 7-17:** Von mises stresses in the beam at different points in time in wrinkled region and collapse

### 7-3-5 Principle stresses in the beam

In the previous section, an example of a visualization of stresses are shown. However, it is difficult to observe what the stresses are in the material. In this section the principle stresses in the inflatable beam are presented. These are the stresses in principle direction, where the shear stress is zero. The stresses in principle direction are calculated with Eq. 7-2 and Eq. 7-2. These are only valid for the taut condition.

$$\sigma_1, \sigma_2 = \frac{\sigma_x + \sigma_\theta}{2} \pm \sqrt{\left(\frac{\sigma_x - \sigma_\theta}{2}\right)^2 + \frac{\tau_{x\theta}{}^2}{2}} \tag{7-2}$$

Where $\sigma_x$, $\sigma_\theta$ and $\tau_{x\theta}$ are stated in Section 3-2-1. The angle at which the shear stresses are zero is calculated with Eq.7-3

$$\tan 2\theta_p = \frac{2\tau_{x\theta}}{\sigma_x + \sigma_\theta} \tag{7-3}$$

The principle stresses have been simulated and calculated on the reference case beam at a distance of 0.14 m from the clamped part. This was done according the St. Venants principle, which states that the local stresses near the clamped part become insignificant at one times the diameter of the largest radius of the beam (Hibbeler, 1997). The stresses were determined at different angles from 0 to $\pi$ rad, where $\theta = 0$, is the bottom side of the beam and $\theta = \pi$ is the top side of the beam. The number of elements of the beam that was simulated was 2500. The 1000 element beam did not give representative results.

In Fig. 7-18, the calculated stress from Eq. 7-2 in first principle direction is shown in Fig. 7-18, the result of the FEM model is shown in Fig. 7-19. The result of the stress in second principle direction is shown in Fig. 7-20 and the result of the second stress of the FEM model is shown in Fig. 7-21.

Both principle stress plots show equal range in stresses. The first principle stress shows a strange effects at $\theta = 30, \theta = 60, \theta = 90 and \theta = 120$. This might be caused by the orientation of the elements and that these are not at exactly the same orientation compared to the theory. The second principle stresses show a good comparison. From Fig: 7-20 and Fig 7-21, it is shown that at 0.14 m from the clamped part, wrinkling occurs at about 15 N at $\theta = 0$.

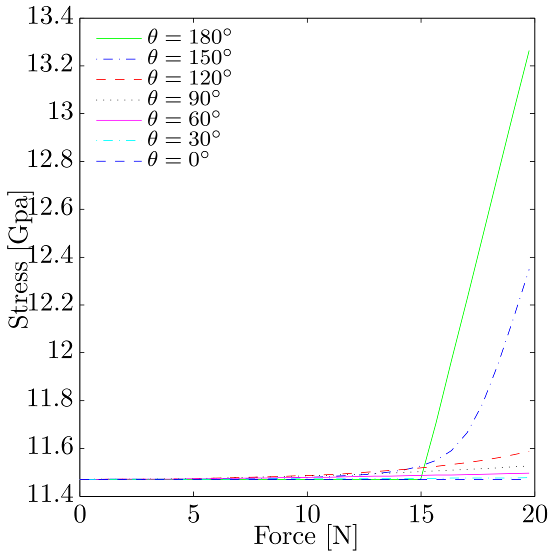


**Figure 7-18:** Stresses in principle 1 direction

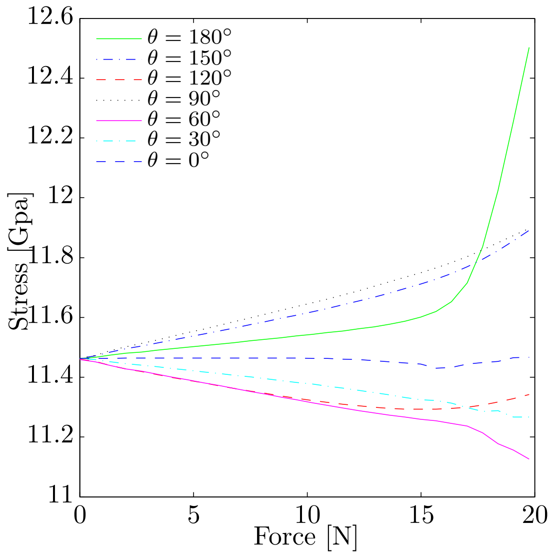


**Figure 7-19:** Stresses from FEM model in principle 1 direction

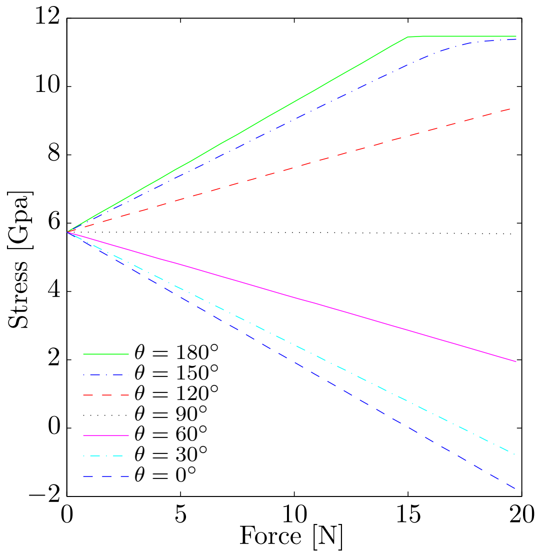


**Figure 7-20:** Stresses in principle 2 direction

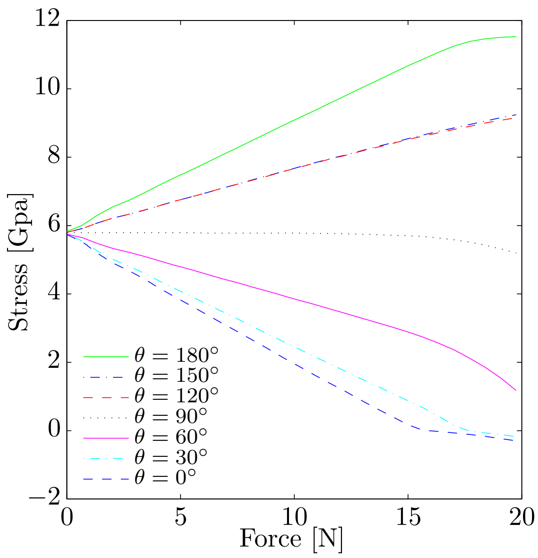


**Figure 7-21:** Stresses from FEM model in principle 2 direction

### 7-3-6 Summary results: Root mean square error (RMSE) and deflection error

The results shown in this section are given in the root mean square error or RMSE analysis. This is shown in Eq. 7-4.

$$RMSE = \sqrt{\frac{\sum_{i=1}^{n} \left(\mathbf{x}_i - \mathbf{x}_{ref,i}\right)^2}{n}} \tag{7-4}$$

Where $\mathbf{x}_i$ is the value at an increment $i$ and $\mathbf{x}_{ref,i}$ is the reference value at the same increment $i$. This RMSE value gives the accuracy of a vector or function with respect to a reference vector or function. The closer the value to zero, the smaller the difference with respect to the reference value. If the RMSE value is equal to zero, the curves coincide perfectly with the reference value.

In the results, two RMSE values are determined. The first RMSE value is with respect to the reference case of the FEM model described in Section 7-5. Only the error in linear part with respect to the reference case is taken into account in this analysis. This RMSE value is an indication of the influence of the change in parameters with respect tot the reference model.

The second value is the RMSE value with respect to the experiments described in (Breukels, 2011). The values are the values of the deflection at a certain applied tip force. The RMSE values are calculated in the complete tip force range of the complete experiment. This RMSE value is an indication of the accuracy of the models with respect to the experiments.

In Table 7-3, the deflections are given for the Element Mass FEM model from Fig. 7-13, Experiment and beam theory.

The second analysis is the error in %. This is calculated by dividing the deflections of the experiment and the beam theory by the deflections of the model at different tip forces. The error values are given in Table 7-4.

In Table 7-3 the deflection of the FEM model of the beam is compared with respect to beam theory and the experiment. Here the beam FEM model is closer to the beam theory compared to the beam experiment.

**Table 7-3:** Deflection of tip force

| Force (N) | Deflection (m) | | |
|---|---|---|---|
| | FEM model | Experiment | Beam theory |
| 3 | 0.0055 | 0.00838 | 0.00545 |
| 4 | 0.00699 | 0.01058 | 0.00691 |
| 5 | 0.0086 | 0.012980 | 0.00853 |
| 6 | 0.01025 | 0.01528 | 0.00101 |
| 7 | 0.011880 | 0.01758 | 0.0117 |
| 8 | 0.0135271 | 0.02068 | 0.01338 |
| 9 | 0.015337 | 0.02318 | 0.01516 |
| 10 | 0.0169637 | 0.02598 | 0.01678 |

In Table 7-4 the error of the model with respect to the experiment and to the analytical beam theory see Eq. 7-1.

**Table 7-4:** Error comparison of the beam FEM model with respect to the beam theory and the experiment

| Force (N) | Error % | |
|---|---|---|
| | Beam theory | Experiment |
| 3 | 0.9 | 34.27 |
| 4 | 1.15 | 33.93 |
| 5 | 0.8 | 33.66 |
| 6 | 1.48 | 32.88 |
| 7 | 1.5 | 32.42 |
| 8 | 1.10 | 34.59 |
| 9 | 1.17 | 33.83 |
| 10 | 1.1 | 34.70 |

In Table 7-5 the average error is computed with RMSE analysis. This is done for the linear part only, because the beam theory is not valid for the non linear behavior at a tip force 13 N approximately. The values are calculated from a tip force from 0 to 10 N. The RMSE values are calculated from the reference case this is the Element Mass with $\alpha = 10$ curve in Fig. 7-13. In Table 7-5, a distinct difference is shown between the comparison with the theory and the experiment.

**Table 7-5:** Root mean square error (RMSE)

| Force (N) | RMSE (m) | |
|---|---|---|
| | Beam theory | Experiment |
| 0 - 10 | $9.5*1^{-5}$ | 0.0132 |

In both Tables 7-4 and 7-5, the beam model is close to the beam theory with an error of approximately 1 %. There is a larger error if the FEM model is compared to the experiment of approximately 34 %. This is also visible from Fig. 7-13.

In Table 7-4, the deviation of different forces of the theory is smaller compared to the experiment. Both theory and FEM model are linear at forces $< 10$ N. The experiment is non linear with a tip force 3 N (Breukels, 2011).

## 7-4 Discussion of the reference case

The discussion of the reference case is based on comparison of the results. The only results that are available from the experiments are measurements of the deflection versus tip force and the collapse load. The focus of the result comparison of the inflatable beam is in the linear part of the curve. This means in the region where the beams are completely in a taut state and wrinkling has not occurred.

**Comparison of the results**

The results are limited by comparing the deflection versus tip force between the model and the experiment. From this the following observations can be made.

1. The inflatable FEM beam model incorporates more stiffness compared to the experiment. This can be seen in difference in slope in the linear part (of the FEM model) of the deflection versus tip force curve. This is not as expected, for sure in the linear region, the model is expected to behave similar compared to the experiment when the beam behaves linearly. However the influence of measurement errors and the correct material parameters should be taken into account.

2. The FEM model is compared with the linear theory including pressure terms. The model proved to be more accurate with respect to the theory compared to the experiment.

3. Comparison with theory proved to be accurate within 2 %, this is similar to the accuracy described in Le & Wielgosz (2005).

4. The inflatable FEM beam model increases in diameter when an internal pressure is introduced in the beam, however, there were no measurements made of the diameter increase of the beam. The inflatable FEM beam model increases in length when an internal pressure is introduced in the beam. This is as expected from theory

5. There is a clear transition between linear (taut) and non linear (wrinkled) regions.

6. The inflatable FEM beam model curve has a similar shape compared to the experiment.

7. The results of the models with tip force applied with a mass with Rayleigh damping $\alpha$ of 1, 5 and 10 are not satisfactory. The beam vibrates and the deflection versus load curve show vibration especially in the region where the tip force applied is low.

8. The results of the models with tip force applied with a mass with Rayleigh damping $\alpha$ of 1000 and the tip force applied with the force at the complete endcap are both very similar. It can be concluded that the slope of the gravity function in the model with a mass is steep enough. The velocity of the beam model including the mass is such that the deflection of the beam including the mass is almost equal to the beam with the tip force. However if the mass is used at the end of the beam, a Rayleigh damping ($\alpha$) of 1000 has to be chosen.

9. The principle stresses of the model were comparable to the principle stresses in theory. The second principle stresses were more accurate compared to the first principle stresses. The first principle stresses showed strange behavior within some angles of the elements.

10. Wrinkling threshold could be predicted with deflection versus force as well as the second principle stress visualization.

**Assumptions, similarities in model inputs (geometry, material and external loads) with respect to the experiment**

The material parameters are difficult to

1. The pressure in the FEM model behaves as expected. The pressure is uniformly distributed at the pre-set pressure. Although there is no pressure measurements recorded during the experiment of the beam.
2. The material inputs are used from uni-axial test data and thickness is as good as possibly measured from actual fabric.

**Other remarks**

1. All that is known is the deflection of the beam and moment of collapse, however not wrinkling load. In the experiment (Breukels, 2011) describes that there was no clear transition from taut to wrinkled. In the simulation of the reference case, there was also no visible transition. However there was a clear transition between the linear part and the non linear part.
2. There are no recordings, photographs or film material so that the kinematic movement of the beam cannot be compared.
3. Due to the use of the strap, the beam model could have had concentrated loads at the edges of this strap.
4. The material thickness is very difficult to measure for a woven material. The thickness is needed for a lot of material input in Madymo, such as: E-modulus, material density, stress/strain relations, shear modulus.
5. The E-modulus, stress / strain relation is based on uni axial test data.
6. CST application of the model might be not the best element, the shell element could also be tested.
7. It is unknown what the effects are of the material input parameters on the deflection behavior of the beam.
8. The input parameters that are necessary for Madymo are based on experience of experts who worked with airbags. This is another field of expertise compared to the model that has been built.

In Fig. 7-13, the curve that represent the experiment measurements clearly sags more than the FEM models in Madymo. This means that the stiffness of the beam in the measurements, is less than the stiffness in the FEM models. With the inflatable beam, there are a lot of uncertainties with respect to the parameters. Not only with the test, but also in material properties like E-modulus, shear modulus, Poisson ratio, in weft and warp (fill direction) of the woven fabric. The thickness measurement of the fabric Dacron there is no standardization.

The E-modulus of fabric is usually expressed is N/m, the thickness of the material is not taken into account. The same holds for the material density. The specific density in fabrics is usually expressed in $kg/m^2$. Madymo there are properties that requires the normal E-modulus in $N/m^2$, but also the density (normally) measured in $kg/m^3$. The thickness of the fabric has to be taken into account, this is difficult to measure, however an estimate has been given. In the observation of the FEM models, the diameter increases gradually during inflation of the inflatable beam. This is as expected in the actual situation, however, this is not recorded during the experiments. The set-up of the models was different on two points: the forces in the models are applied to the complete endcap surface. The forces on the experiment were introduced through a strap. The second difference is the beam length. This results in a small difference in arm introduced by the force. Because the model expands a little, the strap allowed placement at 1 m. The beam length is 1.2 m in the experiment, resulting in a little more weight due to the extra 0.2 m beam length and a moment due to the weight.

There are a lot more uncertainties that are required to actually compare the model to an actual experiment as can be seen in this section. All these uncertainties make it very difficult to create a predictive model, which can be used for a wide variety of beam geometries, materials and loads.

In order to give an idea what parameter show an influence on the beam model, a parameter study is performed. This is done because there are a lot of uncertainties within especially the material of the beam and the parameters that are used in Madymo and to show what input variables have a large impact on the deflection versus tip force curve.

## 7-5 Parameter sensitivity Study

The research subquestion that is answered in this section is:
**What parameters influence the model?**

A reference case is chosen and subsequently each parameter is changed separately. In this way the sensitivity and influence of each parameter individually is tested. Most of the parameters are numerical (for example diameter, length,internal pressure etc). These parameters will be changed to investigate the influence of each parameter. However some parameters such as: reference mesh, mesh element, tension only, element type etc. are not of a quantitative type, so this is on or off for example.

For all the quantitative depended parameters (except for the length) the same grow factors factors are applied. In Table 7-6 all the quantitative parameters are given. Every parameter is changed with the same grow factors as for the internal pressure. Some extra values are needed, see the last column ("extra") of table 7-6. This was necessary because of deviated values in the experiments such as diameter and the E modulus. The reference E modulus was obtained by the uni-axial test data. The E modulus of 2046 $N/m^2$ was obtained by the bi axial test (see chapter 6-2).

Besides the quantitative parameters, there are other parameters that have an influence on the bending of the inflatable beam. These parameters are given in Table 7-6. Some parameters need more explanation.

**Table 7-6:** Parameters that are varied including reference value for the inflatable beam

| Group | Parameter (Unit) | Ref value | Variables | | | | |
|---|---|---|---|---|---|---|---|
| Geometry | Diameter (m) | 0.13 | 0.087 | 0.173 | 0.217 | 0.18 | |
| | Element (-) | CST | | shell | | | |
| Material | Density $\rho$ (kg/m$^3$) | 2046 | 682 | 1364 | 2728 | 3410 | |
| | Thickness (mm) | 0.17 | 0.0567 | 0.113 | 0.227 | 0.283 | |
| | E (N/mm$^2$) | 1360 | 450 | 907 | 1810 | 2267 | 2046 |
| | Poisson's ratio $\mu$ (-) | 0 | 0.1 | 0.2 | 0.3 | 0.4 | |
| | RF TOON* (-) | 0.1 | 0.01 | 0.001 | 0.0001 | | |
| | RF TOOFF** (-) | 0.1 | | | 0.0001 | | |
| | Material model | Isolin | | Material fabric shear | | | |
| | Material Damping $\nu$ (-) | 0.1 | 0.2 | 0.4 | 0.6 | 0.8 | 1.0 |
| External loads | Internal (over)pressure (bar) | 0.3 | 0.1 | 0.2 | 0.4 | 0.5 | |
| | Inflation method | Airbag | | load.press | | | |

* RF TOON: Reduction factor tension only = on.
** RF TOOFF: Reduction factor tension only = off

Tension only = ON (TOON in table 7-6) means a material model with a reduced compressive behavior. In tension only = OFF (TOOFF in table 7-6), the E modulus for compressive behavior is the same as for tensile behavior. The E modulus both for tension and compression is the same. The reduction factor is a factor that reduces the compressive behavior. With a reduction factor of 0.1, the compressive strength is 1/10 $^{th}$ of the tensile strength. With this reduction factor, the behavior of the material can be changed, (TASS, 2010c).

Load.pres for the internal pressure of the cylindrical part of the beam is the other method to impose the internal pressure on the beam. This is a pressure that is directly put on the elements of the beam.

For the beam with shell elements LOAD.PRES is used and compared to the membrane including the LOAD.PRES.

# 7-6 Parameter study results

In this section, the results of the parameter study are shown. In Appendix F, the plots of the deflection as function of the tip force curves are shown.

The following sections are divided into four groups:

1. The first results are results of parameters that influence the model and multiple experiment data is available for comparison. These parameters are diameter and internal (over)pressure.
2. The next results are the results that have only one experiment reference case and the change in parameter value showed a difference in deflection versus tip force curve. These parameters are fabric thickness, E modulus, reduction factor (with tension only off material behavior) and material model.
3. The third result group are the results that show the non linear behavior, however no significant change in deflection versus tip force curve. These parameters are: fabric density, material damping and Poisson's ratio.
4. The last result group shows a different behavior of the inflated beam compared to the experiments and reference models. These parameters are the use of shell elements, tension only off material beaviour and load.press as internal pressure.

## 7-6-1 Results of parameters that influence the model with multiple validation data available

The parameters that are varied are diameter and internal (over)pressure. The RMSE with respect to the reference case, the values are calculated for the influence of the diameter from Fig. F-3 in the linear state. Two experiments have been taken into account, the beam with a diameter of 0.13 m and a beam with a diameter of 0.18 m. The RMSE value with respect to the experiment are calculated from Fig. F-4 for diameter 0.13 m and Fig. F-5 for diameter 0.18 m.

#### Geometry: Diameter

In Fig. F-1,the different diameters (0.0867 m; 0.13 m "reference case"; 0.173 m; 0.18 m; "experiment" and a diameter of 0.2167 m) are displayed in a force range between 0 and 100 N. In Fig. F-1 the overall behavior from different diameters are shown. The element size of the beams is kept the same. The beam with diameter of 0.0867 m, has less elements compared to the beam with diameter of 0.18 m. The curves show increasing stiffness of the beam or, a steeper slope of the deflection versus tip force curves, as the diameter increases. This expected as from theory (Veldman, 2005). When Eq. 7-1 this is shown in the values for L, S, A and I. From Table 7-7 in the In Fig. F-2, a detailed view of the different curves are given. In this Figure at F = 0, the beam is inflated at a pressure of 0.3 bar overpressure, the change in diameter is shown. At F = 0 N, there is already a displacement. This is due to the

**Table 7-7:** Root Mean Square Error of the parameter study multiple experiment data: influence

| Parameter (Unit) | Value | RMSE mm | | |
|---|---|---|---|---|
| | | Reference case | Experiment | Theory |
| Diameter (m) | 0.0867 | 50.5 | 26.2 | |
| | 0.13 EM Reference | 0 | 13.3 | 0.06 |
| | 0.173 | 6.0 | NA | 0.08 |
| | 0.18 | 6.5 | 28.2 | 0.09 |
| | 0.2167 | 8.2 | NA | 0.1 |
| Internal (over)pressure (bar) | 0.1 | 5.5 | NA | 5.4 |
| | 0.2 | 0.5 | 24.0 | 0.49 |
| | 0.3 EM Reference | 0 | 13.2 | 0.11 |
| | 0.4 | 0.19 | 9.8 | 0.38 |
| | 0.5 | 0.15 | 9.2 | 0.13 |

enlargement after pressurization of the inflatable beam. In Fig. F-3, this offset is corrected. In Fig. F-6 the FEM model and theory are plotted. In Table 7-7 the RMSE values of Fig. F-6 are given. Apart from the diameter of 0.0867 m, the error is less than 0.1 mm.

#### External loads: internal pressure

In Fig. F-7, different pressures are displayed. The higher the pressure is, the higher the beam stiffness is. This is according theory of for example, (Stein & Hedgepeth, 1961) and (Wielgosz & Thomas, 2002) and Eq. 7-1. Here the curves of different pressures have an asymptotic behavior with forces in the linear state. This might be explained by the increase in stress ($\sigma_x$ and $\sigma x\theta$) which are a function of the pressure. Due to this increase of the stresses, the principle stresses also increases at $\theta = 0$. The principle stress increases, then the beam behaves at higher loads as a linear beam. In Fig. F-8, the deflection curves for the models of 0.2; 0.3; 0.4 and 0.5 bar overpressure are displayed. The experiments are shown in Fig. F-9.

As an overall comparison between the experiments and the models, Fig. F-8 and F-9 are compared. The curves of the models coincide until the non linear behavior of the beam is shown. this behavior is displayed in Fig. F-8. However, this is inconsistent with the experiment measurements. The curves from the experiment deviate at different pressures even at small loads at the tip. An explanation might be that the force in the experiments is always exerted at precisely 1 m. During inflation, the diameter of the beam increases slightly, therefore the effect of $\sigma_x$ and $\sigma_{x\theta}$. This is comparable with the FEM model. However in the beam model the distance between the clamped end and the tip force increases also. It could possibly be that these two effects might cancel each other in the FEM model, but not in the experiment. This might be the reason that there is little difference between the behavior of the beam at different pressures the FEM model with respect to the experiment. The behavior of the beam can be clearly divided as a linear and a non linear part.

From the observation of the results in the Fig. F-10 to Fig. F-13 it seems that for every pressure, the beam in the models are less stiff compared to the models. However the difference seems to be smaller when the pressure increases. This can be seen in the RMSE, Table 7-7. So at increasing pressure, the difference between the experiment and the FEM model seem smaller. In Fig. F-14, the plots are shown for the data of the RMSE values.

### 7-6-2 Results of parameters that influence the model with one validation data set available

**Table 7-8:** Root Mean Square Error of the parameter study: influence

| Parameter (Unit) | Value | RMSE mm | | |
|---|---|---|---|---|
| | | Reference case | Experiment | Theory |
| Thickness (mm) | 0.0567 | 19.4 | 30.6 | 1.24 |
| | 0.113 | 5.2 | 1.9 | 0.22 |
| | 0.17 EM Reference | 0 | 13.3 | 0.06 |
| | 0.17 Mass Reference | 0.6 | 14.1 | NA |
| | 0.227 | 0.8 | 19.3 | 0.4 |
| | 0.283 | 0.7 | 22.8 | 0.48 |
| E modulus (N/mm$^2$) | 4.530e$^5$ | 18.1 | 27.7 | 1.6 |
| | 9.070e$^5$ | 5.2 | 2.3 | 0.2 |
| | 1.360e$^6$ EM Reference | 0 | 13.3 | 0.1 |
| | 1.810e$^6$ | 2.4 | 19.3 | 0.3 |
| | 2.020e$^6$ | 3.2 | 21.2 | 1.1 |
| | 2.270e$^6$ | 4.0 | 23.1 | 0.48 |
| Reduction Factor (-) | 0.1 EM Reference | 0 | 13.3 | |
| | 0.01 | 0.01 | 10.4 | |
| | 0.001 | 0.01 | 9.7 | |
| | 0.0001 | 0.01 | 9.6 | |
| Material model (-) | Woven Isolin Scaled | 0.3 | 12.0 | |
| | Woven Isolin Unscaled | 0.9 | 10.3 | |
| | Woven MFS 45/45 | 8.2 | 4.2 | |
| | Woven MFS 0/90 | 2.0 | 17.3 | |
| | Isolin Reference | 0 | 13.3 | |

#### Material: material thickness

The different material thicknesses are displayed in Fig. F-15. A clear distinction in slope of the different curves representing different thicknesses is shown in Fig. F-16. In Eq. 7-1, the thickness is incorporated in I, S. In the The material thickness of 0.113 mm is very similar to the experiment data in the range between the 0 and 23 N. The thickness shows also in Table 7-8 a big influence in the column *Reference case*. The FEM models describe within 0.5 mm accuracy the deflection of the inflatable beam, the plots of these calculations are shown in Section F-3 in Fig: F-17.

#### Material: E modulus

The E-modulus is directly linked through the stiffness. The higher the E-modulus of the material, the higher the stiffness of the beam. Beam stiffness is given as $EI$ see for example (Breukels, 2011). This has a direct relation on the behavior of the beam.

In Fig. F-20, a comparison is made between the theory ( 7-1). The plot is shows similar behaviour between the theory and the FEM models. The differences are within 0.5 mm accuracy and the plots of these calculations are shown in Fig: F-17

The curve with E modulus of $9.070e^5$ N/mm$^2$ is close to the experiments of 0.3 bar.

#### Material: Tension Only ON: influence of reduction factor

This tension only = on and the reduction factor defines the material compressive behavior (TASS, 2010c). From Figure F-22, the location in the plot where the curves distinct from the reference case, this is an indication where the beam starts to wrinkle. As aspected from the theory, this is the location where the linear behavior of the beam is converted in the non linear behavior. The reduction factor is used when negative principle stresses occur. The reduction factor scales these principle stresses down such that the principle stresses become zero The collapse of the beam is more in the region of the experiment. There are no measurements of the beam deflection during the collapse, so it is not clear what is a more realistic representation of the collapse. The reference plot shows at approximately 70 N and a deflection of 0.32 m a clear boundary where the beam collapses. The force where the beam collapses is 43 N and a deflection of 0.45 m with a reduction factor of 0.01. The beam with a reduction factor of 0.0001, collapses at approximately 30 N with approximately 0.32 m deflection. The beam in the experiment collapses at approximately 23 N at a deflection of 0.078 m.

#### Material: Woven Material model

In Madymo, it is possible to model woven fabrics. Here, the stress-strain relations can be given as (non)-linear functions. The E-modulus (linear constant relation between the stress and strain, described as Hooke's law). In this case of Dacron, the material behaves linear orthotropic (according to the bi-axial tests results, see 6-2). The E modulus only is given as input.

The Figures F-24 and F-23 are Figures in which the curves of woven materials is shown. There are four different models shown:

The terms scaled and unscaled are given for a correction for the increase in diameter and length due to the internal overpressure. The scaled model behaves stiffer because the increase in length of the beam is smaller (decrease in moment arm) compared to the unscaled model. The orientation of the fabric is at 0/90 degrees.

The woven model with material orientation of 0/90 is the beam that has the most stiffness. The curve follows the trend of the experiments and the reference case. The scaled model is closest to the reference case.

There is a difference between the scaled and unscaled model compared to the reference case. Apparently, the reference mesh behaves a little different than the initial mesh.

The curve of the woven material with material orientation of 45/45, is very strange. It begins linear (see Fig. F-24) and after the linear part it behaves very non linear and unexpected. The Isolin material model proved to be the most accurate model compared to the experiment.

### 7-6-3 Results of parameters that have limited / no influence on the model

**Table 7-9:** Root Mean Square Error of the parameter study: no influence

| Parameter (Unit) | Value | RMSE mm | |
|---|---|---|---|
| | | Reference case | Experiment |
| Density $\rho$ (kg/m$^3$) | 682 | 0.01 | 13.6 |
| | 1364 | 0.01 | 13.4 |
| | 2046 EM Reference | 0 | 13.3 |
| | 2728 | 0.01 | 13.1 |
| | 3410 | 0.01 | 12.9 |
| Material damping $\mu$ (-) | 0.1 | 0.4 | 14.1 |
| | 0.2 | 0.4 | 14.1 |
| | 0.4 | 0.4 | 14.1 |
| | 0.6 | 0.4 | 14.1 |
| | 0.8 | 0.4 | 14.1 |
| | 1.0 | 0.4 | 14.1 |
| | 0 Reference case EM | 0 | 13.3 |
| | 0 Reference case Mass | 0.6 | 14.1 |
| Poisson's ratio $\nu$ (-) | 0.1 | 0.4 | 14.0 |
| | 0.2 | 0.5 | 14.0 |
| | 0.3 | 0.5 | 14.1 |
| | 0.4 | 0.5 | 14.1 |
| | 0.5 | 0.5 | 14.1 |
| | 0 Reference EM | 0 | 13.3 |
| | 0 Reference Mass | 0.6 | 14.1 |

#### Material: material density

In Fig. F-26 the deflection vs force is displaced for different material densities. Because the material volume is very low, the mass of the inflatable beam is also small. This explains the similarity in the results of the models. In theory, Eq. 7-1 the displacement is not a function of the density.

#### Material: material damping coefficients

The material damping coefficients are shown from 0 (reference case) till a damping coefficient of 1.0. The curves of all damping coefficients coincide in the interval shown in Fig. F-27. The different material damping coefficients do not show a significant influence in the curves.

### Material: Poissons's ratio

In Fig. F-28 the curves are shown with different Poisson ratio's. The reference case has a Poisson's ratio equal to zero. The results of different Poisson ratio's show little variation (see Fig. F-28). This is theoretical influence of Poisson's ratio.

### 7-6-4 Other parameters results on model

In this section other parameters results are presented. These parameters did not show the expected behavior of inflatable structures. The parameters are:

- Shell elements
- Tension only OFF
- Load.pres

#### Geometry: Shell elements

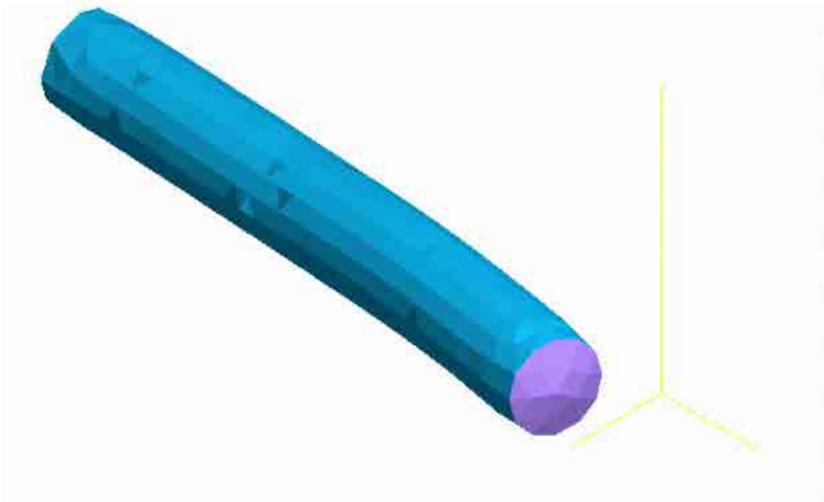

(a) 3D view of the beam

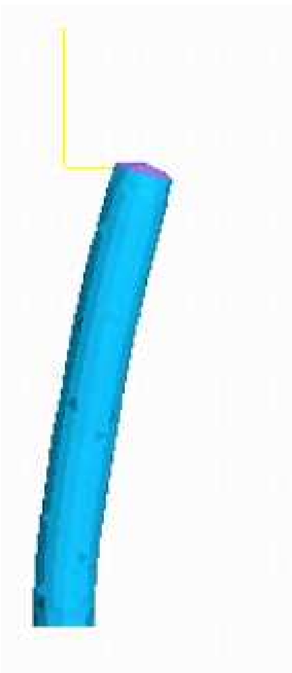

(b) Top view of the beam

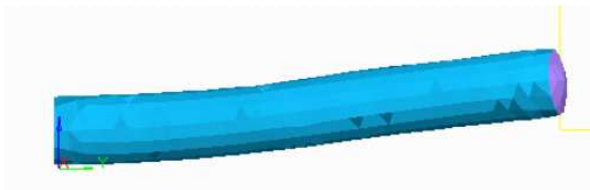

(c) Side view of the beam

**Figure 7-22:** Three views of the inflatable beams wth shell elements only with a constant internal pressure

Only internal pressure is applied on the beam with shell elements. In Figure 7-22, the inflatable beam has a deflection in the x- and the z- directions. This is cannot be correct. With only the internal pressure is applied to the beam, the beam is expected to behave similar to the beam with membrane elements displayed in Figure 7-16b. Test have been performed with MEM.3 element and LOAD.PRES. This resulted only in expansion and not in bending of the beam as displayed in Fig. 7-22.

**Material: Tension Only OFF: influence of reduction factor**

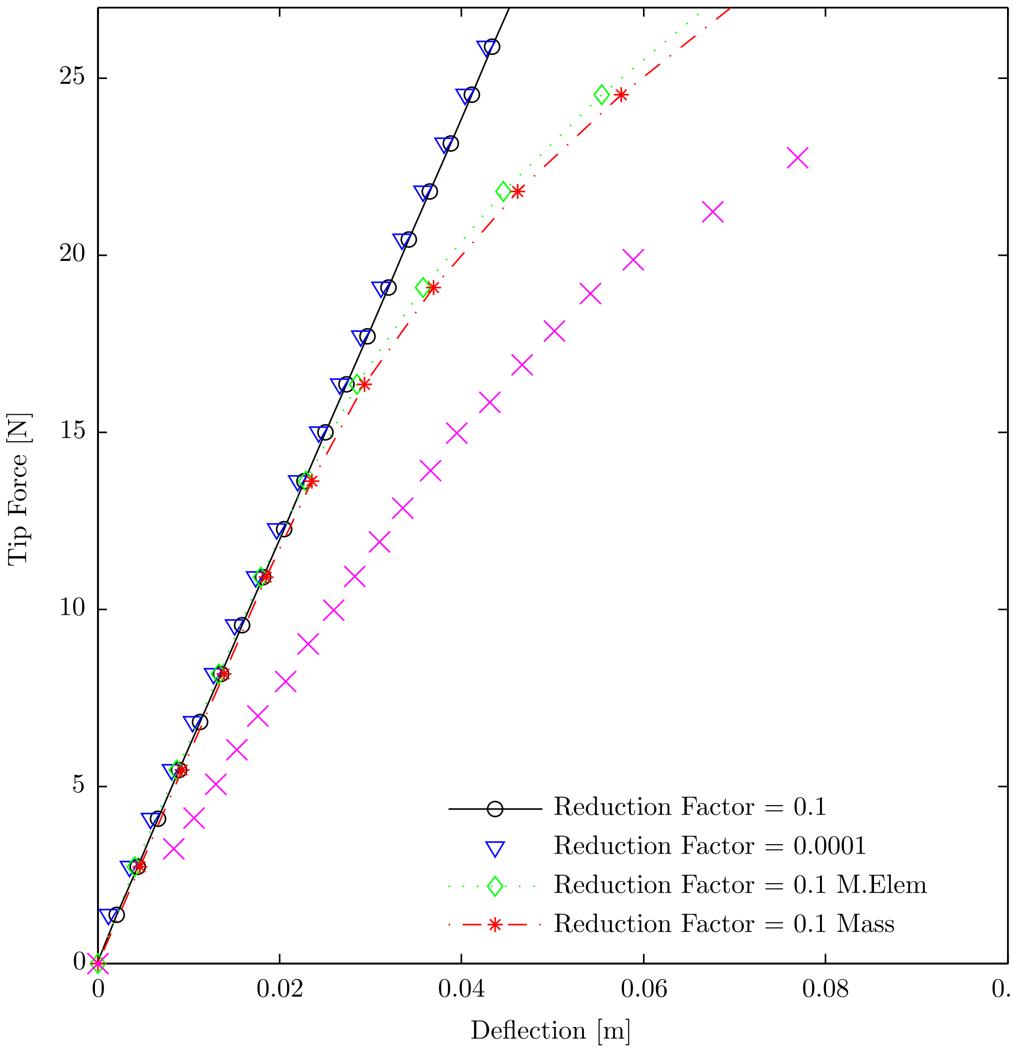


**Figure 7-23:** Results of Tension only OFF (TOOFF)

The curves with tension only off (TOO) and the reference case (with tension only = on) is shown in Figure 7-23. The tension only off can be included in the material properties. The tension only setting is stress strain based. The reduction factor does only have an influence when using tension only = on. With tension only = OFF, the same stiffness or E modulus holds both for compressive and tensile behavior. The curves behave linear, as expected, however, there is a strong indication that this does not represent the inflatable beam behavior.

The curves in Fig. 7-23, the tension only = off, are linear and close to each other. What might cause this behavior is discussed with Madymo FEM experts at TASS, but not solved. The reduction factor showed no influence on tension only = off.

**External loads: LOAD.PRES**

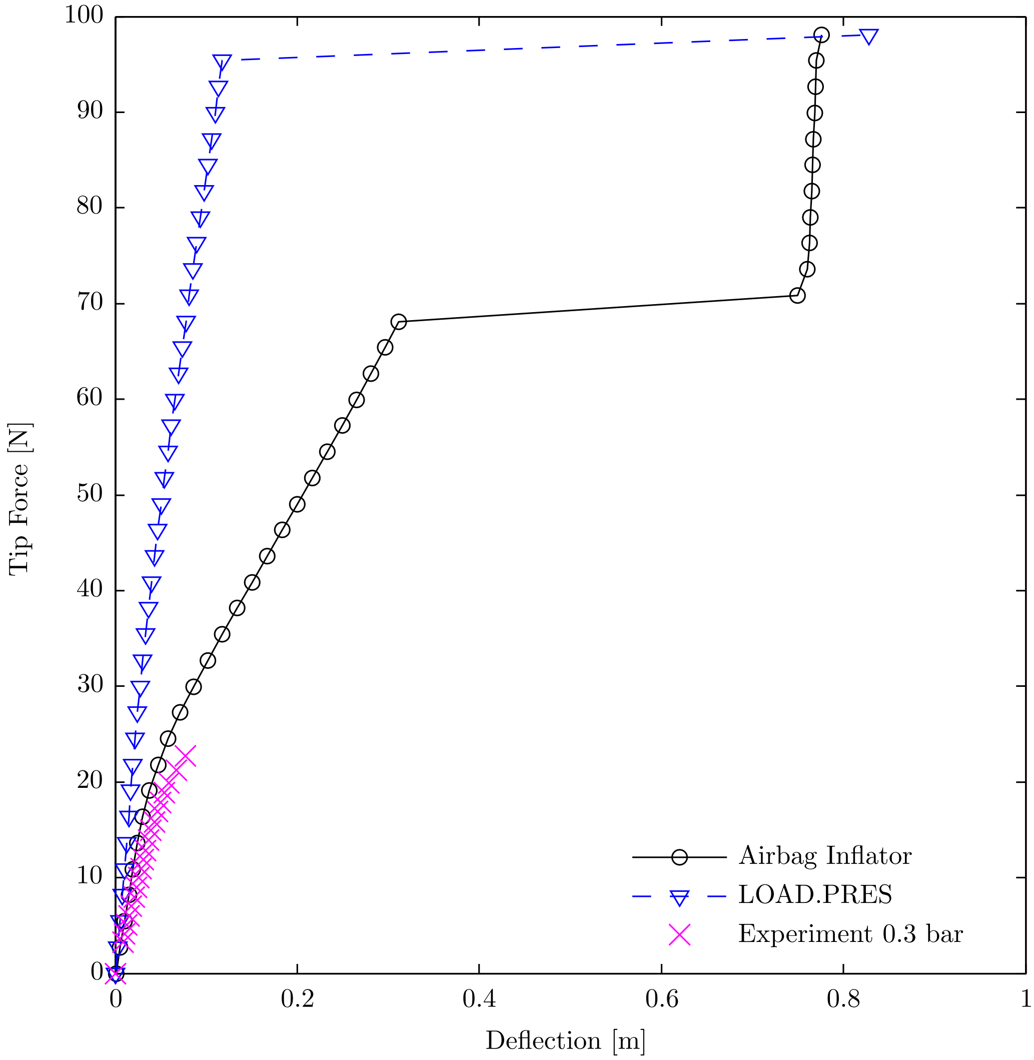


**Figure 7-24:** Results of applying different principles of internal pressures, inflator vs LOAD.PRESS

The results are not similar between the two different internal pressure methods, which have the same pressure when the load is applied. In Fig. 7-26 the pressure vs the tip force is shown of the airbag inflation method vs the LOAD.PRES method. Here it can be clearly seen that the pressure of the inflation has to built up from the mass flow. The LOAD.pres pressure is already at the correct over pressure of 0.3 bar. The pressure is checked with OUTPUT ELEMENT and SELECT.PRES_EXTERNAL. The pressures are equal low forces, however

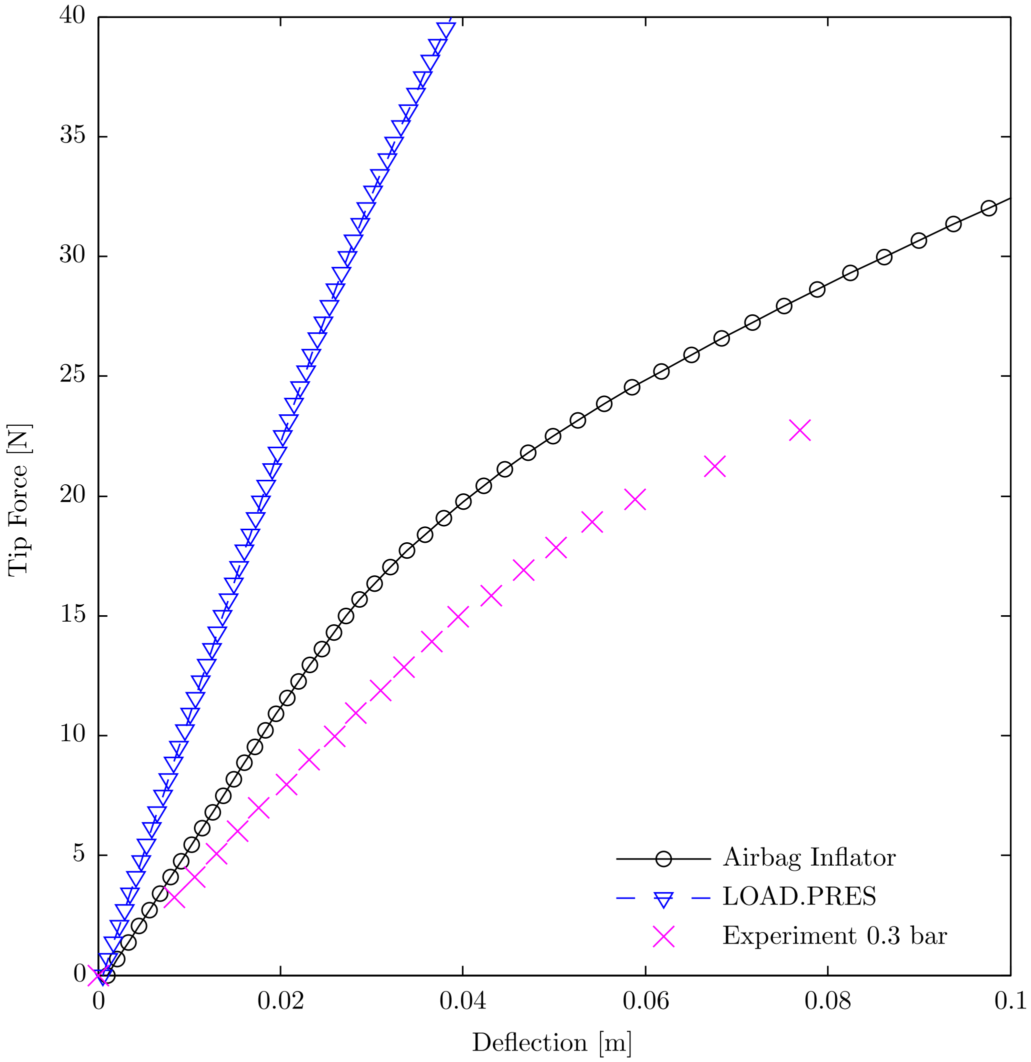


**Figure 7-25:** Detail of applying different principles of internal pressures, inflator vs LOAD.PRESS

when the tip force increases, the load.pres pressure does not increase like expected and as shown with the airbag inflation method. The non linear (wrinkle) part of the plot can also be indicated where the inflation process method increases in pressure at approximately 30 N (see figure 7-25).

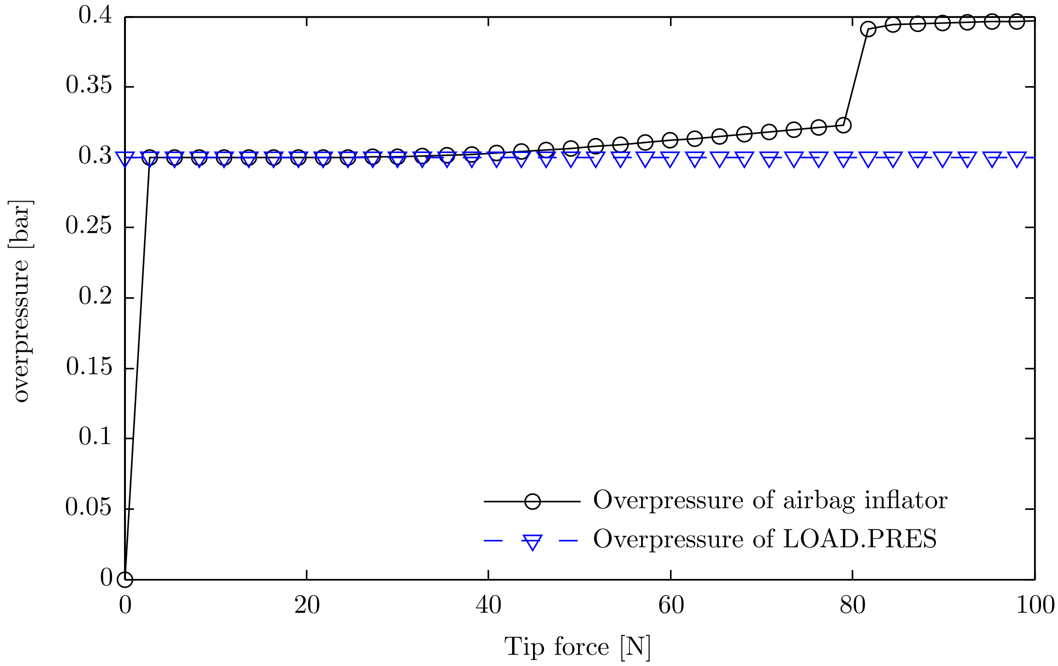


**Figure 7-26:** Detail of applying different principles of internal pressures, inflator vs LOAD.PRESS

## 7-6-5 Discussion and conclusion

The discussion focuses on the linear part of the deflection versus tip force curve. But the influences on the collapse and wrinkling are also discussed.

1. geometrical parameters:

   (a) Reference mesh (flattening) necessary for woven fabrics material model: it appeared to be difficult for a simple geometry such as a cylinder to be flattened in a way that random triangulated shapes could be flattened in the same manner.

   (b) Beam diameter: The curves show increasing stiffness or, a steeper slope of the deflection vs tip force curves, as the diameter increases from the origin of the Fig. F-3. This expected as from theory (Veldman, 2005). The stiffness of the beam increases because the stress in the material in x direction due to the pressure is a linear function with the radius ($r$). The stress in x direction due to the tip force is a function of $1/r^2$ (Veldman, 2005). The latter is because the distance from the outside of the inflatable beam to the neutral line is bigger at larger diameters.

2. material parameters:

   (a) Isolin material behavior shows the best correlation of the both material models that have been tested.

(b) Shell elements: The inflatable beam showed a deflection in the x- and the z- directions, which cannot be correct. With only the internal pressure is applied to the beam, the beam is expected to behave similar to the beam with membrane elements. In this case it is not clear why this occurs.

(c) Material density: The resulting curve is insensitive to density. Because the material volume is very low, the mass of the inflatable beam is also small. This explains the similar results of the models.

(d) Material thickness: There is a distinct difference in slope (stiffness of the beam) with regard to different material thicknesses. This is like expected because the thickness of the material has effect on the stress in x direction directly, the E modulus and material density.

(e) E-modulus: The higher the E-modulus of the material, the higher the stiffness of the beam. Beam stiffness is given as $EI$ see Eq. 7-1. This has a direct relation on the behavior of the beam. The collapse force is at a higher force as expected, however also at a lower displacement. This makes sense if the beam is compared with a more brittle metal beam. It can withstand more stress however it buckles at lower strain.

(f) Poisson's ratio ($\nu$): In Figure F-28 the curves are shown with different Poisson ratio's. The reference case has a Poisson's ratio equal to zero. This is not as expected from theory (Veldman, 2005), here the Poisson's ratio clearly has a big influence on the behavior of the beam, even at low tip forces. Note that (Veldman, 2005) used different materials but including internal pressure.

(g) Tension only = OFF: The curves with tension only off (TOO) and the reference case (with tension only = on) is shown in Figure 7-23. The tension only off can be included in the material properties. With tension only OFF, the compressive stiffness is equal to the tensile stiffness.

(h) Tension only = On: This tension only = on and the reduction factor defines the material compressive behavior (TASS, 2010c). From Figure F-22, the location in the plot where the curves distinct from the reference case, this is an indication where the beam starts to wrinkle. As expected from the theory, this is the location where the linear behavior of the beam is converted in the non linear behavior. The collapse of the beam is more in the region of the experiment. There are no measurements of the beam deflection during the collapse, however, the collapse must be treated with great care, because at 1000 elements the mesh is considered converged for taut state and not for the collapse state.

(i) Material fabric shear, woven fabric material model: The scaled model behaves stiffer because the increase in length of the beam is smaller (decrease in moment arm) compared to the unscaled model. The woven model with material orientation of 0/90 is the beam that incorporates the most stiffness. The curve follows the trend of the experiments and the reference case. The scaled model is closest to the reference case. There is a difference between the scaled and unscaled model compared to the reference case. Apparently, the reference mesh behaves a little different than the initial mesh. The curve of the woven material with material orientation of 45/45, is very strange. It begins linear (see Figure F-24) and after the linear part it behaves very non linear and unexpected.

(j) material damping: The material damping coefficients are shown from 0 (reference case) till a damping coefficient of 1.0. The curves of all damping coefficients coincide in the interval shown in Figure F-27. The different material damping coefficients do not show a significant influence in the curves.

3. External load parameters:

    (a) Internal pressure: As an overall comparison between the experiments and the models, Fig. F-8 and Fig. F-8 are compared. The curves of the models coincide until the non linear behavior of the beam is shown. this behavior is displayed in Fig. F-8. However, this is in contrast to the experiment measurements. The curves from the experiment deviate at different pressures even at small loads at the tip. The collapse of the beams act also in different forces at the tip. This behavior is as expected, both from theory and experiments. The wrinkled region is again small (as with the reference beam see section: 7-2). The behavior of the beam can be clearly divided as a linear and a non linear part.

    (b) Internal pressure with Load.press: The results are not similar between the two different internal pressure methods, which have the same pressure when the load is applied. At low forces, the pressures are equal, however when the tip force increases, the LOAD.PRES pressure does not increase like expected and shown with the airbag inflation method. The non linear (wrinkle) part of the plot can also be indicated where the inflation process method increases in pressure at approximately 30 N.

The stresses in the beam proved to be similar to theoretical calculations. Especially the second principle stress showed a good correlation with theory. Wrinkling could be predicted with stresses or deflection versus force curve.

Chapter 8

# Case study II: modeling the V2 LEI Mutiny kite including the bridle

In this chapter, the objective is to investigate if it is possible to model a complete LE inflatable kite (in this case the 25 $m^2$ V2 Mutiny kite. It is not the objective to validate the model, but to show that a kite model can be created and a stable simulation is able to run in Madymo.

The research subquestions that are answered in this chapter are:

- Is it possible to create a structural model of the LE inflatable kite with the LE and the struts inflated to a desired internal pressure?
- Is it possible to model the LEI kite including the bridle and does the bridle interact with the kite at different loads?
- Does the response qualitatively match the actual kite?

The complete kite model in Madymo should consist of the kite and the bridle system. The kite is build up out of different parts like described in the process development chapter 6-1:

1. The inflatable leading edge.
2. Inflator.
3. Connection between the beam and the inflator.
4. Seven struts.
5. Seven connections between the leading edge and the struts.
6. Eight holes: one between the inflator and the leading edge and seven between the struts and the leading edge.

7. Canopy parts.

In Madymo the bridle system is the next part of the geometry that completes the kite. the bridle system consists of (see also chapter 2-4):

1. Bridle lines
2. Pulleys
3. Knots
4. Bridle points

In Fig. 8-1 the complete kite including the parts of the bridle system is shown. The bridle lines are modeled in Madymo by BELT segments and the pulleys are modeled by BELT tyings, see (TASS, 2010d) for the theory of the BELTS. Both applications are multibody entities. The BPs are attached to the kite by connecting bodies to the nodes at the exact initial location of the actual bridle points. The bodies of the BPs are set to be at a very small mass (0.000001 kg) not to disturb the geometry, inertia and the weight of the kite.

Each pulley in the multibody system has a mass of 0.008 kg, this is measured with a scale.

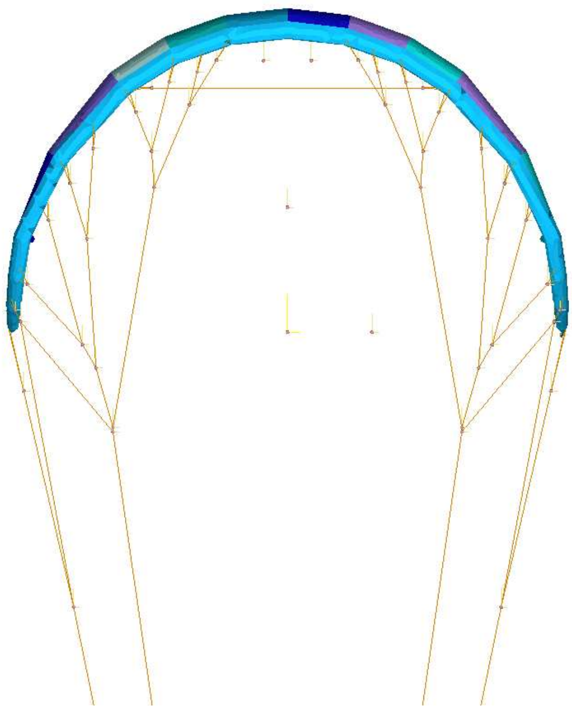

**Figure 8-1:** Complete kite including the bridle system from Madymo

Before the kite could be simulated loaded with forces, the kite first has to be inflated. This is a base case after which three different simulation cases that are qualitatively compared with an experiment. The three simulations that are to be tested are:

1. Kite upside down under gravity.
2. Kite upside down under a single load at the middle of the LE.
3. Falling mass into the kite.

## 8-1 Experiments set-up of the leading edge inflatable kite

The V2 Mutiny kite is quite a large object with 25 $m^2$ canopy surface (projected area $\approx$ 17 $m^2$), a maximum chord length of the kite of approximately 2.7 m and a height from tip to the top of the center strut of approximately 3.8 m. If the complete bridle system and the POD are included, then the height of the kite becomes approximately 19 m. In order to perform static tests, the kite should not be disturbed by for example the wind. As a result, the kite should be positioned indoors.

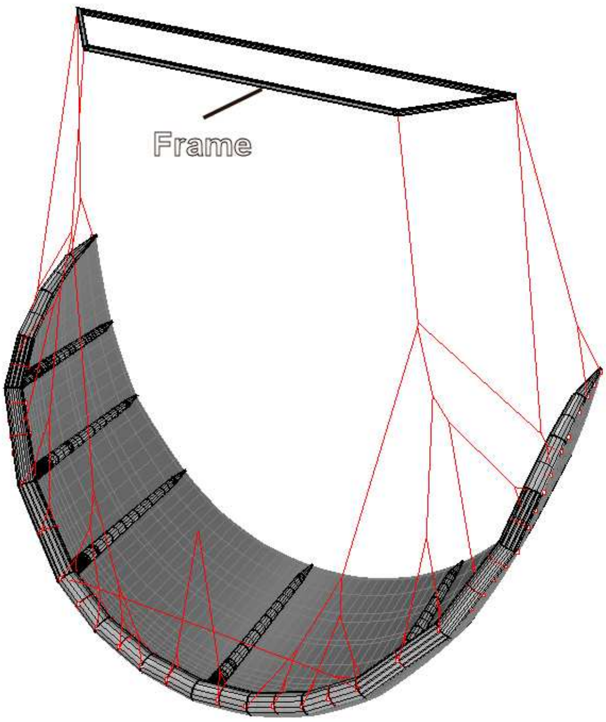


**Figure 8-2:** Kite plan for the test

The kite could not be placed in upright position on the tips and the bridle system has a big influence on the behavior of the kite. An option not to interfere with the geometry of the kite is to hang the kite upside-down. However, if the complete bridle system should be included, then a height of at least 21 m would be necessary. There were no buildings in the vicinity that have such space available for the test.

Another test concept was built and tested, as shown in Fig. 8-2. In order to reduce the height, but keep the kite intact, the bridle was shortened see Figure 8-2. The minimal height needed for the test was now approximately 8.0 m (the height of the kite is 7.1 m) including 1.0 m of attachment height and sagging height (due to loads and own weight). This is still a huge height to overcome indoors. The test was performed in the sport centre of the DUT, the height inside the sport center was approximately 8.5 m see Fig. 8-3.

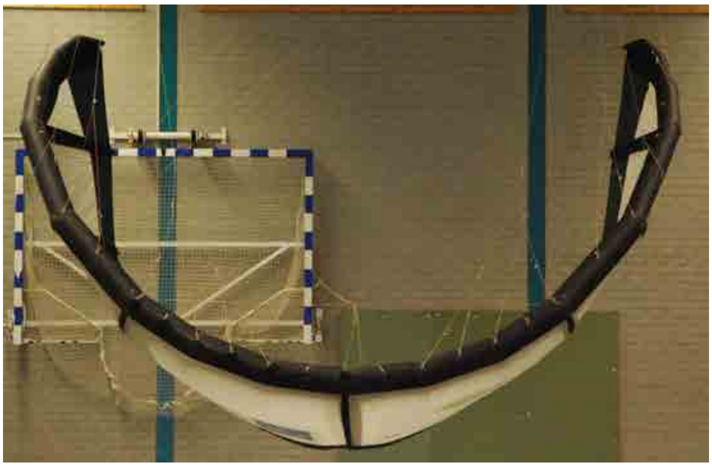

**Figure 8-3:** Actual test overview of the kite

### 8-1-1 Kite Geometry

The "frame" of the kite (see Fig. 8-2) is made from a nylon chord, this frame was attached to the ceiling. The geometry of the kite is shown in Section 2-4 in Fig. 2-6.

### 8-1-2 Kite material

In Verheul (2010), the complete mass breakdown of the kite is performed for the V2 Mutiny kite. The mass of the kite consists of:

1. Ripstop cannopy
2. Sponsor logo's
3. Dacron (inflatable LE,struts and reinforcements)
4. TPU bladder

The pulleys have a weight of approximately 8 grams per pulley. The bridle lines assumed to have a specific weight of 0.01 kg/m (Southern Ropes, 2012).

### 8-1-3 External loads

#### Inflation Process

The kite was inflated by a pump using a manometer to ensure the overpressure of 0.3 bar.

### Forces on the kite

There are three different load cases that have been tested in the experiment. The first load is gravity on the kite, see Fig. 8-3.

The second force on the kite is a distributed force on a small surface and considered a point load applied at the LE of the kite. This load applied ranged from 0 N to 343 N in steps of 49.05 N (5 kg), see Figure 8-4 and Figure 8-5.

**Figure 8-4:** Kite under gravity and center load

As a last case, the kite is loaded with a mass (ball) to simulate a dynamic behavior with the kite. See Fig. 8-6.

## 8-1-4 Support and constraints

The kite was attached to the ceiling via four pulleys that were pre-attached to the ceiling. The frame of the kite and the attachment to the ceiling is shown in Fig. 8-7 and a side view is shown in Fig. 8-8.

**Figure 8-5:** Kite under gravity and center load

**Figure 8-6:** Dynamic interactive test between the kite and a mass

### 8-1-5 Measurements of the experiments

The measurements of the experiments are qualitatively. This can give a first indication whether the model of the kite is comparable to the experiment. When the model seems to have acceptable results, photogrammetry could be used for the measurement of the displacements and deformations.

**Figure 8-7:** Bottom view of the attachment to the ceiling

**Figure 8-8:** Side view of the attachment to the ceiling

## 8-2 Finite Element model set-up

In this section, the FEM model set-up of the kite is explained. First the geometry of the kite will be shown, next the kite bridle system will be explained. In Section 8-2-2 the kite materials that are used in the model are implemented. In Section 8-2-4 three external load cases will be described and in Section 8-2-5 the supports and the constraints of the kite will be displayed. Section 8-2-6 the method for comparing the measurements and the model.

### 8-2-1 Kite Geometry

The kite geometry is made in ICEM and described in Section 6-1-5. However there is one important note for the kite. The BPs should be located at the nodes. The coordinates of the BPs, pulleys and knots should be manually imported into Madymo. For the pulleys, knots and bridle points multibody parts have to be made. First a "BODY.RIGID" and a "JOINT.FREE" have to be made. The BODY.RIGID part can have entities like mass, a name and center of gravity. For the center of gravity is given in the local body coordinates. The default coordinates are: 0,0,0 (this is in the center of the body itself). Next to the BODY.RIGID part a JOINT.FREE has to be made. This joint accompanies the BODY.RIGID and here the position of the body is entered. Another important entry is the status of the JOINT.FREE. If the joint must move with the body in all directions, the option "FREE" must be chosen. This is the case for all the BPs (here the BODY.RIGID and JOINT.FREE are connected to the nodes of the FEM part thus the kite). The pulleys and knots also have the "FREE" option. However there are also BODIES and JOINTS that must be "locked". In this option all the DOFs of the BODY and JOINT are fixed. This is the case for the four points of the frame and the Kite Control Unit (KCU) in the simulations without the frame.

### 8-2-2 Kite material

In this Sub section, the material input for the kite FEM is discussed.

In the kite, three materials are modeled. In Section 7-1-2 the input of the inflatable beam given which is made out of Dacron. The uni axial input of the beam is used for the input of the FEM model of the kite. The stiffness of the FEM model of the beam showed to be higher compared to the experiments, Section 7-3. In the FEM model, this should be predictive. So the input as measured is used and then the result is shown. As a result of the beam study it was concluded that the Isolin material model was best for prediction and the input that resembles the beam best was the uni axial stress test input discussed in Chapter 6-2-2. So for Dacron this leads to:

- Material damping (NU) = 0.1 -
- E-modulus = 1360 N/m$^2$
- Density = 2046 kg/m$^3$
- Poisson ratio (MU) = 0

From the inflatable beam reference results in Section 7-3 showed that the input is probably not correct. However this is measured and the bi axial test resulted in a yet higher E modulus, thus leading to a stiffer beam compared to the experiment discussed in Section 7-6-2. The need for correct input is an advantage, because the input physically corresponds to the actual material properties, however in this case it is not known if the material properties measured that are correct, see Section 7-6-5.

In Chapter 6-2-2, the results of the uni-axial stress test of Ripstop are:

- Material damping (NU) = 0.1 -
- E-modulus = 600 N/m$^2$
- Density = 750 kg/m$^3$

- Poisson ratio (MU) = 0

The Dacron reinforcements are quite evenly spread over the complete LE and the struts. The Dacron reinforcement at the Trailing Edge (TE) of the kite is not included in the model. For the inflatable structure the weight of the Dacron itself, the Dacron reinforcements and the TPU bladders are included in the density of Dacron. The weight of the TPU bladder is included in the density of Dacron is justified because tensile strength of the TPU is assumed <<< tensile strength of Dacron. So the mass of the TPU bladder is taken into account, however not in the strength. This is also done with the beam see 7-1-2.

### 8-2-3 Bridle system

For the bridle lines results are obtained by using two belts with a specific weight (Mass Belt) and without a specific weight. For the bridle lines a specific weight of 0.01 kg/m is assumed (Southern Ropes, 2012), material damping can only be used as an input with the Mass Belt.

The weight of the pulleys were measured on a scale, an example of a pulley used in the kite is displayed in Fig. 8-9 The weight measured was 8 grams ($8*10^{-3}$ kg).

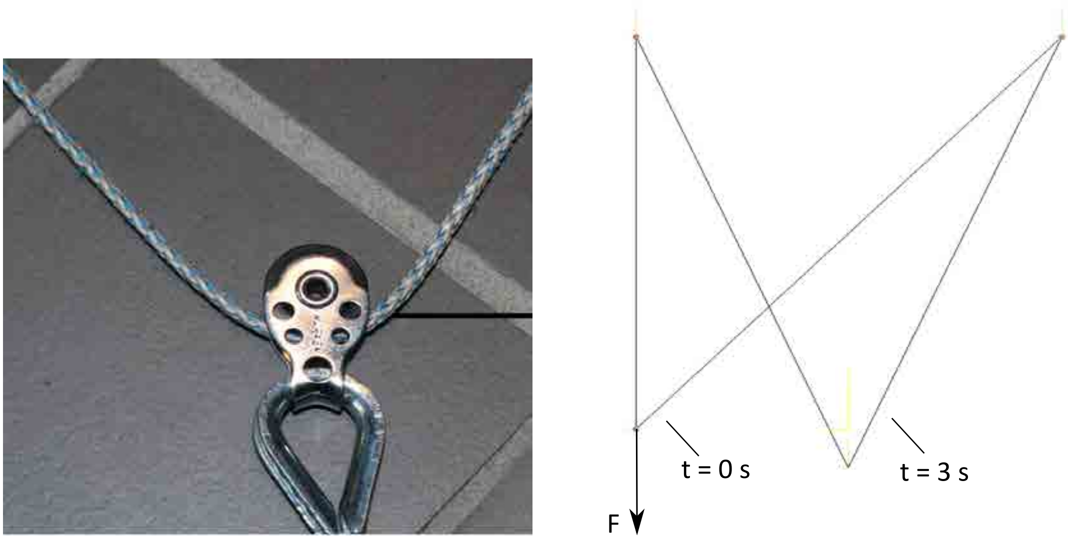


**(a)** Actual image of the pulley **(b)** Model

**Figure 8-9:** Actual and model of the pulley

#### Simple pulley model

In Madymo a simple pulley construction was first tested. This contains two lines and a pulley shown in Figure 8-9b. On the pulley there is a force of 10 N in negative z direction

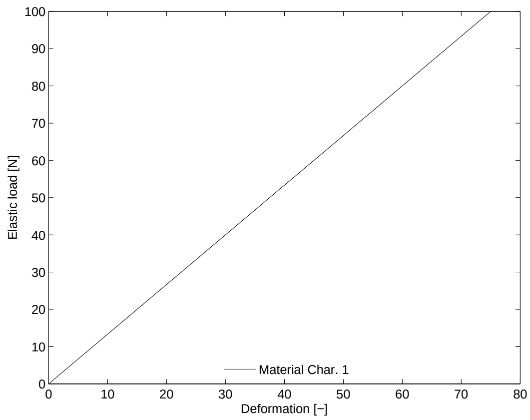


**(a)** Material Characteristic 1

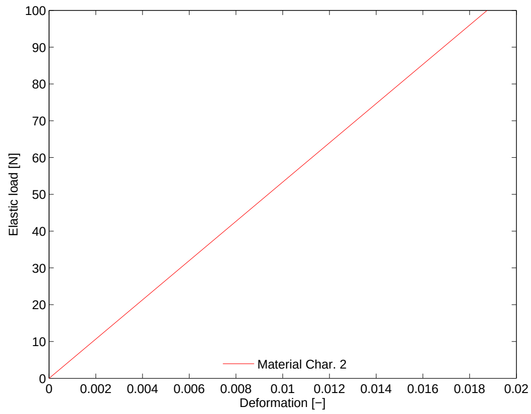


**(b)** Material Characteristic 2

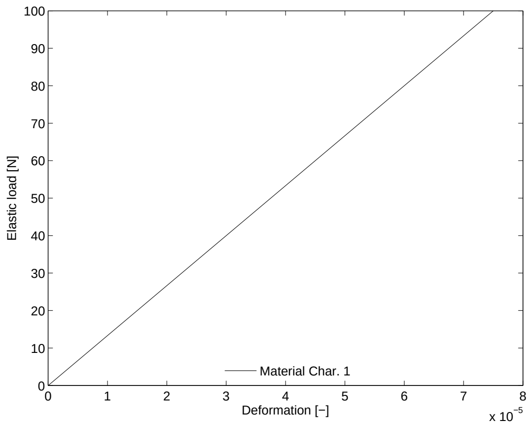


**(c)** Material Characteristic 3

**Figure 8-10:** Material Characteristics

(downward). Three material characteristics have been tested for the belts, see Fig. 8-10. The characteristics are fictive, but used to get as stable simulation of Madymo.

The characteristic of the belt contains a force versus elongation curve. In this case there was no input present so different characteristic cases were tested. In Fig. 8-11a and Fig. 8-11b a sensor, that measures the distance between the begin position and the position during simulation. This sensor is attached to the pulley. In Fig. 8-11a and Fig. 8-11b, the results are shown using two massless belt characteristics 1 and 3. In Fig. 8-11a, the displacements are very large. What is also noticeable is that the vibration is not damped out. No damping can be set for the mass less belts. Fig. 8-11b seems to respond more realistically, although also in this plot, the vibration is shown because no damping was added to the mass less belts. Another test has been performed with mass belts with the same material characteristics. This is shown in Fig. 8-12. The vibrating behavior is damped at with damping coefficients of 0.15. This was the value, where the behavior was damped out, but still ended up in the correct position, in the middle between the two constraints. For the kite two belts are tested with the kite: a massless belt with characteristic 3 and a mass belt with characteristic 2 and a

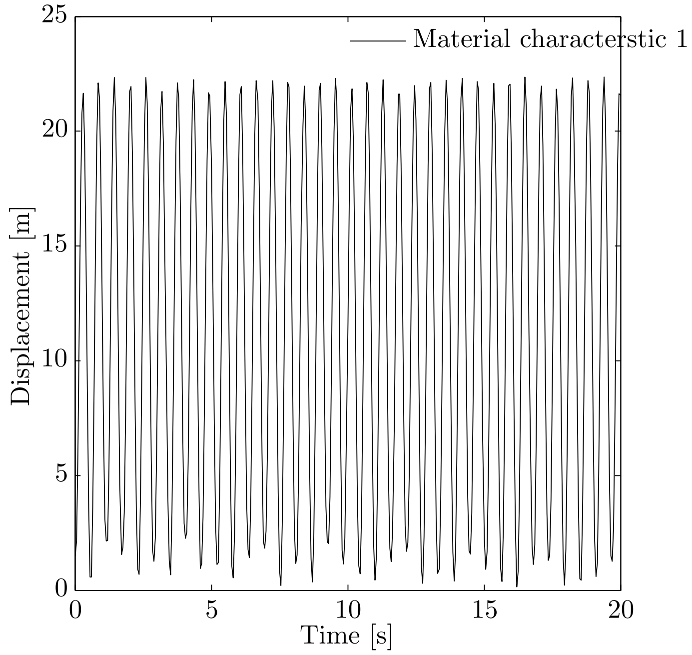


**(a)** Material characteristic 1

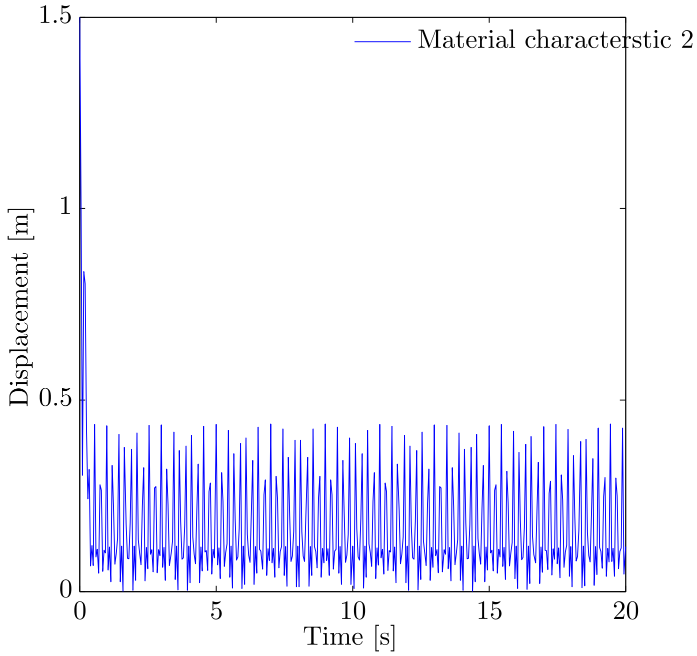


**(b)** Material characteristic 3

**Figure 8-11:** Results of two material characteristics in simple pulley model without damping

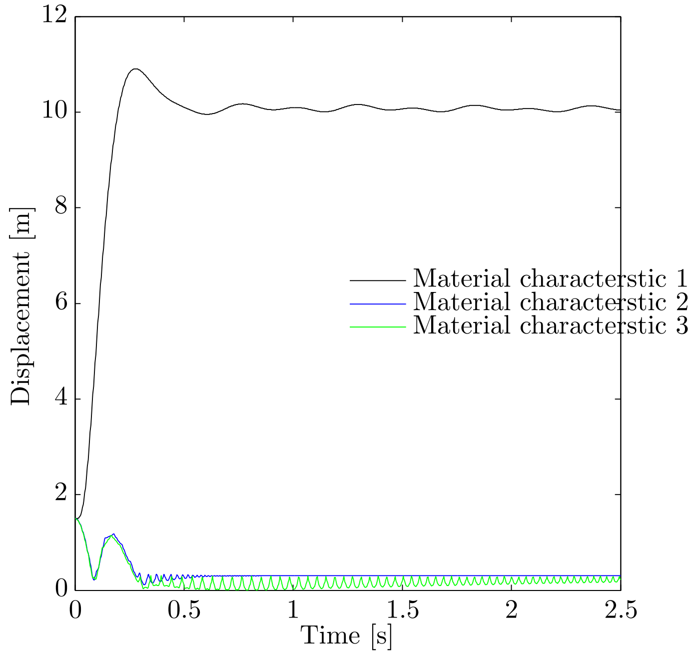


**Figure 8-12:** Result comparison mass belts

damping coefficient of 0.15. The influence of the bridle on the kite is shown.

Then the last input that was required was the bridle belt in the bridle system. With the belt characteristics used in Fig. 8-11b, the complete bridle has been tested. It proved also difficult to incorporate a bridle system that incorporated a realistic bridle system. No test is done to validate and verify the behavior of the pulley system. In the test set-up all the bridle points that are normally fixed to the bridle, are now locked by freezing all the degrees of freedom (DOF) of the bridle points. The bridle points are the points that are attached to the kite. The pulleys and the knots of the bridle system are able to move freely in 3D space. A force in positive x direction (to the right) is applied on the bottom of the bridle system see Fig. 8-13a. The result is shown in Fig. 8-13b. The material characteristics both of material characteristic 1 and 2 were almost identical.

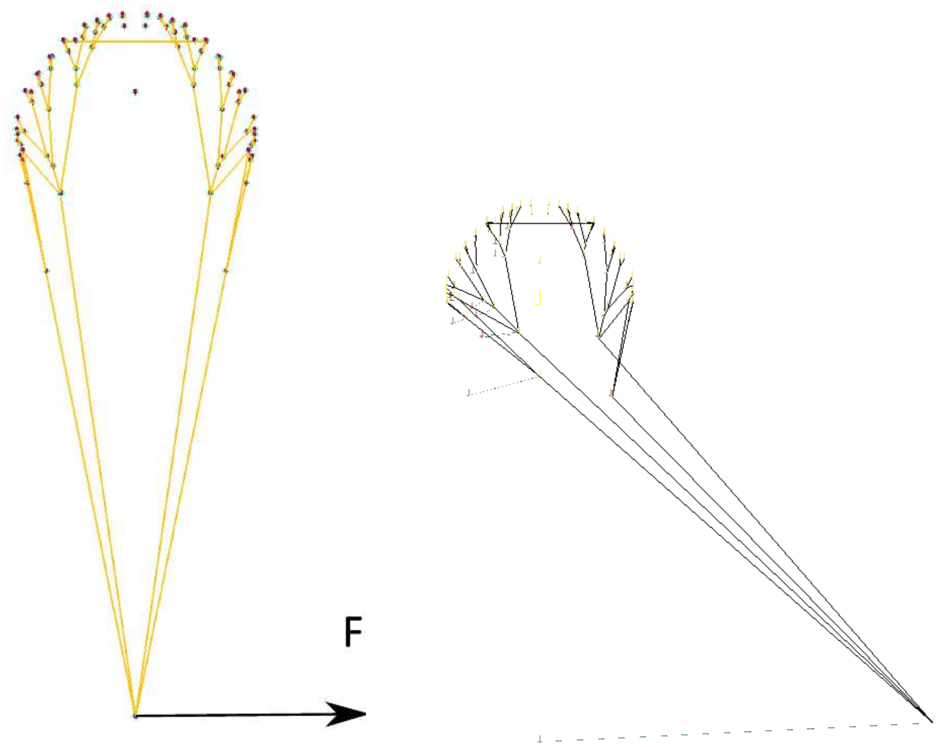


**(a)** Model setup of the kite bridle **(b)** Result under load

**Figure 8-13:** Model set-up and result of the complete bridle system under static load

## 8-2-4 External loads

In this sub section, the four external loads are described: internal pressure, gravity, point load at the center of the LE of the kite and a round mass falling on the kite.

### Inflation Process

The inflation process is similar to the inflation process of the inflatable beam. There is a major difference, because the kite had to be "released" in contrast to the beam, which was clamped at all times.

When the tips of the kite were fixed then the situation was similar to the inflatable beam. The difference was that there were more airbag chambers present in the kite. The inflation mechanism worked exactly the same as in the beam with multiple switches for each airbag chamber in the struts and LE. The first trial was without bridle system. There was one downside. Because the kite approximated 30.000 elements with multiple system models the computation time to inflate the kite was reduced. So instead of gradually pumping up the kite in 5 minutes (like in real time), the kite was inflated in less than 5 seconds. The momentum of the inflated air caused the kite to go up (bend open), as shown in Figs. 8-14.

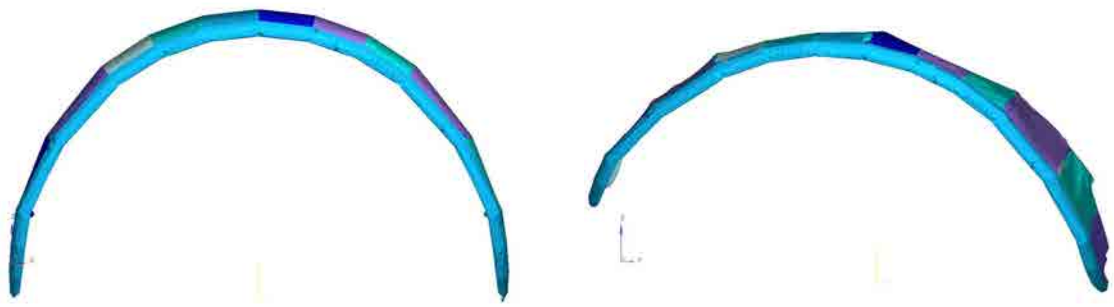

**(a)** t=0 s **(b)** t=5 s

**Figure 8-14:** Inflation process of the kite at several points in time

In order to prevent this "opening" of the kite, the kite was fixed during the inflation period. This was done in order to keep the shape of the kite. The DOFs of the nodes of both tips were fixed. The DOFs can be set to FREE with a SWITCH. So when the inflation process is done and the target pressures are met the kite is relaxed a little while and then finally the SWITCH is turned on, releasing the DOFs.

There is one important factor, and this has to do with the set-up inside Madymo. With the beam, the inflator mass flow could be set as much as possible because the beam was clamped. With the kite, the kite is set completely free with the switch. If the inflator is not completely empty and the target pressures have not been met, then there is a resultant force that spins the kite. A sequence of this phenomenon can be seen in Figure 8-15. The cause of this phenomenon is probably because the normals (pointing outside) are not everywhere pointing in the outside direction, leaving a resultant force. There was not enough time to investigate this thoroughly. By using just enough mass flow as an input for the inflator the desired pressure inside the LE and struts is reached.

### Gravity

The kite is placed upside down and the first test is the kite behavior, if the only load is gravity. The gravity is pointing downward acting only at the kite, not at the bridle system. The bridle system needs more research then done in this thesis discussed in Section 8-2-3.

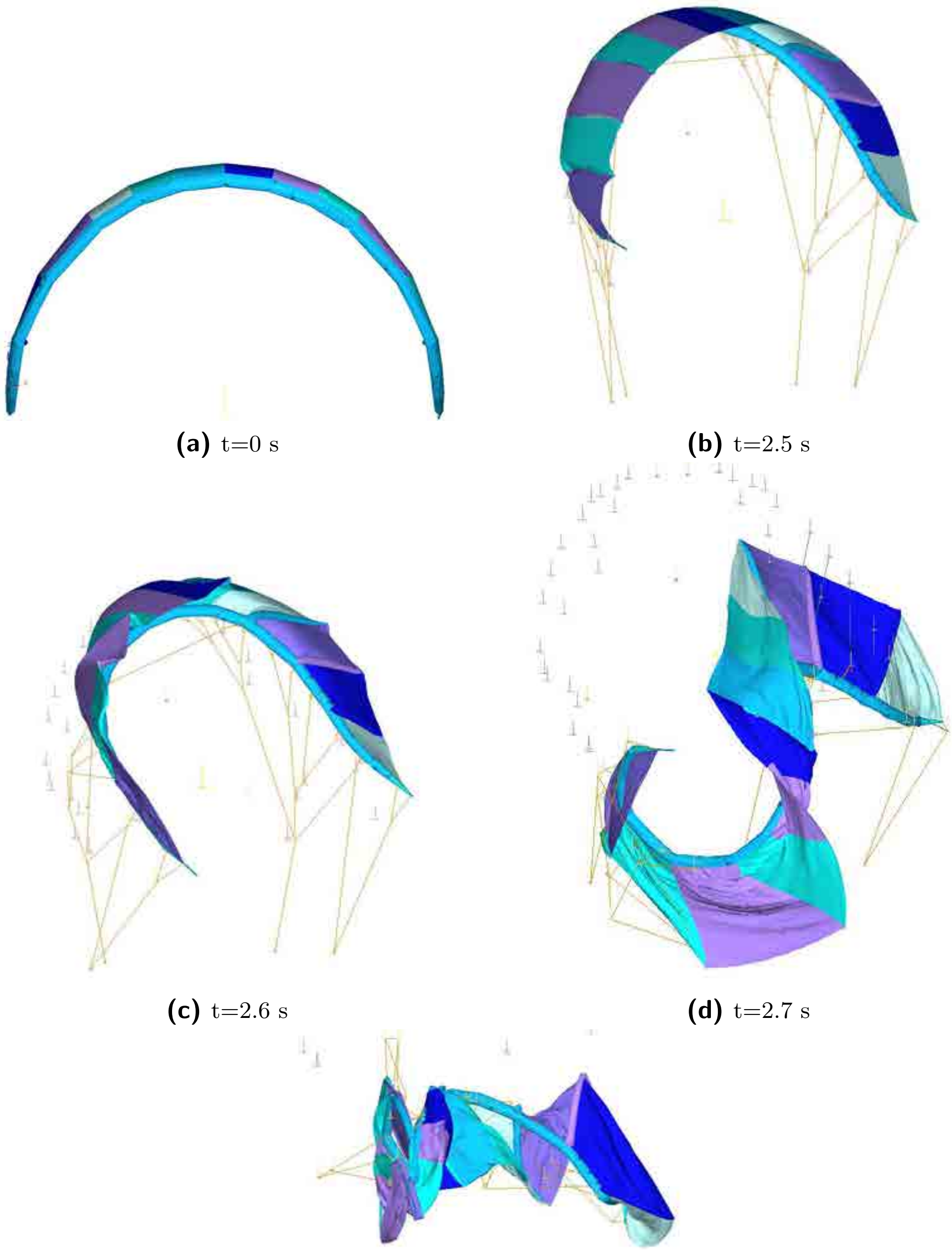

**(a)** t=0 s
**(b)** t=2.5 s
**(c)** t=2.6 s
**(d)** t=2.7 s
**(e)** t=2.9 s

**Figure 8-15:** Inflation process of the kite turned into a spiral

### Kite point loads

The forces are just point Force functions on nodes close to the position of the loads in the experiment. This point Force acting on the LE of the kite. This is modeled by loading one node at the middle of the LE of the kite with a force function like with the beam untill collapse of the kite. The force is applied after the kite is inflated and released.

#### Falling ball

The last load that is modeled is the falling mass in the kite. A multi-body mass is dropped down and contact between the ball and the kite is modeled.

### 8-2-5 Support and constraints

The attachment to the ceiling is not really applicable in the FEM model. At the corner points of the frame, the BODIES and JOINT are created on the right position from Rhino. The JOINT status is set to "LOCK". It is in reality not possible to fix all the DOFs, this is a compromise.

### 8-2-6 Measurements of the experiments

The first result is to compare the actual images of the experiment and the images of the model. The shape of the kite is the first focus. When the overall shape of the model is similar to the shape in the experiment, the deflections at different locations on the kite will be measured from the images in Rhino, where both the images of the model and the experiment will be measured. Although this is quite rough, it will give a good indication for further testing.

## 8-3 Results of the Finite Element model

The shape of the kite is captured in the experiment from the front with every load step that is applied to the kite. These images are put next to the model images from the front, applied with the same load.

### 8-3-1 Results gravity load

In this Section, only gravity acting on the kite is displayed. Two images are shown in Fig. 8-16a where the kite in the experiment is shown. In Fig. 8-16b the FEM model applied with a gravity load is shown.

The shapes of the FEM model and the experiment are quite different. The biggest difference is shown in the kite tips. As shown in the actual experiment, the kite wing tips are rotated inside. This is due to the weight especially of the center strut, this is bend down more than is shown in the model. The model seems to incorporate more stiffness compared to the experiment. There is no difference between the two bridle systems that are tested. The stiffness of the kite in this condition is assumed to be provided mostly from the kite itself.

### 8-3-2 Results point load

The next Figures show the result of the experiments and the FEM model applied with a point load at the LE of the kite.

**(a)** Experiment **(b)** FEM Model

**Figure 8-16:** Gravity applied to the kite in the experiments and the FEM model

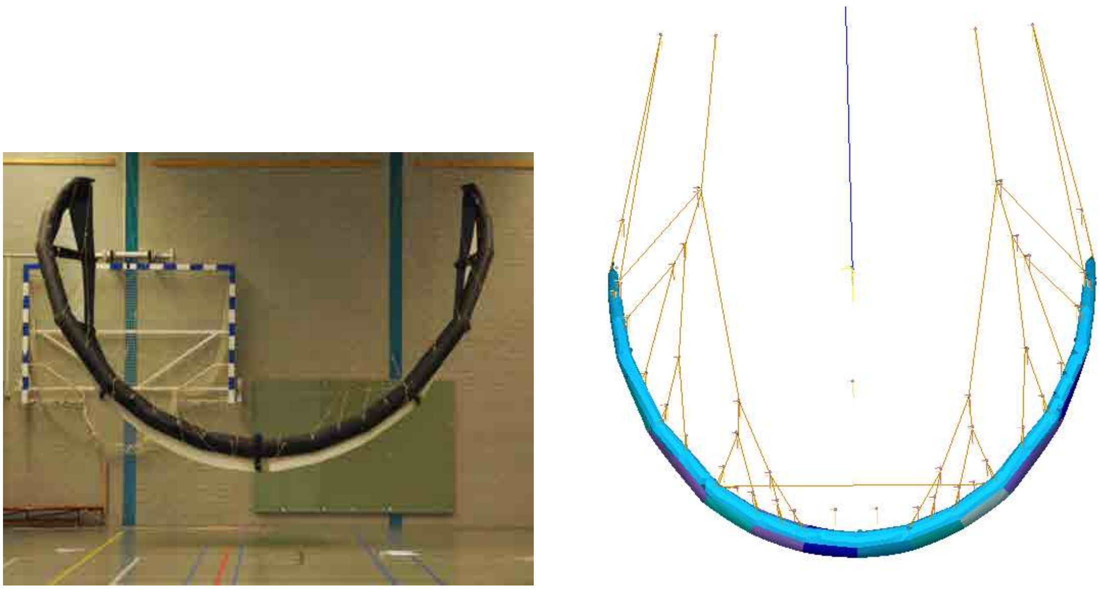

**(a)** Experiment **(b)** FEM Model

**Figure 8-17:** Force = 49 N

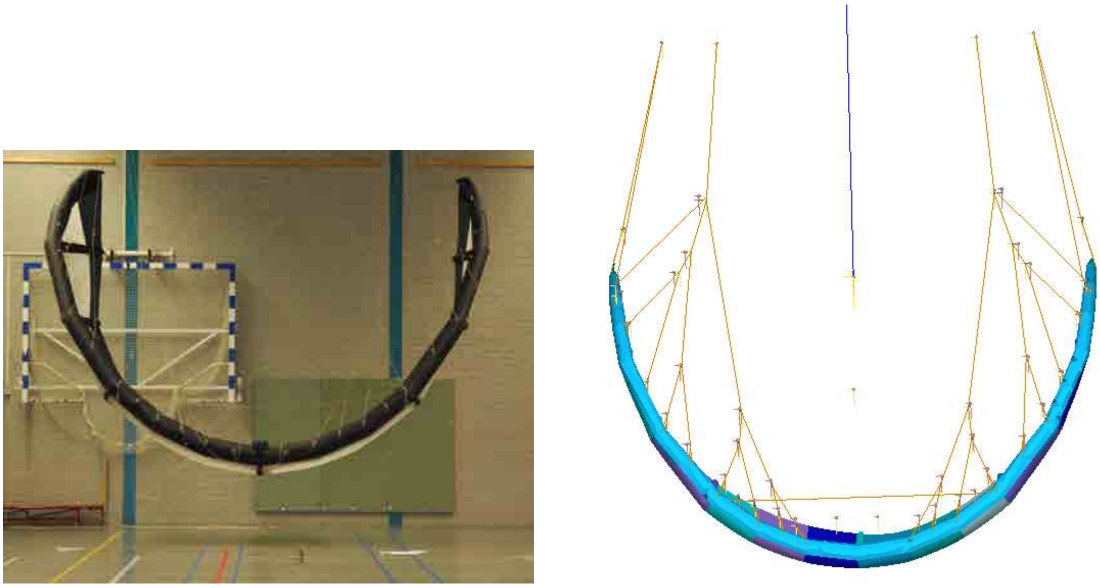

**(a)** Experiment **(b)** FEM Model

**Figure 8-18:** Force = 98 N

**(a)** Experiment **(b)** FEM Model

**Figure 8-19:** Force = 147 N

**(a)** Experiment **(b)** FEM Model

**Figure 8-20:** Force = 196 N

**(a)** Experiment

**(b)** FEM Model

**Figure 8-21:** Force = 245 N

**(a)** Experiment

**(b)** FEM Model

**Figure 8-22:** Force = 245 N

**(a)** Experiment

**(b)** FEM Model

**Figure 8-23:** Force = 343 N

**(a)** Just before Collapse

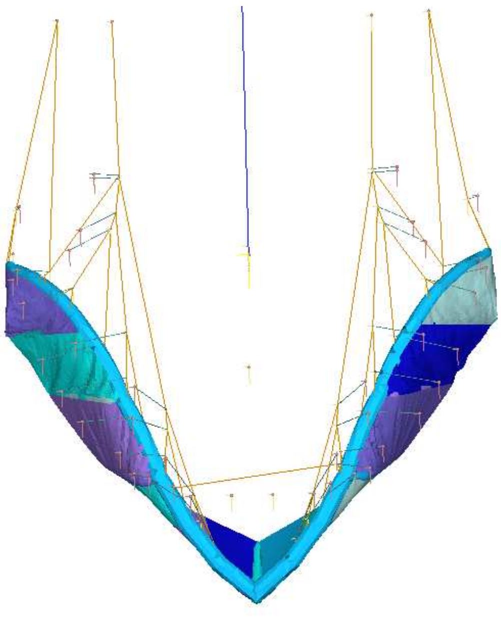

**(b)** Full Collapse FEM Model F = 635 N

**Figure 8-24:** Collapse FEM model

In Fig. 8-17 to Fig. 8-23 there is a big difference between the kite behavior of the experiment compared to the FEM model. The FEM model appears to incorporate stiffness compared to the experiment. This was expected because of the more stiffness because of the material input that was tested with the beam in Section 7-3. However there are three other important factors that could increase the stiffness of the complete kite structure. The first factor could be the attachment of the struts to the leading edge. This connection appears to be more solid compared to the actual kite. In the actual kite, the struts are sewed onto the leading edge. Some uniform stress tests have been performed (Verheul et al., 2009) of the stitched Dacron materials. However, these stitched seams were not modeled in FEM model in Madymo. The second factor is the bridle system. There is little difference between the two bridle systems that are tested. The stiffness of the kite in this condition is assumed to be provided mostly from the kite itself. The bridle has not been tested and if the characteristics are completely different, this test should be redone. However, if the characteristics are in the same order of magnitude, little differences are expected to be observed. Topics for this are the material that resulted in increased stiffness, the connection between the leading edge and the struts and the bridle system. The third factor could be the mesh refinement of the inflatable structure. There was no convergence study performed, but the output from the beam experiment (1000 elements) was taken as a starting point for the inflatable structure of the kite. Therefore, the collapse of the kite cannot be compared to the actual kite in the experiment. The force is much higher, this is similar compared to the results of the reference case of the inflatable beam, but also the shape of the collapse kite is very different.

### 8-3-3 Results falling mass

The mass was dropped from a height on the kite, to see if the kite and bridle interact. A comparison was made qualitatively of the experiment.

**(a)** Experiment

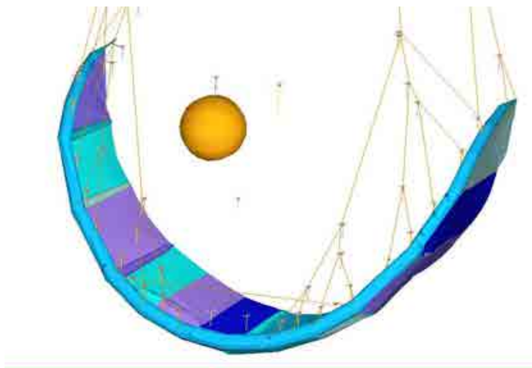

**(b)** Model

**Figure 8-25:** Falling mass comparison t = 0 s

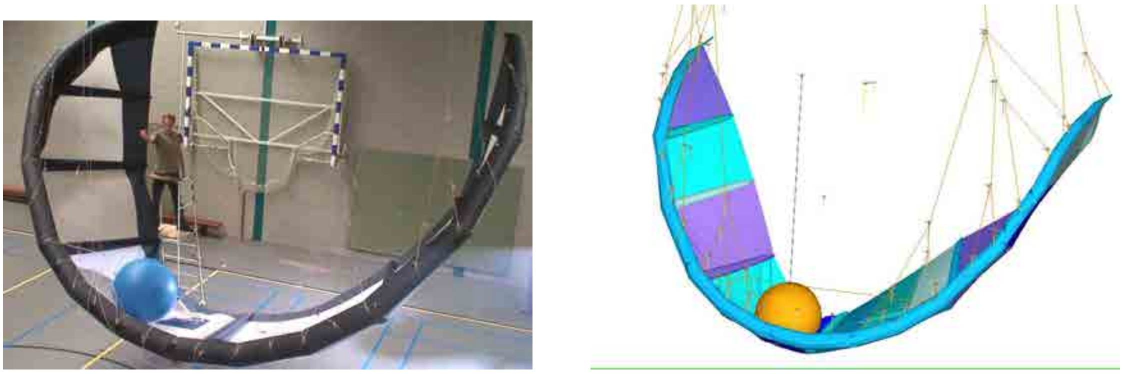

**(a)** Experiment **(b)** Model

**Figure 8-26:** Falling mass comparison t1

**(a)** Experiment **(b)** Model

**Figure 8-27:** Falling mass comparison t2

**(a)** Experiment **(b)** Model

**Figure 8-28:** Falling mass comparison t3

**(a)** Experiment

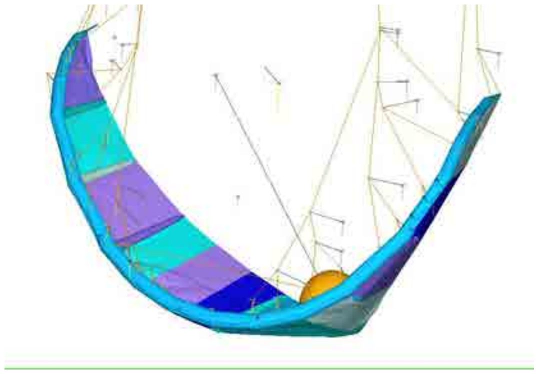

**(b)** Model

**Figure 8-29:** Falling mass comparison t4

In the Fig. 8-25 to Fig. 8-29, the interaction between the mass and the kite is displayed. The increase in stiffness is incorporated in this result to as was discussed in Section 8-3-3. The bridle system interacts with the interaction between the mass and the kite and this interaction looks realistic. The falling mass bounces of the canopy in the FEM model, in the experiment the mass sinks more or less in the kite. This is another indication of the increase in stiffness of the FEM model of the kite. The kite in the experiment tends to move entirely, while the bridle in the FEM model withstands the force.

## 8-4 Discussion

Three load cases are modeled with FEM in Madymo and compared with an experiment. All three results from the load cases imply that the kite FEM model incorporates an increased stiffness compared to the experiments. There are many uncertainties with respect to the material inputs that are used. The input that is used for the kite was derived from actual uni axial stress tests. For Dacron this uni axial stress test result appeared to be more accurate compared to the bi axial stress test, from the beam model. Not only the material input is questionable. Also the connections between the different parts of the kite seem to behave more rigid compared to the actual tests. The two different bridle characteristics that were tested did show only a little difference in behavior of the kite. However no tests were performed for the bridle and the characteristics were estimated. The kite seem to have the stiffness due to the inflation of the kite. There are a lot of research opportunities for the kite, some specific tests should be performed to investigate the increase in stiffness:

- Test T-junction with two beams to test the rigidity of the connection between the leading edge and the struts.
- Test the characteristic of the bridle lines
- Test a simple pulley case.

- Perform a mesh convergence for the complete kite.

It must be noted that the use of shell elements might result in unreliable behavior of the inflatable kite, however also this is something that should be tested properly. For this see Section 7-6-4.

Chapter 9

# Conclusion and recommendations

This Chapter provides conclusions and recommendations based on this thesis.

## 9-1 Conclusions

There are four main research questions answered in this thesis.

Is it possible to describe a FEM model of an inflatable structure with UP (uniform pressure) method with a triangular membrane mesh? The UP method equally distributes the internal pressure on the surface inside an enclosed inflatable structure?

Two inflatable structures with FEM and UP were successfully created in Madymo. The input of geometry, material and external loads describe the behavior of the FEM model. A process was developed to create the discretized input geometry for Madymo, with this process all kinds of shapes can be prepared for a mesh and then imported into Madymo. Ansys Icem proved to be a good mesh package with CAD implementation to deal with non manifold surfaces. For the materials Dacron and Ripstop only uni-axial stress test data was available. In this research a bi-axial stress test was performed by EMPA. From these tests, it was shown that both Dacron and Ripstop behave linear orthotropic. There was however a large difference between the E modulus of Dacron and Ripstop of the uni-axial tests compared to the bi-axial tests. The uniform pressure is applied on the structure by using an inflator, this ensured the internal pressure was indeed uniformly distributed on the enclosed volume. Giving the results of the inflatable beam with respect to the theory this leads to a strong indication that a triangulated mesh with FEM using the UP method could be used for modeling inflatable structures in the taut state. For the non linear states, especially collapse, further research is necessary.

How accurate will a cylindrical beam model be able to predict the behavior in comparison with experiments and theory using a model that has a reasonable computation time?

The inflatable beam was compared to an experiment and theory in the taut or linear region. A reference case is created and modeled. The model was within 2 % accurate with respect to the theory. The accuracy with respect to the experiment was significant with an average of 35% in tip deflection. The FEM model has a higher stiffness compared to the experiment.

Due to uncertainties with respect to the material inputs, possible measurement errors, details about the local behavior of the beam during the experiment and the fact that the model is not exactly similar to the model make it difficult to state what the cause was for this difference. The mesh that was used was considered converged in the taut region, however this does not count for the collapse. For the collapse behavior the results should be treated with care and there is a strong indication that more refinement has to be done. The convergence study has been done up to 15.000 elements.

What is the influence of changes in the model parameters to the inflatable beam model performance?

Due to these uncertainties, a parameter sensitivity study is performed. From the reference case one parameter is changed at the time, with one exception. A different type of element is used together with a different type of internal pressure with respect to the reference case. The root mean square error (RMSE) analysis is used to quantitatively determine the error between the deflection versus tip force curve. Two RMSE values are determined, the first value is the RMSE value of the parameters with respect to the reference case. The second is the RMSE value of the parameter with respect to the experiment.

There are four groups of results that can be distinguished. The first group consists of parameters were multiple experiments could be used as a comparison and show an influence in changing the parameters on the behavior of the beam. The parameters are beam diameter and internal pressure.

The second group consists of parameters that show an influence but could only be compared to the reference experiment. These are thickness, E modulus, Reduction factor and material model.

The third group showed limited or no influence with respect to the reference case. These are Density, material damping and Poisson's ratio.

The fourth group showed other results for with respect to the inflatable beam theory. The parameters are: shell elements, tension only = OFF and Load.Pres. This does not mean that the results are actually wrong, however there is an indication that the these model settings are not reliable to use for modeling inflatable beams.

Is it possible to model the structural dynamics of a LEI kite model including the bridle system with FEM method using the UP assumption applied to the inflatable tubular structure?

The belts in Madymo were used as bridle lines and tyings were used as pulleys. For the bridle lines, the force versus elongation input is not based on true data of the bridle lines. Two bridle line characteristics were used for the model and there was only little difference between the two characteristics. The kite could be inflated with the desired pressure, however the holes could not be closed and the mass flow of the inflator had to be tuned to ensure the correct internal pressure of the kite. The internal volumes of the leading edge and the struts remained interconnected. Based on all three load case, the kite seemed to incorporate more stiffness compared to the experiment. It is difficult to indicate what exactly causes the increased stiffness, because there are a lot of factors that influence the behavior of the inflatable structure.

Concluding: the FEM showed to be a promising approach for modeling complex inflatable structures such as the LEI kite, however a lot of research still has to be performed in order to get a accurate FEM model of the kite using UP method.

## 9-2 Recommendations

In this Section recommendations are given with respect to the potential continuation of FEM research for inflatable structures.

### 9-2-1 Material input

The are a lot of uncertainties concerning the correct material inputs. Not only the E modulus and Poisson's ratio in both thread directions is questionable, but also the material thickness was proved to be difficult to measure and lead to discussions in the kite group of DUT. The E modulus of the uni axial test and the bi axial test differed significantly. It might be good to test Dacron and Ripstop again with the uni-axial test machine at the DUT and perform the tests in both directions. The most important recommendation when such a test is performed is that a test report is made. In this way it is always clear what and how the tests have been performed. The use of shell elements, quadrilateral elements could be used to gain computation time. However it must be noted that the use of shell elements resulted in unreliable behavior of the inflatable beam see Section 7-6-4, so this could be validated with another FEM package.

### 9-2-2 Modeling the bridle system

The bridle system was proven to be easy to implement but difficult to model. The characteristics of the bridle lines should be tested and a simple pulley test is advised to be performed to increase the knowledge needed for modeling bridle system in Madymo.

### 9-2-3 Modeling a cylindrical inflatable beam

An extension to the inflatable beam research is needed to validate the FEM model of the beam in Madymo. If the FEM model is created of the inflatable beam, another test of the inflatable beam should be performed. Preferable with pure bending. The shear force has influence on the behavior of the beam and in order to get feeling for inflatable structures and beams, such a test is crucial. All the important components that could be vital for validation can be recorded. Examples are: take different images at different loads to compare the overall shape, make images of the wrinkling behavior. In order to show wrinkling visibly in the dynamic output file, the number elements should be increased. This thesis is limited at the linear analysis of a beam, however if collapse is taken into account further study must be performed on mesh convergence and maybe local refinement.

### 9-2-4 Modeling a complete kite including bridle

Recommendations with regard to the kite regarding modeling of the kite is to investigate in detail all the connections of the inflatable tubular structure, the connections between the tubular structure and the canopy and the connection between the kite and the bridle system. It might be good to divide the kite into smaller sections were every section is tested, modeled and validated. Also an extensive mesh refinement, or convergence, study has to be performed of the complete kite.

### 9-2-5 Complete kite including bridle experiment

It was a great challenge to create an experiment for the kite, mainly due to the size. For the positioning of the kite it is preferred to hang the kite at the position of the KCU. The dimensions of the "frame" were taken out of the CAD representation. If the "frame" of the kite is used, it should be made of a rigid material. The nylon ropes were elastic and were stretched during positioning of the kite. It is best when the kite is positioned at the height of the KCU. If a more detailed model is made of the kite including mesh refinement, or convergence study, and the kite behaves more similar compared to the experiment, more test cases could be performed. In order to validate the shape, photogrammetry could be used as a benchmark. The a more accurate comparison could be made of the kite.

### 9-2-6 Madymo

Madymo was a great program to work with, however, it took a long time to incorporate the basic inputs for the models. Such as inflating the beam at a correct pressure, correct output generation, building the complete model etc. It might be beneficial for both the DUT and TASS to join forces and be more directly involved with experts of Madymo.

# Bibliography


Ansys. (2007). *Ansys icem cfd 11.0 tutorial manual.*

ASTM, I. (2003). *Standard test method for breaking force and elongation of textile fabrics (strip method).* ASTM International.

Axelrad, E., & Emmerling, F. (1987). Intrinsic shell theory relevant for realizable large displacements. *International Journal of Non-Linear Mechanics*, *22*(2), 139 - 150.

Baruch, J., M. and Arbocz, & Zhang, G. (1992). Imperfection sensitivity of the brazier effect for orthotropic cylindrical shells [Internal report].

Bathe, K.-J. (1982). *Finite element procedures in engineering analysis.* Prentice-Hall, Inc., Englewood Cliffs, New Jersey 07632.

Brazier, L. G. (1927). On the flexure of thin cylindrical shells and other thin sections. *Proceedings of the Royal Society of London. Series A, Containing Papers of a Mathematical and Physical Character*, *116*(773), 104 - 114.

Breukels, J. (2011). *An engineering methodology for kite design* [Dissertation]. Uitgeverij BOXPress, Oisterwijk.

Chatzikonstantinou, T. (1999). Problems in ram air wing modeling and their solution in the three dimensional simulation code 'para3d'.

Comer, R., & Levi, S. (1963). Deflections of an inflated circular-cylindrical cantilever beam. *AIAA Journal*, *1*, 1652-1655.

Davids, W. G., & Zhang, H. (2008). Beam finite element for nonlinear analysis of pressurized fabric beamcolumns. *Engineering Structures*, *30*(7), 1969 - 1980.

Filippa, C. (2000a). *Nonlinear finite element methods (asen 6107).* College of engineering University of Colorado.

Filippa, C. (2000b). *A systematic approach to the element-independent corotational dynamics of finite elements* (Tech. Rep.). College of engineering University of Colorado.

Flugge, W. (1932). Die stabilitat der kreiszylinderschale. *Archive of Applied Mechanics*, *3*, 463-506.

Galliot, C., & Luchsinger, R. (2009). A simple model describing the non-linear biaxial tensile behaviour of pvc-coated polyester fabrics for use in finite element analysis. *Composite Structures*, *90*(4), 438 - 447.

Geuzaine, C., & Remacle, J.-F. (2010). *Gmsh reference manual.*

Heuvel, J. v. d. (2011). *Kitesailing.* Delft University of Technology.

Hibbeler, R. (1997). *Sterkteleer.* Prentice Hall Academic Service.

Jamal, A. (1998). [Dissertation].

Jetteur, P., & Bruyneel, M. (2008). *Advanced capabilities for the simulation of membrane and inflatable space structures using samcef* (Vol. 8). Springer Netherlands.

Kroeplin, B., & Wagner, R. (2004). On the applications, the potential and the limits of inflatable membrane structures.

Lampani, L., & Gaudenzi, P. (2010). Numerical simulation of the behavior of inflatable structures for space. *Acta Astronautica*, *67*(34), 362 - 368.

Le, v. A., & Wielgosz, C. (2005). Bending and buckling of inflatable beams: Some new theoretical results. *Thin-Walled Structures*, *43*(8), 1166 - 1187.

Loyd, M. L. (1980). *Crosswind kite power* (Vol. 4).

MacNeal, R. (1994). *Finite elements: their design and performance.* M. Dekker.

Ockels, W. J. (2001). Laddermill, a novel concept to exploit the energy in the airspace. *Aircraft Design*, *4*(23), 81 - 97.

Ockels, W. J., Lansdorp, B., Breukels, J., & Spierenburg, G. (2004). The laddermill: Work in progress.

Pappa, R. S., Lassiter, J. O., & Ross, B. P. (2001). Structural dynamics experimental activities in ultra-lightweight and inflatable space structures.

Schmehl, R. (2011a). Die kraft des drachens. *Erneuerbare Energien*(8), 64 - 69.

Schmehl, R. (2011b). Kite power technologie. *Windnieuws*(2), 22 - 24.

Schmehl, R. (2012). Large-scale power generation with kites. *Leonardo Times Journal of the Society of Aerospace Engineering Students 'Leonardo da Vinci'*(1), 21 - 22.

Schmehl, R., & Fechner, U. (2012). Design of a distributed kite power control system. *Multi-Conference on Systems and Control, Dubrovnik, Croatia*.

Seide, P., Weingarten, V., & Peterson, J. (1965). Buckling of thin-walled circular cylinders. *NASA SPACE VEHICLE DESIGN CRITERIA (Structures)*, 56.

Southern Ropes, U. (2012). *Southern ropes.* Available from `www.southernropes.com/products/sailmakers-catalogue/leech-lines`

Stein, M., & Hedgepeth, J. M. (1961). *Analysis of partly wrinkled membranes* (Tech. Rep.).

TASS. (2010a). *Madymo application manual 7.3.* Author.

TASS. (2010b). *Madymo introduction presentation finite element module.* Author.

TASS. (2010c). *Madymo reference manual 7.3.* Author.

TASS. (2010d). *Madymo theory manual 7.3* (Vol. 9) (No. 2). Author.

Thomas, J. (2008, February). *Metaefficient the guide to efficient living.* Available from `www.metaefficient.com/news/new-record-worlds-largest-wind-turbine-7-megawatts.html`

Thomas, J., & Wielgosz, C. (2004). Deflections of highly inflated fabric tubes. *Thin-Walled Structures*, *42*(7), 1049 - 1066.

TRW, O. R. S. G. . C. (2003). *Seitenairbag:bio adapted side airbag system* (Tech. Rep.).

Tsunoda, H., & Senbokuya, Y. (2002). Structural dynamics experimental activities in ultra-lightweight and inflatable space structures.

Veldman, S. (2005). *Design and analysis methodologies for inflated beams.* Ios Pr Inc.

Veldman, S. (2006). Wrinkling prediction of cylindrical and conical inflated cantilever beams under torsion and bending. *Thin-Walled Structures*, *44*(2), 211 - 215.

Veldman, S., Bergsma, O., Beukers, A., & Drechsler, K. (2005). Bending and optimisation of an inflated braided beam. *Thin-Walled Structures*, *43*(9), 1338 - 1354.

Verheul, R. (2010). *Mass and geometric properties of the 25m mutiny v2 kite* (Tech. Rep.).

Verheul, R., Breukels, J., & Ockels, W. (2009). Material selection and joining methods for the purpose of a high-altitude inflatable kite.

Wachter, A. de. (2010). Power from the skies. *Leonardo times*(4), 18-20.

Wielgosz, C., Le, v. A., & Thomas, J. (2008). Mechanics of inflatable fabric beams. *International Conference on Computational & Experimental Engineering and Sciences*, *5*(2), 93-98.

Wielgosz, C., & Thomas, J. (2002). Deflections of inflatable fabric panels at high pressure. *Thin-Walled Structures*, *40*(6), 523-536.

# Appendix A

# Uinform pressure theory

The composition of air consists of the mass mixture fractions $Y_i$ and these fractions remain constant see Eq. A-1.

$$Y_i = \frac{M_i}{M_{tot}} = \quad \text{Constant} \quad \Rightarrow dY_i \equiv 0 \quad \text{and} \quad \frac{dY_i}{dt} \equiv 0 \tag{A-1}$$

With the additional assumption of ideal gas behavior the mass-specific internal energy is constructed as:

$$u = \sum_{i=1}^{n} Y_i \, u_i, \qquad \text{where} \quad u_i = u_i(T), \tag{A-2}$$

The total differential can be decomposed as follows

$$du = \sum_{i=1}^{n} Y_i \, du_i, \tag{A-3}$$

$$= \sum_{i=1}^{n} Y_i \, c_{v,i} \, dT, \tag{A-4}$$

$$= c_{v,m} \, dT, \quad \text{where} \quad c_{v,m} = \sum_{i=1}^{n} Y_i \, c_{v,i} \tag{A-5}$$

The first expression in equation A-5 represents the change of internal energy due to changing temperature where $c_{v,m}$ represents the heat capacity of the ideal gas mixture. The total time derivative of the internal energy content $U = mu$ contained in each chamber can be formulated as

$$\frac{dU}{dt} = m\frac{du}{dt} + u\frac{dm}{dt} \tag{A-6}$$

$$= mc_{v,m}\,\frac{dT}{dt} + \sum_{i=1}^{n} Y_i\, u_i \frac{dm}{dt} \tag{A-7}$$

The first term on the right hand side in equation A-7 describe the temporal variation of $U$ for changing temperature and the second term in equation A-7 describes the changing mass content of the chamber.

The relation between pressure $p$, temperature $T$, gas volume $V$ and mass $m$ is described by the ideal gas law:

$$m = \frac{p\,V}{R_s\,T} \tag{A-8}$$

$R_s = R/M$ is the special gas constant and $M$ the variable molar mass of the mixture which depends on the molar mixture fractions $X_i$ and the component molar masses $M_i$ in equation A-9

$$M = \sum_{i=1}^{n} X_i M_i. \tag{A-9}$$

The mass balance of each chamber is given by equation A-10.

$$\frac{dm}{dt} = \sum_{j=1}^{p} \dot{m}_j, \tag{A-10}$$

Where the $\dot{m}_j$ represent the mass flows $j = 1, \ldots, p$ entering (from inflators or from other chambers) or leaving (through holes to other chambers) the chamber control volume. Per chamber, individual mass balance equations can be formulated for each gas substance in equation A-11.

$$\frac{dm_i}{dt} = \sum_{j=1}^{p} \dot{m}_{j,i}, \qquad \text{where} \quad i = 1, \ldots, n \tag{A-11}$$

In case of the inflatable kite the gas that is used to inflate the kite is air. The chemical composition of air in each chamber is assumed to remain constant after inflation. Neglecting the kinetic energy of the gas in the airbag chambers, the energy balance of each chamber is given in equation A-12.

$$\frac{dU}{dt} = \dot{Q} + \sum_{j=1}^{p} \dot{m}_j \left( h_j + \frac{v_j^2}{2} \right) - \dot{W}. \tag{A-12}$$

The first term on the right hand side of this equation represents the net heat flux transfered to the chamber. It can be modeled by the following discretization:

$$\dot{Q} = \int_S \dot{q}\, dS = \sum_{l=1}^{q} k_l\, S_l(T - T_l) \tag{A-13}$$

Where $\dot{q}$ is the local heat flux density at the chamber surface, $k_l$ are the heat transfer coefficients and $S_l$ the areas associated with the surface patches $l = 1, \ldots, q$ and $T - T_l$ are the corresponding driving temperature differences. The second term of Equation A-12 comprises the convective energy transfer to the airbag chamber coupled to the mass flows $\dot{m}_j$. It consists of a static part, $h_j$, and a kinetic part, $v_j^2/2$. For a multi-component gas mixture the associated enthalpies $h_j$ are calculated in equation A-14.

$$h_j = \sum_{i=1}^{n} Y_{j,i}\, h_i, \qquad \text{where} \quad j = 1, \ldots, p \tag{A-14}$$

The $h_i$ terms are the mass-specific enthalpies of the gas components at a specific temperature level associated with the in- or outflow. Characteristic velocities $v_j$ of the mass flows $\dot{m}_j$ can be derived from the following approximation:

$$\dot{m}_j = \rho_j\, A_j\, v_j, \tag{A-15}$$

where $A_j$ is the cross sectional area of the in- or outflow region.

The third term in equation A-12 represents the work rate due to expansion or compression of the chamber volume $V$ and can be described as:

$$\dot{W} = p\frac{dV}{dt}. \tag{A-16}$$

Combining equations A-7 and A-12 the ime derivative of the temperature of each chamber is described as:

$$\frac{dT}{dt} = \frac{1}{m\, c_{v,m}} \left[ \sum_{l=1}^{q} k_l\, S_l(T - T_l) + \sum_{j=1}^{p} \dot{m}_j \left( h_j + \frac{v_j^2}{2} \right) - p\frac{dV}{dt} - \sum_{i=1}^{n} Y_i\, u_i \frac{dm}{dt} \right] \tag{A-17}$$

Starting from an initial state of the gas in an airbag chamber, defined by $p^0, T^0, m^0$ and $Y_i^0$, equations A-10, and A-17 can be integrated numerically for given mass flow rates $\dot{m}_j$, internal energies $u_i(T)$, enthalpies $h_i(T)$, volume change $dV/dt$ and heat transfer model $k_l$ and $S_l$. The pressure increases (equal to a preset pressure) compared to the ambient pressure. Consequently also the volume increases compared to the initial volume of each chamber due to the expansion of the chamber.

# Appendix B

# Output/Input Process from CAD to Mesh

**NOTES** The curves and the points (if there exist any) for all extension have to be removed from the CAD drawing. Only surfaces can be exported to the mesh program.

## B-1 Output/Input Process from CAD to Mesh for GMSH

The output of the CAD (Rhino) in order to import the CAD geometry in GMSH is a .STP (or step) file extension. NonManifoldMerge should not be used, because this functionality is not supported for .STP extension.

## B-2 Output/Input Process from CAD to Mesh for Icem

The output of the CAD (Rhino) in order to import the CAD geometry in Icem is a .sat (acis) file extension. NonManifoldMerge should not be used, see for figure B-1a of a CAD representation of half of the kite before the NonManifoldMerge was applied and see figure B-1b after applying NonManifoldMerge. In figure B-2, a partof the mesh inside of the kite is shown. The strut of the kite (which is completely flat) is not attached tot the canopy parts, where it should be attached. This is no problem, because Icem has got an extensive CAD tool box.

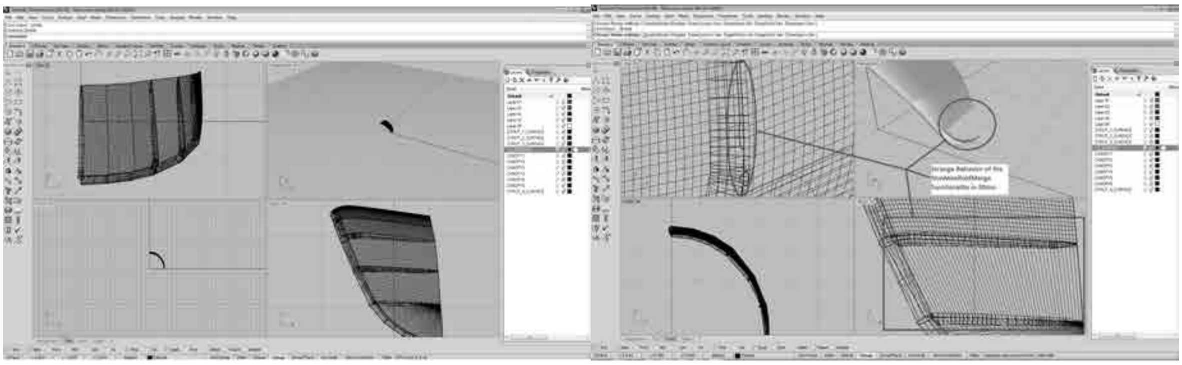

**(a)** CAD representation of half of the kite before applying NonManifoldMerge

**(b)** CAD representation of half of the kite after applying NonManifoldMerge

**Figure B-1:** Mesh of a cylinder in GMSH

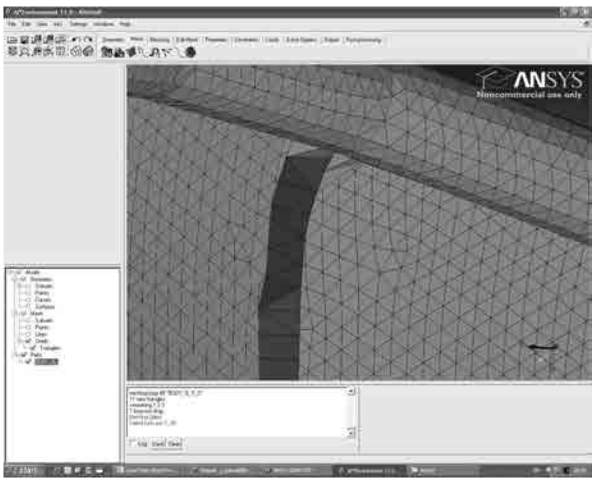


**Figure B-2:** Result of NonManifoldMerge function of Rhino in Icem

# Appendix C

# Output/Input Process from Mesh to Madymo

This is an example of one of the scripts that was needed in order to get the correct input for Madymo.

@author: jschwoll

```
from future import with_statement
import time

class Timer(object):
def __enter__(self):
self.__start = time.time()

def __exit__(self, type, value, traceback):
# Error handling here
self.__finish = time.time()

def duration_in_seconds(self):
return self.__finish - self.__start

class MeshConverter:

Class to convert mesh data from icem radioss.txt file into
madymo tables

def __init__(self):
self.nodes = []
```

```
self.elements = []
self.partno = []
self.meshReader = None
self.elementReader = None

def readMeshFile(self, inputFile):
” read the file and store it into the meshReader property ”
print ”Looping through the file, line by line.”
self.meshReader = open(inputFile, ’r’)

def writeResultNode(self, NodeFileName):
””” Process the input mesh and write the elements into a file
with the name of the NodeFileName parameter; ””” print ”Writing file: ” + NodeFileName
node = open(NodeFileName, ’w’)
i = 0
for line in self.meshReader:
if i ¿ 0:
if len(line) ¿ 60:
l = line.split()
n = l[0:4]
print ’ ’.join(n)
node.write(’ ’.join(n) + ”n”)
i = i+1
node.close()
self.meshReader.seek(0)

def writeResultElement(self, ElementFileName):
””” process the input mesh and write the elements into a file with the name of the
ElementFileName parameter;
Then read the new file into the elementReader- property.
””” print ”Writing file: ”+ElementFileName
element = open(ElementFileName, ’w’)
i = 0
for line in self.meshReader:
if i > 1:
if len(line) < 50:
l = line.split()
m = int(l[0]), int(l[1]), int(l[2]), int(l[3]), int(l[4])
I = str(m)
#print m
O = I.replace(”,”,””)
#print O
P = O.replace(”(”,””)
Q = P.replace(”)”,””)
print ”.join(Q) + ”n”
element.write(”.join(Q) + ”n”)
```

```
i = i+1
#print count
element.close()
self.elementReader = open(ElementFileName, ’r’)

def writeResultPart(self, PartFileName):
””” process the input elements and write the nodes of each part into a file with the name of the PartFileName parameter;
””” print ”Writing file: ” + PartFileName
largest = 0
for line in self.elementReader:
numlist = line.split()
del numlist[0]
self.partno.append(numlist)
#print list
if numlist[0] > largest:
numlist[0] = int(numlist[0])
largest = numlist[0]
print numlist

L = []
for j in range(largest):
L.append(set())
print L

for numlist in self.partno:
for i in range(3):
L[numlist[0]-1].add(str(numlist[i + 1]))
print L[i]
#filename = ’resultpart.txt’
partnode = open(PartFileName, ’w’)

for i in range(largest):
partnode.write(str(i + 1) + ’: ’ + ’ ’.join(L[i]) + ”n”)

partnode.close()

if __name__ == ’__main__’:
timer = Timer()

with timer:
oConv = MeshConverter()
INPUT_FILE = ”testini.k”
NODE_FILE_NAME = ”resultnodesini.txt”
```

```
ELEMENT_FILE_NAME = "resultelemini.txt"
PART_FILE_NAME = "resultpart.txt"

oConv.readMeshFile(INPUT_FILE)
oConv.writeResultNode(NODE_FILE_NAME)
oConv.writeResultElement(ELEMENT_FILE_NAME)
oConv.writeResultPart(PART_FILE_NAME)

print "'Execution time: %.2f seconds. "' % (timer.duration_in_seconds())
```

# Appendix D

# Results of the bi-axial stress tests of Dacron and Ripstop performed by EMPA Switzerland

The bi-axial material tests were performed by EMPA in Switzerland. EMPA designed a specific bi axial stress and shear test (see (Galliot & Luchsinger, 2009)) for woven fabrics. In the test for the pumping kite power system project they performed material test for Dacron and Ripstop. Dacron is the material for the inflatable tubes and ripstop is the material for the canopy. For both materials there are two tests performed: Bi axial stress test (this test is performed in two runs to verify the test) and a bi axial shear test is performed.

**Comments from Cedric Galliot, test engineer at EMPA, Switzerland**

> *"I estimated the materials properties ($E_w$, $E_w$ and $\nu_{wf}$) based on the results of the last cycles, which are actually the data I sent you today. Then I used the Solver in Excel to find the best match between the experimental data and a linear elastic orthotropic model with the given properties. Actually for both materials these models give quite a good match for all tested load ratios. This is not the case in the paper you read because the structure in the fabrics is different. For PVC coated polyester for example the crimp is pretty high, that means that the yarns are initially curved, so when you pull in one direction they tend to straighten in that direction and to be curved even more in the orthogonal direction, which is called "crimp interchange". We found out that it was not possible to capture this effect with the Poisson's ratio, and that it would be necessary to have a non linear model with varying elastic moduli. But this does not significantly appear for the kite materials."*

> *"I made some more biaxial tests with the Dacron and the Ripstop materials. These tests are made with another machine configuration (5 grips per side on the*

*sample instead of 1). This configuration allows to apply a shear loading to the specimen with the shear ramp test procedure that we developed at EMPA. You will find here enclosed four files, two new biaxial tests and two shear tests. The new biaxial tests give very similar results in comparison to the first series so I think it won't be necessary to test a third sample. It took me some time to perform the shear tests because with such materials we reach the lower limit of our test machine capabilities. It is also more difficult in the case of shear to give a single value for the shear modulus, so I gave some boundaries instead. You will probably see that a stress correction factor is used for the shear tests. This allows to obtain an estimation of the shear stress in the centre of the sample from the tensile stresses that are applied and measured on the sample. This factor is determined by FEA. If you have any question concerning the tests do not hesitate to ask. I could also send you some pictures of the samples and the test setup if wish.*"

## D-1 Dacron bi-axial stress test

Center for Synergetic Structures

EMPA Materials Science & Technology

**Biaxial test report**

Date: 16.08.2011 Temperature: 22°C Specimen ID: Dacron_01

**Material reference:** **Dacron (black)**

| | | | |
|---|---|---|---|
| Yarn material: | Polyester | Coating material: | |
| Yarns (dtex): | | Weave pattern: | |
| Weight (g/m$^2$): | approx. 150 | Thickness (mm): | approx. 0.17 |
| Warp tensile strength (kN/m): | 26 | Fill tensile strength (kN/m): | 26 |

**Loading history:**

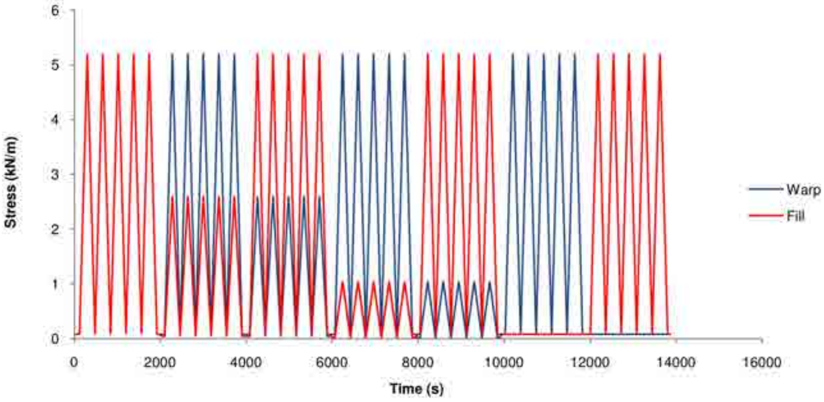


| | | | |
|---|---|---|---|
| Pre-stress Warp (kN/m): | 0.08 | Max. stress Warp (kN/m): | 5.2 |
| Pre-stress Fill (kN/m): | 0.08 | Max. stress Fill (kN/m): | 5.2 |
| Max. loading rate ((N/m)/s): | 29.4 | | |

**Additional informations:**

Mechanical properties based on plane stress linear elastic orthotropic model:

$E_w$ = 358.9 kN/m

$E_f$ = 326.0 kN/m

$\nu_{wf}$ = 0.33

Page 1

Center for Synergetic Structures

EMPA Materials Science & Technology

**Cycles #1: Load ratio 1:1**

*Measured stress:*

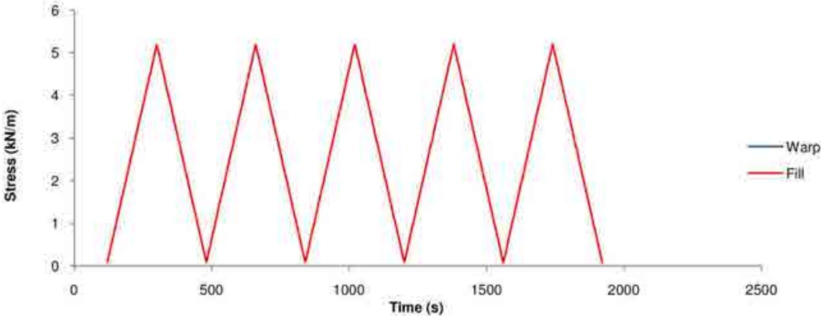


*Measured strain:*

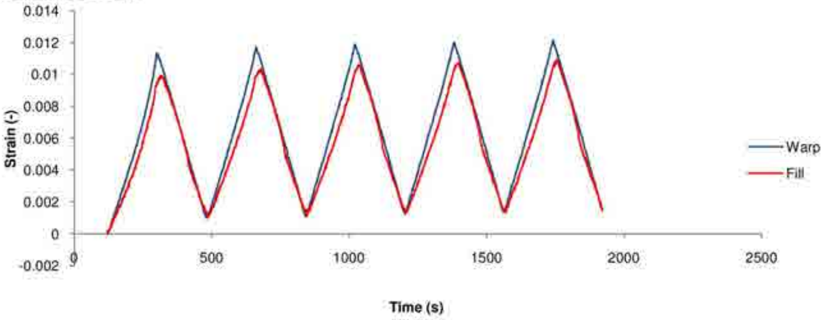


*Stress-strain behaviour:*

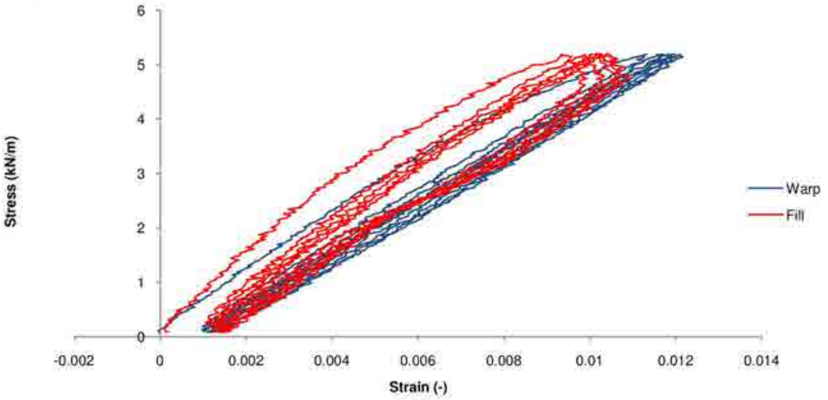


Page 2

Center for Synergetic Structures

EMPA Materials Science & Technology

**Cycles #2: Load ratio 2:1**

*Measured stress:*

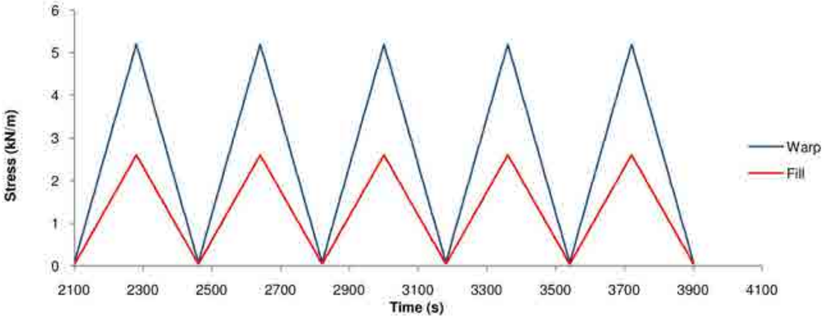


*Measured strain:*

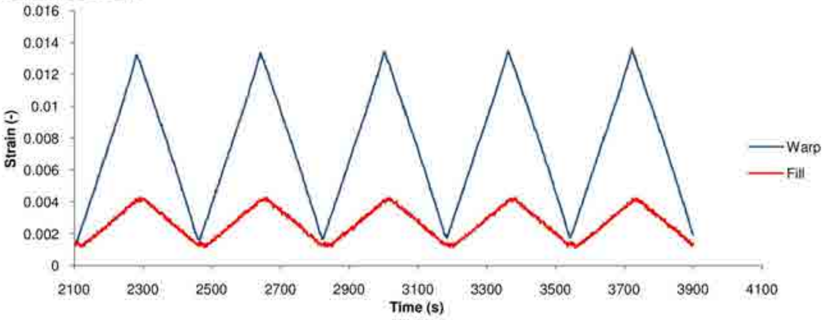


*Stress-strain behaviour:*

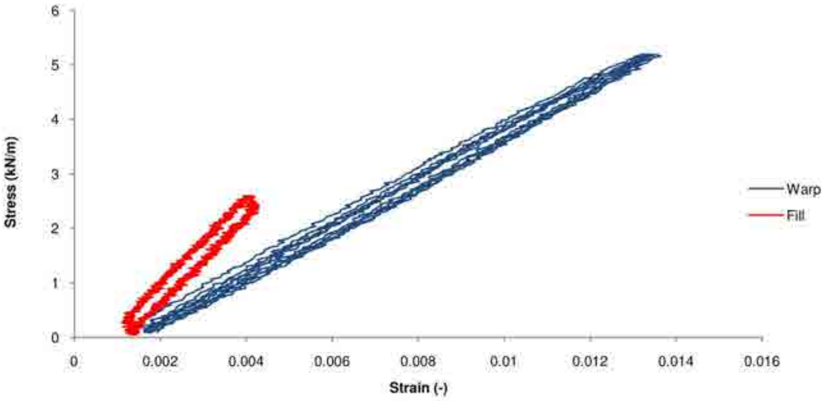


Page 3

Center for Synergetic Structures

EMPA Materials Science & Technology

**Cycles #3: Load ratio 1:2**

*Measured stress:*

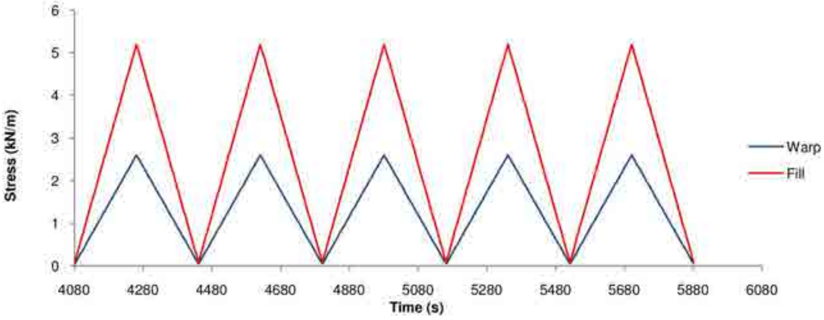


*Measured strain:*

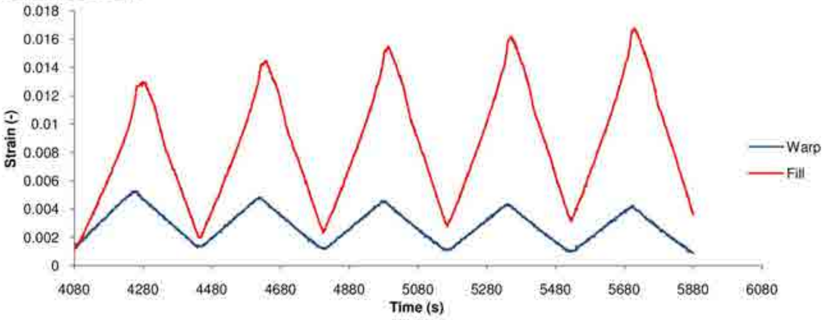


*Stress-strain behaviour:*

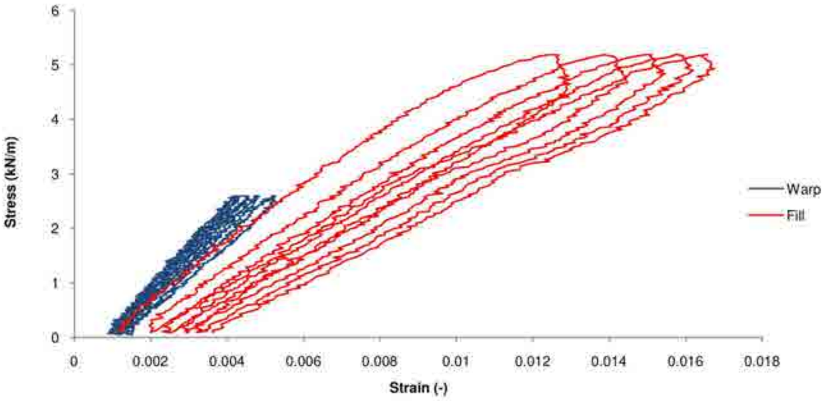


Page 4

Center for Synergetic Structures

EMPA Materials Science & Technology

**Cycles #4: Load ratio 5:1**

*Measured stress:*

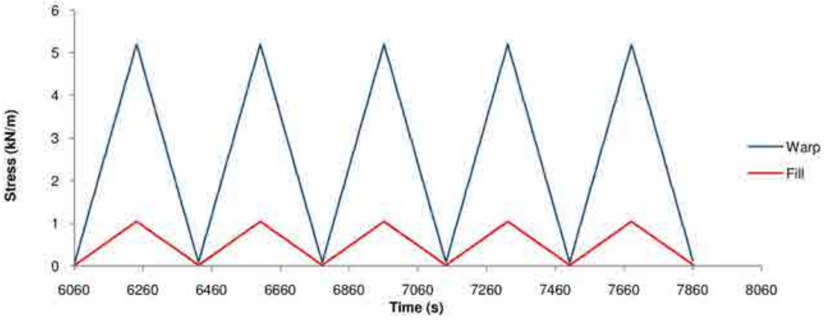


*Measured strain:*

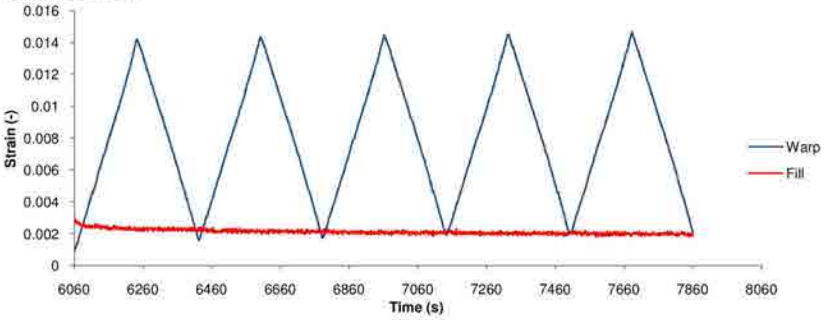


*Stress-strain behaviour:*

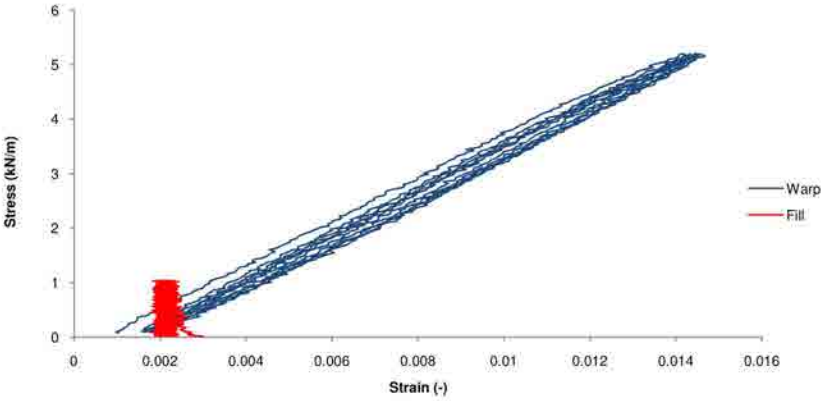


Page 5

Center for Synergetic Structures

EMPA Materials Science & Technology

**Cycles #5: Load ratio 1:5**

*Measured stress:*

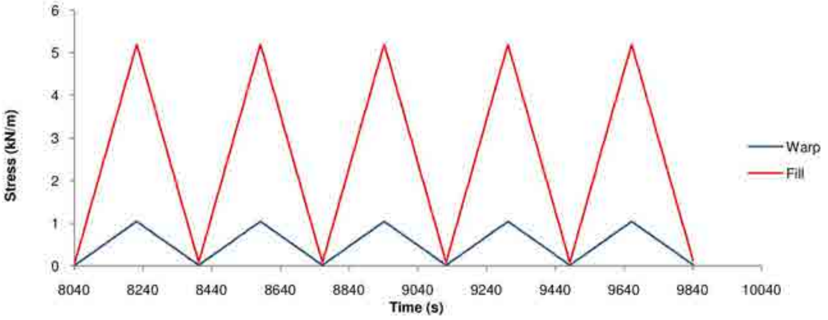


*Measured strain:*

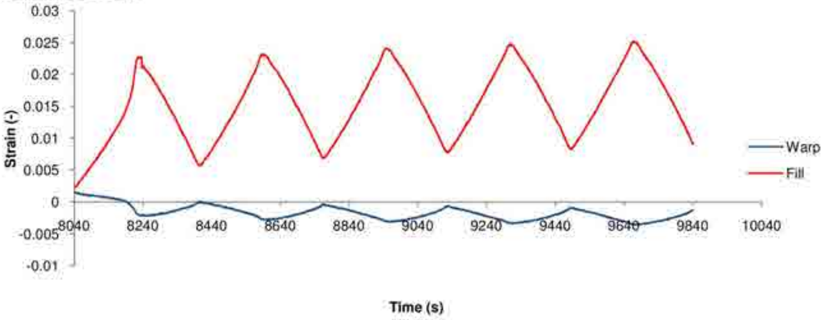


*Stress-strain behaviour:*

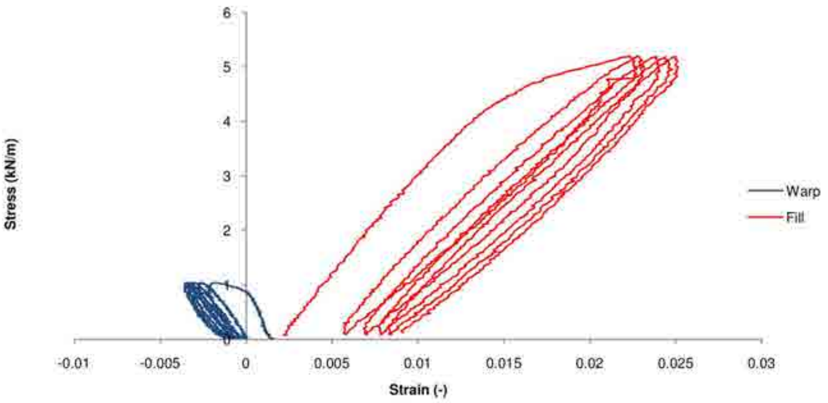


Page 6

Center for Synergetic Structures

EMPA
Materials Science & Technology

**Cycles #6: Load ratio 1:0**

*Measured stress:*

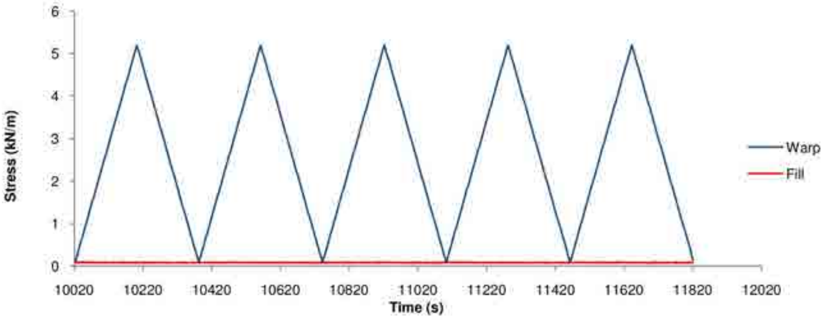


*Measured strain:*

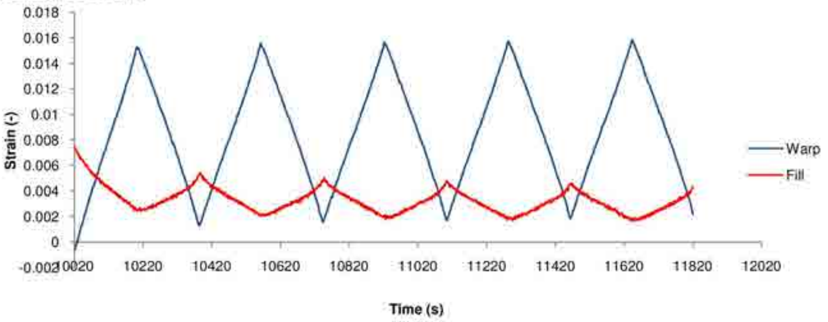


*Stress-strain behaviour:*

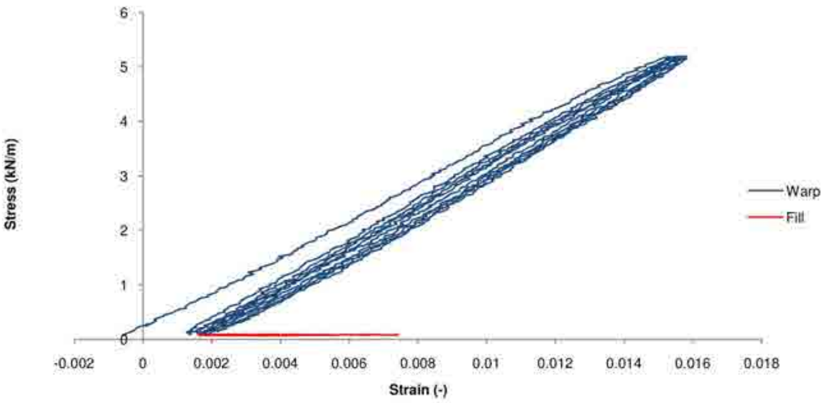


Page 7

Center for Synergetic Structures

EMPA Materials Science & Technology

**Cycles #7: Load ratio 0:1**

*Measured stress:*

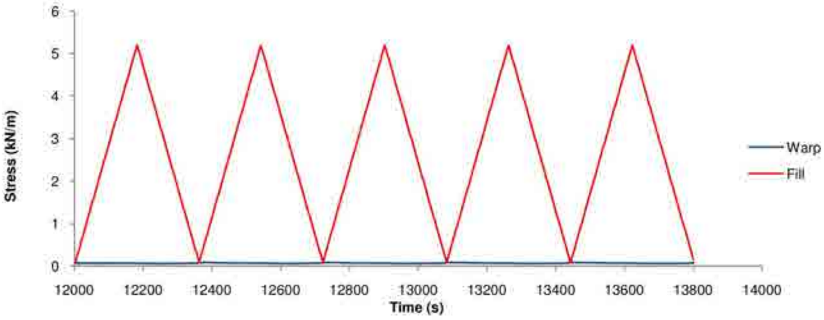


*Measured strain:*

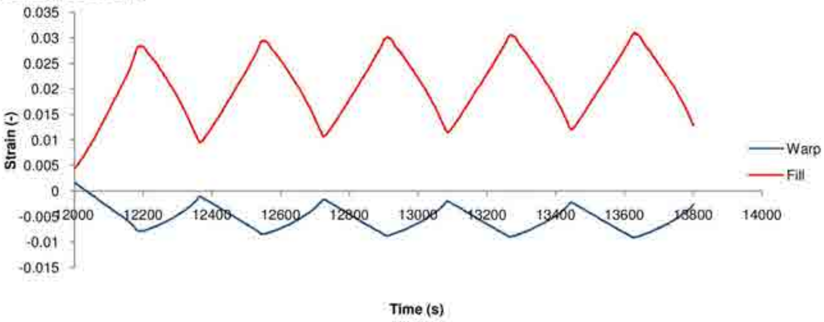


*Stress-strain behaviour:*

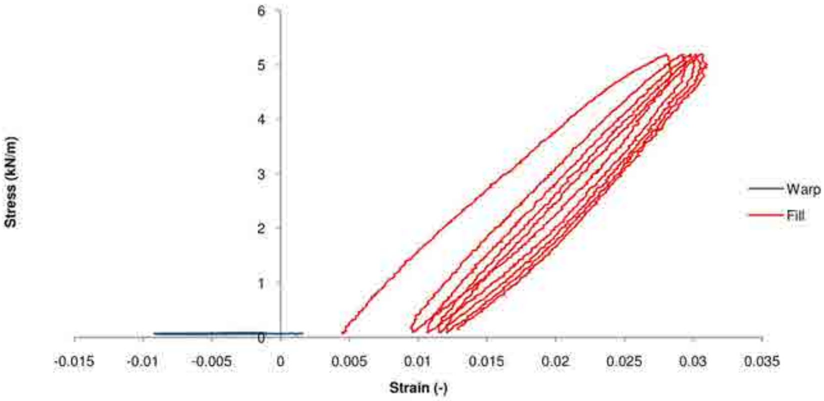


Page 8

## D-2 Ripstop bi-axial stress test

Center for Synergetic Structures

EMPA Materials Science & Technology

**Biaxial test report**

Date: 29.07.2011 Temperature: 22°C Specimen ID: Ripstop_01

**Material reference:** **Ripstop Nylon (Spinnaker)**

Yarn material: Nylon

Coating material:

Yarns (dtex):

Weave pattern:

Weight (g/m$^2$): approx. 50

Thickness (mm): approx. 0.08

Warp tensile strength (kN/m): 8.6

Fill tensile strength (kN/m): 8.6

**Loading history:**

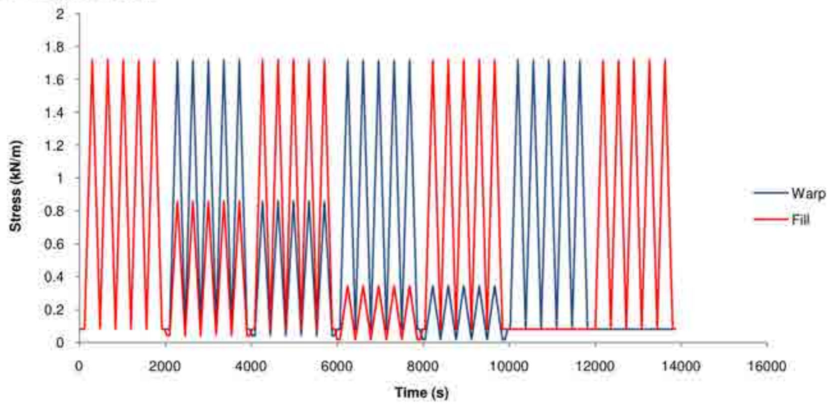


Pre-stress Warp (kN/m): 0.08

Pre-stress Fill (kN/m): 0.08

Max. loading rate ((N/m)/s): 9.6

Max. stress Warp (kN/m): 1.72

Max. stress Fill (kN/m): 1.72

**Additional informations:**

Mechanical properties based on plane stress linear elastic orthotropic model:

$E_w$ = 104.4 kN/m

$E_f$ = 71.2 kN/m

$\nu_{wf}$ = 0.36

Page 1

Center for Synergetic Structures

EMPA Materials Science & Technology

**Cycles #1: Load ratio 1:1**

*Measured stress:*

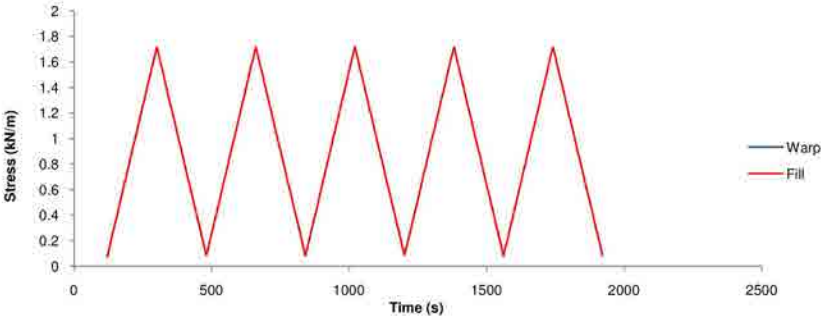


*Measured strain:*

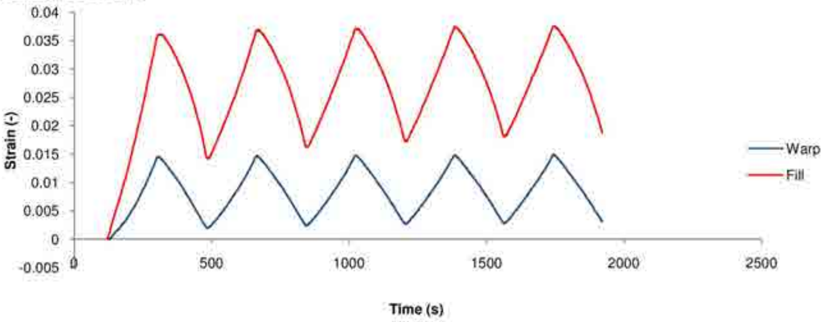


*Stress-strain behaviour:*

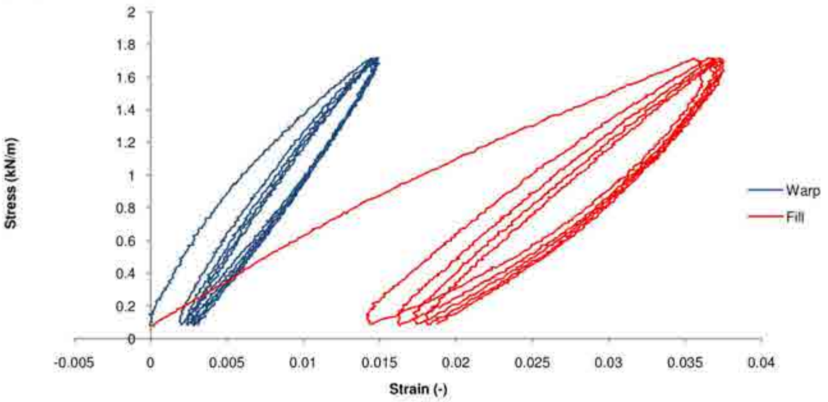


Page 2

Center for Synergetic Structures

EMPA Materials Science & Technology

**Cycles #2: Load ratio 2:1**

*Measured stress:*

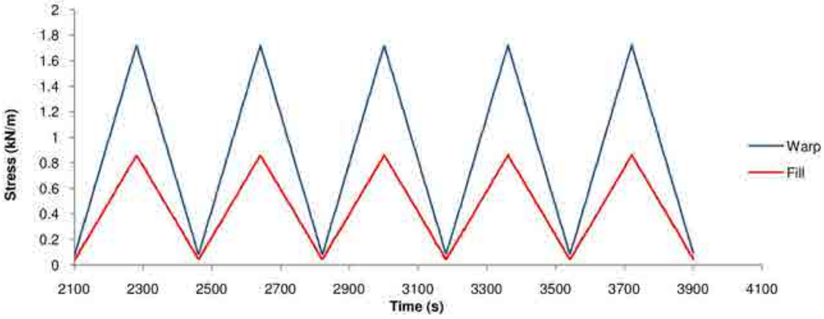


*Measured strain:*

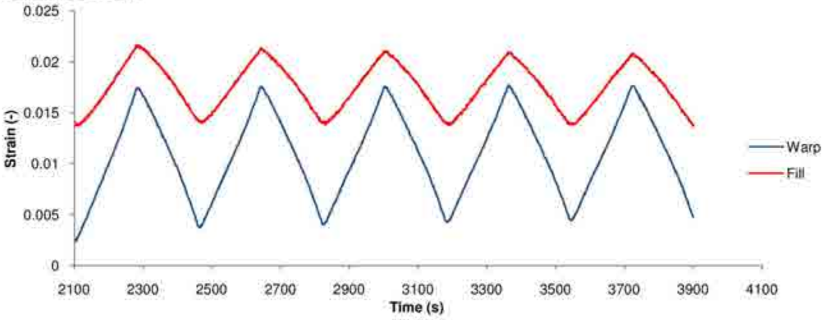


*Stress-strain behaviour:*

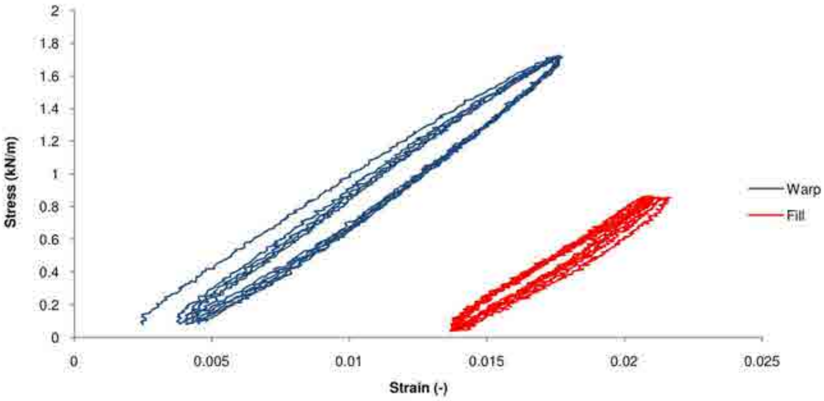


Page 3

Center for Synergetic Structures

EMPA Materials Science & Technology

**Cycles #3: Load ratio 1:2**

*Measured stress:*

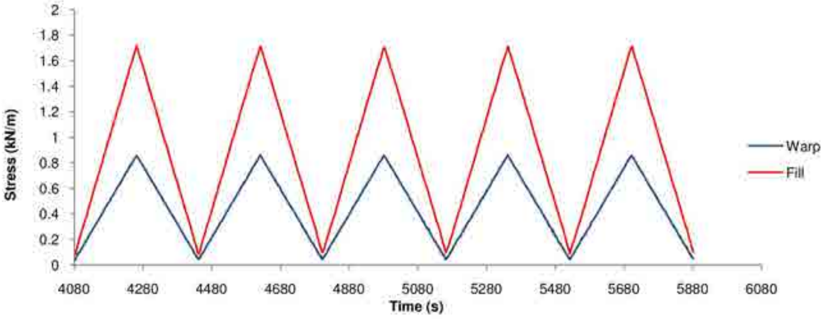


*Measured strain:*

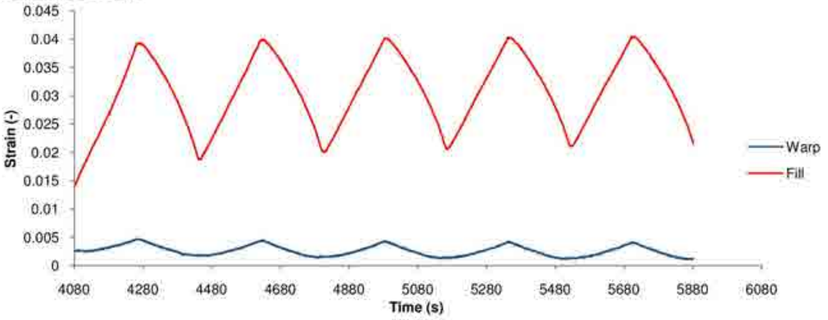


*Stress-strain behaviour:*

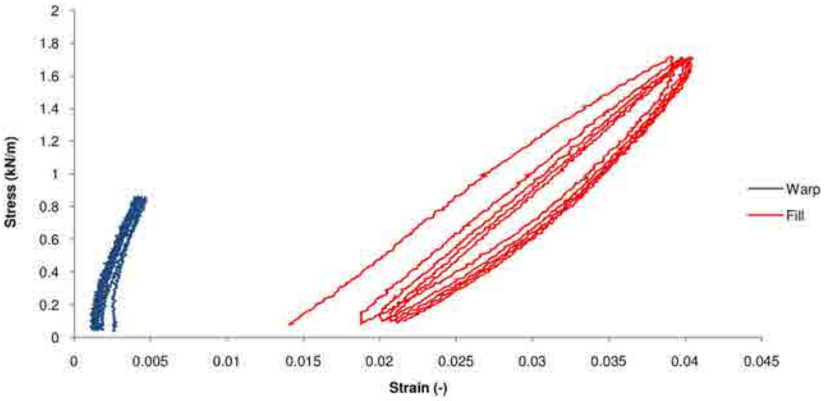


Page 4

Center for Synergetic Structures

EMPA Materials Science & Technology

**Cycles #4: Load ratio 5:1**

*Measured stress:*

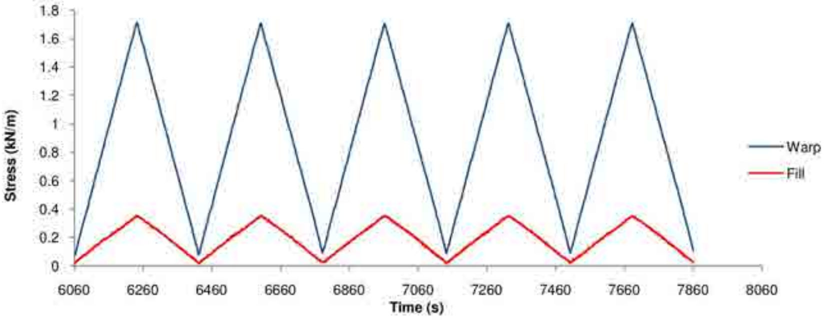


*Measured strain:*

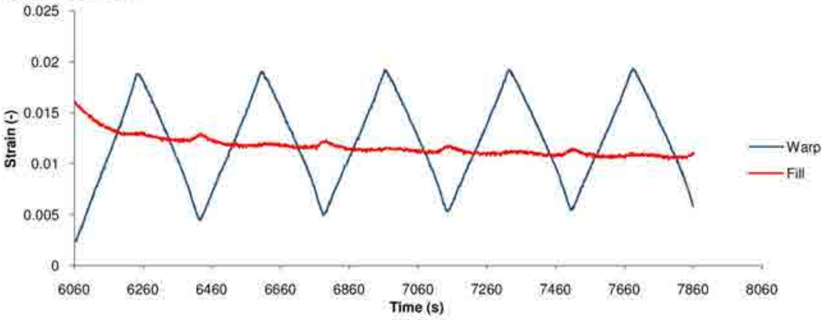


*Stress-strain behaviour:*

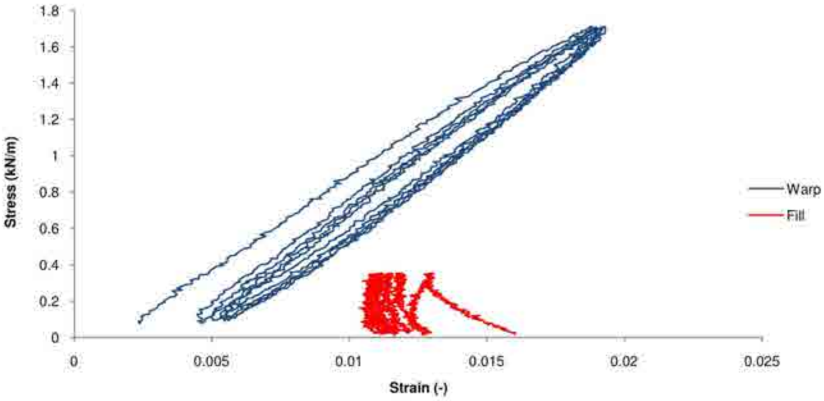


Page 5

Center for Synergetic Structures

EMPA Materials Science & Technology

## Cycles #5: Load ratio 1:5

*Measured stress:*

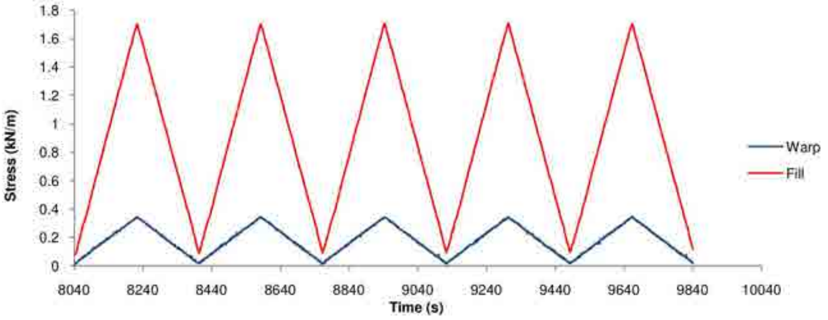


*Measured strain:*

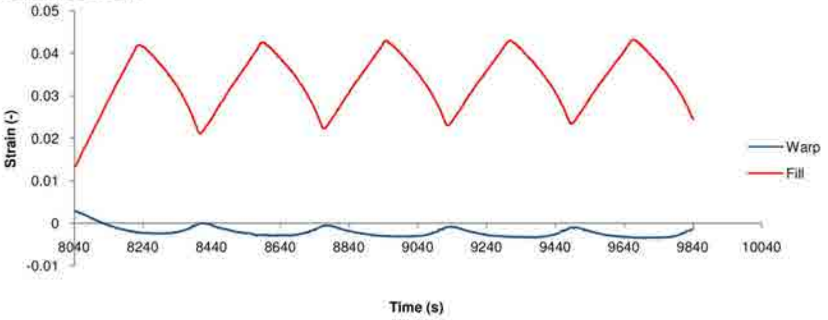


*Stress-strain behaviour:*

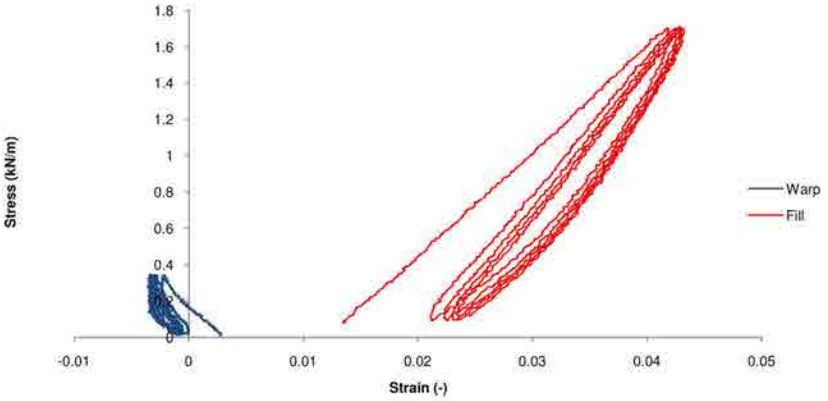


Page 6

Center for Synergetic Structures

EMPA
Materials Science & Technology

**Cycles #6: Load ratio 1:0**

*Measured stress:*

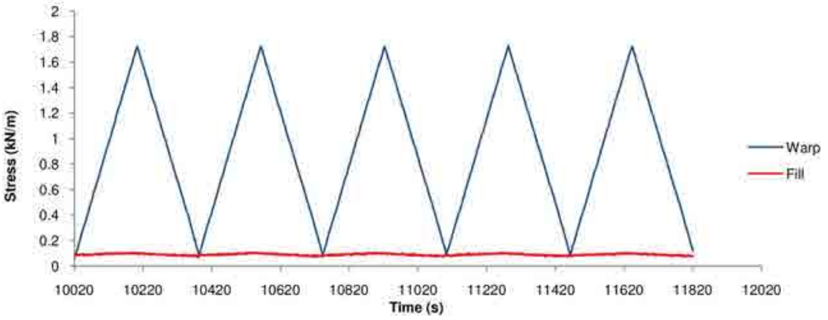


*Measured strain:*

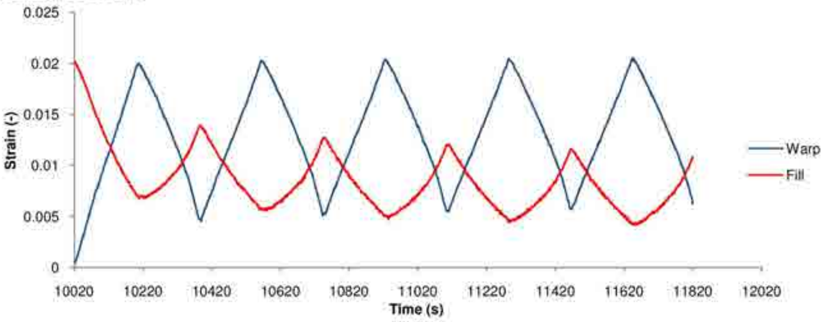


*Stress-strain behaviour:*

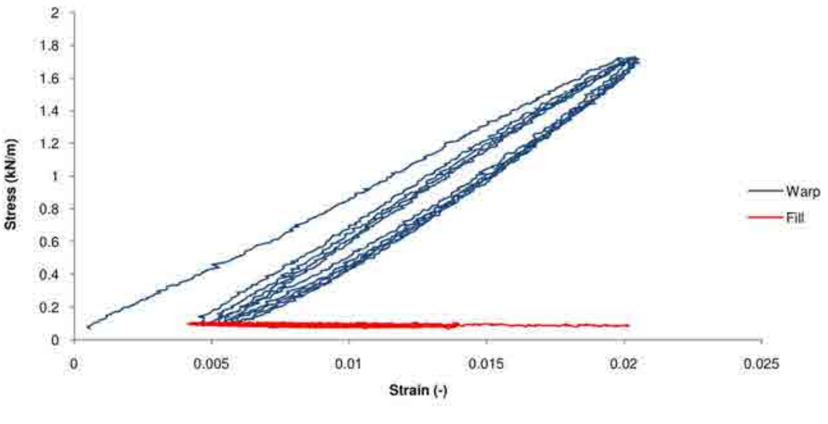


Page 7

Center for Synergetic Structures

EMPA Materials Science & Technology

**Cycles #7: Load ratio 0:1**

*Measured stress:*

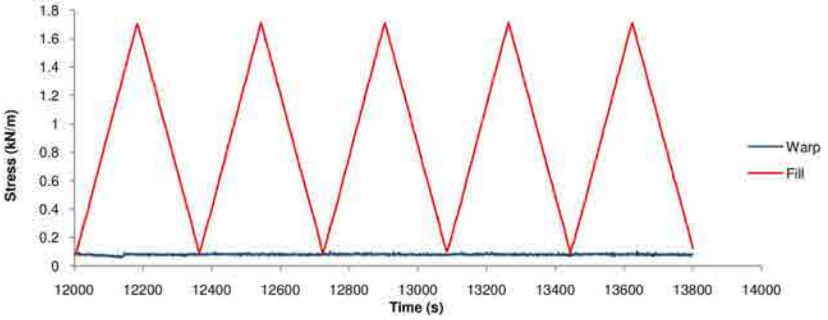


*Measured strain:*

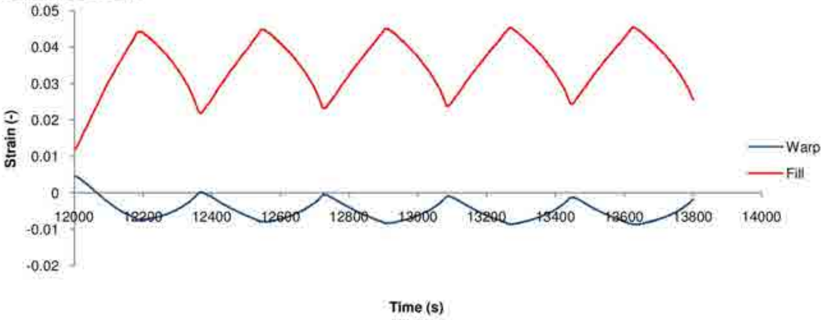


*Stress-strain behaviour:*

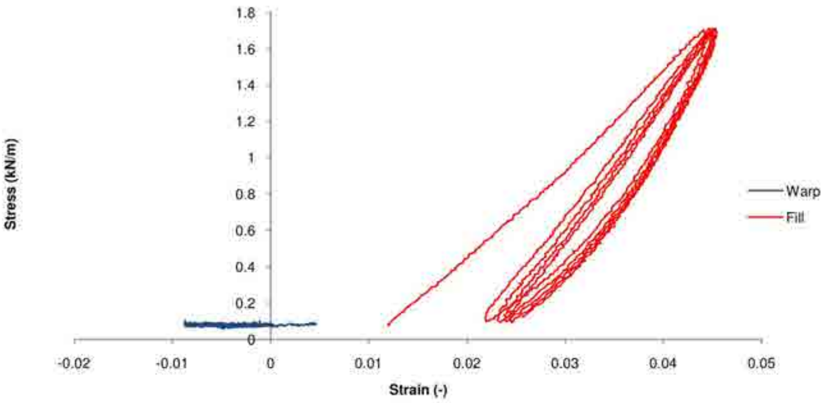


Page 8

## D-3 Dacron bi-axial shear test

Center for Synergetic Structures

EMPA Materials Science & Technology

**Biaxial shear test report**

Date: 05.09.2011 Temperature: 22°C Specimen ID: Dacron_03

**Material reference:** **Dacron (black)**

Yarn material: Polyester

Coating material:

Yarns (dtex):

Weave pattern:

Weight (g/m$^2$): approx. 150

Thickness (mm): approx. 0.17

Warp tensile strength (kN/m): 26

Fill tensile strength (kN/m): 26

**Loading history:**

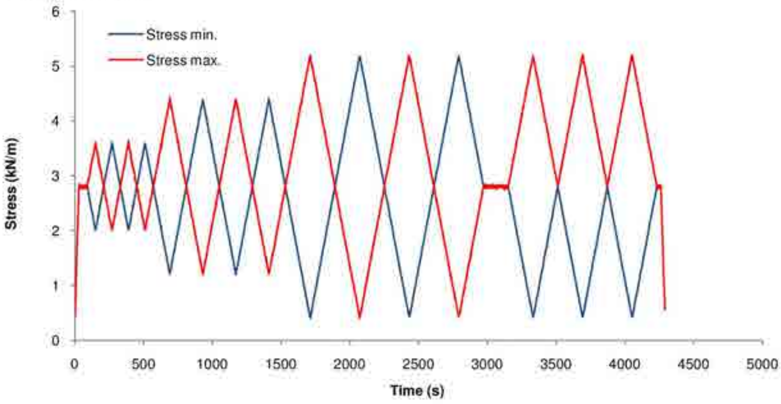


Constant pre-stress (kN/m): 2.8

Max. stress (kN/m): 26

**Stress correction factor: 0.81**

**Additional informations:**

Estimated shear modulus:

28 kN/m < $G_{wf}$ < 50 kN/m

Page 1

Center for Synergetic Structures

EMPA Materials Science & Technology

**Shear stress based on the correction factor 0.81**

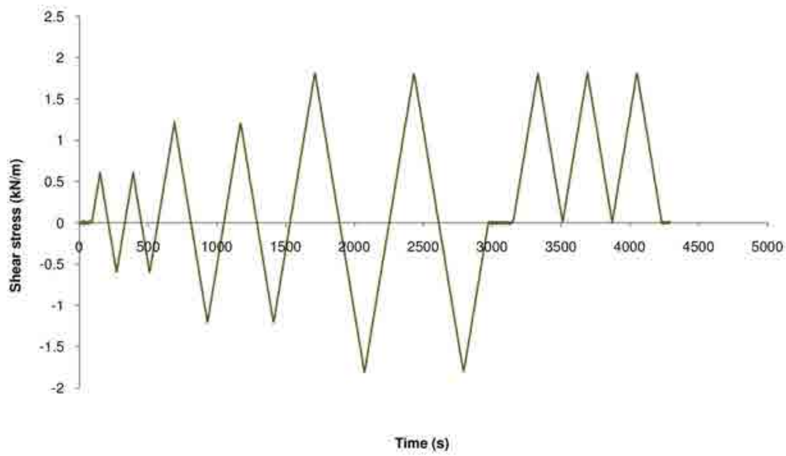


Max shear stress (kN/m): 1.82

**Measured strains**

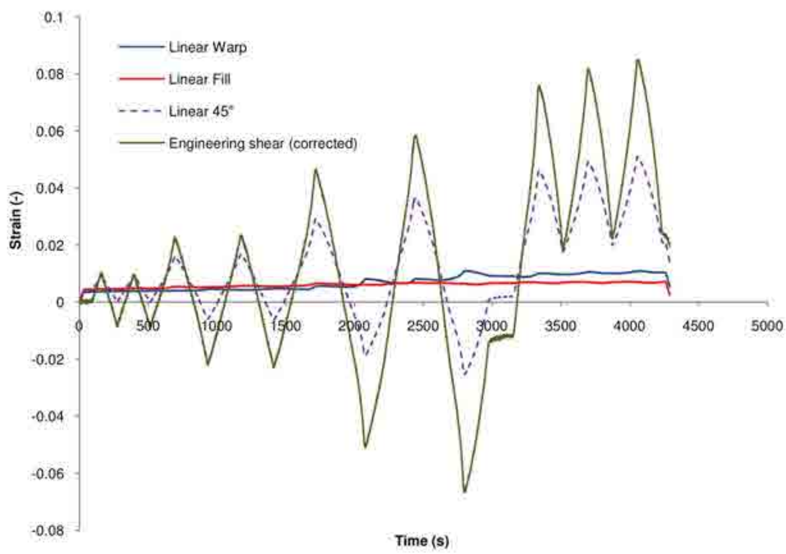


Page 2

Center for Synergetic Structures

EMPA
Materials Science & Technology

**Shear stress strain response**

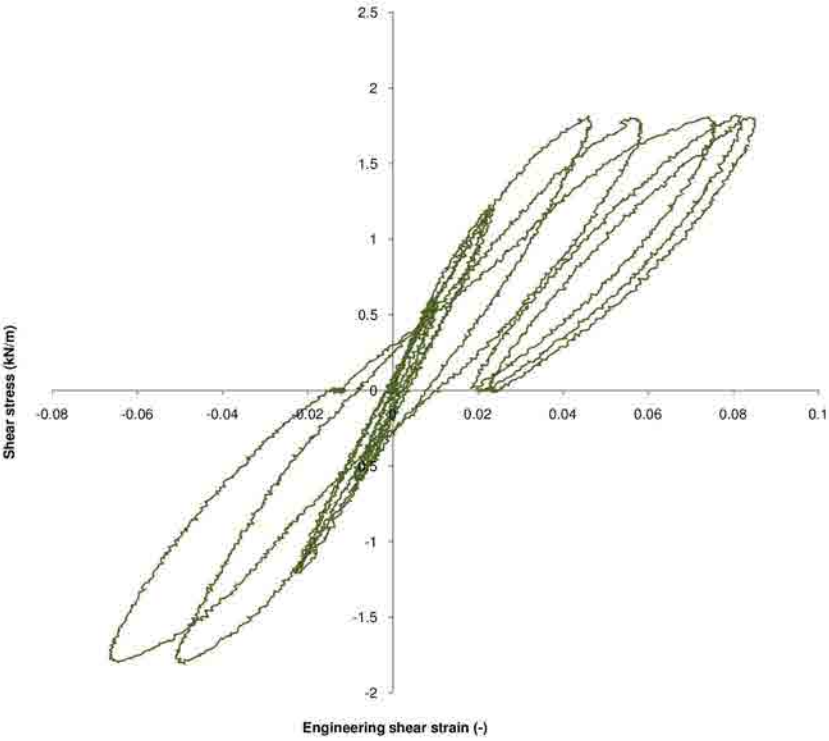


Page 3

# D-4 Ripstop Bi axial Shear

Center for Synergetic Structures

EMPA Materials Science & Technology

## Biaxial shear test report

Date: 02.09.2011 Temperature: 22℃ Specimen ID: Ripstop_02

**Material reference:** **Ripstop Nylon (Spinnaker)**

Yarn material: Nylon Coating material:

Yarns (dtex): Weave pattern:

Weight (g/m$^2$): approx. 50 Thickness (mm): approx. 0.08

Warp tensile strength (kN/m): 8.6 Fill tensile strength (kN/m): 8.6

**Loading history:**

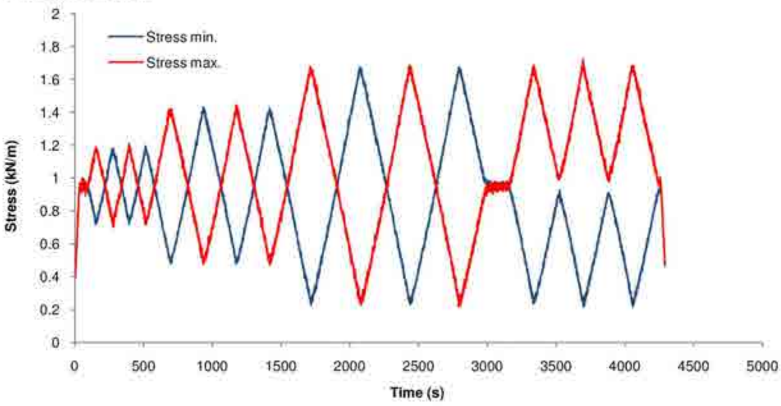


Constant pre-stress (kN/m): 0.95 Max. stress (kN/m): 8.6

**Stress correction factor: 0.76**

**Additional informations:**

Estimated shear modulus:

1.8 kN/m < $G_{wf}$ < 2.2 kN/m

Page 1

Center for Synergetic Structures

EMPA Materials Science & Technology

**Shear stress based on the correction factor 0.76**

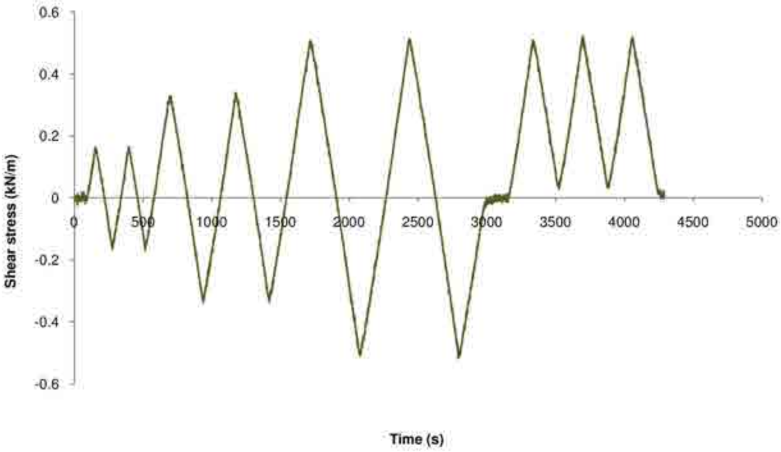


Max shear stress (kN/m): 0.52

**Measured strains**

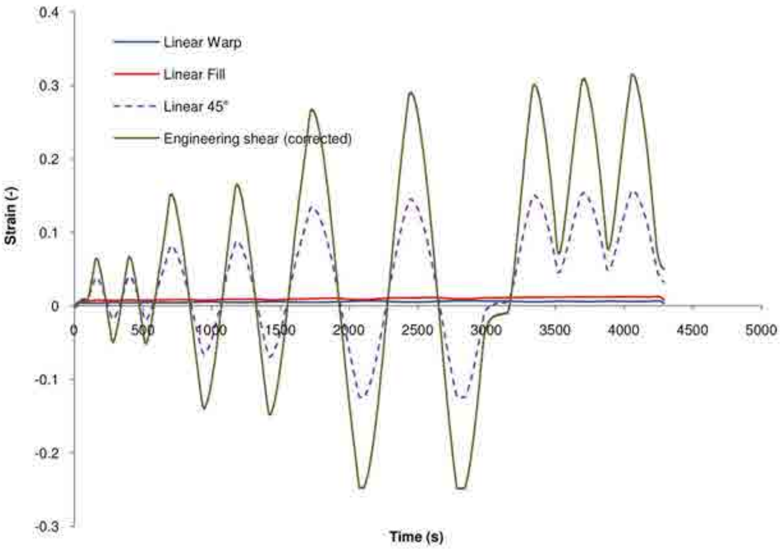


Page 2

Center for Synergetic Structures

EMPA Materials Science & Technology

**Shear stress strain response**

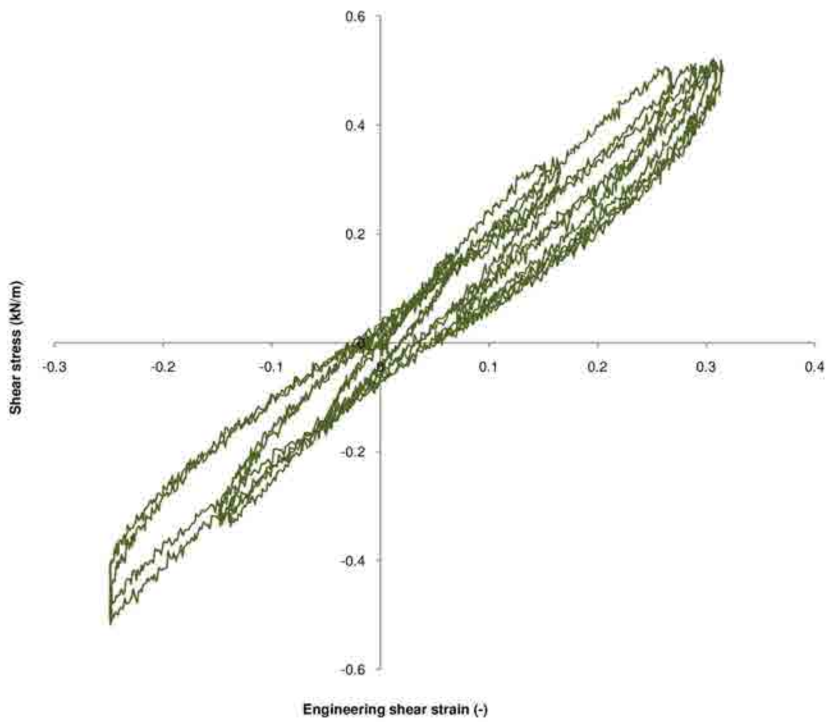


Page 3

# Appendix E

# Experiment of the cantilever beam

In this section, the experiment by (Breukels, 2011) is described. The Inflatable beam experiments consists of beams with different diameters, different internal pressures and different loads. The results are deflection versus the tip load curve of each beam.

The experiment overview is given and shown in Figure E-1.

**Figure E-1:** Overview of the experiment (Breukels, 2011)

## E-1 Beam geometry

In this section the geometry is described. Two cylindrical beams with different diameters (0.18 m and 0.13 m) have been tested for bending with different internal pressures. The beams have a length of 1.2 m, however the load is applied at 1 m from the root of the beam. The test set-up of the experiment is shown in Fig. E-1.

## E-2 Beam material

The inflatable beam has a cylindrical shape and consists of a TPU bladder, to ensure the beam can be inflated and to minimize leakage. The stiffness of the beam is provided by Dacron material. This is a woven material, that is rolled at high temperature, for material properties see chapter 6-2. See Figure E-2 for a layout of the inflatable beam, with the TPU bladder and the Dacron outer material providing the stiffness. The TPU bladder is assumed not to contribute to the strength of the beam.

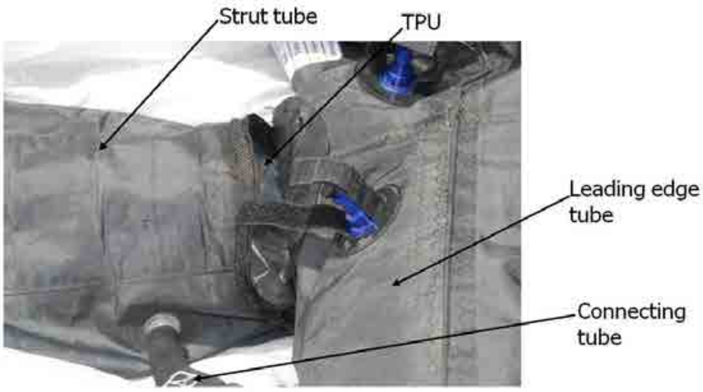


**Figure E-2:** Inflatable beam with TPU bladder and Dacron (Breukels, 2011)

## E-3 External loads

This section describes the external loads that are applied in the experiment. These external loads are: internal pressure and tip force.

### E-3-1 Internal pressure

In this Section the inflation process of the experiment is described.

The beam with diameter of 0.13 m was tested with internal (over)pressures of 0.3 bar, 0.4 bar and 0.5 bar. The beam with diameter of 0.18 m was tested with internal (over)pressures of 0.2 bar and 0.4 bar.

The beam is inflated with a compressor. The pressure is measured with a manometer and when the pressure reached the required pressure, a valve was shut. This leads to a situation in which there is an inflatable beam with a fixed volume. On this beam the loads are applied. So the pressure in the beam increases when the loads on the inflatable beam increase. This is because the volume decreases under a load, however the volume is fixed, so the pressure is expected to rise. In the experiments of bending and torsion, this set-up is used for the experiments. This is also the case for the inflatable tubes in the tube kite when the kite

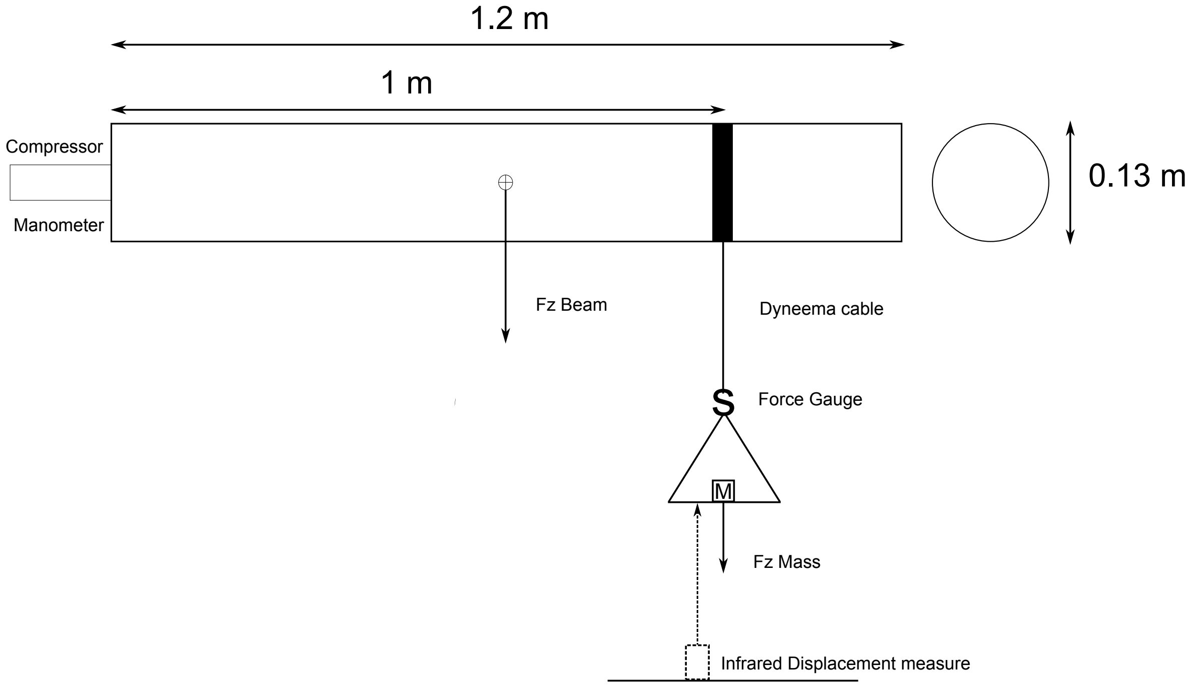


**Figure E-3:** Experiment set-up for bending

experience a load, (Breukels, 2011). See Figure E-3 for the test set-up for bending of the beam.

### E-3-2 Tip force

See Figure E-3 for the test set-up for bending of the beam. The beams are clamped at one end and loaded at the tip. The loads at the tip of the inflatable beam that were applied, were applied in varying step sizes, from 0 N until the inflatable beam collapsed. This is different for the beams with different diameters and this load is different for the different internal pressures. The results of the experiments is the tip deflection as a function of the tip force where the loads were measured with a load cell.

## E-4 Beam support and constraints

The beam is clamped at one end, in Figure E-4 it is shown how the DOFs of the endcap are restraint. From discussion with Dr. Ir. J.M.A Hol (professor at the Aerospace Engineering faculty) and Dr. Ir. R. Ruijtenbeek (professor at the 3ME faculty), the behavior of inflated beams at the clamped end (see Figure E-5) has a huge influence on the deflection of the beam. There are no pictures or records of the experiment regarding this phenomenon under pressure, however in Figure E-4a the overview of the beam is shown. The restraint in the actual experiment is done by two actions. First the beam is bolted onto a plate that is connected to a steel fixed beam see Figure E-1. This is done by putting a wooden cylinder at the inside of the beam see Figure E-4b. Secondly the beam is constraint by constraining the fabric to slide due to the force. This is done by tightening a metal strap on the outside of the fabric onto the wooden cylinder that is inside of the beam, this is shown in Figure E-4c.

**(a)** Overview of the beam

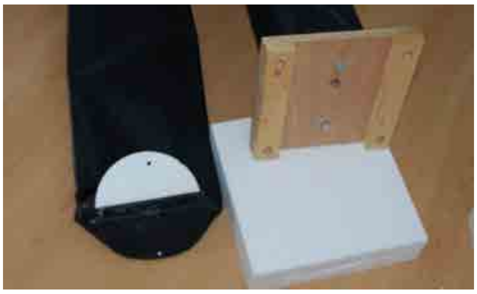

**(b)** Wood cylinder and connection to the plate

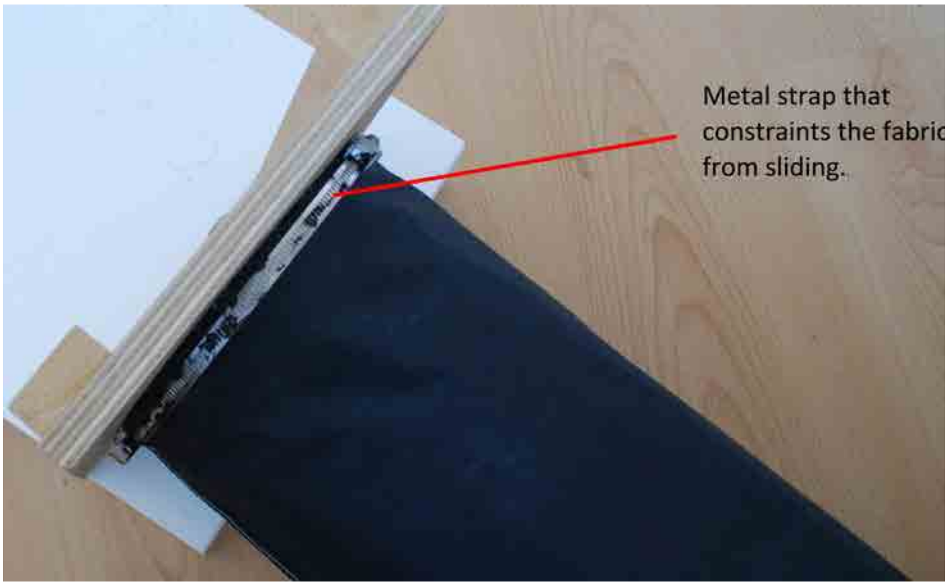


**(c)** Metal strap prevents material sliding

**Figure E-4:** Restraint DOFS endcap

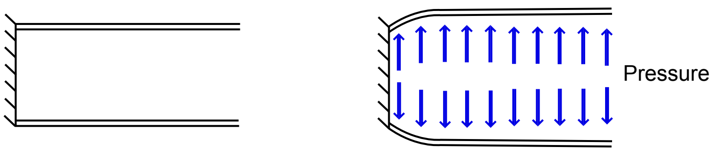


**Figure E-5:** reaction after inflation of the beam near the clamped end

## E-5 Measuring deflection

The tip deflection is measured with a laser (Breukels, 2011). The deflection is not directly measured at the beam, however at the lower side of the plate. The connection of the beam was made of a Dyneema line and the distance was assumed to be short enough, to exclude influence on the deflection on the beam. In this assumption means that the deflection at the beam is assumed equal to the deflection of the plate.

In Figure E-3, the measurement of the deflection of the beam is shown.

# Appendix F

# Results of the parameter study of the inflatable beam

In this section the results of the parameter study are given.

In Table F-1 the parameters are given and sorted in groups, this is a recap of Table 7-6.

**Table F-1:** Parameters that are varied including reference value for the inflatable beam

| Group | Parameter (Unit) | Ref value | Variables | | | | |
|---|---|---|---|---|---|---|---|
| Geometry | Diameter (m) | 0.13 | 0.087 | 0.173 | 0.217 | 0.18 | |
| | Element (-) | CST | | | shell | | |
| Material | Density $\rho$ (kg/m$^3$) | 2046 | 682 | 1364 | 2728 | 3410 | |
| | Thickness (mm) | 0.17 | 0.0567 | 0.113 | 0.227 | 0.283 | |
| | E (N/mm$^2$) | 1360 | 450 | 907 | 1810 | 2267 | 2046 |
| | Poisson's ratio $\mu$ (-) | 0 | 0.1 | 0.2 | 0.3 | 0.4 | |
| | RF TOON (-) | 0.1 | 0.01 | 0.001 | 0.0001 | | |
| | RF TOOFF (-) | 0.1 | | | 0.0001 | | |
| | Material model | Isolin | | Material fabric shear | | | |
| | Material Damping $\nu$ (-) | 0.1 | 0.2 | 0.4 | 0.6 | 0.8 | 1.0 |
| External loads | Internal (over)pressure (bar) | 0.3 | 0.1 | 0.2 | 0.4 | 0.5 | |
| | Inflation method | Airbag | | | load.press | | |

## F-1 Geometry: Beam diameter

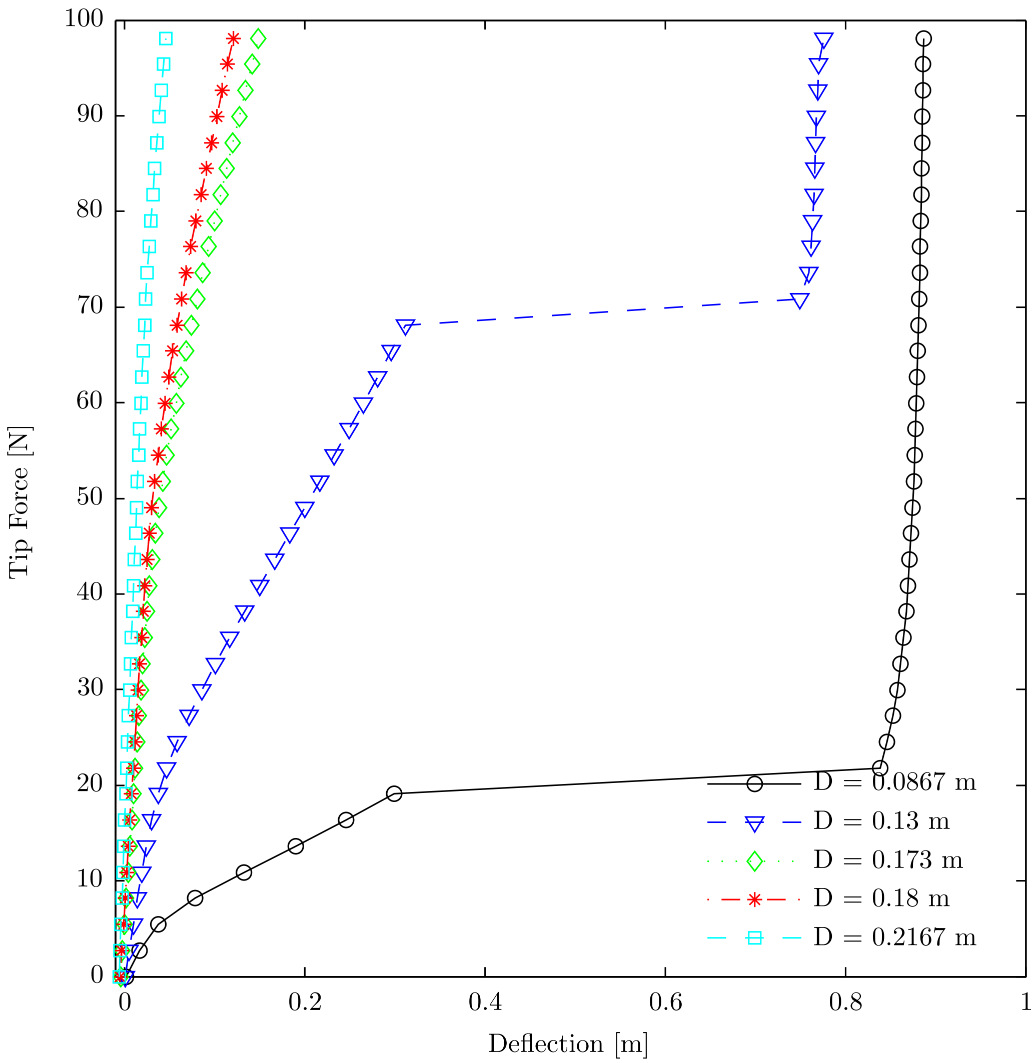


**Figure F-1:** Results of different diameters

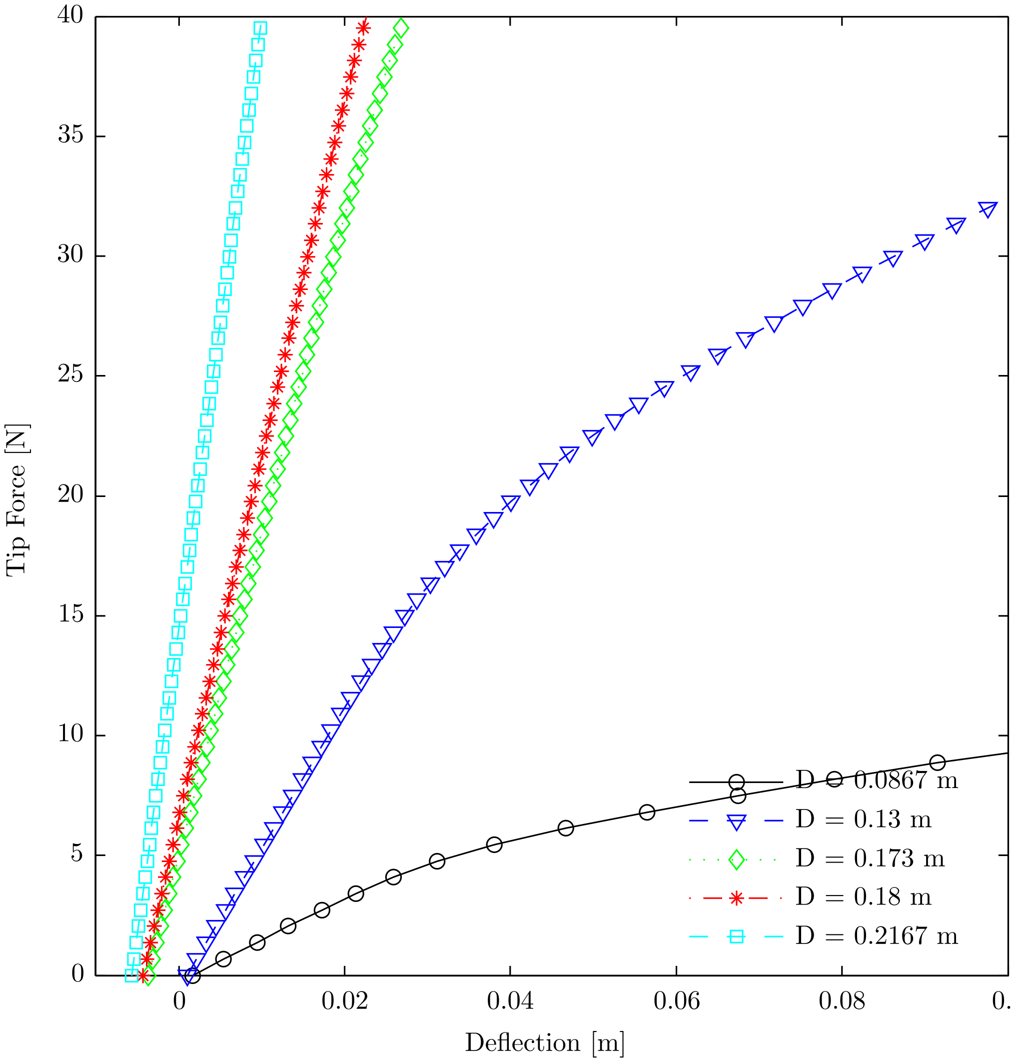


**Figure F-2:** Detail results of different diameters

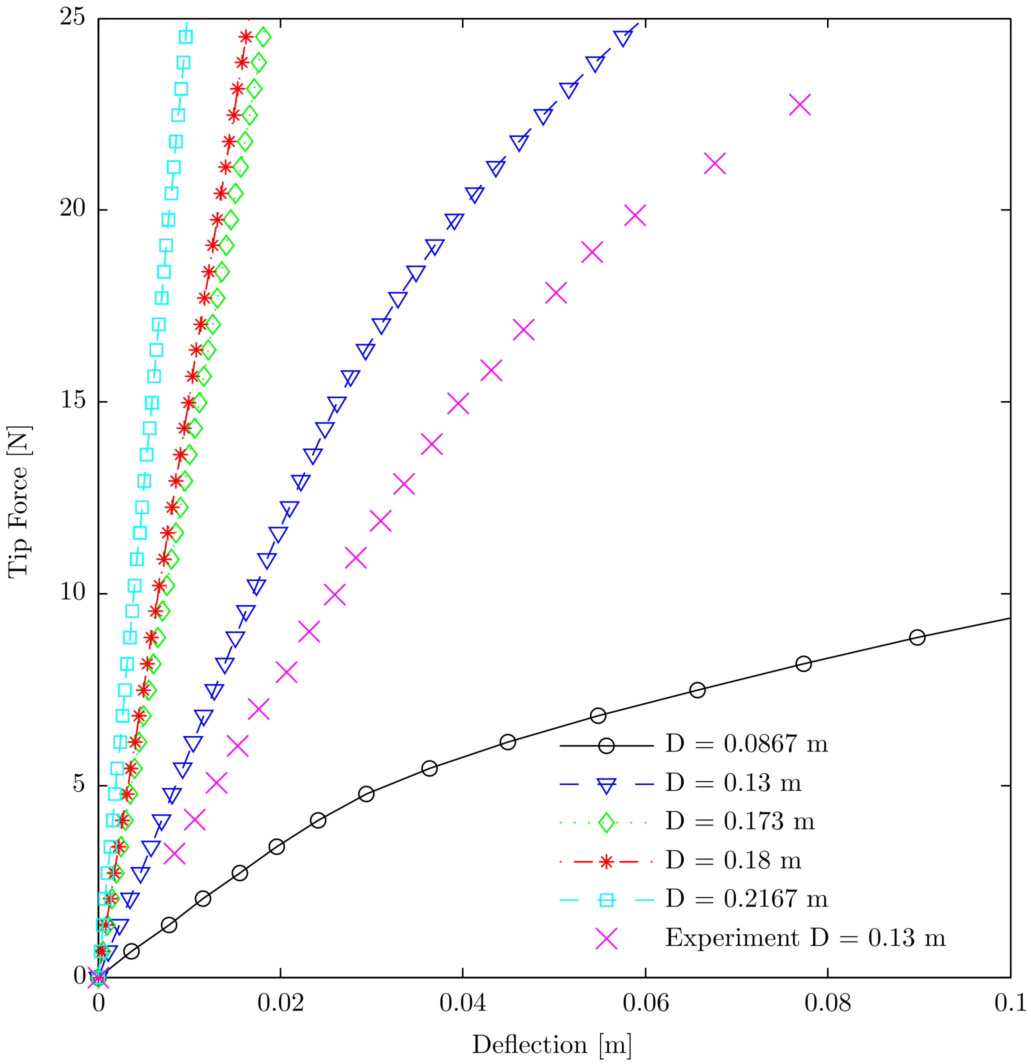


**Figure F-3:** Corrected detailed results of different diameters

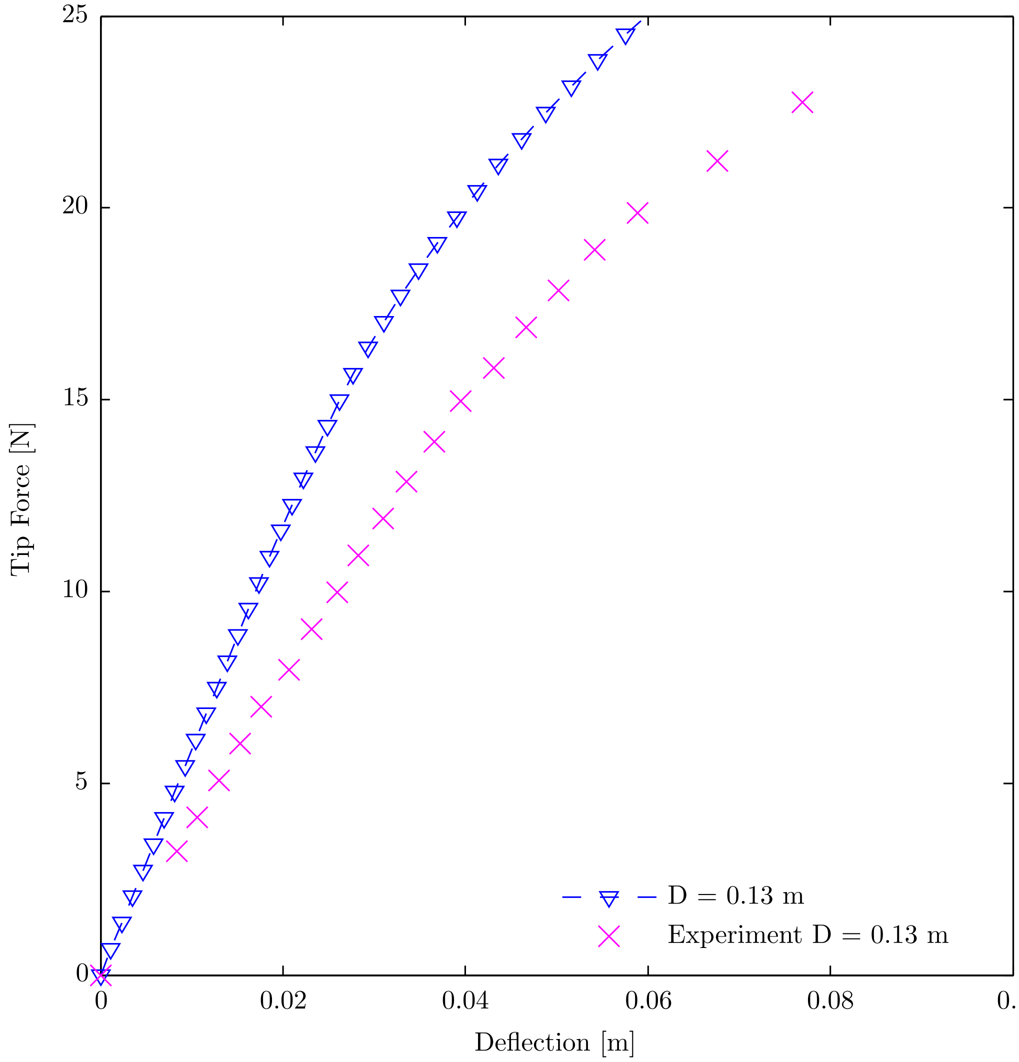


**Figure F-4:** Comparison between experiment and model of a beam with diameter is 0.13 m

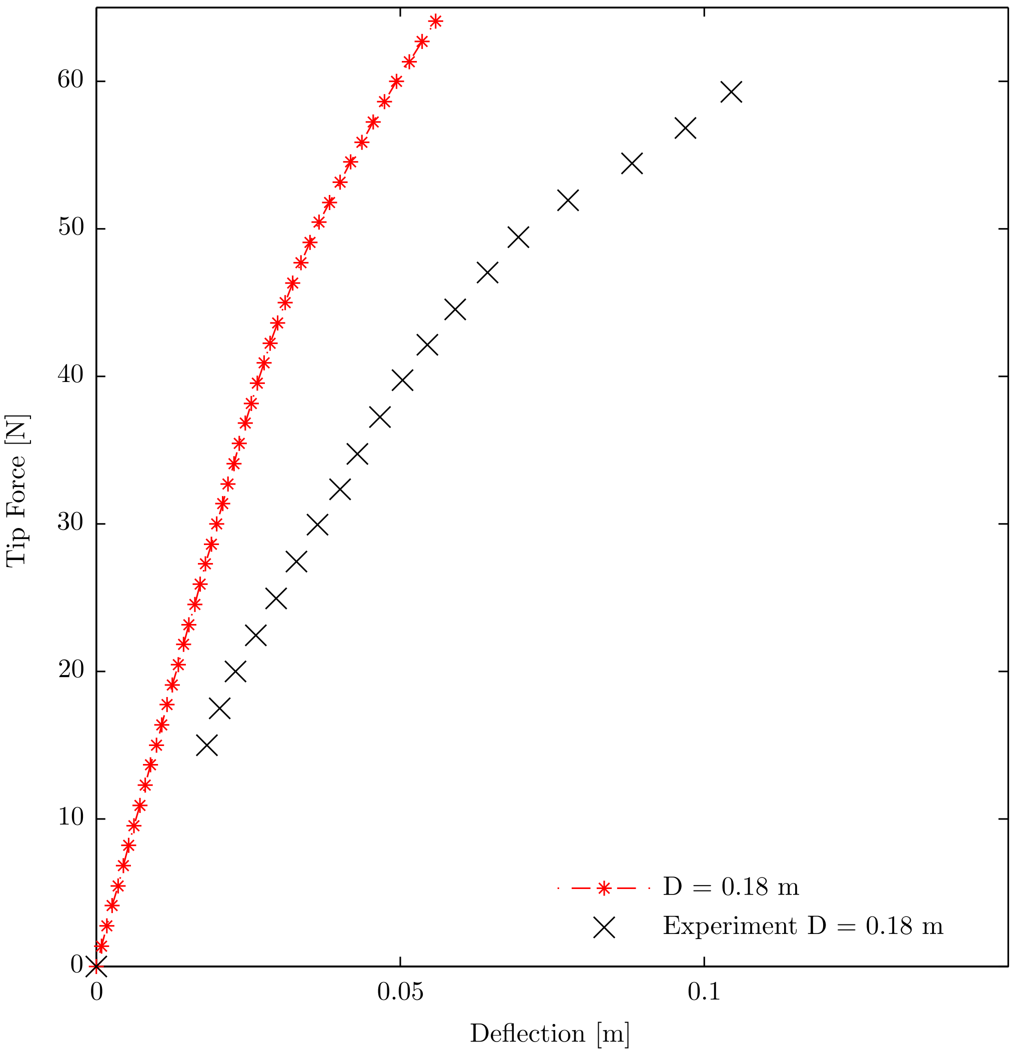


**Figure F-5:** Comparison between experiment and model of a beam with diameter is 0.18 m

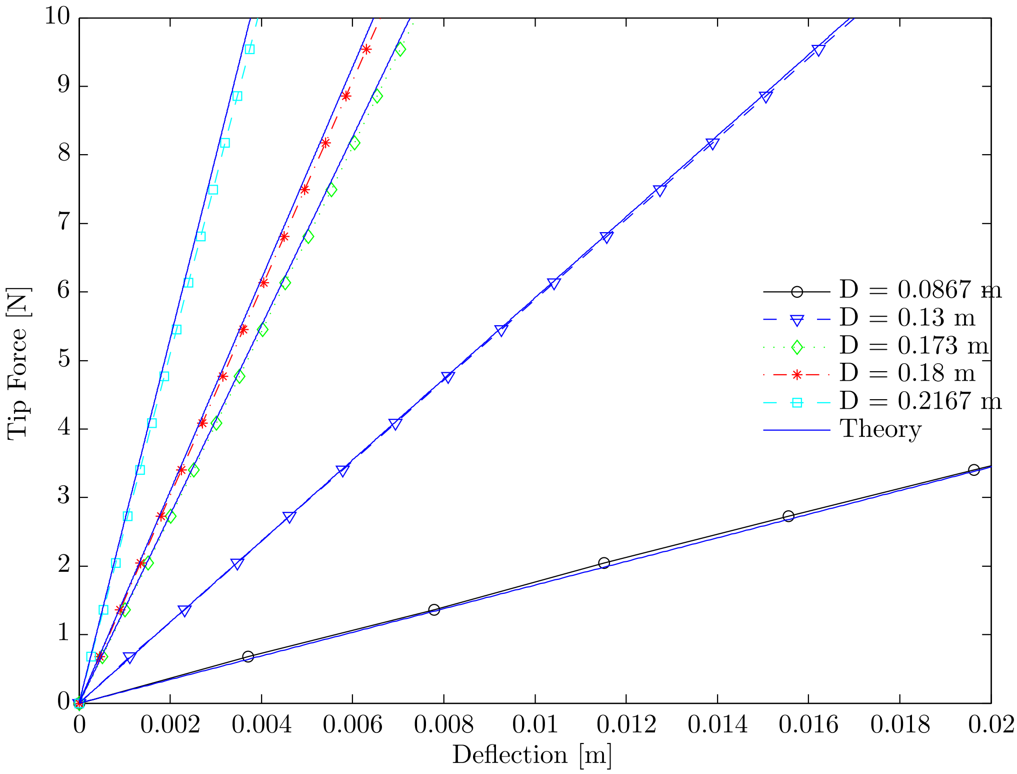


**Figure F-6:** Comparison between theory and FEM model with different diameters

# F-2 External loads: Internal pressure

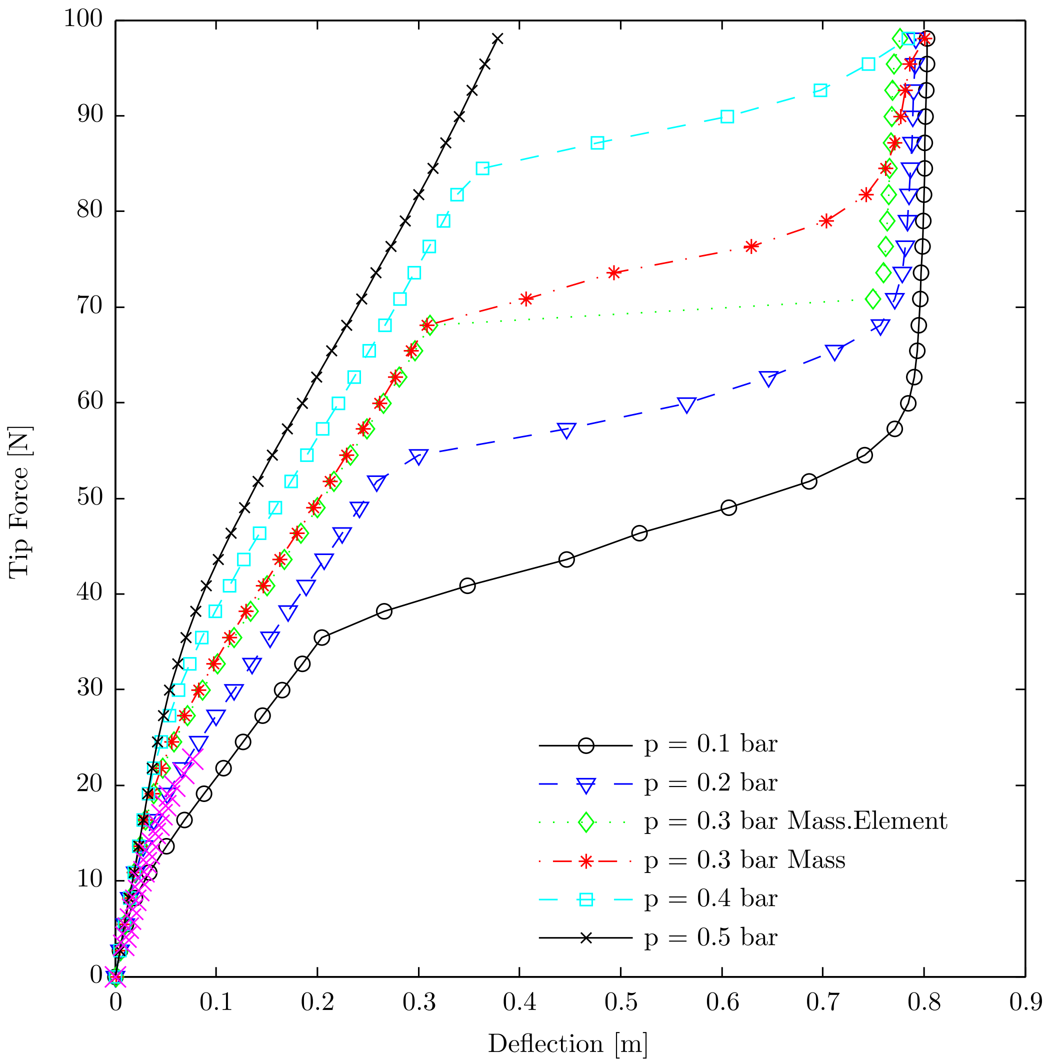


**Figure F-7:** Results of different pressures

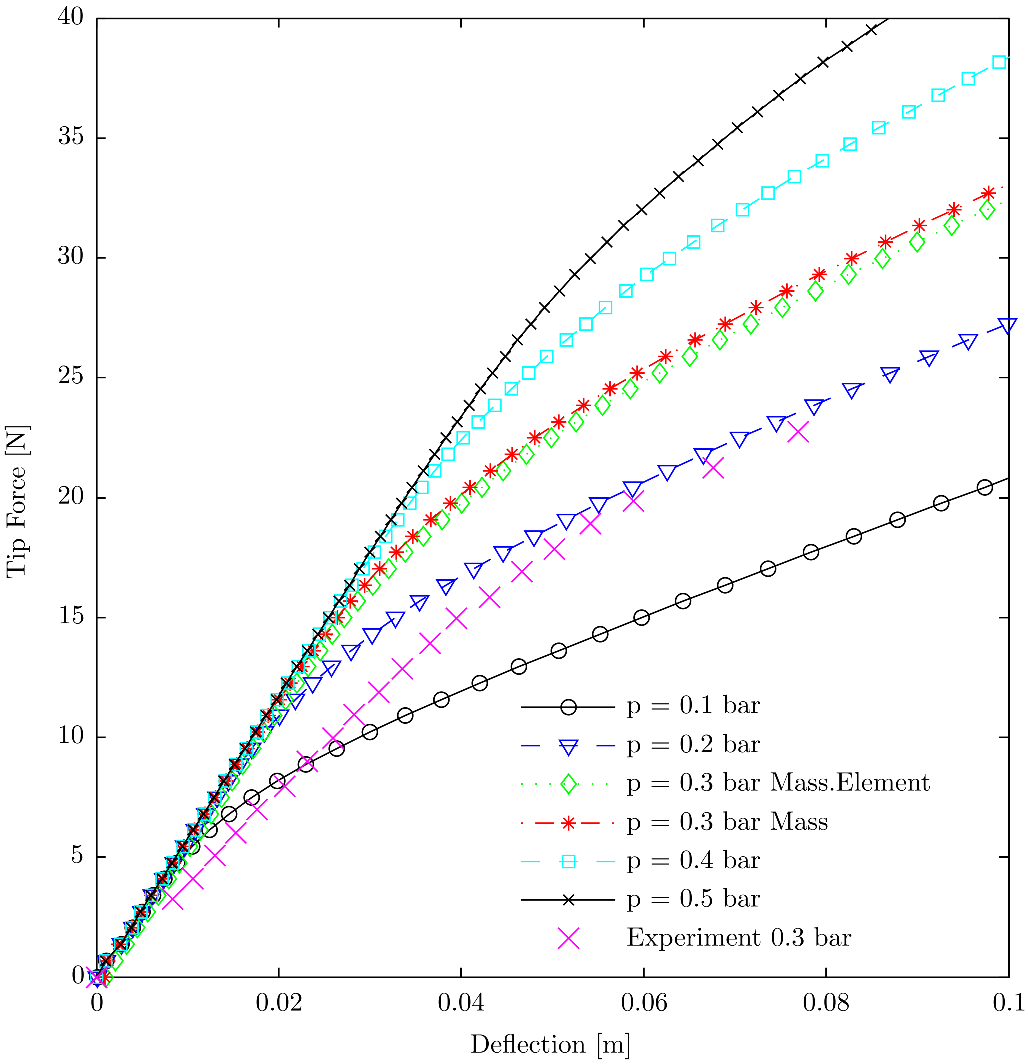


**Figure F-8:** Detail results of different pressures

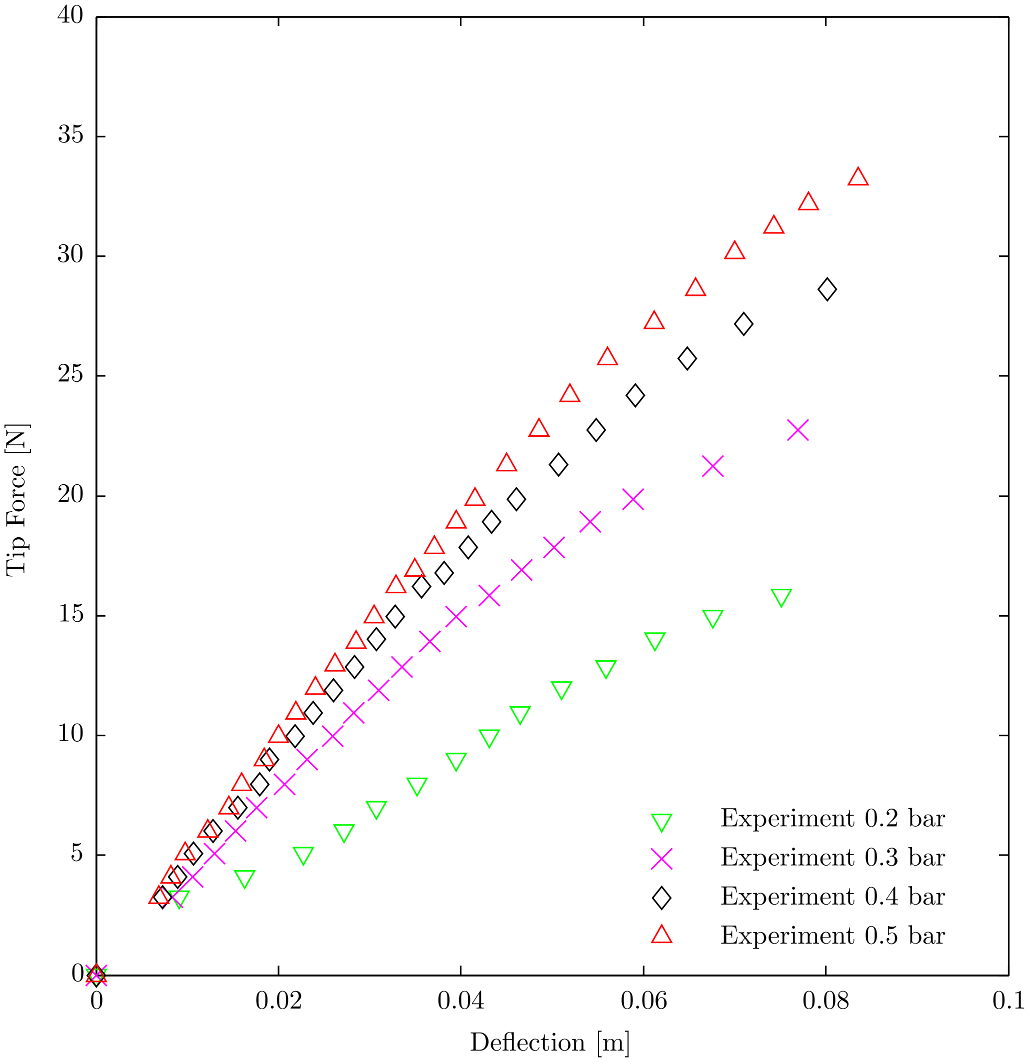


**Figure F-9:** Experiment results

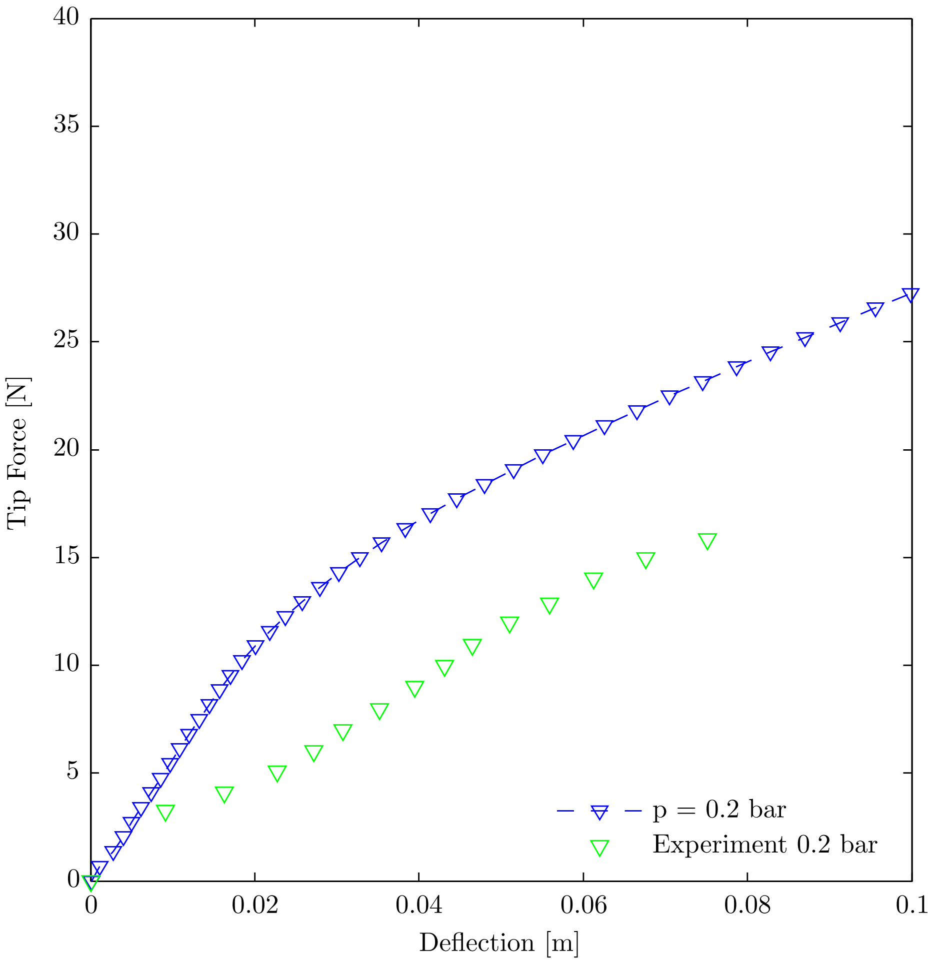


**Figure F-10:** Comparison between experiment and model at 0.2 bar

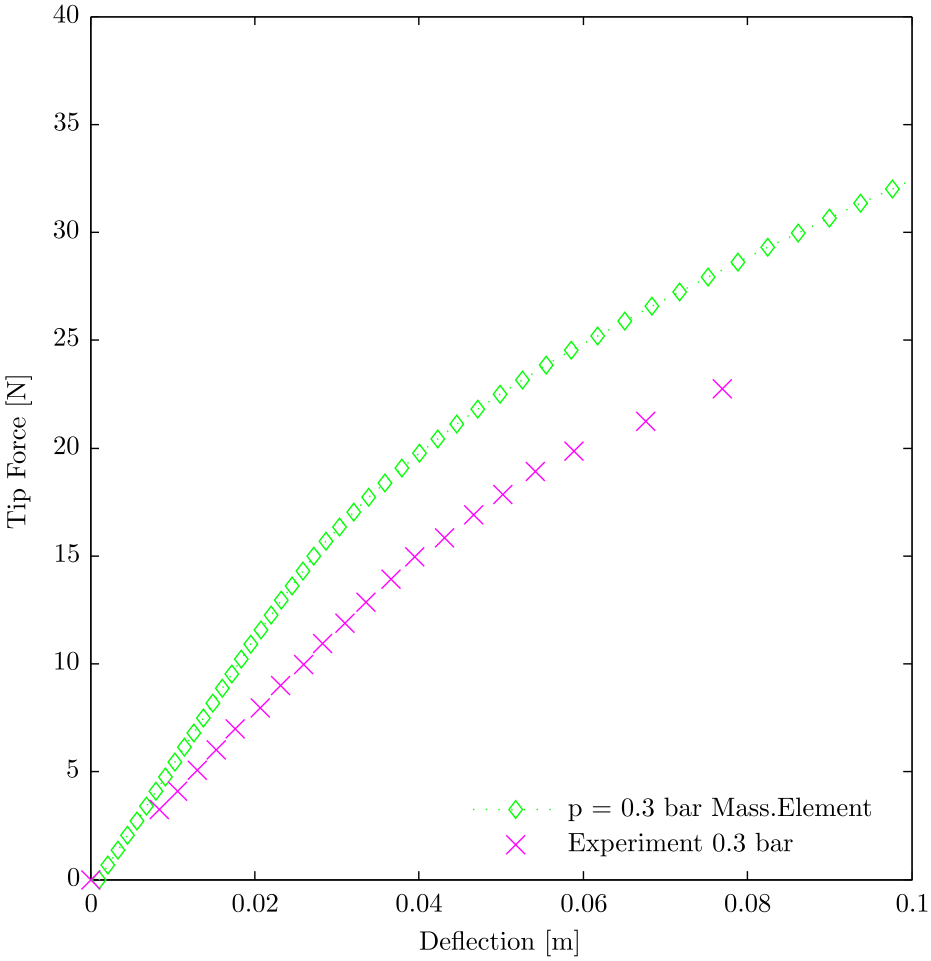


**Figure F-11:** Comparison between experiment and model at 0.3 bar

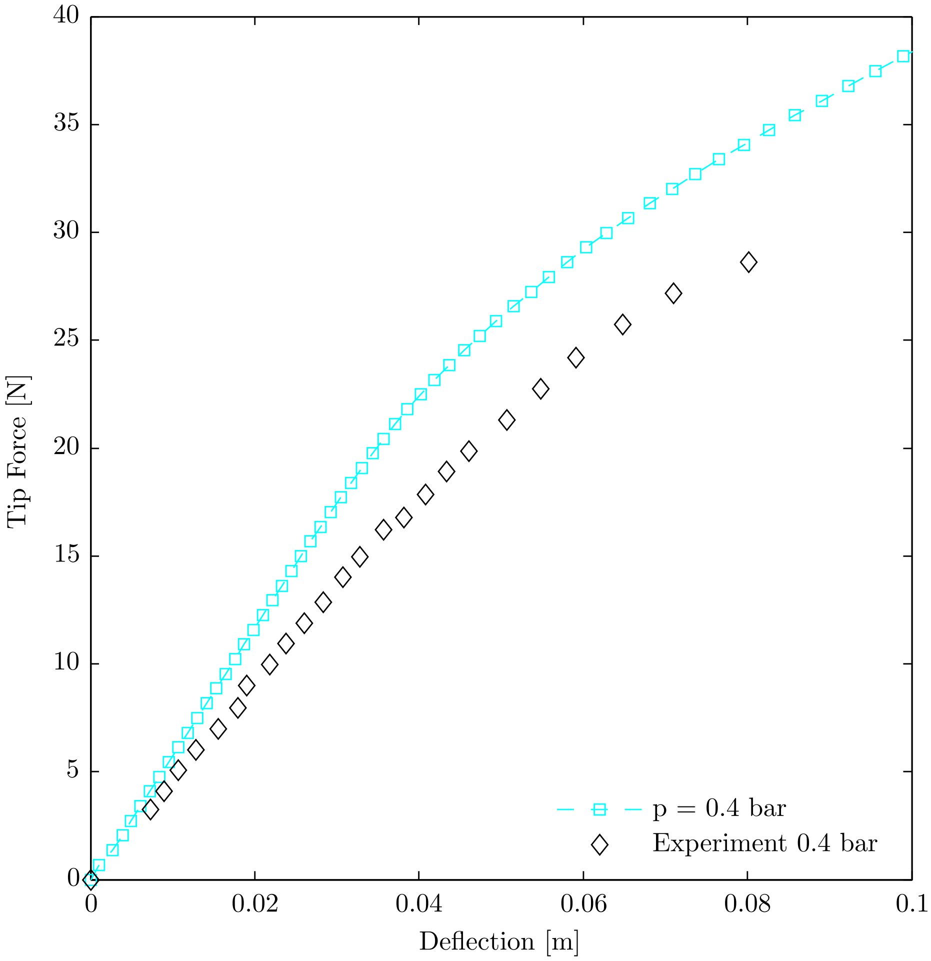


**Figure F-12:** Comparison between experiment and model at 0.4 bar

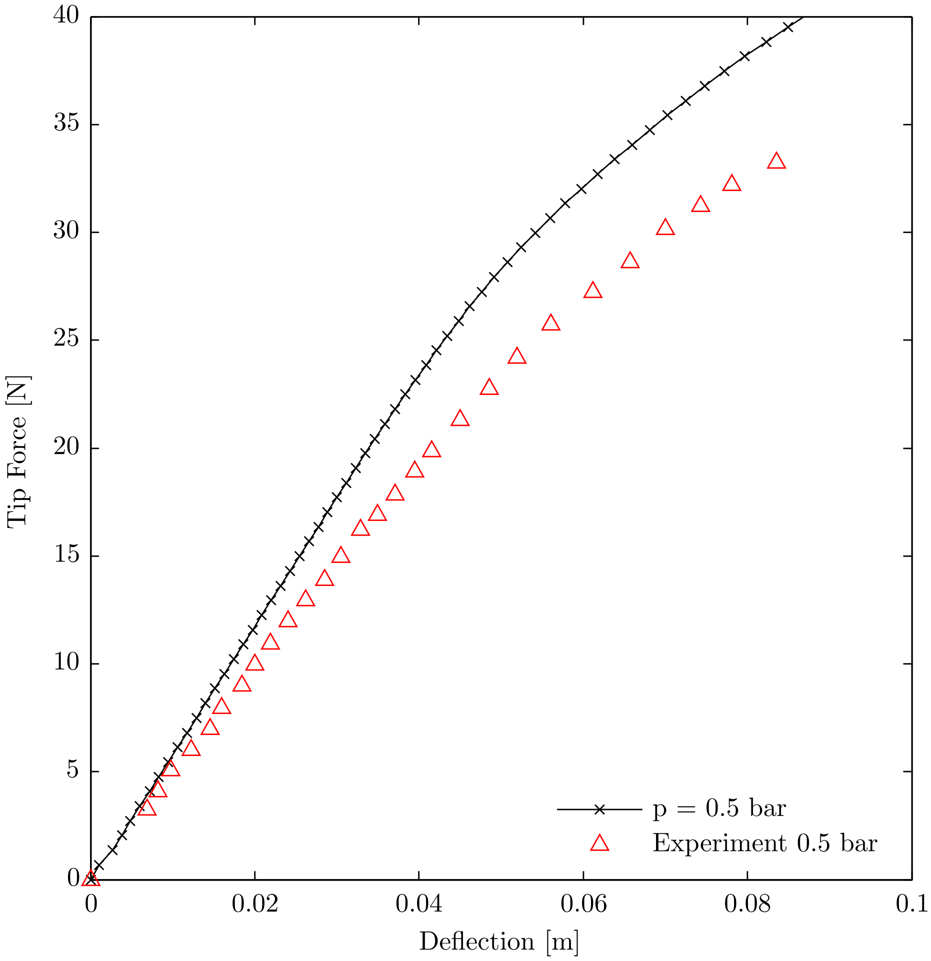


**Figure F-13:** Comparison between experiment and model at 0.2 bar

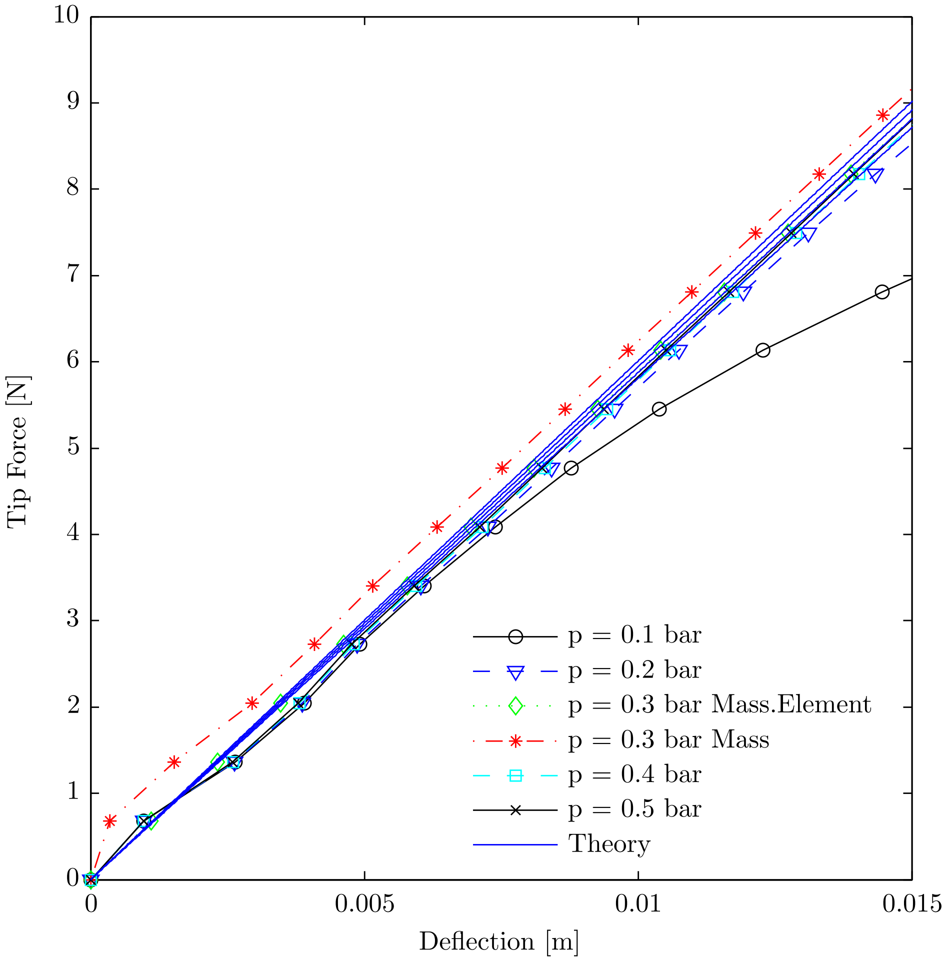


**Figure F-14:** Comparison between theory and FEM model with different pressures

## F-3 Material: Thickness

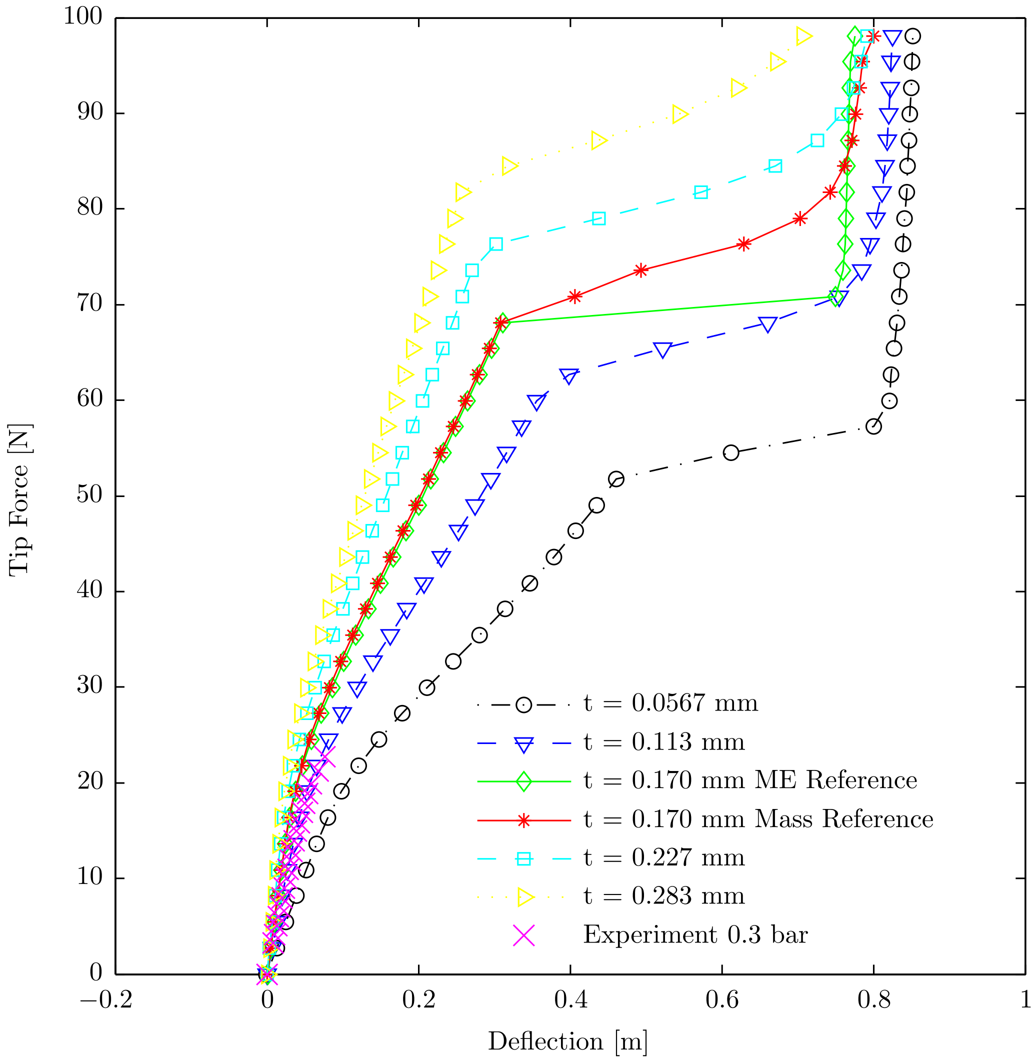


**Figure F-15:** Results of different material thicknesses

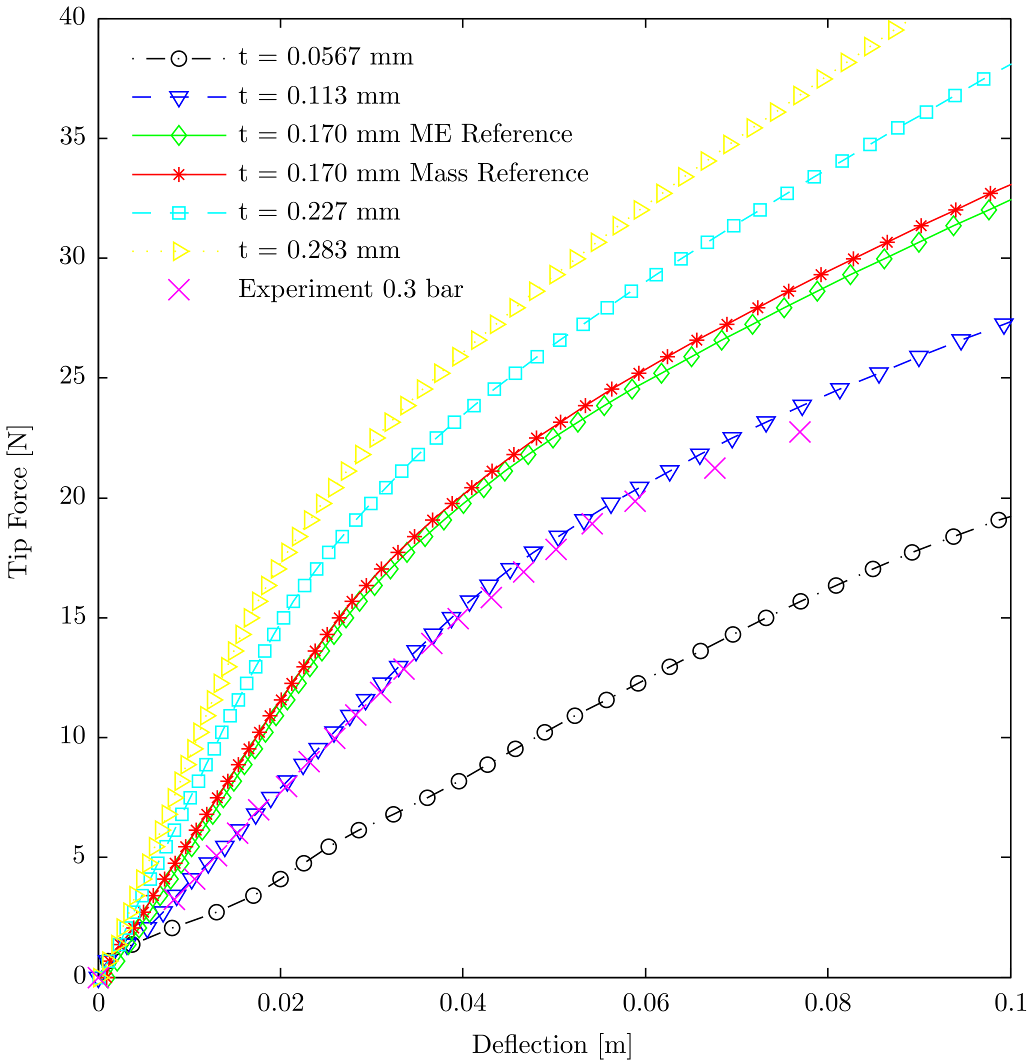


**Figure F-16:** Results of different material thicknesses

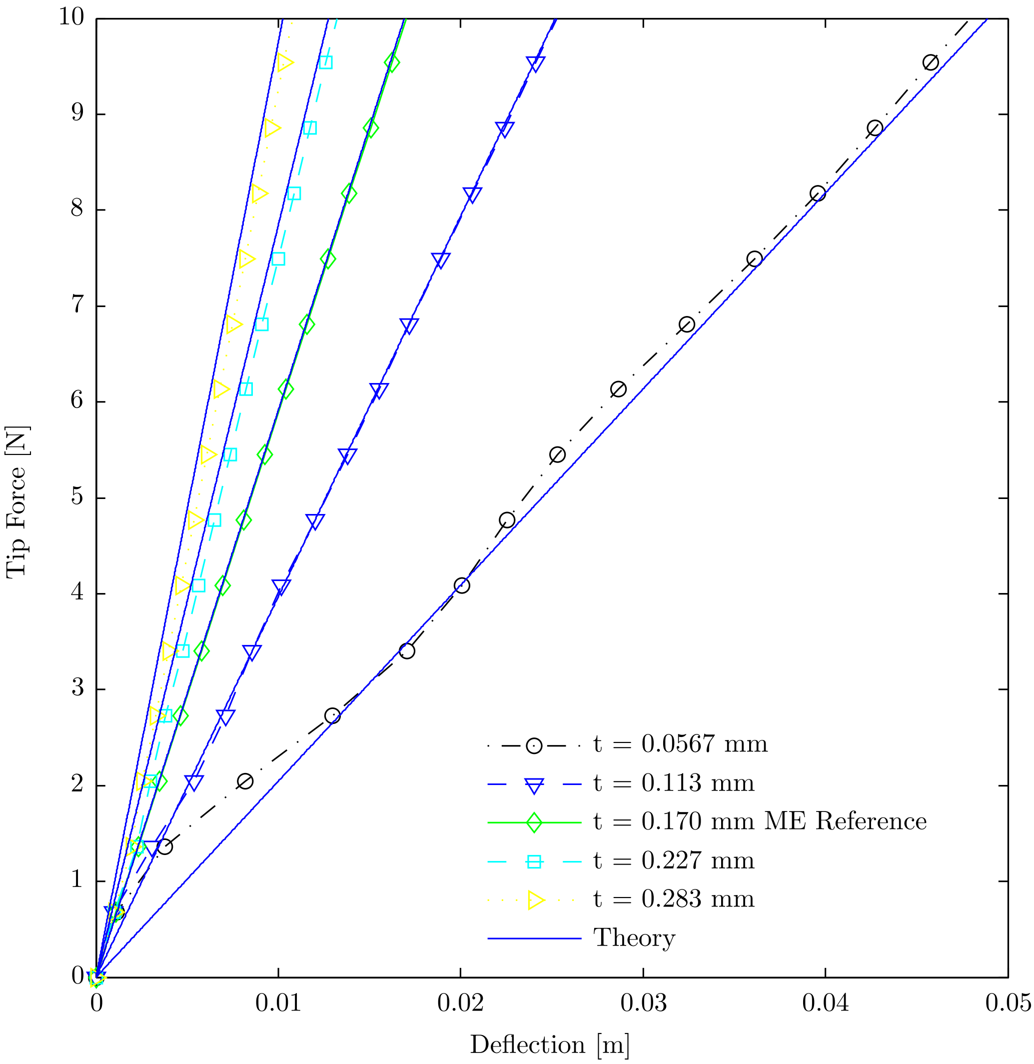


**Figure F-17:** Comparison theory and FEM model with different thicknesses

# F-4 Material: E modulus

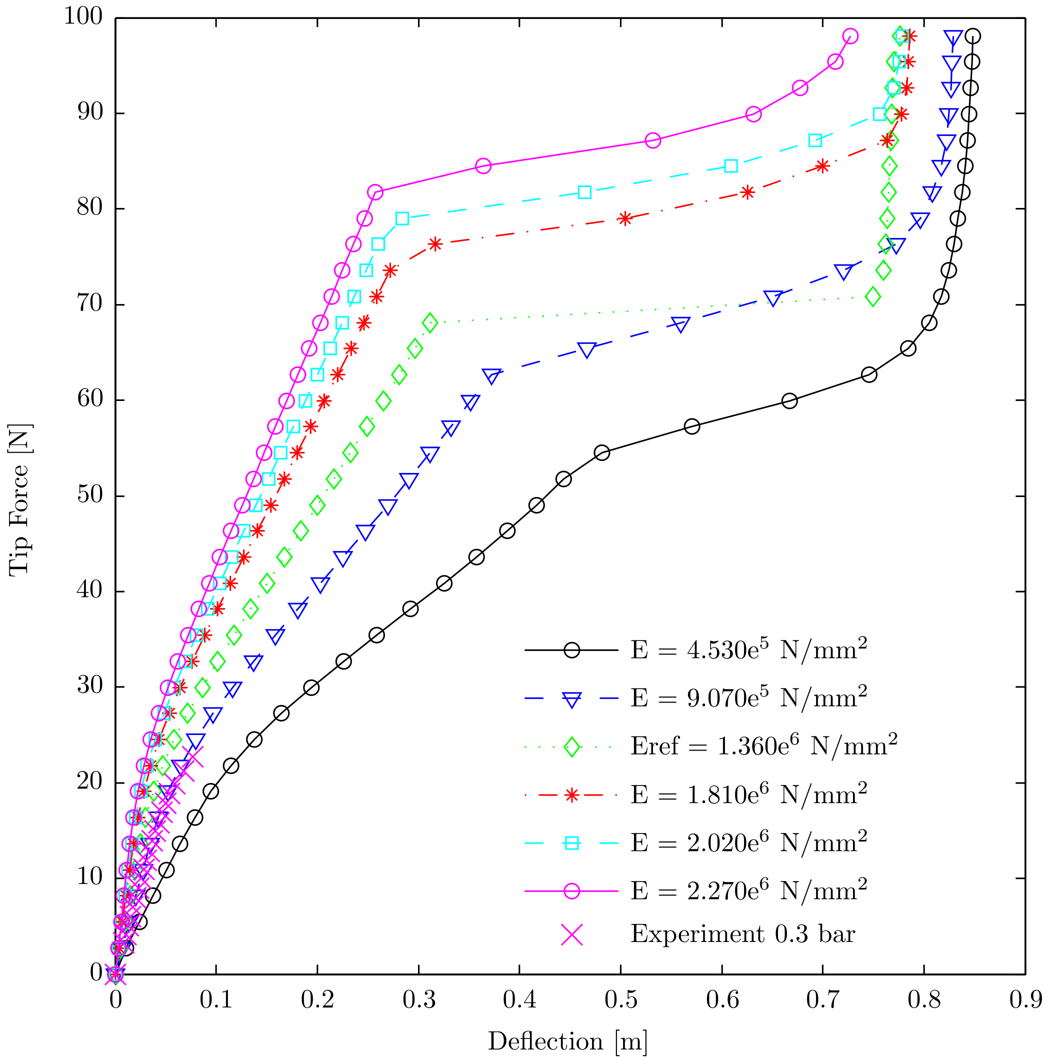


**Figure F-18:** Results of different E moduli

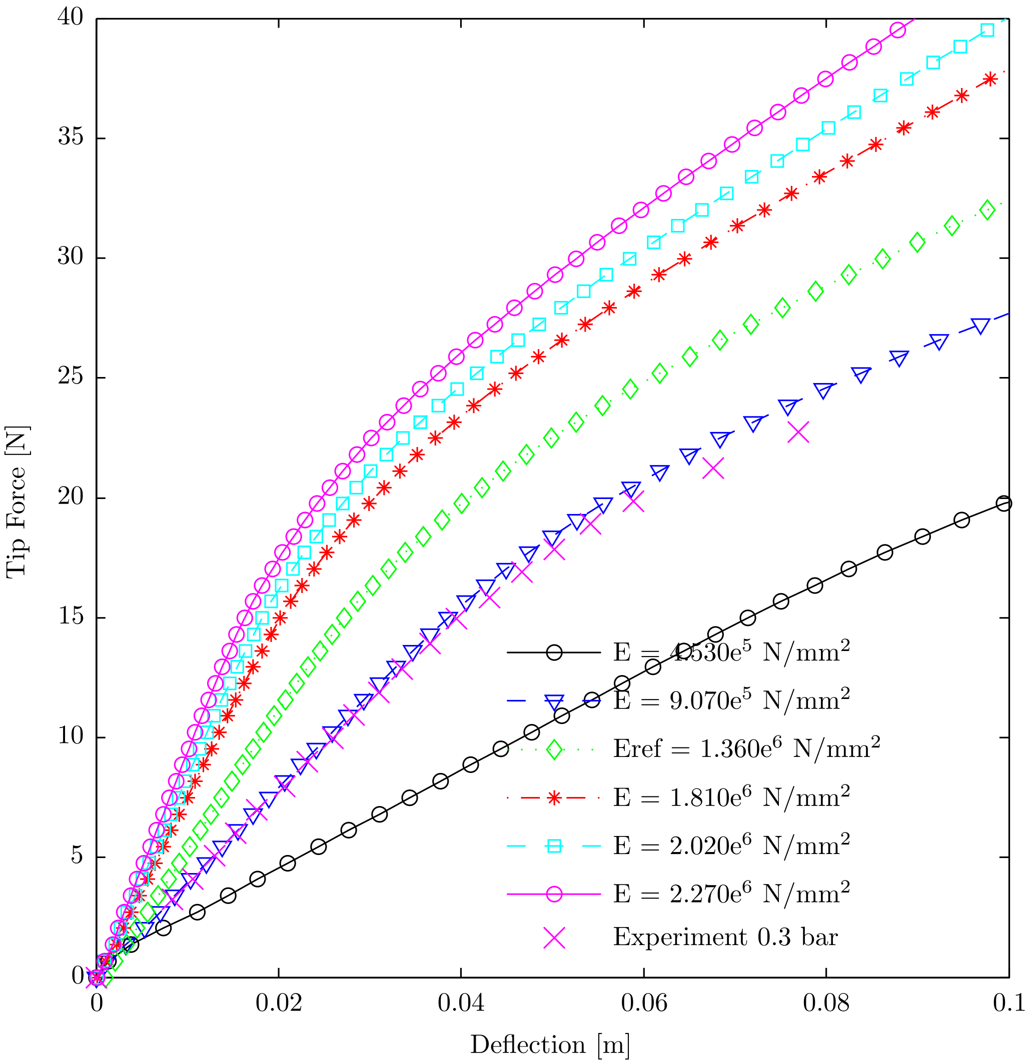


**Figure F-19:** Results of different E moduli

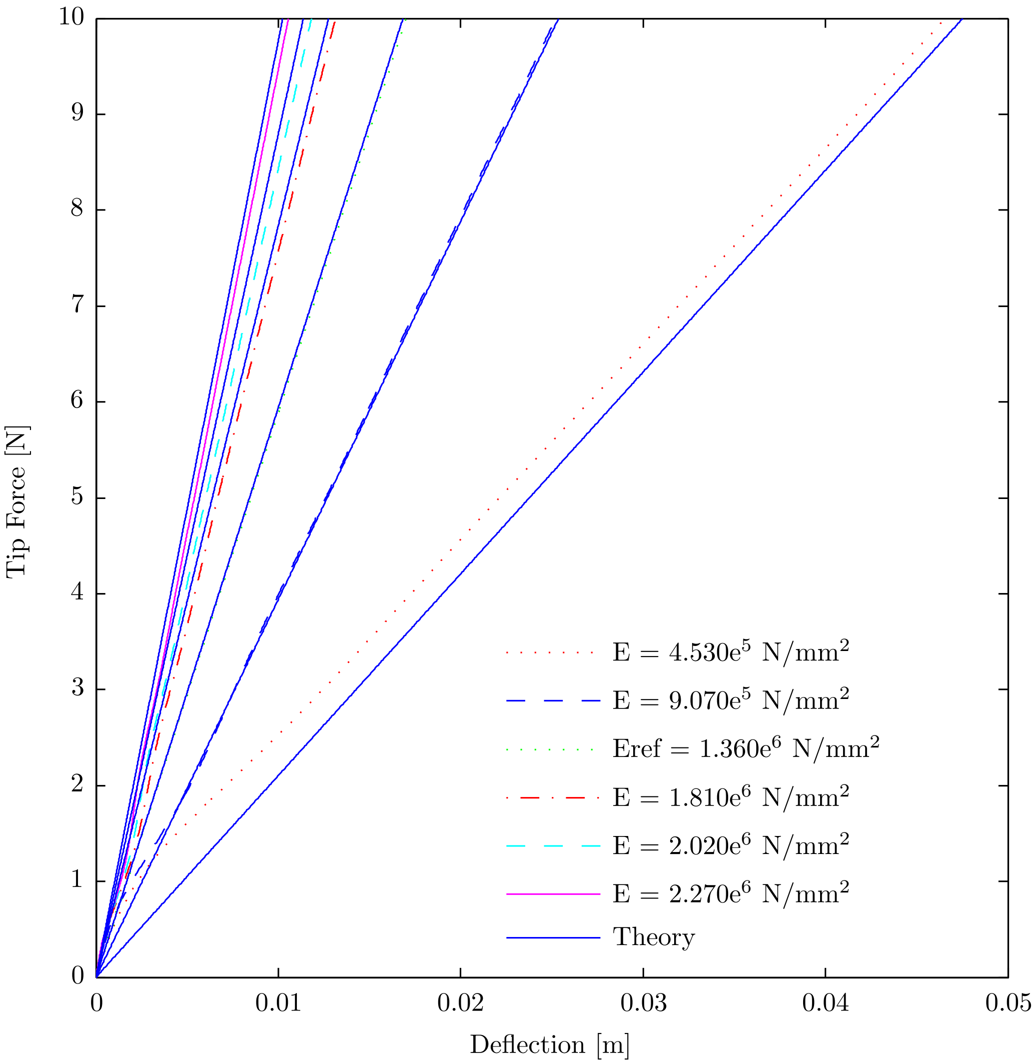


**Figure F-20:** Comparison theory and FEM model with different E moduli

## F-5 Material: Tension Only ON and influence of reduction factor

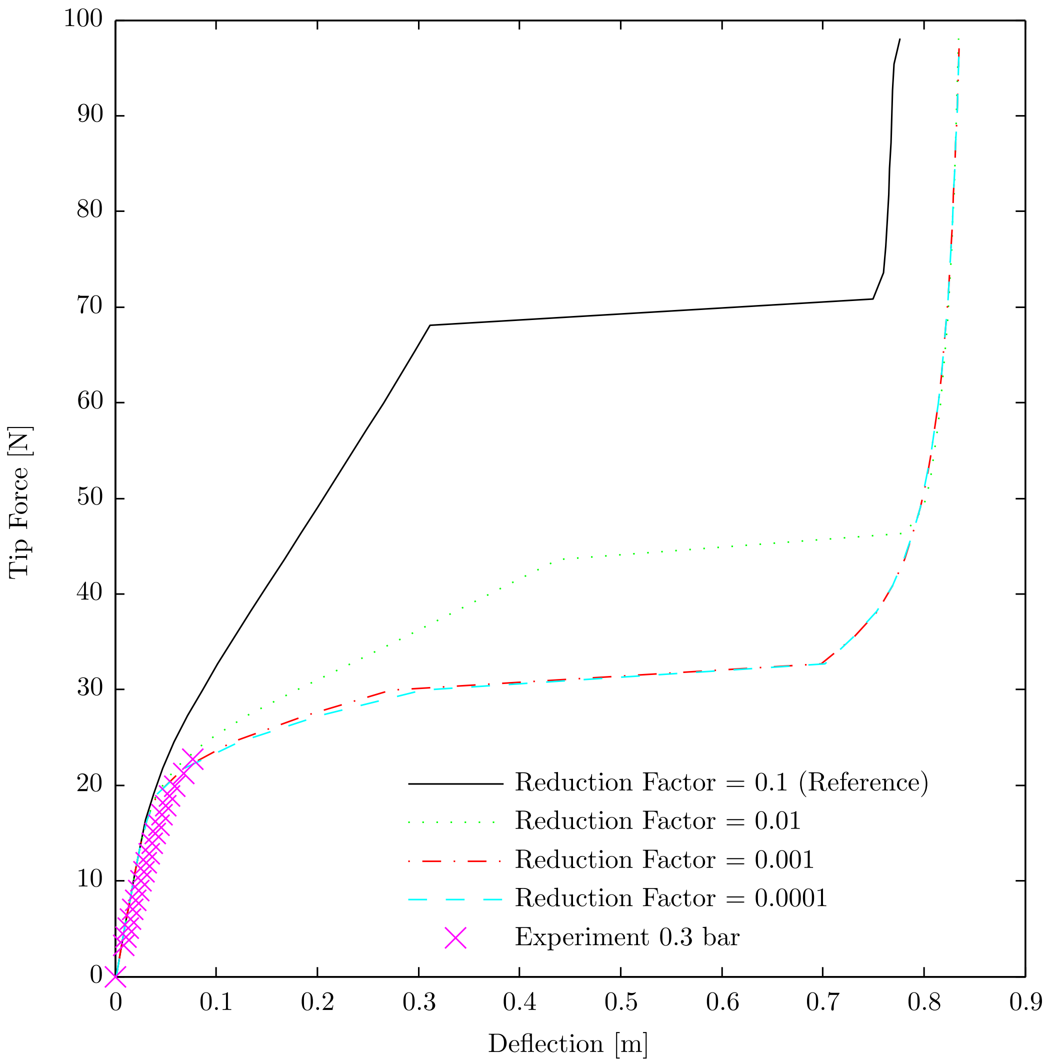


**Figure F-21:** Results of different reduction factors

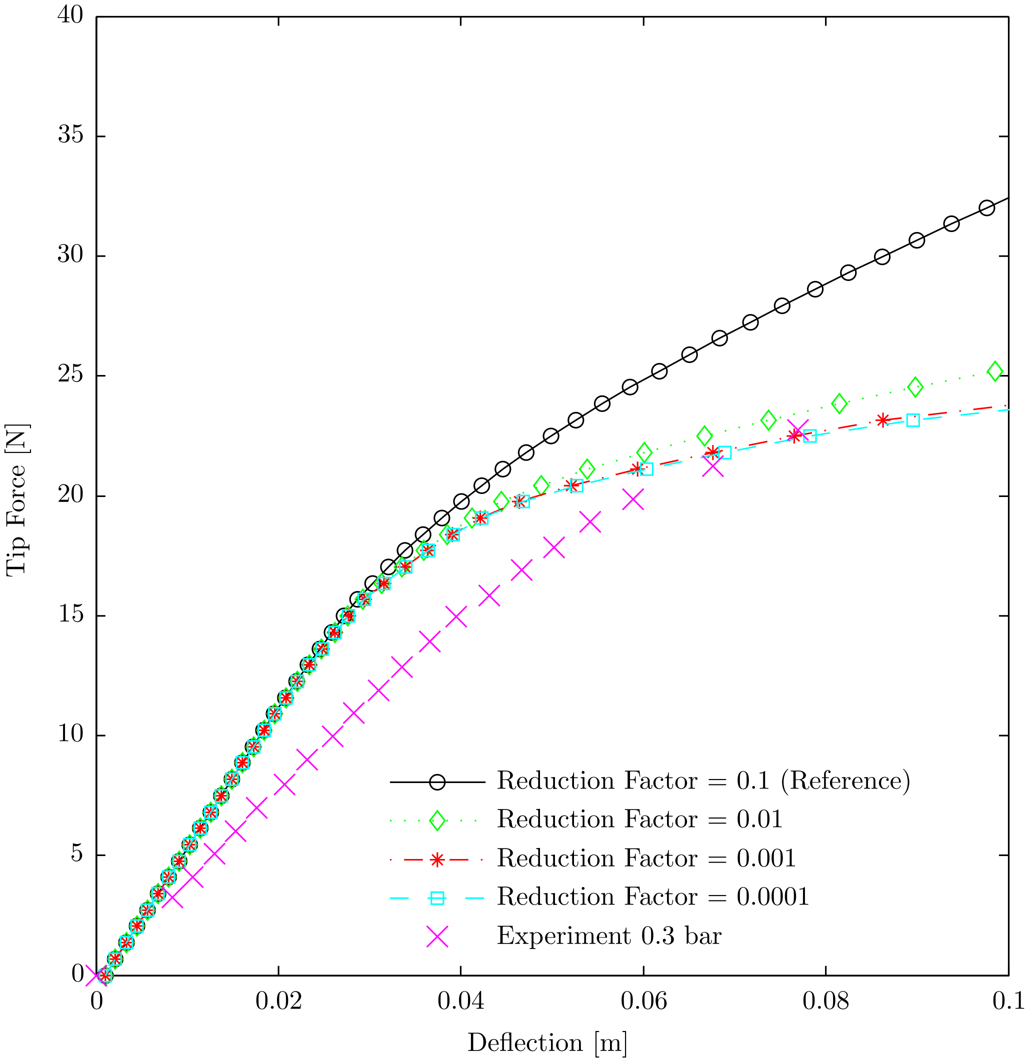


**Figure F-22:** Detail results of different reduction factors

# F-6 Material: Woven Material model

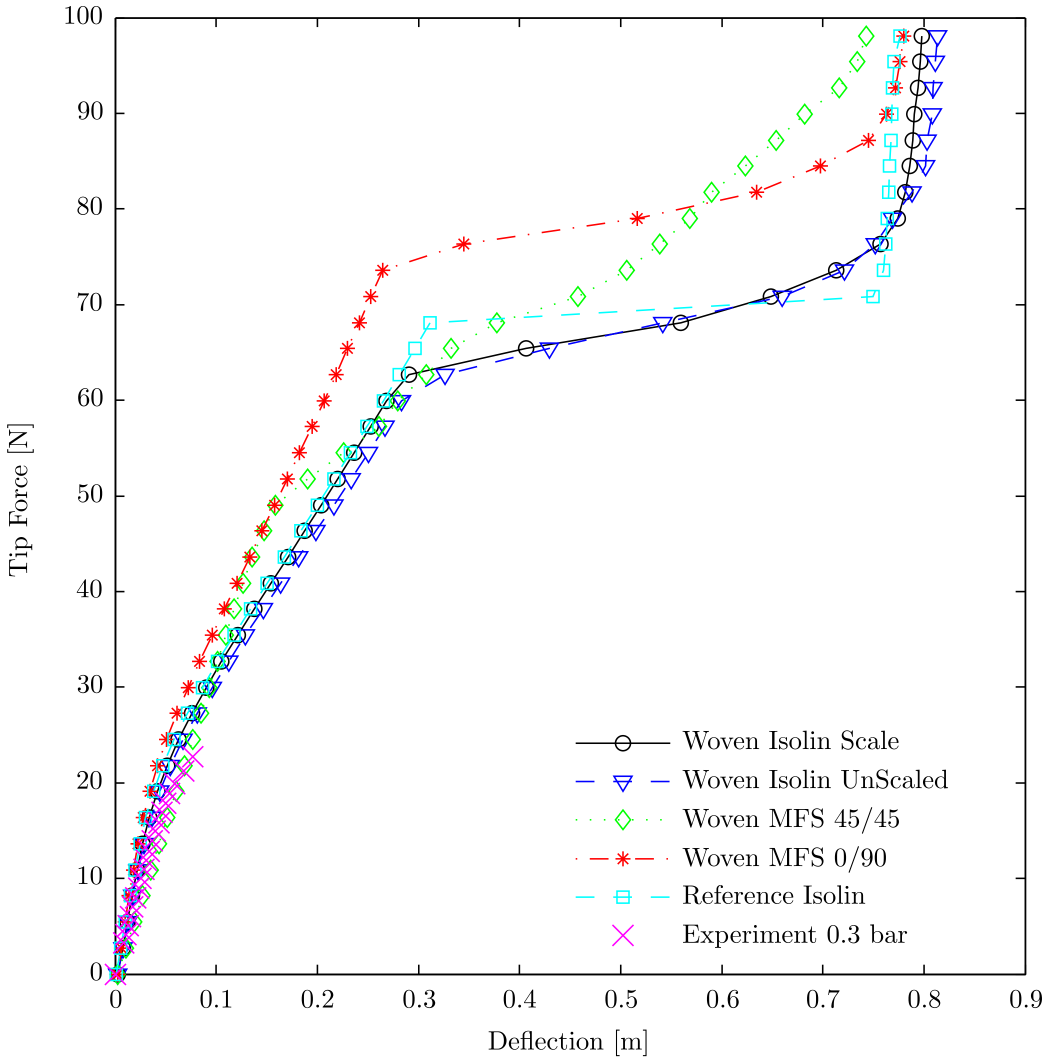


**Figure F-23:** Results of different material models

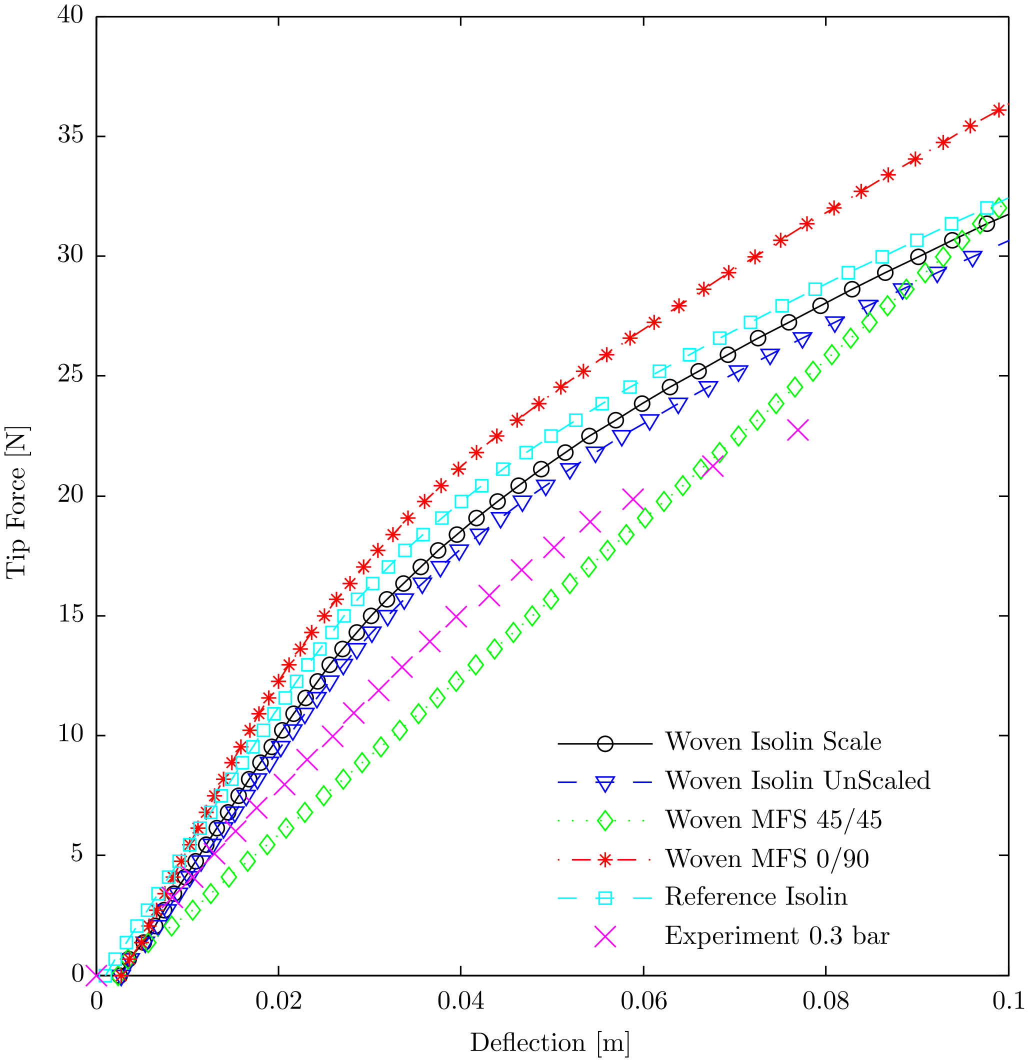


**Figure F-24:** Results of different material models

## F-7 Material: Density

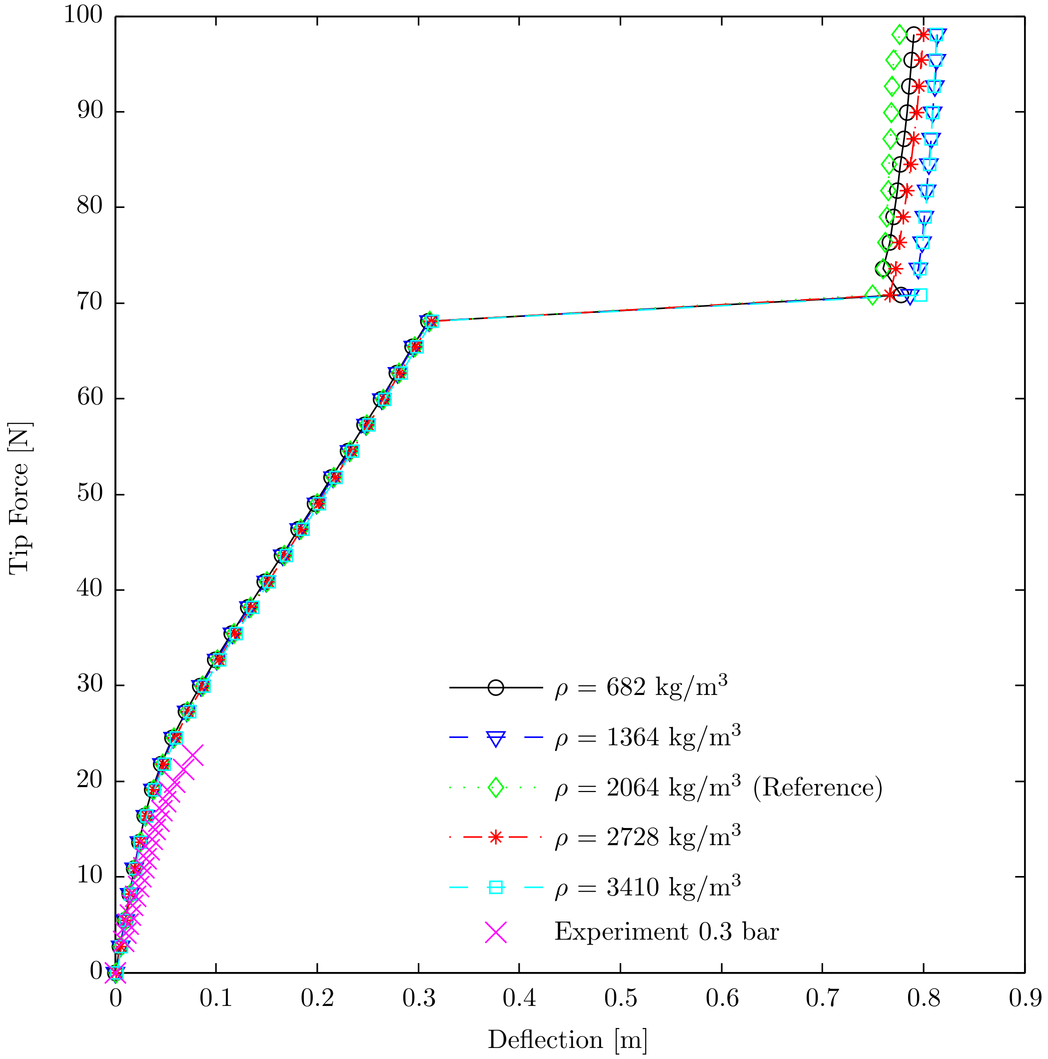


**Figure F-25:** Results of different densities

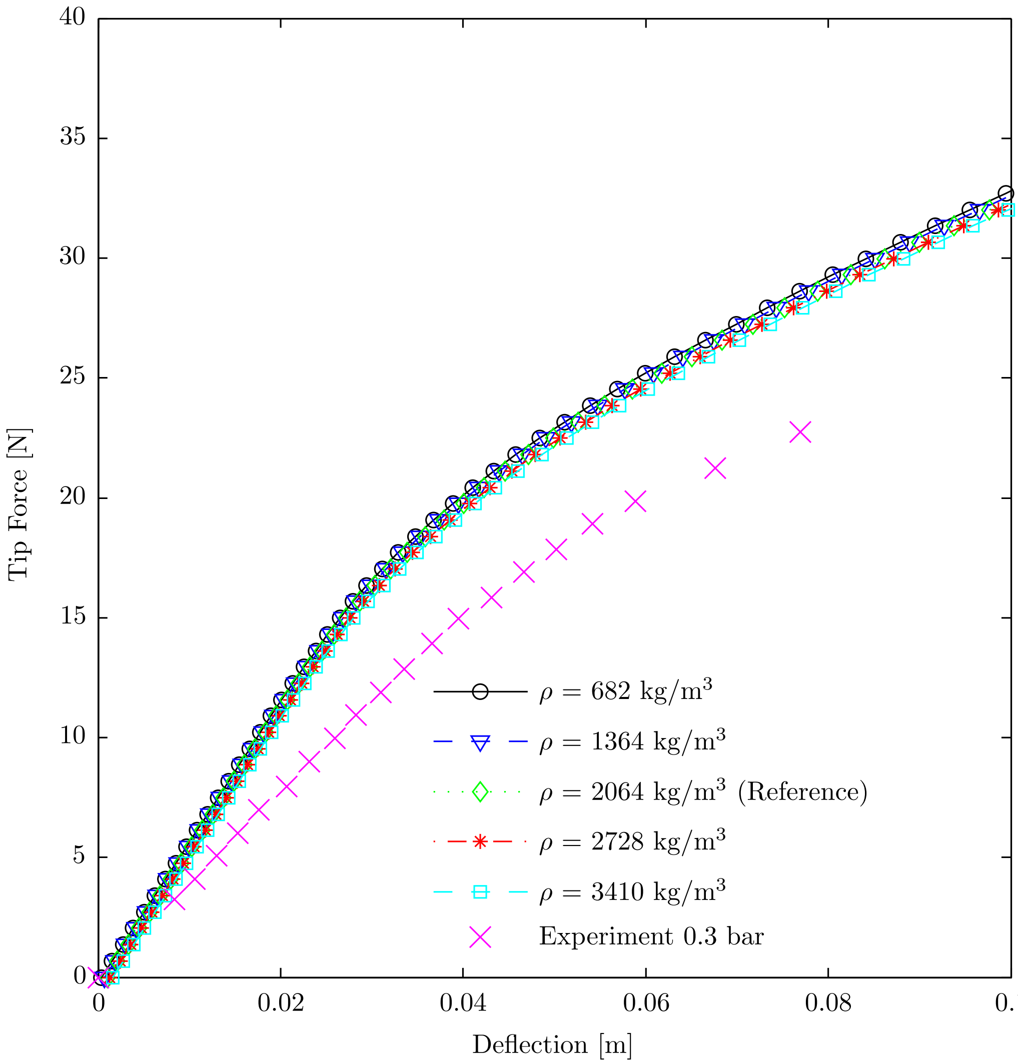


**Figure F-26:** Results of different densities

## F-8 Material: Damping coefficients

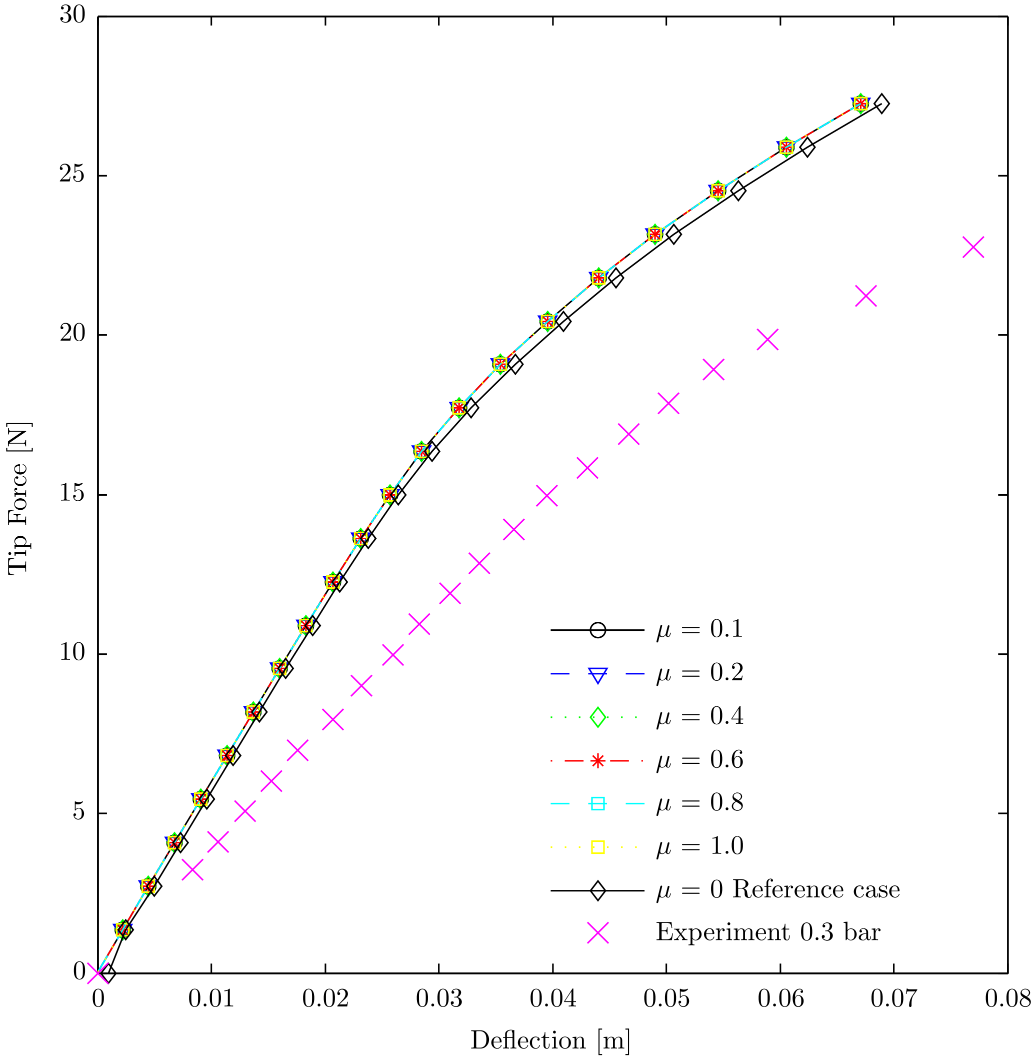


**Figure F-27:** Results of different Material Damping Coefficient $\mu$

# F-9 Poissons's ratio

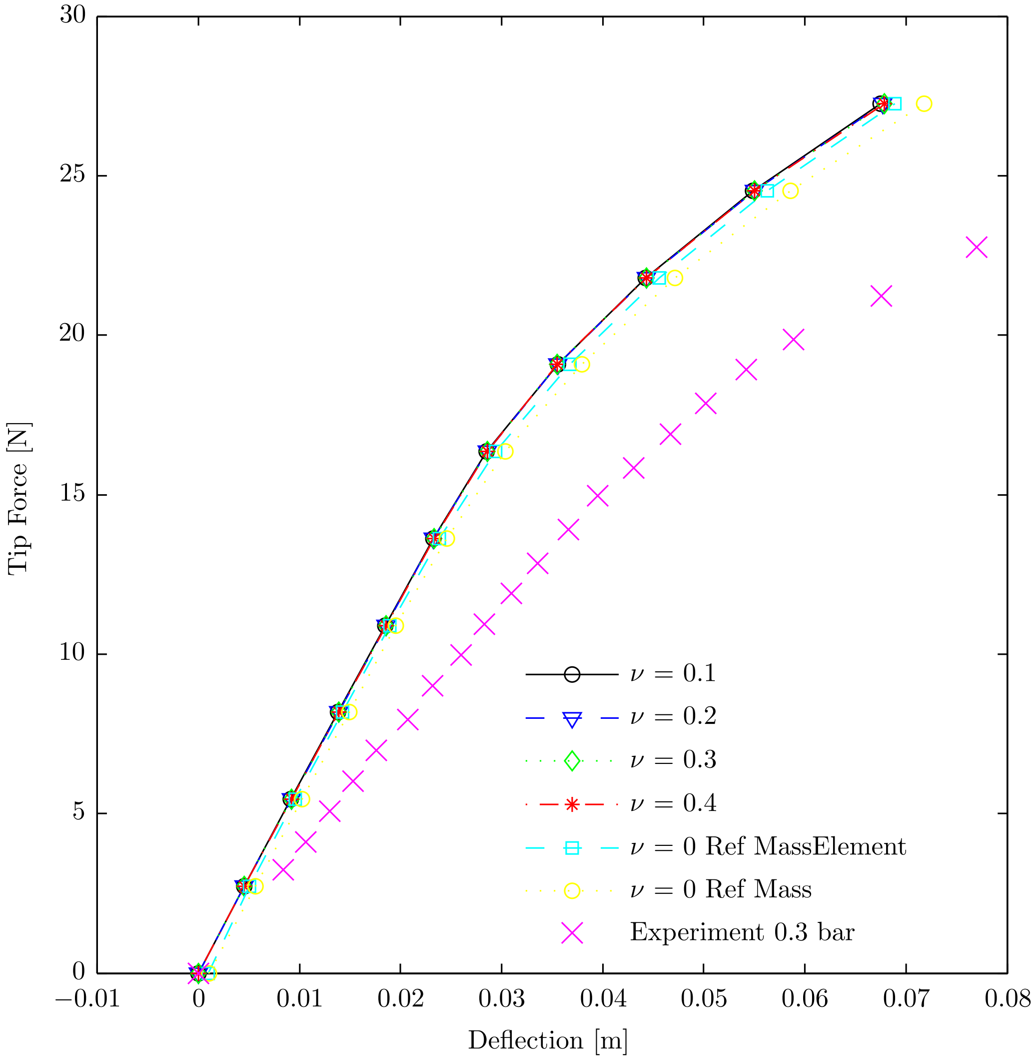


**Figure F-28:** Results of different Poisson's ratios

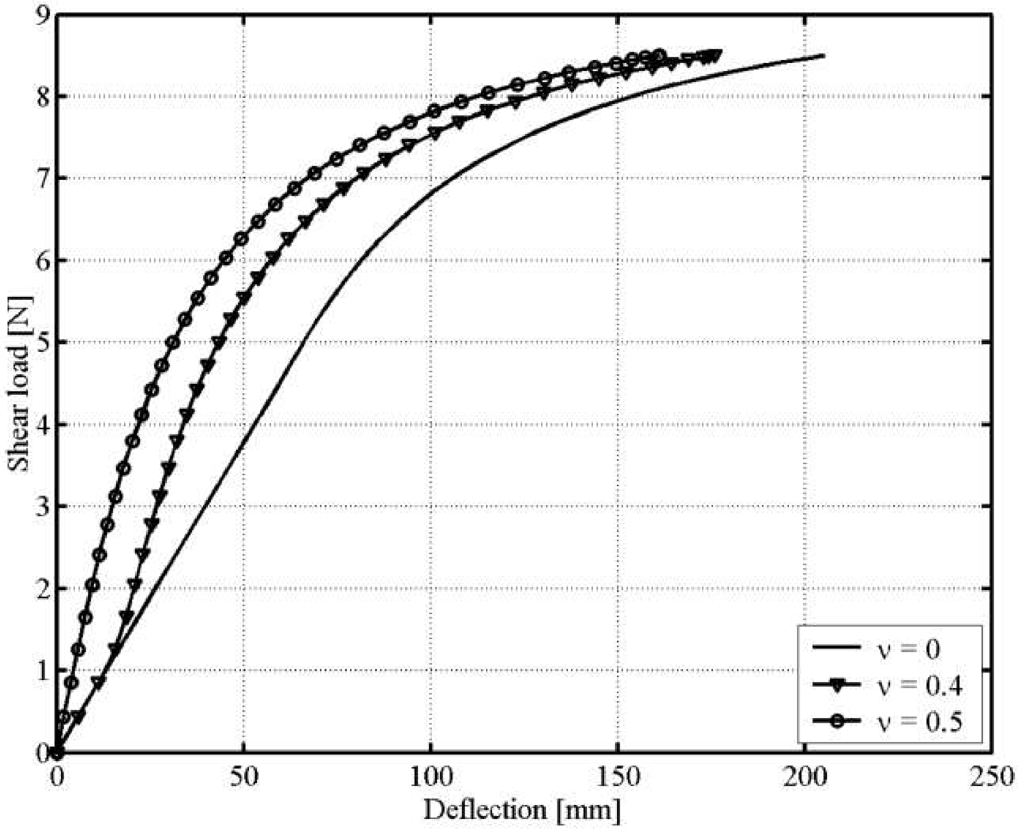


**Figure F-29:** Results of different Poisson's ratios in (Veldman, 2005)